Hydro-mechanical behaviour of a residual soil slope in Malaysia

MD-RAHIM, MOHD,SYAZWAN,BIN

Durham University

Hydro-mechanical behaviour of a residual soil slope in Malaysia

Mohd Syazwan Md. Rahim

Thesis submitted towards the
degree of Doctor of Philosophy in the Faculty of Science

Geotechnical Group
School of Engineering and Computing Sciences
Durham University
United Kingdom

January 2016

Hydro-mechanical behaviour of a residual soil slope in Malaysia

ABSTRACT

Climate change poses real threats to the sustainability of slopes, particularly in the tropical region of the world. Its effects have caused a greater occurrence of extreme climate events that are reflected in a greater occurrence of slope failure incidents for this region. The hydro-mechanical characteristics of soils linked with climate variation are factors that can explain deterioration in slope stability. Therefore, the ability to analyse the hydro-mechanical behaviour properly is worthy of investigation and this can be done by the use of experimental investigation and numerical modelling using both saturated and unsaturated soil properties. In this thesis, the description of the important effects of climate impacts on slope stability has been made for a failed tropical residual soil slope located in Precinct 9, Putrajaya, Malaysia. Part of the work involved soil sampling for the acquisition of undisturbed soil samples from the slope. Series of advanced saturated and unsaturated laboratory testing for both hydrological and mechanical properties have also been implemented and were used in transient, unsaturated numerical modelling of slope stability analysis (using Plaxis 2D). The results demonstrate that within a slope the mobilised shear strength drops quickly during a rainfall event (due to rainfall infiltration) but recovers much more slowly during drying. This shows how a series of regular rain storms with short periods of drying in between can cause a ratcheting effect, with rapid loss of strength during each period of rain that is not recovered during the intermediate drying periods. In addition, the results also show that the adoption of critical state soil parameters is more suitable to match the observed failure. The failure was due to a very extreme amount of rainwater infiltration in the two days before the incident, including the largest daily rainfall in 2007 of 140mm.

DECLARATION

The work in this thesis is based on research carried out in the Geotechnical Group, School of Engineering and Computing Sciences, Durham University. No part of this report has been submitted elsewhere for any other degree or qualification and it is all my own work unless referenced to the contrary in the text. Parts of this work have been published in the following:

MD. RAHIM, M. S. & TOLL, D. G., 2014. Fully Coupled Flow-Deformation Analyses of Infiltration and Matric Suctions within a Tropical Soil Slope. *Unsaturated Soils: Research & Applications. (Eds. N. Khalili, A. Russell & A. Khoshghalb),* London: Taylor & Francis (CRC Press), pp. 1453-1458.

TOLL, D. G., MD. RAHIM, M. S., KARTHIKEYAN, M. & TSAPARAS, I. 2015. Soil atmosphere interactions for analysing slopes in tropical soils. *Computer Methods and Recent Advances in Geomechanics.* (Eds. F. Oka, A. Murakami & R. Uzuoka), London: Taylor & Francis (CRC Press), pp. 1333–1338.

ACKNOWLEDGEMENTS

In the Name of Allāh, the Most Gracious, the Most Merciful

First and foremost, I would like to express my greatest love and gratitude to both of my parents - Md. Rahim Ahmad and Fatimah Hj. Abdul Rahman. Their support, encouragement, quiet patience and unwavering love were undeniably the bedrock upon which made this journey is possible. It was from their prayers that I gained the courage and the ability to tackle challenges head on. The tolerance of my occasional vulgar moods is evidence in itself of their unfading affection and love.

I am deeply indebted to Professor David G. Toll for the guidance, encouragement and advice provided throughout my period of study. His confidence in me is a constant source of inspiration and for always motivating me not to quit in the face of difficulties. I would like to thank Dr Ashraf Osman for his continuous support as well as for his expert advices. I have been extremely lucky to have a great supervising team who cared so much about my work, and who provided me huge support during the time of research and writing of this thesis.

A special word of thanks also goes to Mr. Jimjali Ahmed, Business Director of IKRAM, for his response and help on the acquisition of soil samples from the slope in Putrajaya, Malaysia. An ambitious project of this nature is only possible with the help of kind people like him. Not to forget Mr. Stephen Richardson and Mr. Kevan Longley for the assistance given during the implementation of laboratory works. Without their presence as well as my fellow PhD friends (Dr. Asem Hassan, Dr. Jonathan Asquith, Piotr Osinski, Dr. Salma Hashim and Dr. Thomas Birchall), I don't think my time in Durham University would be interesting.

To my siblings (Along, Ateh and Abang Na'man) and my in laws, thanks very much for inspiring me to follow my dreams and with all the support, help, and assistance that all of you have given me all this while. I would also like to thank the Malaysian community in Bowburn for the companionship that makes the longing for home is very much

bearable. My sincere thanks also go to my sponsor (Majlis Amanah Rakyat – MARA) without which, all this would only be and remained as an ambition like others.

Last but not least, to my wife Rimma Melati Abdul Karim, thank you for your patience by being with me throughout this journey. Your unconditional love inspires me to keep on moving despite the hardship. To my sweet little princess –Ameera Surfina Mohd Syazwan, I hope someday when you read this, you will understand that learning is a never-ending journey.

And to my beloved brother who was never forgotten,
Allahyarham Mohd Syahrizan Md. Rahim.

CONTENTS

CHAPTER 3

Mechanical behaviour of Tropical Residual Soils

CHAPTER 4

Hydrological behaviour of Tropical Residual Soils

CHAPTER 5

Numerical Modelling of Tropical Residual Soil Slope

LIST OF FIGURES

LIST OF TABLES

LIST OF SYMBOLS

ρ	Bulk density	M_s	Saturated critical state stress ratio
ρ_{dry}	Dry density	M_{p^*}	Unsaturated critical stress state ratio
G_s	Specific Gravity	M_a	Critical state stress ratio with respect to mean net stress
σ	Total stress	M_b	Critical state stress ratio with respect to suction
χ	Bishop's 'effective stress' coefficient	p'_e	Equivalent stress on the normal compression line
τ_m	Mobilised shear strength	p'_c	Equivalent stress on the critical state line
τ	Shear strength	ν_λ	Equivalent specific volume intercept
c'	Effective cohesion	E'	Young's modulus
ϕ'	Angle of internal shearing resistance	ν	Poisson's ratio
ϕ_{cr}	Angle of internal shearing resistance at critical state	e	Void ratio
ϕ_p	Angle of internal shearing resistance at peak state	V_s	Volume faction of solid
ϕ^a	Angle of internal shearing resistance with respect to changes of net stress	V_v	Volume faction of voids
ϕ^b	Angle of internal shearing resistance with respect to changes of suction	Ψ	Total suction
Γ	Specific volume at p' = 1.0kPa	Π	Osmotic suction
λ	Slope of critical state line	u_a	Pore-air pressure
Γ_{adj}	Adjusted specific volume at p' = 1.0kPa	u_w	Pore-water pressure
λ_{adj}	Adjusted slope of critical state line	w	Gravimetric water content
q_{cr}	Deviatoric Stress at critical state	θ_w	Volumetric water content
q_p	Deviatoric Stress at peak state	$\emptyset_p$	Suction head
g_p'	q intercept (in terms of q/p'_c)	$k_{rel}(S)$	Relative permeability
H	Gradient of peak strength envelope	k_w	Hydraulic conductivity with respect to water
g'	q intercept in kPa	k_s	Saturated hydraulic conductivity

m_{final}	Targeted mass after drying or wetting procedure	K_0	Input permeability value
$m_{initial}$	Initial mass of the specimen	i	Hydraulic gradient
$w_{initial}$	Initial water content of the specimen	a, m, n	SWRC curve fitting parameter in terms of gravimetic water content
w_{final}	Desired water content for SWRC	g_a, g_n, g_l	SWRC curve fitting parameter in terms of degree of saturation
S_r	Degree of saturation	N	Normal force acting at the base of each slice
S_e	Effective degree of saturation	R	Radius of the potential slip surface
S_{res}	Degree of saturation at residual state	x	Horizontal distance from center of each slice to the center of moments
S_{sat}	Degree of saturation at saturated state	b	Width of each slice
$(\mathrm{FOS})_m$	Moment equilibrium factor of safety	W	Weight of each slice
$(\mathrm{FOS})_f$	Force equilibrium factor of safety	α	Inclination of the base of the slice
$\emptyset_r$& c_r	Shear strength parameters at failure	f	Offset distance from the force to the center of moments

Chapter 1
Introduction

1.1 Overview

Climate plays an important role in constructing the environment, natural resources, infrastructure and other living aspects in the world. Even with small changes, the implication can be enormous as it influences the human environment in many ways. In 2013, the Intergovernmental Panel on Climate Change (IPCC) 5th Assessment Report (IPCC, 2013) has indicated that since about 1950, the number of heavy precipitation events over land has increased in more regions than it has decreased. Confidence is highest for North America and Europe where there have been likely increases in either the frequency or intensity of heavy rainfall infiltration with some seasonal and regional variations. The condition is also likely to become greater due the likelihood of the occurrence or strength of extreme weather and climate events or both. Therefore, this real-time scenario should not be taken lightly as it can lead to an unfavourable implication, particularly towards the safety of public infrastructure such as slope stability (Liew, 2004, Toll et al., 2012, Toll, 2001, Huat et al., 2007, Premchitt et al., 1994, Rahardjo et al., 2000).

To best illustrate the effects of climate change on slope stability, the simple depiction by Rahardjo et al. (2007) is presented in Figure 1.1. Based on the diagram, it can be recognised that the effects are generally associated with the changes in soil conditions within the slope (Toll et al., 2012). In general, the simultaneous occurrence of evapotranspiration process during dry seasons may cause desiccation cracks (or tension cracks) to occur and this will produce a major change in soil characteristics (Toll et al., 2014). Then, during wet seasons, these characteristics may change again as swelling develops due to the wetting and infiltration processes. The variation of climate events also causes soil layers above the groundwater table to mostly exist under unsaturated conditions; resulted from a greater evapotranspiration than infiltration that leads to soil moisture deficits. The vertical extent of this unsaturated soil zone can be very substantial especially for locations where the groundwater tables are significantly deep.

The development of a wetting front is also another important effect that can be produced through climate variation. This hydrological term is defined as the accumulation of rainwater infiltration due to permeability contrasts within the unsaturated region of the slope (Vaughan, 1985). With the occurrence of greater extremes of infiltration that often exceeds evapotranspiration; the development of the wetting front will become even larger and this can eventually result in an elevation of groundwater position, which gives a greater possibility to trigger slope failures (Tsaparas, 2002). Therefore, it is clear that in order to explain these long-term adverse behaviours of a slope, the incorporation of unsaturated soil concepts for slope assessment is imperative (Toll et al., 2012, Md. Rahim and Toll, 2014). Also, with the adoption of this advanced soil theoretical concept, the complexity of climate-soil interaction can be assessed and this gives confidence to engineers to arrive at a design that can sustain the current climate patterns as well as predicting its serviceability when faced with different climate patterns.

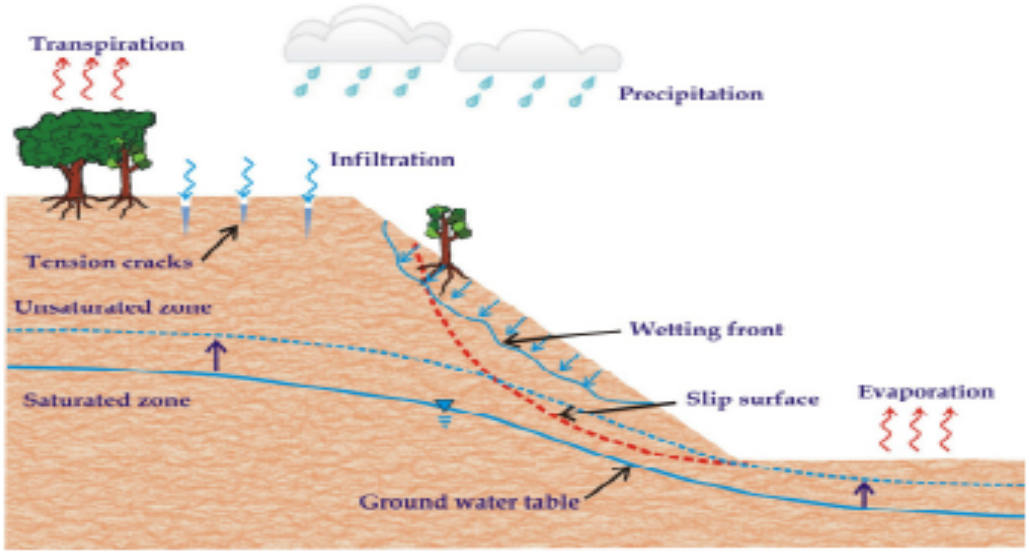

Figure 1.1 The effects of climate change on the mechanism of slope failure (after Rahardjo et al., 2007)

The adoption of unsaturated soil concepts is also essential when dealing with residual soil slopes, commonly found in tropical regions. This is because it has been observed that failures are more likely to occur on residual soil slopes than in any

other types of geotechnical structures (Liew, 2004). The apparent challenges when analysing a tropical residual slope can be attributed to the inherent variation of earth material properties with depth, groundwater regime and subsequent weathering process in the material. The natural heterogeneity of the degree of weathering that reflects the differences in degree of cementation between soil particles, is also amongst the problems, which are frequently unforeseen and also difficult to identify during the design stage (Singh and Huat, 2004). Therefore, it is important to understand the natural characteristics of residual soils in order to describe the actual behaviour of these unsaturated tropical residual soil slopes in correspondence to extreme climate changes.

Malaysia, that is geographically located in the climatic zones enclosed between the latitudes 20° North and 20° South of the equator, is underlain by widespread residual soils. Furthermore, it is also subjected to high temperatures and high humidity throughout the year and therefore can be expected to experience the same extreme climate variations. The impacts of climate change through high volume of rainfalls occurring in the seasonal and monsoonal sequences have caused numerous disastrous slope failure incidents and resulted in not only extensive damage to public properties but also loss of lives (Ahmed et al., 2011). With the tremendous increase in construction of residential buildings on hill sites over the last 15 years, it has been recognised that extra precautions in the geotechnical design are required, especially to further understand the mechanism that is causing these slope failures (Gue and Tan, 2004).

Hence, in 2006, the Malaysian Public Works Authority implemented a major initiative by producing the National Slope Master Plan Study for the mitigation of this slope instability issue. The objective of the study is to provide a comprehensive and effective national policy, strategy and action plan in reducing losses from slope failures that is predominantly based on ‘precautionary principles’ (Huat et al., 2007). However, looking at the potential risk that can be produced by this extreme climate variability, a comprehensive and exhaustive measure of mitigation based on scientific analyses is crucial. The technical study should be able to emulate the wetting and drying process, utilising both classical and unsaturated soil mechanics.

To analyse the effects of climate change on the stability of tropical residual soil slopes will inevitably require the use of numerical modelling (Toll et. al., 2012). This means such studies must involve the adoption of advanced modelling methodologies that can deal with the complexity of climate-soil interaction. The interrelation of hydraulic and mechanical behaviour during and after rainfall infiltration is also a subject of great interest in geotechnical engineering practice (Khalili et al., 2008). This proves that the ability to analyse them properly is worthy of investigation and highly relevant especially to those complex slope problems that could not be explained using conventional techniques.

Therefore, in May 2013, soil-sampling works have been successfully carried out at the top of a failed tropical residual soil slope located in Precinct 9, Putrajaya, Malaysia. The purpose of this soil sampling works is to acquire undisturbed soil samples for the advanced investigations of the cause of a disastrous failure that took place at around 4:30am, on the 22nd March 2007. Using these undisturbed soil samples, the actual unsaturated soil hydrological and mechanical properties can be obtained and be used as input parameters for the implementation of numerical modelling of slope stability analysis with time dependent boundary conditions. However, in order to ensure the actual representation of these properties for the area of concern, the sampling procedure must be executed in a way to avoid disturbance to the sample, especially changes to the water content of the soils.

There are various techniques that can be used to determine unsaturated hydrological and mechanical properties of the residual soils (i.e. Toll et. al., 2013, Toll et. al., 2015, Fredlund and Rahardjo, 1993, Ridley and Burland, 1993, Rahardjo and Leong, 2006, Bulut and Leong, 2008, Lourenço, 2008, Mendes et. al., 2012, Li and Standing, 2014 among others). These techniques are mostly implemented for soil suction measurement and control, as this soil component represents the natural ability of the soil to exert a tensile pull due to the existence of air elements within the pores. The state-of-the-art unsaturated soil laboratory available in Durham University can provide investigation of the water retention properties, permeability and strength behaviours. Nevertheless, it has to noted that the implementation of these testing demands special care due to the sensitivity of the soil that may change drastically even by partial drying.

Lastly, it is common for numerical modelling for stability assessments to calculate the flow (hydrological) and deformation (mechanical) assessments in two separate analyses. However, in actuality, both aspects are highly interlinked as the characteristics of water flow, changes of pore-water pressure, and shear strength of soils are the main parameters associated with the flux boundary condition at the soil-atmosphere interface (Hamdhan and Schweiger, 2011). Thus, the analyses reported here will be done by coupling the equations for the flow (hydrological) and deformation (mechanical) assessments using the concept introduced by Bishop (1959); where “effective” stress in unsaturated soils is used to represent the hydro-mechanical coupling effects. Hopefully, the findings from this numerical study can be put into use as further guidance in order to mitigate the effects and the impacts of rainfall on slopes, and in return would help to reduce the public fear and trepidation.

1.2 Research Objectives

The main objectives of the work described in this thesis are:

1) To study the physical characteristics and index material properties of tropical residual soils through the implementation of high quality soil sampling fieldwork and soil classification laboratory work.
2) To perform unsaturated laboratory testing for the characterization of the hydro-mechanical behaviour of the undisturbed tropical residual soils.
3) To perform numerical modelling of slope stability analysis by coupling the equations for the flow (hydrological) and deformation (mechanical) assessments in order to better understand the actual cause of failure for the studied research slope.

1.3 Thesis Structure

The thesis is divided into 6 chapters. It has to be noted that the theoretical and research background and basis of each aspects of work are presented in each relevant chapter. This thesis format was chosen as to provide convenience of reading especially for the process of literature reviewing.

Following this introductory chapter is Chapter 2 that describes the engineering geology of tropical residual soils from the studied research slope. The chapter starts by introducing definitions and information regarding tropical residual soils, followed by the descriptions of the research slope. This includes the implementation of soil sampling fieldwork. The chapter continues with the soil index and classification laboratory work to further characterise and classify the types of soil materials and to compare the variation in each property against depth.

In Chapter 3, the details of the mechanical behaviour of the unsaturated tropical residual soil are presented. The differences in strength characteristics for this this type of soil are discussed as well as the descriptions of several available constitutive models proposed for unsaturated soil. Then, a detailed description for a series of Multistage triaxial testing is outlined, following with the presentation of the results of strength testing. Comparisons of the soil strength properties (critical state parameters) using different constitutive models are also presented at the end of this chapter.

Next is the chapter that describe the hydrological behaviour of the tropical residual soil (Chapter 4). Similarly, the unsaturated soil theoretical background is presented that includes the influence of suction on the water retention behaviour. The description of the different hydrological testing procedures as well as the experimentation on the residual soil samples for Soil water retention curves (SWRC) are also presented. At the end of the chapter, the production of SWRC using different suction measurement or control techniques are shown and discussed.

The numerical modelling of slope stability analysis for two different tropical residual soils slopes are presented in Chapter 5. The key aspects that influence the changes of flow of water within the slope are discussed as well as the description of numerical modelling procedures. This chapter also includes a review of tropical

residual soil slope failure incidents that has happened in Malaysia. Subsequently, the slope stability analysis by coupling the equations for the flow (hydrological) and deformation (mechanical) assessments are shown as these analyses were carried out for two different tropical residual soils slopes; a reanalysis of a previous numerical study reported from Singapore reported by Tsaparas and Toll (2002) and a back analysis of the studied research slope in Putrajaya, Malaysia.

Finally, Chapter 6 summarises the results of the research study, provides conclusions and also gives recommendations for future work.

Chapter 2
Engineering Geology of Tropical Residual Soil Slope in Malaysia

2.1 Introduction

In tropical regions, specifically Malaysia, the construction of residential buildings on hill-sites is becoming a substantial trend due to the depletion of flat land and other influential commercial factors (i.e. beautiful scenery, freshness, exclusiveness and etc.) (Gue and Tan, 2004). Such hill site development could result in the erection of many geotechnical structures and construction of engineered cut slopes as part of the earthworks. However, as the region is predominantly underlain with residual soils, extra precautions in the geotechnical design are needed as it has been reported that failures are more likely to occur on residual soil slopes than in any other circumstances (Liew, 2004).

The inherent variation of earth material properties, groundwater regime and subsequent weathering process in the material are amongst the problems which are frequently unforeseen and also difficult to identify during the design stage (Singh and Huat, 2004). Therefore, it is important to understand the engineering geology of residual soils in order to describe the actual behaviour of these tropical residual soil slopes in correspondence to climate changes.

In this chapter, the definition and information regarding tropical residual soils are presented together with the descriptions of the studied research slope including the implementation of soil sampling fieldwork and soil classification laboratory work.

2.2 Literature review

2.2.1 Tropical residual soil and geology of Malaysia

Residual soils are defined as soils originated from the outcome of weathering processes on the parent bedrocks, such that they remain at the place where they were formed. This definition was made based on different interpretations provided by different authors as to describe of what might be defined as 'residual soil', compared to other conventional soils (i.e. Brand and Phillipson, 1985, Blight, 1985, Sowers, 1985, and The Public Works Institute of Malaysia, 1996 and etc.). The weathering process, which can be separated into chemical and mechanical forms, takes place over a very long period of time and is highly dependent on the fabric or structure of the parent bedrocks. The processes of chemical weathering contribute to changes of the rock minerals, whilst, the decomposition of the rock material into small fragments is accelerated by the mechanical processes (Sowers, 1985). Nevertheless, these developments of residual soils depend on several major factors such as climate, geology, topography, biotical factor and chronology (Bergman and McKnight, 1993).

The weathering process essentially proceeds from the ground surface downward. This perpetual in-situ disintegration process produces a weathered subsoil profile that is parallel or sub parallel to the ground surface, which means the stratigraphy would be sub-horizontal for flat ground and sloping in parallel with sloping ground. The degree of weathering may extend until the original structure of the rock mass is completely destroyed and removed, as a result, usually leaving a clay-based deposit (Huat et al., 2004).

To further illustrate the stratification, the simple scheme proposed Little (1969) can be used (Figure 2.1). The scheme that was derived from work on granites (igneous rock) is used to define weathering grade of rock (I to III) and soils (IV to VI) and can be applied to sedimentary and metasedimentary rocks, although, ideally with some experience. The thickness also depends on the types of parent bedrock and can only be determined from boreholes and open excavations. In general, based on the generalization from previous experiences, weathering profiles in granitic soil often extend nearly down to 50m deep whereas sedimentary and metasedimentary residual soil (i.e. shales and schists) are reported to be thinner, that is approximately 10m deep (Bergman and McKnight, 1993).

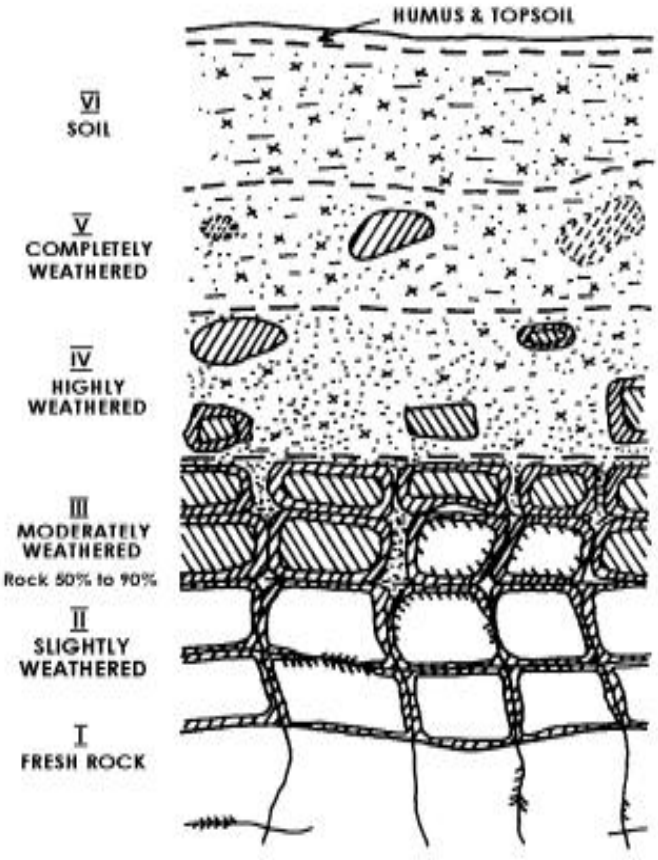

Figure 2.1 Weathering profile (after Little, 1969)

Malaysia, that is geographically located in the climatic zones enclosed between the latitudes 20° North and 20° South of the equator, is underlain by widespread residual soils. It is due to the extent of this climatic zone, the tropical areas, the types of residual soils in this region are referred to as tropical residual soils (Tan, 2004). However, the term tropical residual soil is also used to describe these upper three weathering grades that are dominated by soil material (note the distinction between **tropical** residual soil, which incorporates all three weathering grades IV, V and VI, and residual soil, which only describes Grade VI) (Toll, 2012b). With regular cyclic fluctuations of high and low temperatures, high humidity and heavy rainfalls which are experienced in this region, the weathering processes are easily accelerated and may extend deeper to a significant thickness (Sowers, 1985).

In Peninsular Malaysia, the types of tropical residual soil can be classified by three major classes of rock types, which are igneous, sedimentary and meta-sedimentary. The distributions for these various rock types are closely related to their

topographical location (Bergman and McKnight, 1993). Figure 2.2 shows the distributions of these three classes. It has to be noted that the distributions should only be taken as a preliminary guide due to the very small scale and the lack of distinction between sedimentary and meta-sedimentary rock types. With large geologic map scale of 1:2,000,000, the precision to describe the site variation or details would be limited. This in fact, is further confused by the actual characterization of sedimentary and meta-sedimentary rocks which include a host of different rock types, with very contrasting characteristics and are capable of producing different residual soils (i.e. schists, sandstones, shales, limestones etc.) (Bergman and McKnight, 1993).

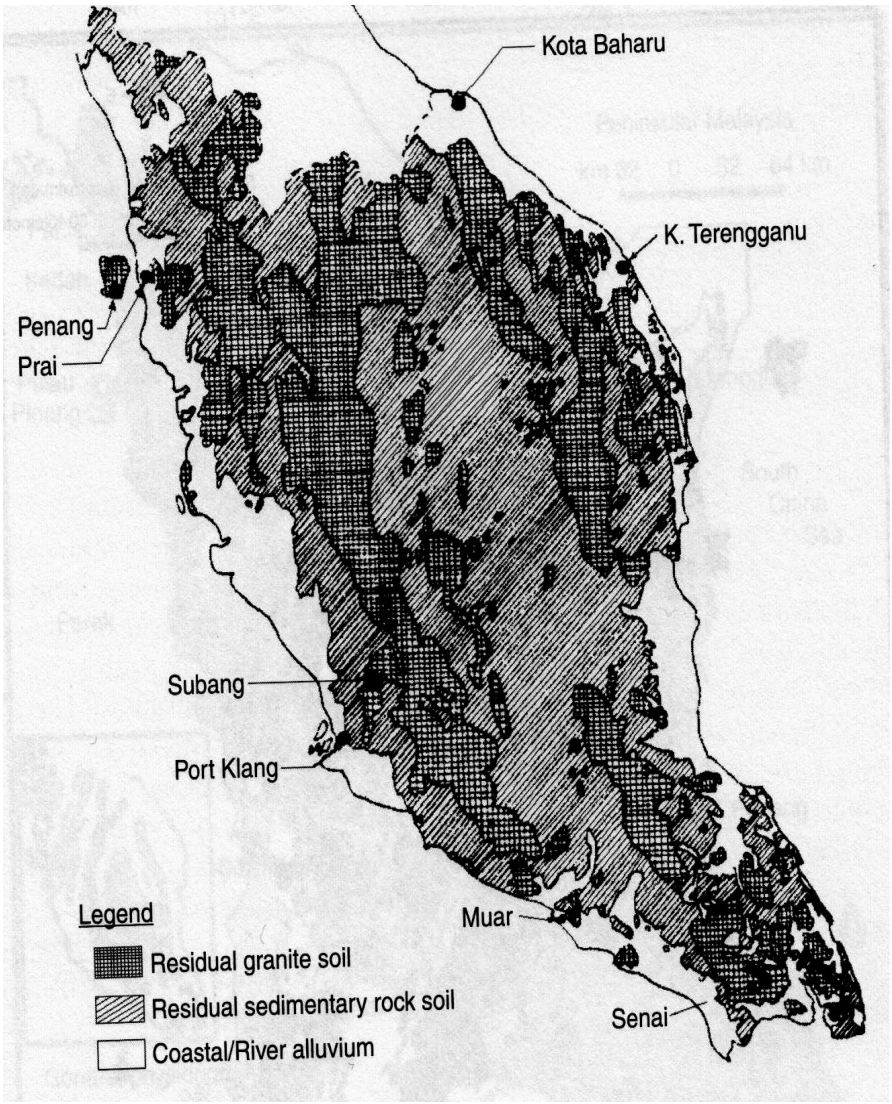

Figure 2.2 The distribution of Tropical Residual Soils in Peninsular Malaysia (Ooi, 1982)

2.2.2 Soil sampling of tropical residual soils

A collection of research papers on sampling processes for residual soils was presented at a symposium held in Singapore in 1979, organised by International Society for Soil Mechanics and Foundation Engineering (ISSMFE) (Nicholls, 1990). These papers were presented due to the growing awareness among researchers, at that time, pertaining to the differences in behaviour and characteristics for residual soils from other conventional soils, particularly in relation to the properties and structure. As a result, special criteria were highlighted for soil sampling procedures that depend on various factors and should be demonstrated by the designers in order to obtain 'representative' soil samples. Further descriptions on the criteria based on these various factors such as purpose of sampling, location of samples, sampling methodology and handling process are briefly discussed, as depicted by Tan (2004).

2.2.2.1 Purpose of sampling

The validity of the geotechnical properties obtained from laboratory testing is highly dependent on the quality of the sample (Cooling, 1949). Ladd and Lambe (1963) suggested the definition of 'Good Quality samples' as samples, which have not been disturbed by boring, sampling and trimming, however, have experienced stress release. The assessment on these samples should be carried out with great care and should not be influenced either by optimistic estimations of a lack disturbance or by the requirements of any analytical programs to be used for the design (Brand and Phillipson, 1985, Geoguide 3, 1996, Schnaid and Huat, 2012).

The importance to minimise disturbance of the samples for residual soils is essential especially for tests such as shear strength, compressibility and permeability. The mechanical force disturbance experienced by the samples during sampling and handling may alter the structure or soil fabric. Therefore, it is important to really understand the purpose of sampling as in whether it should be undisturbed or disturbed types of samples that are actually needed.

2.2.2.2 The method of sampling

There are various sampling techniques that can be applied for residual soils. Open hand dug pit, machine dug pit and drilling techniques are amongst the

common technique used with the latter being the most popular. The utilisation of water as the drilling fluid should be avoided, particularly for soil regions above the water table. This is due to the likelihood to cause sample disturbance such as erosion and loss of core (Huat et al., 2004). Misunderstandings in determining groundwater level and the imposition of additional moisture on the surface of the sample are also consequences of the utilisation of water as the drilling fluid.

It is suggested that foam, mud, air or special drilling fluid are the best alternative to be utilised when dealing with tropical residual soils. By using these materials as the drilling fluid, the sample disturbance can be reduced.

2.2.2.3 Sample handling process

The handling of residual soil samples, especially undisturbed samples, should be carried out in as gentle way as possible due to its sensitivity. The bonding between particles either by cementation or interlocking, value of void ratio and moisture content are among soil characteristics that require extra attention once the samples are brought up to the surface. Any changes in one of these soil characteristics caused either by shaking and vibration during transportation or storage may provide false results. Head (1992) suggested that the samples should be kept in a temperature-controlled room to protect them from extremes of cold and heat. The samples should also be sealed all the time during storage and stored upright to prevent segregation of water.

2.2.3 Index properties of Tropical residual soils in Malaysia

Soil index properties are generally used by engineers to classify different kinds of soil into broad categories (i.e. clay and sand) and into further sub-groups. The variation in values for these properties for tropical residual soils, however, may change drastically even by partial drying. This sensitiveness is due to alteration of the clay minerals on partial dehydration, or due to aggregation of fine particles to form large particles, which remain bonded together, even on rewetting (Fookes, 1997, Blight, 1997). A study of typical index properties for tropical residual soils in Malaysia has been reported by Shukri et al. (2004) and shall be described as the following.

2.2.3.1 Water content

It has been reported that for tropical residual soils, the value of water content ranges between 16% to 49% (Nixon and Skipp, 1957). These variations are depending to the dominant type of soils. Table 2.1 shows some of the reported values of natural water contents for tropical residual soils in Malaysia.

Table 2.1 Water content of some tropical residual soils in Malaysia
(after Shukri et al 2004)

Parent Material	Natural Water Content (%)	Source
Andesite	26	Newill & Dowling (1996)
Granite	30	Ting et al. (1982)
Granite	31	Taha et al. (1999)
Rhyolites	76	Soong et al. (1973)
Schists	10 to 48	Komoo (1985)
Schists	7 to 49	Nithiaraj et al. (1996)
Sandstone	46	Soong et al. (1973)
Shale	47	Mun (1985)

2.2.3.2 Atterberg limits

Due to the sensitivity of tropical residual soils to drying, it has been recommended that the process to determine Atterberg Limits should be carried out as soon as possible and with an appropriate method of drying application (Blight, 1997). The observation made upon various pre-test treatments on Atterberg limits of tropical residual soils showed that drying process may change the physical and chemical properties of the affected soils (Muttaya and Huat, 1994). Table 2.2 shows some typical values of plasticity index for different types of tropical residual soils in Malaysia.

Table 2.2 Atterberg limits of some tropical residual soils in Malaysia (after Shukri et al 2004)

Parent Material	Liquid limits (%)	Plastic Index (%)	Source
Basalt	92 to 105	48 to 59	West &Dumbleton (1970)
Basalt	46 to 52	15 to 19	West &Dumbleton (1970)
Granite	42 to 107	20 to 21	West &Dumbleton (1970)
Granite	79	44	Ting et al. (1982)
Granite	69	33	Taha et al. (1999)
Schists	25 to 90	18 to 38	Komoo (1989)
Schists	59.5	28.5	Raj (1988)
Shale	64	22	Mun (1985)

2.2.3.3 Particle size distribution (PSD)

Particle size distribution is normally obtained through sieving and sedimentation tests. For sieving tests on tropical residual soils, sample preparation by crushing it into individual particles must be avoided (Fookes, 1997). It is also suggested to implement wet sieving instead of dry sieving process due to its natural characteristic to aggregate upon drying (Newill and Dowling, 1969). For example, a red clay from Sasumua, Kenya showed a clay fraction of 79% when testing at natural moisture content, but this reduced to an apparent value of 47% after oven drying (Terzaghi, 1958).

Moreover, in Figure 2.3, it can be seen that the process of oven drying reduces the apparent fine particles of the soil compared to air-dried sample (Muttaya and Huat, 1994). This is associated with the aggregation between fine particles that are bonded to form larger particles. Thus, it is suggested to use dispersion agent (sodium hexametaphosphate) in order to produce an adequate degree of separation between the individual fractions of the soil into fine silt and clay contents. The composition and particle size distribution of residual soils are also depending on the characteristics of their parent rocks. Table 2.3 presents the reported percentage of composition of particles after weathering for different rock types in Malaysia.

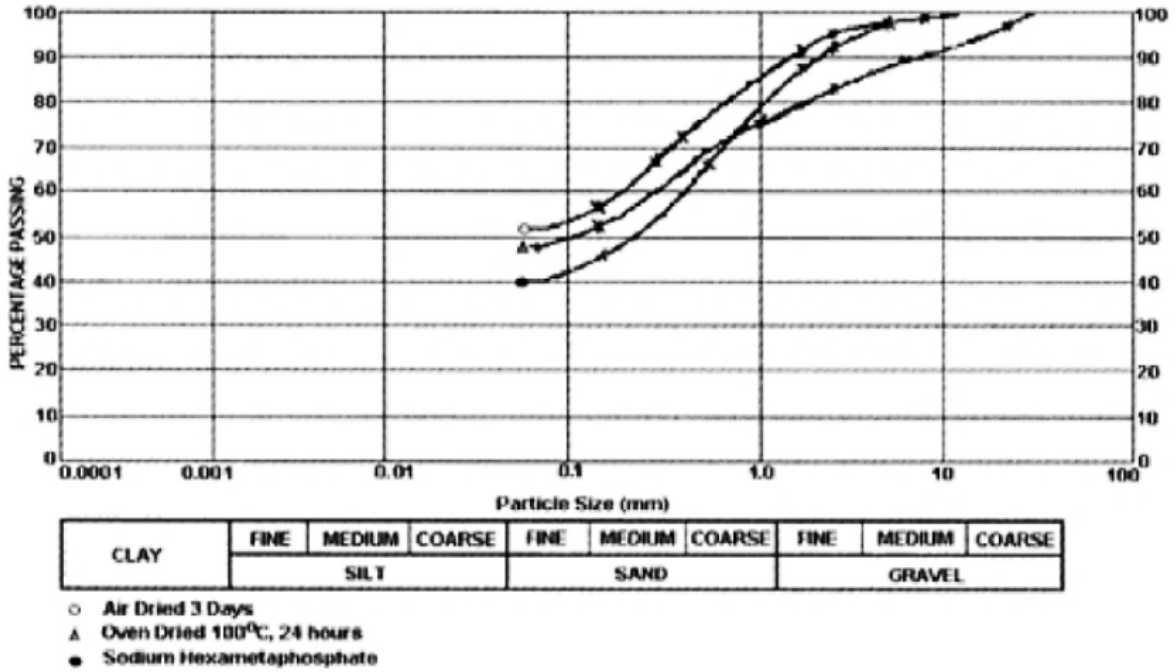

Figure 2.3 Effect of sample preparation on tropical residual soil (weathered shale) (after Muttaya and Huat, 1994)

Table 2.3 Particle size distributions of some tropical residual soils in Malaysia (after Shukri et al 2004)

Parent Material	Clay (%)	Silt (%)	Sand(%)	Source
Andesite	57	15	4	Pushparajah & Amin (1977)
Basalt	63	20	11	Pushparajah & Amin (1977)
Granite	52	4	5	Pushparajah & Amin (1977)
Granite	28	17	48	Ting et al. (1982)
Granite	42	23	35	Taha et al. (1999)
Rhyolites	53	14	9	Pushparajah & Amin (1977)
Schists	5 to 58	9 to 40	7 to 49	Nithiaraj et al. (1996)
Sandstone	27	2	27	Pushparajah & Amin (1977)
Shale	67	14	8	Pushparajah & Amin (1977)

2.2.3.4 In-situ densities and specific gravity

The densities of tropical residual soils are normally obtained from the measurements on undisturbed samples. The variation of density and specific gravity (particle density) are unusually large.

Rahardjo et al. (2004) reported that the variation in total density of residual soil is due to the weathering process, which produces a porous structure by the leaching of minerals from the soil. For the upper layers of residual soils, water and air phases occupy more space, thus, giving less density. However, the porosity of the soil decreases with depth. In west Malaysia, the addition of small proportions of cement or lime that particularly applies to the concretionary nodular laterite is also among reason that contributes to the variation to these engineering properties (Newill and Dowling, 1969).

In Table 2.4, typical values of density and specific gravity are presented based on the study done by different authors.

Table 2.4 Densities and specific gravity of some tropical residual soils in Malaysia (after Shukri et al 2004)

Parent Material	Bulk Density (mg/m^3)	Dry Density (mg/m^3)	Specific Gravity	Source
Andesite	NA	1.7	3.4	Newill & Dowling (1996)
Granite	NA	NA	2.6	Pushparajah & Amin (1977)
Granite	1.9	1.9	2.6	Ting et al. (1982)
Schists	1.4 to 2.0	NA	2.6 to 2.7	Nithiaraj et al. (1996)
Sandstone	1.3	NA	2.6	Pushparajah & Amin (1977)
Shale	NA	NA	2.6	Pushparajah & Amin (1977)
Shale	NA	2.1	3.3	Newill & Dowling (1996)

2.3 Descriptions of Research Slope in Putrajaya, Malaysia

2.3.1 General background of Putrajaya, Malaysia

Putrajaya is a planned city, located 25 km south of Kuala Lumpur and 20 km north of the Kuala Lumpur International Airport (KLIA). It serves as the federal administrative centre of Malaysia to replace the capital city of Kuala Lumpur. Planned as a garden and 'intelligent' city, the total land area of Putrajaya covers up to 4,931 hectares and lies within Malaysia's Multimedia Super Corridor. The city was also designed as a residential suburb for thousands of civil servants and estimated to have a population of around 320,000 with 64,000 housing units (Perbadanan Putrajaya, 2015).

2.3.2 Background of research slope

The selected research slope is located at Precinct 9, Putrajaya, where it is sited next to 3 blocks containing 334 units of Malaysian government quarters. The slope was designed as a cut slope before a landslide incident took place at around 4:30am, on the 22nd March 2007. There was no injury or fatality reported, however, 27 cars were totally or partially buried by the debris material. The event also caused the evacuation of about 1200 surrounding residential occupants. Photographic views of the landslide are shown in Figure 2.4 and provide graphic illustration of the landslide, the location of the site and further indication of the distance from the slope to the adjacent apartment buildings (Ahmed et al., 2011).

A private consulting engineers company, Kumpulan IKRAM Pte. Ptd. (IKRAM) was appointed by Perbadanan Putrajaya (PPj), the city Authority body, to investigate the landslide and recommend immediate action on the design for stabilisation and remedial works. As part of the investigations, IKRAM performed field geological and geotechnical investigation, field instrumentation and monitoring and laboratory testing of soil samples. Data from the field and laboratory investigation were used to perform stability analyses that led to the conclusion that the slope failure was caused by a rise in the groundwater table. It was believed that the main cause of the water table rising was due to the high intensity of rainfall that occurred at Putrajaya prior to the incident. The total amount of rainfall between 21 and 22 March was recorded to be as high as 140mm. The possibility of leakage from the water tank located at the

top of the hill was also raised; however, leakage tests performed by Malaysia Water Resources department showed no leaks were detected neither from the reservoir nor the inlet and outlet pipes. For the remedial works, forty deep horizontal drains were installed into the intact parts of the slope on each side of the landslide immediately after the failure. The drains were intended to relieve the inherent water pressure within the slope. For the collapsed section, a reconstruction using a crib wall was carried out at the toe of the slope. Further details on the application of the horizontal drains can be seen in (Ahmed et al., 2011).

Figure 2.4 Photographic views of the slope failure

(after IKRAM 2007).

2.3.3 Topography and geological conditions

IKRAM (2007) reported that the landslide was located on the western face of a ridge that has its crest close to the upper edge of the slide scarp. The size of the landslide was observed to be 40m wide, 35m in length and 15m in height from the toe of the ridge. The ridge was described to be a combination of a cut slope with gradient of 27° (1V: 2H) and natural slope with less than 27° gradient that continues from the cut slope top edge up to a road that leads to a 36 million-litre water tank at the hilltop. The water tank is partially buried on a part of the hill that had been cut to prepare a flat site for it. The distance of the tank to the edge of the ridge where the slide occurred was about 25m. Further illustrations can be seen in the Digital Terrain Model as shown in Figure 2.5.

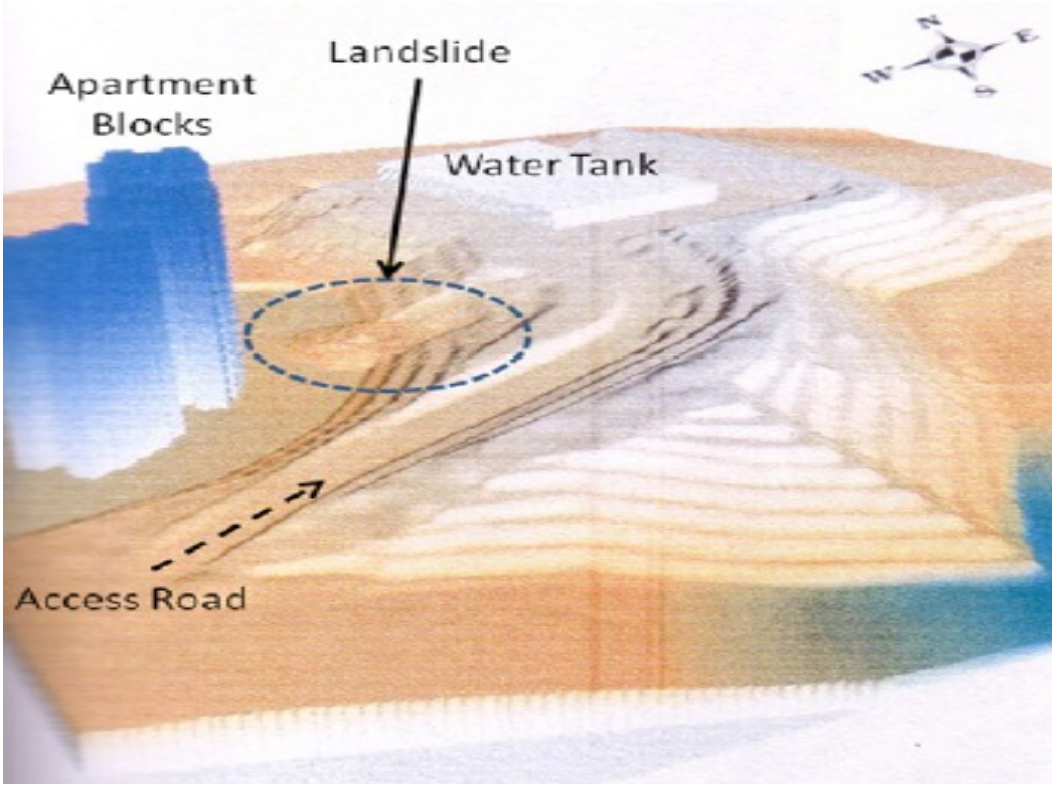

Figure 2.5 Digital terrain model of the slope area

(after Ahmed et. al. 2011).

The geological profile of the slope is reported to be underlain by graphitic Quartz-mica Schist from Kajang Formation (Figure 2.6). From the inspection made on site by IKRAM, the outcrops that could be seen along the cut slope surface had seemed to experience intense weathering processes with weathering grade ranges from Grade III to VI. Nevertheless, Grade II material could still be noted at certain areas.

The outcrops (Grade II to IV) were dark grey to black in colour with clear foliation planes. These foliation planes were thin white quartz lamination. Whilst, for Grade V-VI outcrops, the colour was reddish brown to brownish red due to existence of laterite, which is rich in ferrous oxides. Yellowish orange very soft clayey soil was found in the failed area (Figure 2.7)

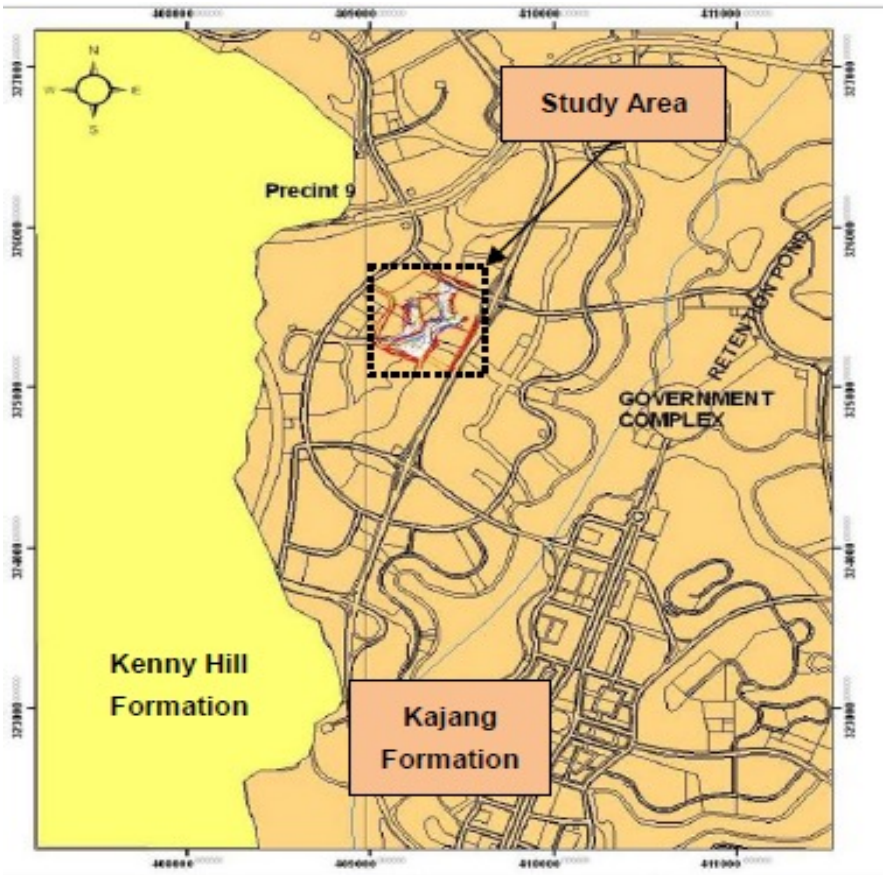

Figure 2.6 Geological map of the study area

(after Ahmed et. al. 2011).

Figure 2.7 Soft soil observed in the mass of collapsed material

(after IKRAM 2007)

2.3.4 Subsoil Investigations and instrumentations

Subsurface investigations and instrumentation programmes were undertaken consisting of 17 boreholes (BH1 to BH17). Seven standpipes (SP1 to SP7) and 5 vertical inclinometers (IC1 to IC5) were installed and implemented by IKRAM in order to further understand the subsoil profile of the entire section of the slope (Figure 2.8). The programme that was commenced in March and completed in April 2007 can be divided into two packages; (i) before the installation of horizontal drains and (ii) after the installation.

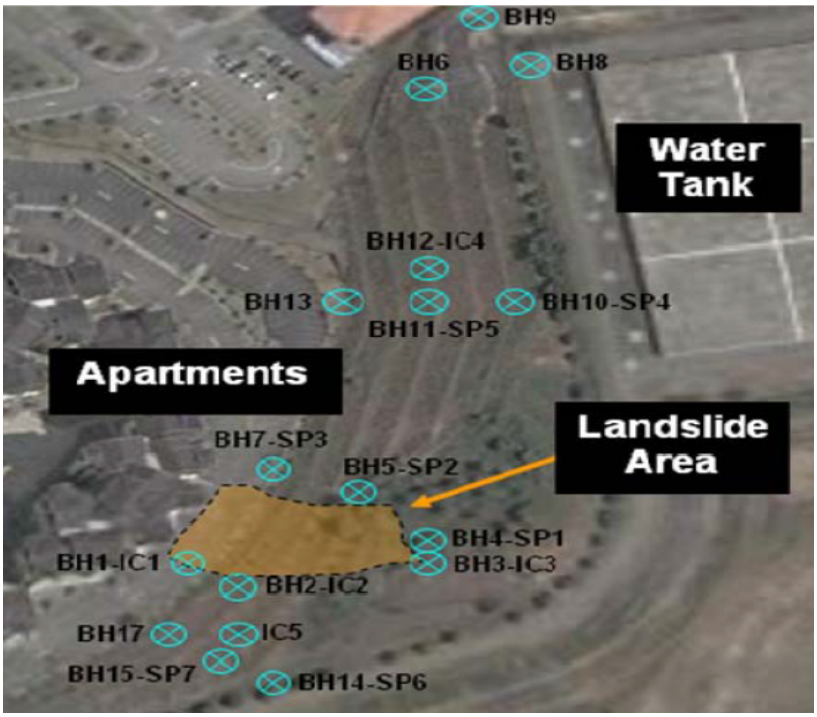

Figure 2.8 Location of boreholes and instrumentation.

(after Ahmed et. al. 2011)

These boreholes were executed using a rotary drilling technique with foam as flushing medium and standard penetration tests (SPT) were carried out generally at 1.5m intervals. When rock was encountered, a diamond- studded bit was used for rock coring.

A total of seven standpipe piezometers were installed to obtain the groundwater level readings, with 3 nos. installed before the horizontal drains installation and 4 nos. after the installation. The groundwater table recorded for SP1 and SP2 were approximately 5m and 1.5m, from the ground surface, and indicated

as zero for SP3. These readings were manually taken once to three times a day using a water level indicator, before the implementation of remedial works.

Vertical inclinometers were installed to detect zones of movement and to determine whether the slope was responding to the immediate remedial measures. However, very little movements were detected from the readings.

2.3.5 Subsoil profile and hydrological conditions

Based on the soil investigation data obtained by IKRAM, the details of the subsurface profile of the slope can be categorised as follows;

i. ***Residual soil layer (Grade VI)***

This top layer consists of silt to sandy clay material that is reddish brown, to brownish grey in colour. The colour varies slightly with weathering grade and depth. The layer thickness is approximately 1m to 9m from ground level depending on subsurface topography.

ii. ***Highly to completely weathered Schists of Kajang formation (Grade IV to V)***

The layer consists of very hard silt material with its colour varying from yellow to grey depending on weathering grade and depth. The layer thickness ranges between 1m to 10m.

iii. ***Fresh to moderately weathered Schists of Kajang formation (Grade I to III)***

The depth of the bedrock was reported to be at 1m (toe) to 11m (crest) from ground level. The colour is consistent with the soil above, which is dark grey with white stripes. These white stripes are believed to have formed due to penetration of quartz mineral to form thin quartz veins.

The groundwater level was taken from all 3 nos. of standpipe piezometers, namely SP1, SP2 and SP3, which were installed before the implementation of remedial works. From the data measurements, it can be seen that the groundwater level within the failed slope was high, ranging from ground surface (toe) to 5m below ground level (crest). Figure 2.9 presents the simplified geometry of the slope together with the generalised subsoil profile and hydrological condition of the failed slope.

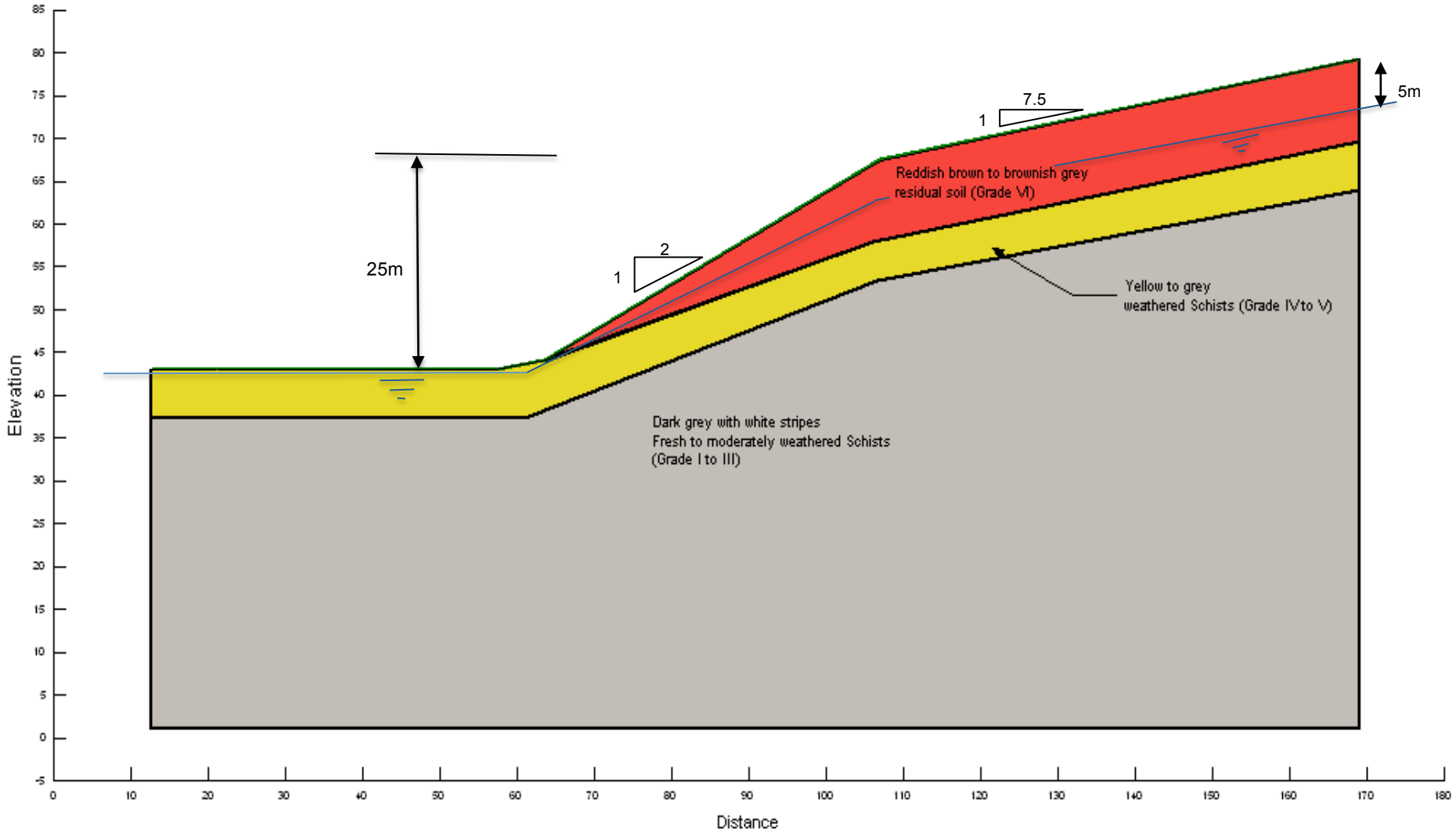

Figure 2.9 The simplified geometry of the failed slope together with the generalised subsoil profile and hydrological condition.

2.4 Sampling of Undisturbed Tropical Residual Soils samples

Research collaboration was established between Durham University, IKRAM and PPj for the acquiring of undisturbed soil samples from the failed slope in Putrajaya. The purpose of the collaboration was for knowledge sharing between organisations with the implementation of advance investigations using Durham University's state-of-the-art unsaturated soil testing facilities. The undisturbed soil samples obtained from the site were used for the determination of unsaturated hydrological and mechanical properties of the residual soils. Then, the results obtained from these soil testing were also utilised as input parameters for the advance numerical modelling works, described in Chapter 5.

2.4.1 Location of soil sampling works

Soil sampling works were successfully carried out during the fourth week of May 2013. The process was completed in 2 days and was conducted by IKRAM with standing supervision and advice provided by Durham University. PPj was the funder for this ground investigation activity.

Several discussions had been made between Durham University and IKRAM in order to implement a suitable approach for ground investigation works. These comprehensive discussions were organised primarily to ensure that the retrieved undisturbed soil samples were representative of the area of concern and also not subjected to any irreversible damage either during the sampling process or transportation (e.g. volumetric strains). The non-homogenous and anisotropic conditions that are well known to occur for tropical residual soils were also taken into account before any suggestion was made.

It was decided that the borehole location for the soil sampling works would be located at the top of the slope, approximately 10m away from BH4 (Figure 2.8). This decision was made based on the logging profile (Figure 2.9) that is representative of the original subsoil stratigraphy at the failed area. The site observation made by IKRAM also indicated that the slide took place mainly through the top layer (residual soil layer). This provided better reason for this borehole location. The accessibility of the drilling rig and equipment used on site were also amongst factors looked at prior to the finalisation of this soil sampling works.

2.4.2 Configuration and equipment of soil sampling technique

The sampling works were carried out using foam flush rotary drilling technique. The decision to use foam as the drilling fluid (or flushing fluid) was made corresponding to the criteria outlined in previous sections to avoid disturbance to the sample, especially on changing the water content of the soils. The flushing fluid is also used to cool the mechanical parts during drilling and at the same time to bring up the 'cuttings' of ground.

The rotary drilling procedures produce rotary action that is combined with downward force to grind away the material, which would result in less disruption to the samples than percussive methods. Full configuration of the technique implemented on site is shown in Figure 2.10. There were five main components used in order to carry out the soil sampling procedures. The flushing fluid (foam) was produced by foam liquid that was pumped into one of the 'Y' connector pipe inlet and injected with air pressure supplied by an air compressor. The amount of foam produced was controlled at a constant rate and volume.

Detailed descriptions of rotary drilling can be referred to Heinz (1989). The layout of the drilling rig is presented in Figure 2.11. The major elements required for rotary drilling rig are described as the following:

i. A drilling machine or 'rotary rig', which delivers torque and thrust.
ii. Flushes pump, which pumps flushing fluid down the hole and to bring up the 'cuttings' of soil to the ground surface as drilling continues.
iii. A 'string' of hollow drill rods, which transmit the torque and thrust from produced by the drilling rig, and also flushing fluid from the flush pump to the bottom of the drilled hole.
iv. A drilling tool (core barrel), which grinds away the hard material (e.g. rock), and also for sample retrieval.

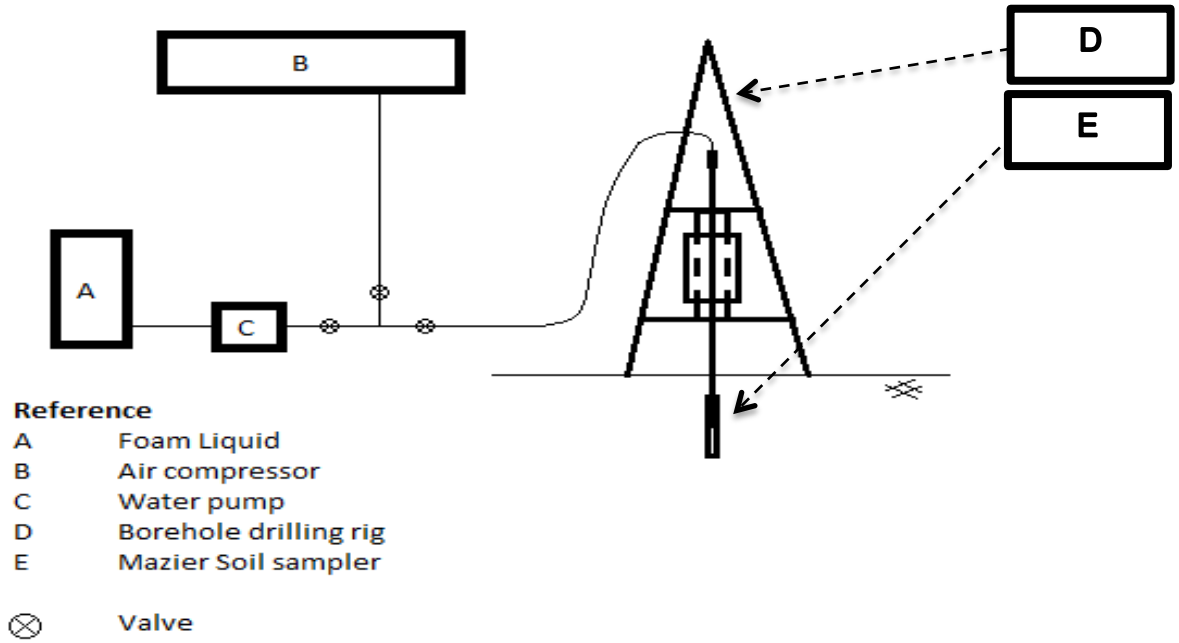

Figure 2.10 Configuration of rotary drilling technique.

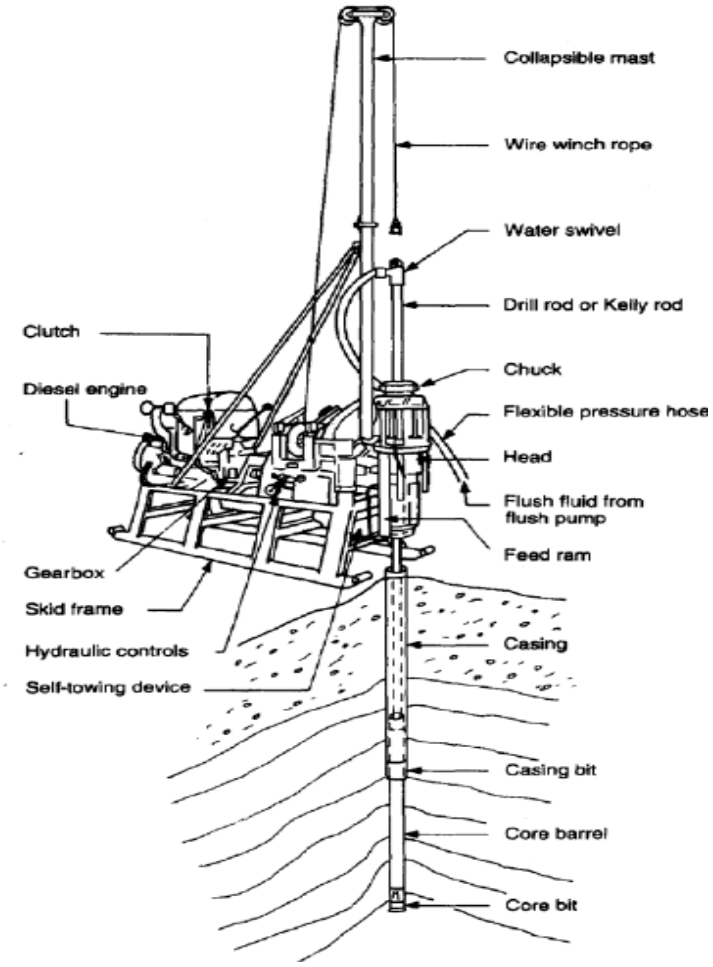

Figure 2.11 Layout of rotary core drill. (after Heinz 1989)

Triple tube Mazier sampling method was adopted to obtain high quality undisturbed samples. The advantage of using a triple tube sampler is due to its secure procedure of sample removal (as it is taken from the ground), assuring the 'in-situ condition' of the soil (Huat et al., 2004). The apparatus consists of a rotary triple tube sampler with an outer and an inner barrel, a PVC tube and a sampler head, a cutting shoe and a drill bit. Typical details of the rotary triple tube sampler (Japanese Geotechnical Society, 1998) are presented in Figure 2.12.

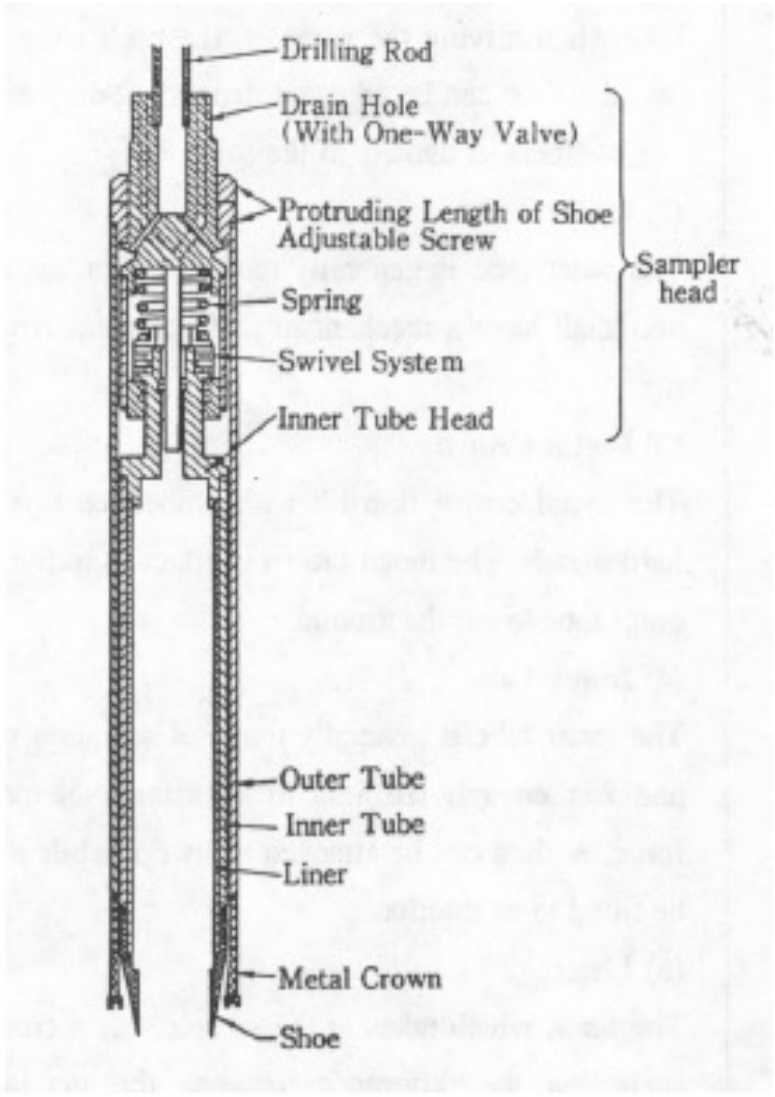

Figure 2.12 Layout of rotary core drill. (after Japanese Geotechnical Society, 1998)

2.4.3 Soil sampling procedures

The implementation of the sampling process was initially carried out by connecting the hollow drilling rod from the drilling rig to the upper part of the sampler head. Then, a 1000mm by 75mm diameter sized PVC tube (liner) was placed inside the inner tube that was separately connected to the outer tube, both held by sampler head (Figure 2.12). After that, a drill bit was firmly attached to the bottom part of the sampler (outer tube) before the whole combined part was pulled up using the wire winch rope close to the drilling rig.

Next, the triple tube sampler was lowered into the clean-flushed borehole, which was supported by seamless steel casings, in 1m depths. These steel casings were used to prevent the collapse of the borehole wall. Once the drilling rod was securely tightened to the drilling head, the flush fluid (foam) was pumped through the drill rods at a controlled rate and volume. Following to the complete of these procedures, the sample drilling process was started.

During sampling, the inner tube (with PVC tube) remained stationary as the rotated downward thrust of the drilling rod was transmitted only to the outer tube. The movement was controlled by the swivel system that is connected to a spring inside the sampler head. However, in order to secure a high recovery of residual soil sample, the drilling process was executed slowly at a controlled speed and pressure. After the required penetration length was met (1m), the triple tube sampler was carefully pulled out from the borehole for the retrieval of the soil sample contained within the PVC tube. Lastly, this sample-containing tube was immediately sealed with wax and labelled for further reference.

Similar procedures were implemented for each 1-metre interval after flushing out of the “cuttings” of ground of the previously drilled depth. The termination of the sampling process, however, was made when the drilling speed was observed to be very slow, indicating penetration into a hard soil rock layer. This termination criterion was suggested due to the primary objective for the research works that focussed only on the overburden soil. Figure 2.13 presents the photographic views of the equipment and the sampling works carried out on site.


Air compressor

(a)

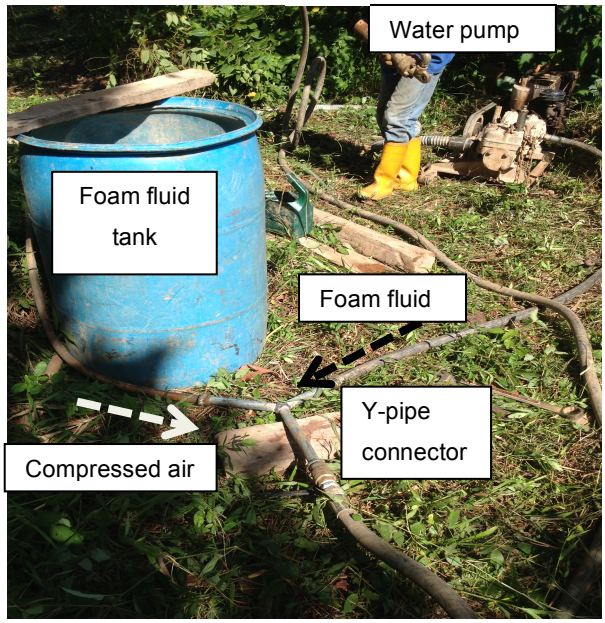
Water pump
Foam fluid tank
Foam fluid
Y-pipe connector
Compressed air

(b)

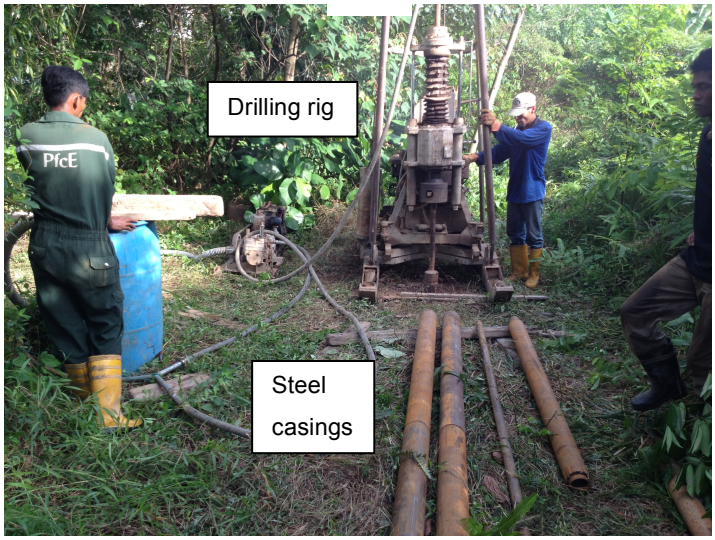
Drilling rig
Steel casings

(c)

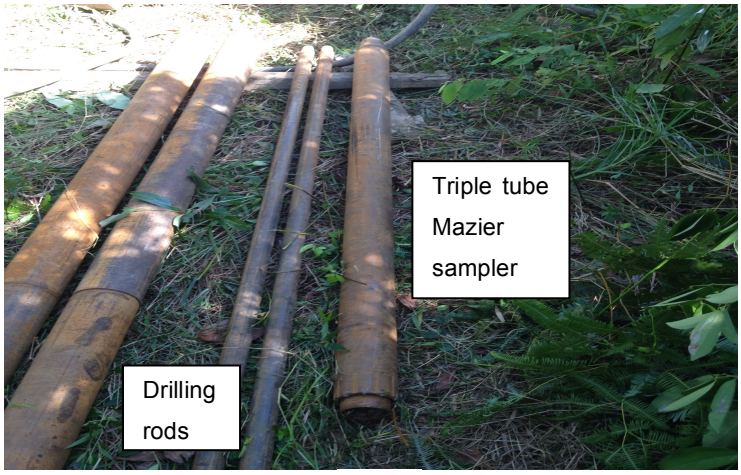
Triple tube Mazier sampler
Drilling rods

(d)


The retrieval of residual soil sample contained PVC tube.

(e)


PVC tube being placed upright position immediately.

(f)

(g)

(h)

Figure 2.13 Photographic views of the equipment required and sampling works carried out on site.

2.4.4 Tropical residual soils samples

A total number of five PVC tubes were successfully obtained from the soil sampling process. These tubes were retrieved from two boreholes that were located at the top of the slope (BH1 and BH2), close to the western face of the ridge where the slide took place (slope details in Section 2.3.3). The distance between these two boreholes was approximately 0.5m. Initially, four tubes were obtained from BH1 to represent the soil profile of 1m to 5m deep. However, due to the requirement for additional samples for the unsaturated laboratory tests, an additional tube was taken from BH2 for depth of 1m to 2m deep. Each tube was labelled as MZ1, MZ2, MZ3, MZ4 and MZ1a, based on the starting depth when it was retrieved (e.g. MZ1 is the tube sample for depth 1m to 2m depth). MZ1a is the additional tube sample from BH2.

All residual soil sample tubes, with total weight of approximately 40 kg, were then transported to Durham University by airfreight. The shipping preparations (such as additional sealing, bubble wrapping etc.) were done to prevent samples from being damaged during the shipping process. UK custom declaration documents were prepared prior to the shipment in order to ensure a smooth delivery of the samples.

Figure 2.14 presents the photographic views of samples contained in tubes MZ1, MZ2, MZ3, MZ4 and MZ1a. From the figures, it can be seen that natural fissures and tree roots are clearly visible in each sample, especially samples from the upper depth. None of the samples seem to have experienced disturbance due to transportation. Further details for each sample are summarised in Table 2.5.

Table 2.5 Typical details of the residual soil samples contained in each sampler tubes.

Mazier	Depth (m)		Sample length	Recovery ratio	Remarks
	From	To	mm	%	
MZ1	1.0	2.0	890	89	reddish brownto brownish grey in colour
MZ2	2.0	3.0	910	91	reddish brownto brownish grey in colour
MZ3	3.0	4.0	530	53	yellow, reddish brownto brownish grey in colour
MZ4	4.0	5.0	510	51	dark grey with white stripes
MZ1a	1.0	2.0	960	96	reddish brownto brownish grey in colour

(a) MZ1

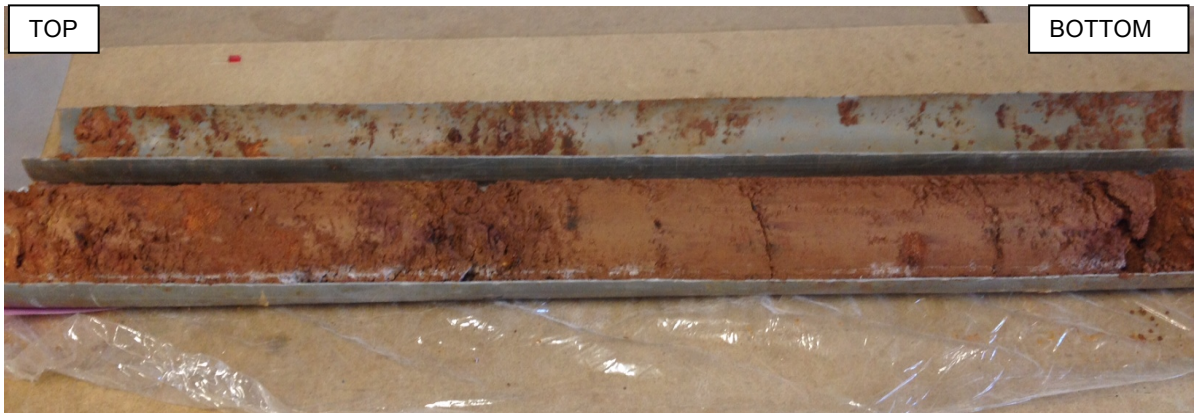

(b) MZ2

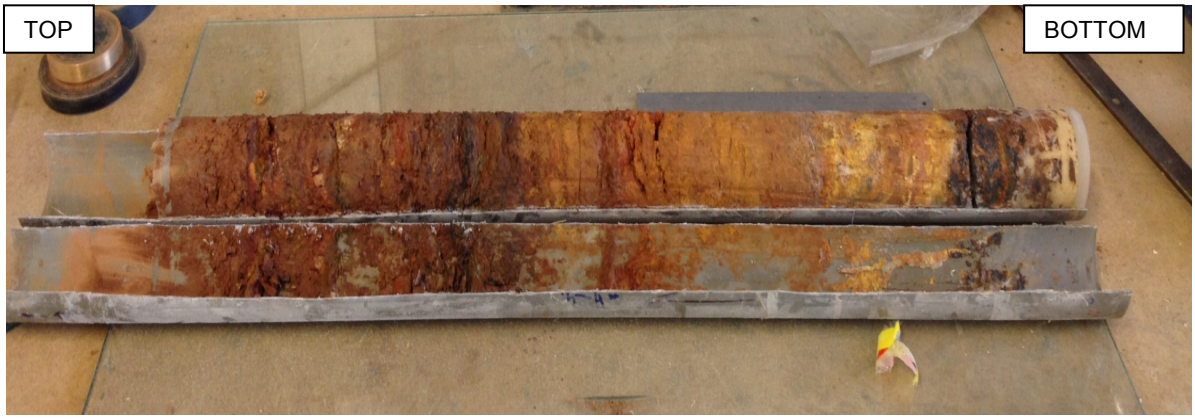

(c) MZ3

(d) MZ4

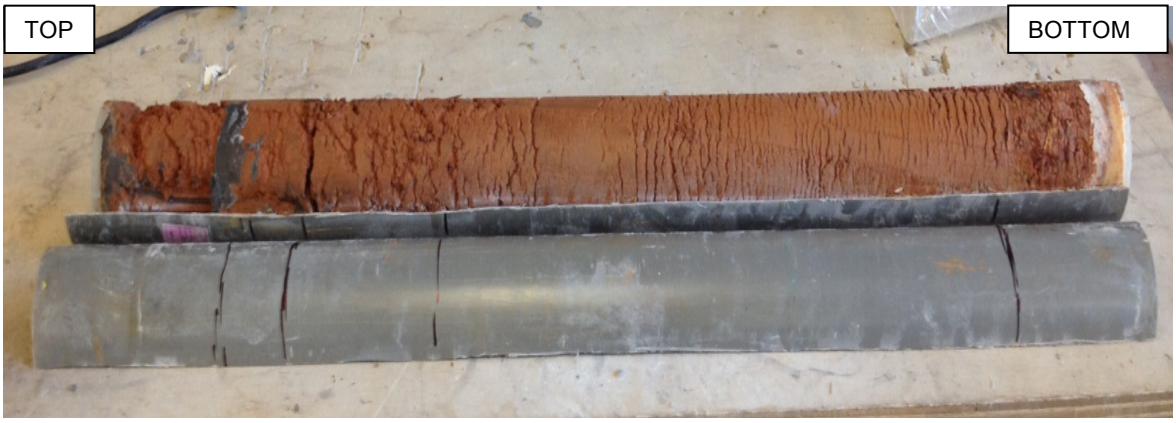

(e) MZ1a

Figure 2.14 Photographic views of samples contained in tubes.

From observation, samples from MZ1, MZ2 and MZ1a were similar in physical characteristics. Each samples from these tubes exhibited similarity in colour that is reddish brown to brownish grey. However, for residual soil samples in MZ3, a variation in colour can be seen clearly which can be associated with the variation in degree of weathering for residual soil. The variation starts from brown to yellowish in colour. In addition, there was a recovery ratio less than for the upper sample tubes (around 50% rather than 90% as reported in Table 2.5). The sample was also observed to be stiffer than the samples from the upper tubes.

Likewise, similar variation can be seen on sample obtained in MZ4 that shows the colour of dark grey with white stripes. This layer is part of the underlain bedrock due to its structural rigidity.

2.5 Tropical Residual Soils Index and Classification tests

A series of index and classification tests were executed in order to further characterise and classify the types of samples contained in each tube. The results from each tube were compared to obtain the variation in each property against depth, which will be explained at the final part of this section. The respective results of each test, however, are presented in the following sections.

2.5.1 Natural water content

The determination of natural water content of residual soil sample in each tube was made from the respective soil specimens prepared for both mechanical and hydrological tests. These soil specimens were taken from different parts of the tube covering from top to the bottom. The values are presented in Table 2.6 for each tube.

Table 2.6 Natural water content of the residual soil samples contained in each tubes.

Mazier	Depth (m)		Test type	Specimen label	Natural water content
	From	To			%
MZ1	1.0	2.0	Mech.	S1	31
				S2	36
				S3	29
			Hydro.	S1	34
MZ2	2.0	3.0	Mech.	US1	26
				US2	27
				US3	27
			Hydro.	S1	27
				S2	29
				S3	29
MZ3	3.0	4.0	Mech.	S1	24
			Hydro.	S1	24
MZ4	4.0	5.0	Mech.	S2	27
				S3	14
MZ1a	1.0	2.0	Mech.	US4	30
				US5	29

Referring to the results, it is apparent that the overall natural water content ranges from 14% up to 36%. These variations are believed to be due to the effects of climatic controls as well as the distinction in weathering grade in each tube.

2.5.2 Atterberg limits

It has been recommended that the process to determine Atterberg limits for residual soil should be carried out as quickly as possible and with an appropriate method of drying (Blight, 1997). This recommendation is due to the sensitiveness of residual soil to drying, which could cause the alteration of physical and chemical properties of the soils. Thus, the determination of these parameters for each tube was made from the soil trimmings obtained from the soil specimen preparation for both saturated and unsaturated tests. These soil trimmings were not oven-dried, thus, gave less alteration to the original characteristics. The results are presented in Table 2.7.

Table 2.7 Atterberg limits parameters of the residual soil samples contained in each sampler tubes.

Mazier	Depth (m)		Atterberg limits			Description
	From	To	PL	LL	PI	
			%	%	%	
MZ1	1.0	2.0	38	85	47	Very high plasticity CLAY
MZ2	2.0	3.0	39	65	26	High plasticity SILT
MZ3	3.0	4.0	30	38	8	Intermediate plasticity SILT
MZ4	4.0	5.0	29	40	11	Intermediate plasticity SILT
MZ1a	1.0	2.0	35	86	51	Very high plasticity CLAY

The general description for fine soils presented in the table was made based on plasticity chart in BS 5930: 1999. From the table, it shows that sample MZ1 and MZ1a are similar and classified as very high plasticity clay. The plasticity indexes for each tube seem to reduce with the greater depth (51% down to 8%). Similar to the result from previous tests, the cause to this variation is attributable to the weathering grade resulted in the decomposition of the parent rock material (differences in clay-based content).

2.5.3 Particle size distribution (PSD)

Several suggestions have been put forward by researchers for the determination of particle size distributions of tropical residual soils (Tan, 2004). These suggestions that have been described in earlier sections are mainly linked to the sensitiveness of residual soils towards the drying process that could result in aggregation between fine particles to forming larger particles. Without adhering to any of these suggestions, false assessments could be made on the PSD of these residual soil samples.

An approximate 1kg mass of residual soil sample from each tube was initially used for PSD tests. To ensure that discrete particles were separated, a wet sieving procedure was implemented. The soil sample was passed through sieves from 2.80mm down to the size of 0.063 mm, supported by sprayed water, to break the particles down and separates the fine silts and clay contents. However, it was discovered that the sample continued to breakdown and subsequently passing the 0.063mm sieve as higher water pressure was applied to the material. This caused difficulties in defining the actual amount of particles that was larger than 0.063mm. Therefore, a different approach was investigated for the particle size analysis of the tropical residual soil samples.

Consequently, it was decided that the determination of the PSD for samples in each tube would be done by using a commercial laser diffraction particle size analyser, as shown in Figure 2.15. This particle size analyser (model LS13320), available in the Department of Geography, Durham University, is a laser diffraction analyser system that utilizes polarization intensity differential scattering (PIDS) technology to produce fast and reliable particle size analysis results for dry, aqueous and non-aqueous samples. The LS13320 analyser can measure light scattering measurement across the widest dynamic range, from 0.017μm (clay) to 2000 μm (sand), in a single scan with no extrapolation.

The study of the comparison between sedimentation analysis and laser diffraction for the determination of particle size distribution can be seen from the papers prepared by Gee and Or (2002) and Eshel et al. (2003). The comparison was made based on the results gathered from 50 soil samples collected at a 70 acre experimental field of Button and Turkovitch Farms, United States. The results

showed that high correlation (not much difference in PSD) between both methods were observed, with laser diffraction method giving greater precision. The laser diffraction analysis made fast calculations that were easy to recreate after a one-time analysis, did not need large sample sizes, and produced large amounts of data. It is also indicated that the analysis process using this modern technique is relatively quick compared to the traditional sedimentation tests. Therefore, due to the sensitivity of tropical residual soils, the use of this equipment is appropriate.

Figure 2.15 The commercial laser diffraction particle size analyser; model LS13320.

To carry out the procedure, two sets of 0.45g of trimmings (in natural water content state) from each tube were used for the particle size analysis. These samples were initially pre-treated by mixing, with 20ml of distilled water and 2mL dispersion agent (sodium hexametaphosphate), following BS 1377: 1990, to produce an adequate degree of separation between the individual fractions of the soil into fine silt and clay contents. The assessments of the shaken and non-shaken effects on the pre-treated samples were also executed. This was done by having one of collected sample placed in an end-over-end shaker and shaken for a period up to 2 hours. Figure 2.16a, 2.16b; 2.16c, 2.16d and 2.16e present the plots for PSD for each sample (for both shaken and non-shaken conditions) from each tube, respectively.

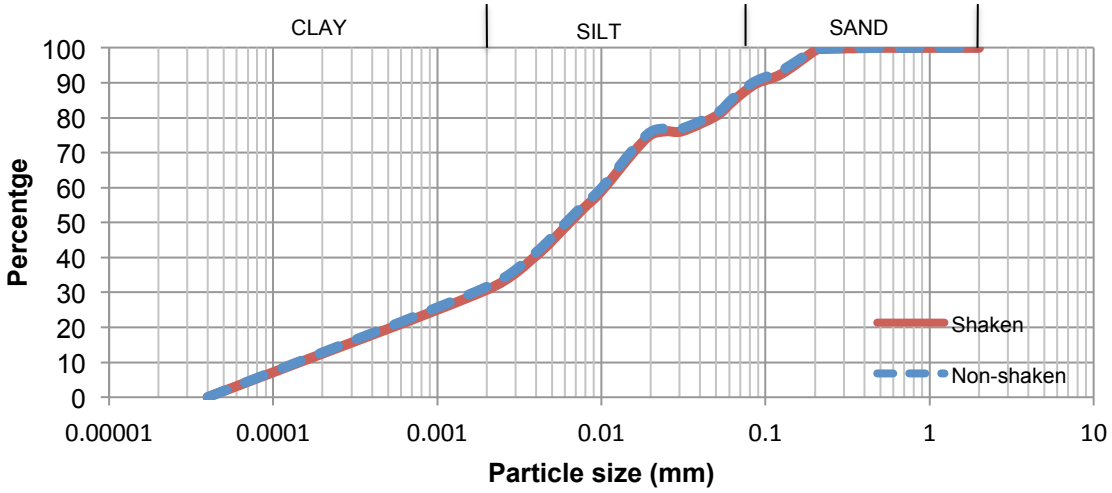

(a) MZ1

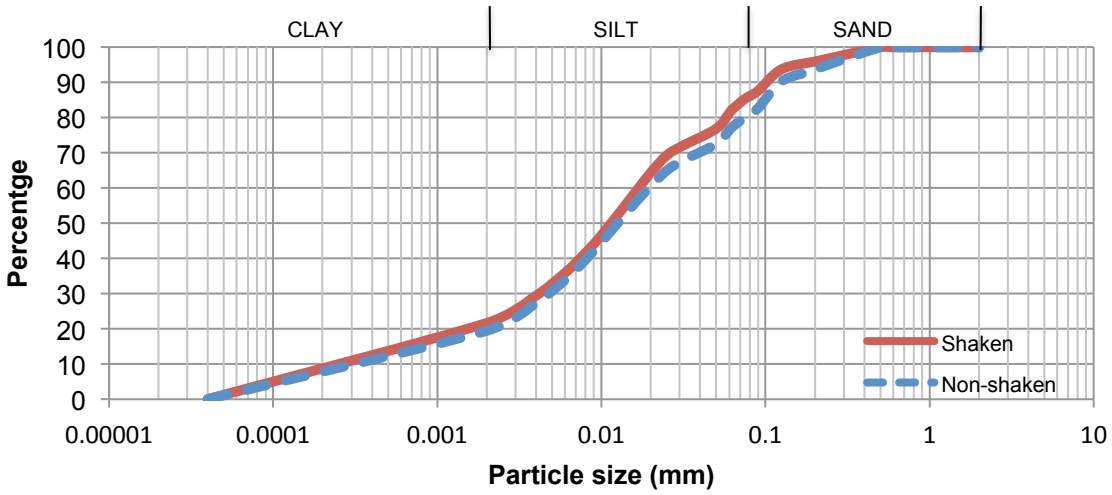

(b) MZ2

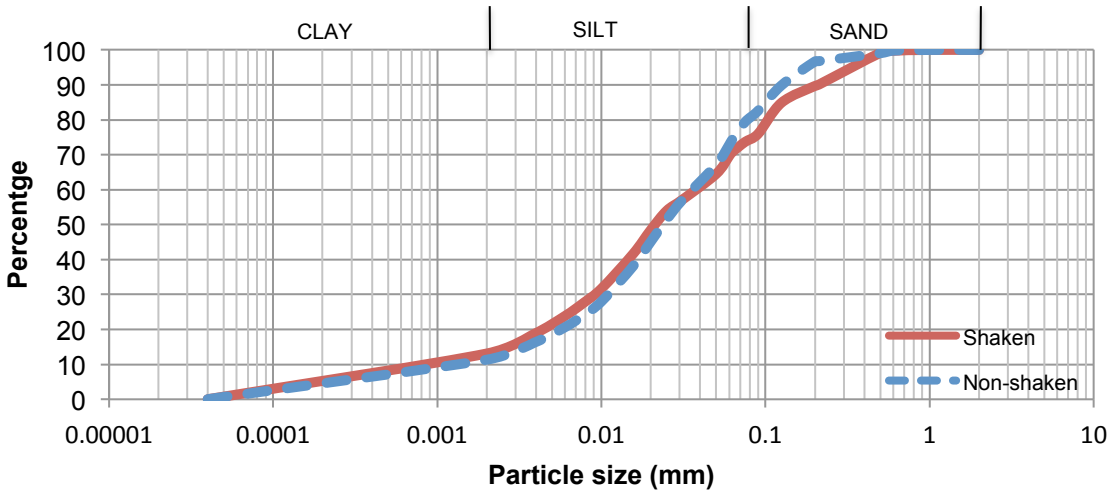

(c) MZ3

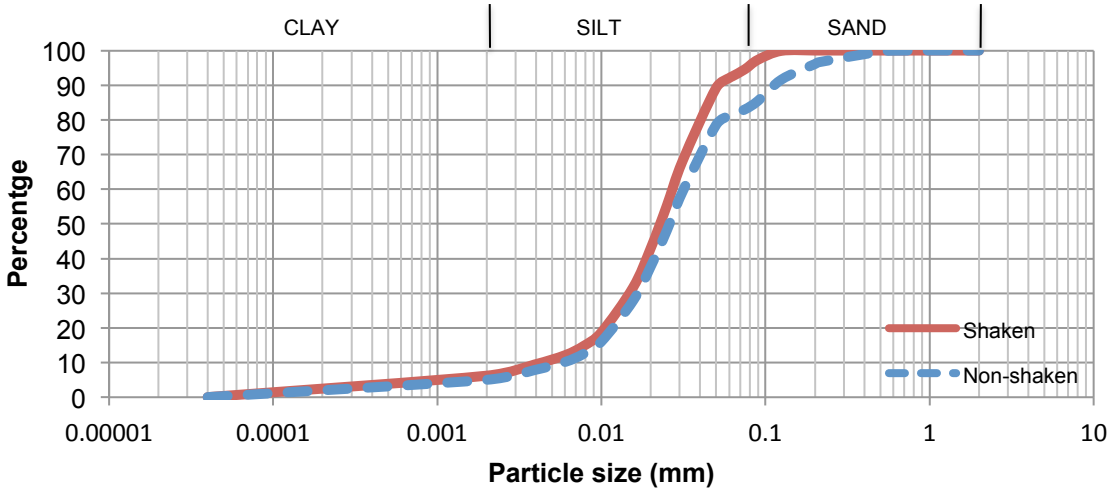

(d) MZ4

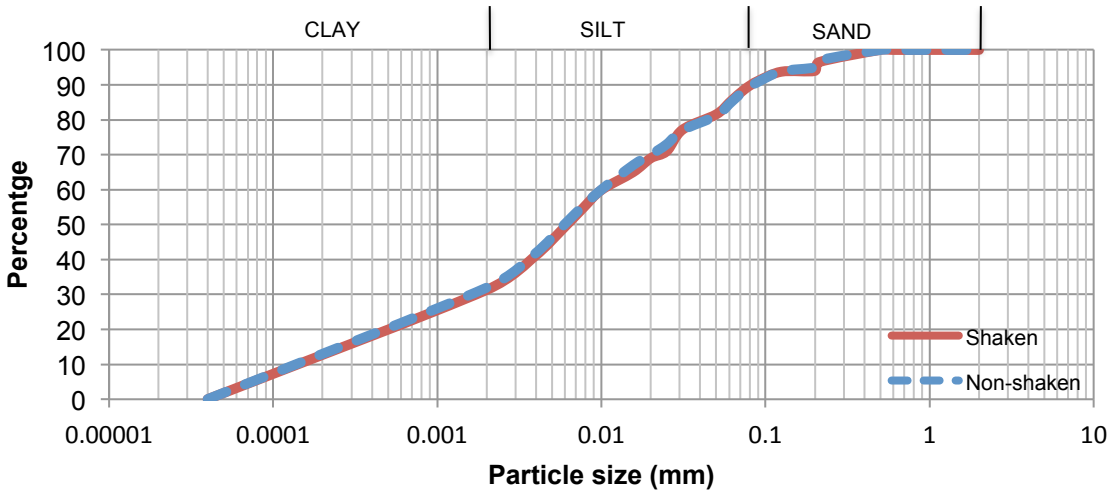

(e) MZ1a

Figure 2.16 Particle size distributions for each sample for both shaken and non-shaken conditions from each tube.

From the plots, it can be seen that every sample shows an increase in percentage for the smaller sized particles after shaking procedure. However, the variation appears to be very minimal for samples from MZ1 and MZ1a. This suggests that the gradation for samples from these tubes was very much well distributed under both conditions. On the other hand, for samples from MZ2, MZ3 and MZ4, the variations in percentage are more significant with the difference in percentage up to 10%. Interestingly, this condition can be correlated to the degree of cementation between particles that is based on the differences in weathering grade. For samples with lower degree of weathering, the effects from shaking procedures are more substantial, resulting in a higher degree of separation between the individual

fractions. The comparison of PSD for the shaken samples between each tube is also presented in Figure 2.17. On average, each sample presents a well-graded particle distribution except for samples from MZ4, where a narrow range of particle sizes can be seen (poorly graded). Similarly, these differences are attributable to the degree of weathering effects of each sample. A greater degree of weathering results in a larger clay fraction. Table 2.8 summarises the percentage of PSD of tropical residual soil samples in each tube.

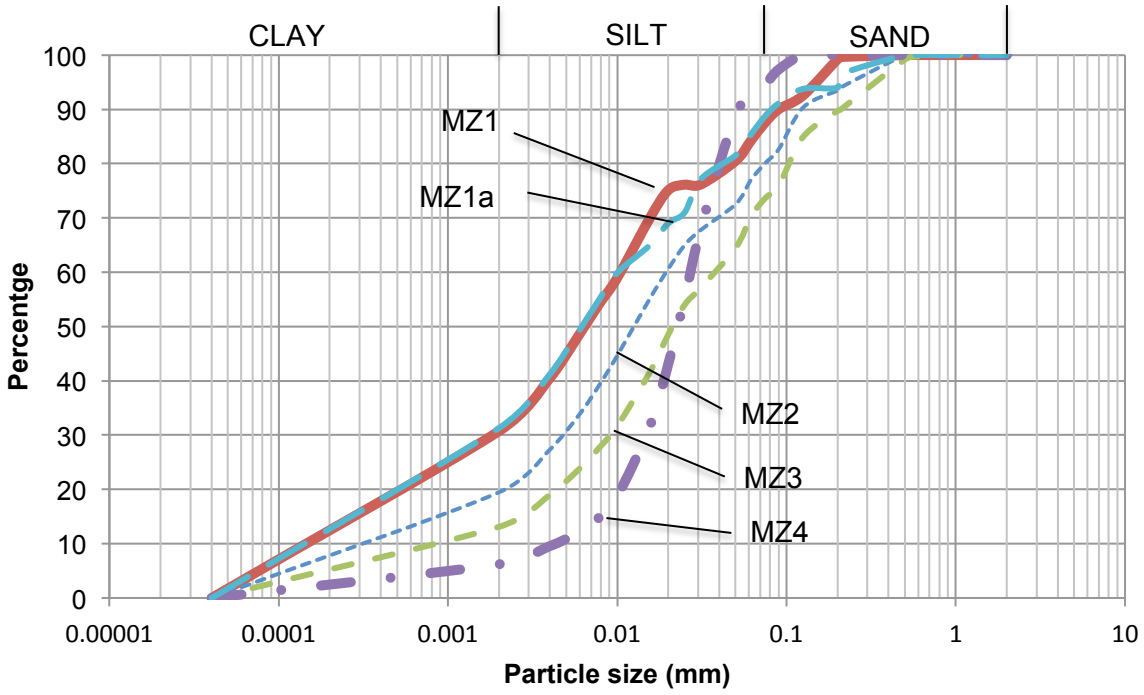

Figure 2.17 Comparison of the particle size distributions (shaken conditions) from each tube.

Table 2.8 Details of the particle size distributions of residual soil samples contained in each sampler tubes.

Mazier	Depth (m)		Particle Size Distributions		
	From	To	Clay	Silts	Sands
			%	%	%
MZ1	1.0	2.0	32	52	16
MZ2	2.0	3.0	19	57	24
MZ3	3.0	4.0	11	62	27
MZ4	4.0	5.0	5	76	19
MZ1a	1.0	2.0	31	53	16

2.5.4 In situ densities and specific gravity

The in situ density of the tropical residual soils in each tube was obtained by weighing and measuring the volume of the undisturbed specimens prepared for the hydrological and mechanical tests. The details of the results are presented in Table 2.9. In general, the calculated density values for each layer increases with depth. However, the results for samples from MZ2 are higher as compared to the rest of the samples from different tubes. Furthermore, the values for specific gravity are also presented in the Table 2.10, which ranged from 2.69 to 2.86. The determination of these parameters was made from the soil trimmings taken from different parts at top, mid and bottom of the tubes.

Table 2.9 Details of the total density, dry density and specific gravity of residual soil samples contained in each sampler tubes.

Mazier	Depth (m)		Test type	Specimen label	Density	
	From	To			Bulk ρ Mg/cm^3	Dry ρ_{dry} Mg/cm^3
MZ1	1.0	2.0	Mech.	S1	1.8	1.37
				S2	1.79	1.31
				S3	1.75	1.36
			Hydro.	S1	1.76	1.36
MZ2	2.0	3.0	Mech.	US1	1.99	1.59
				US2	1.95	1.55
				US3	1.94	1.54
			Hydro.	S1	1.96	1.57
				S2	1.88	1.47
				S3	1.94	1.53
MZ3	3.0	4.0	Mech.	S1	1.77	1.42
			Hydro.	S1	1.82	1.53
MZ4	4.0	5.0	Mech.	S2	1.84	1.45
				S3	2.01	1.75
MZ1a	1.0	2.0	Mech.	US4	1.81	1.41
				US5	1.84	1.43

Table 2.10 Details of the total density, dry density and specific gravity of residual soil samples contained in each sampler tubes.

Mazier	Depth (m)		Sample loc. in tube	Specific Gravity
	From	To		G_s
MZ1	1.0	2.0	top	2.86
			mid	2.86
			bottom	2.85
MZ2	2.0	3.0	top	2.77
			mid	2.79
			bottom	2.84
MZ3	3.0	4.0	top	2.85
			mid	2.80
			bottom	2.69
MZ4	4.0	5.0	top	2.85
			mid	2.80
			bottom	2.82
MZ1a	1.0	2.0	top	2.85
			mid	2.84
			bottom	2.87

2.5.5 The variation of index properties with depth

Rahardjo et al. (2004) has reported that the variation in index properties of residual soil reflects the variation in the degree of weathering. For higher weathering grades, the considerable leaching of minerals from the soil results in a porous structure that causes variation to these soil properties. Moreover, the heterogeneity of residual soil is also one of the factor that may influence the accuracy of the results (Singh and Huat, 2004).

To better illustrate this variability, the results of index properties from each tube against depth were plotted and are shown in Figure 2.18. These plots consist of natural water content, Atterberg limits, specific gravity, densities and particle size distribution. They show evidence of variation with depth that can be related to the differences on the mineralogy of the soil and degree of weathering (Tuncer and Lohnes, 1977).

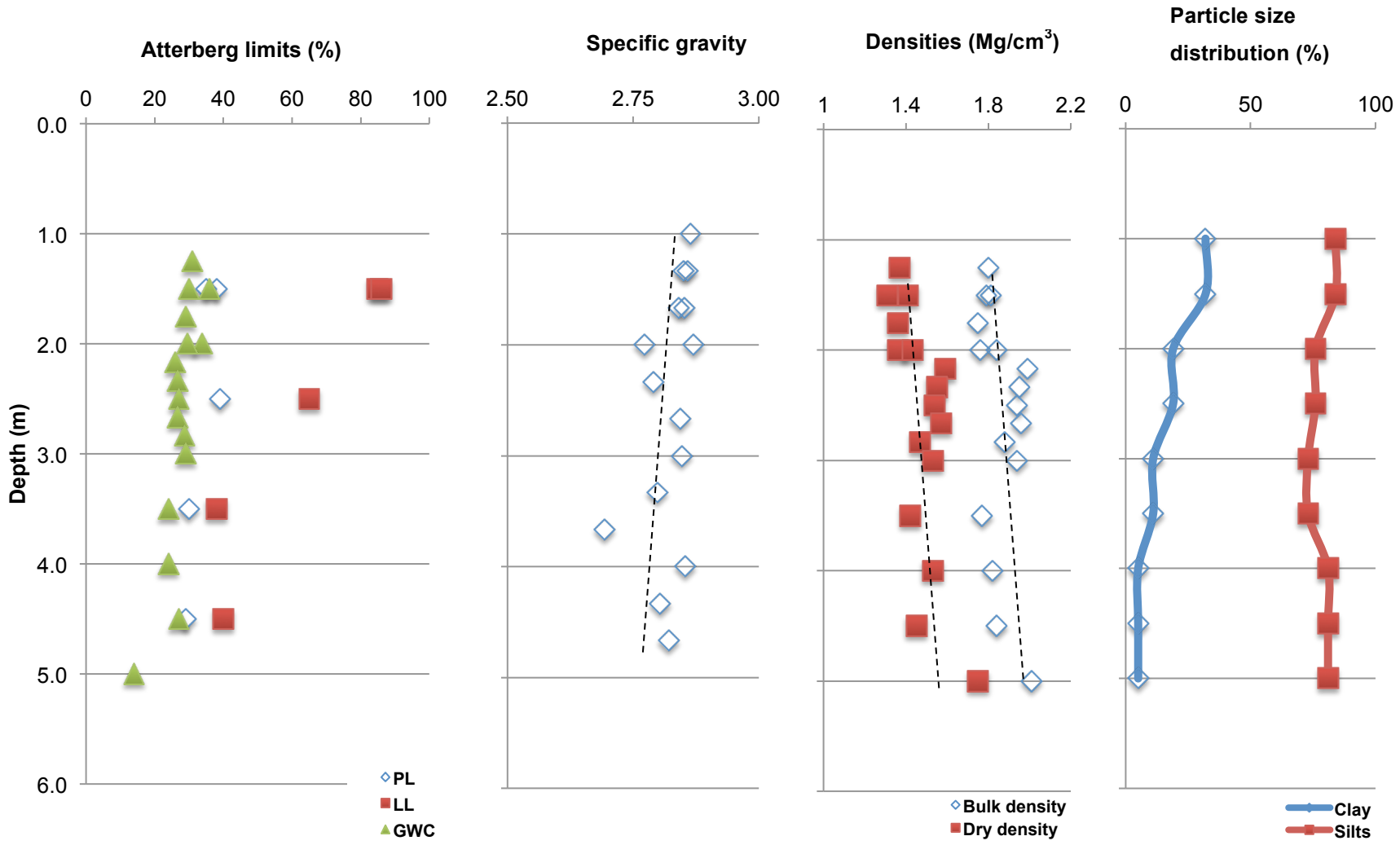

Figure 2.18 Comparison on natural water content, Atterberg limits, specific gravity, soil densities (bulk and dry) and particle size distribution against depth.

For depths near to the ground surface, the high amount of clay-based material in the soil (produced by weathering process) causes water to be retained instead of flowing down to the lower depth. This explains the variation in natural water content, where a higher value is observed to be concentrated at the upper layer and decreases with depth. However, it can also be seen that the results for bulk density is lower near surface. To explain this, the plots for degree of saturation against depth are presented (Figure 2.19). From the results, it can be seen that the degree of saturation for depth of 1m to 3m, ranges from 80% to 95% with higher value calculated for lower layer (2m to 3m) as compared to the upper layer (1m to 2m). This condition can be related to the porous structure that was produced within this depth due to the leaching of minerals from the soil. With further exposure to climate variation that occurred at the ground surface, it has caused the air phase to occupy more space within the soil and this reflects in the slightly lower degree of saturation.

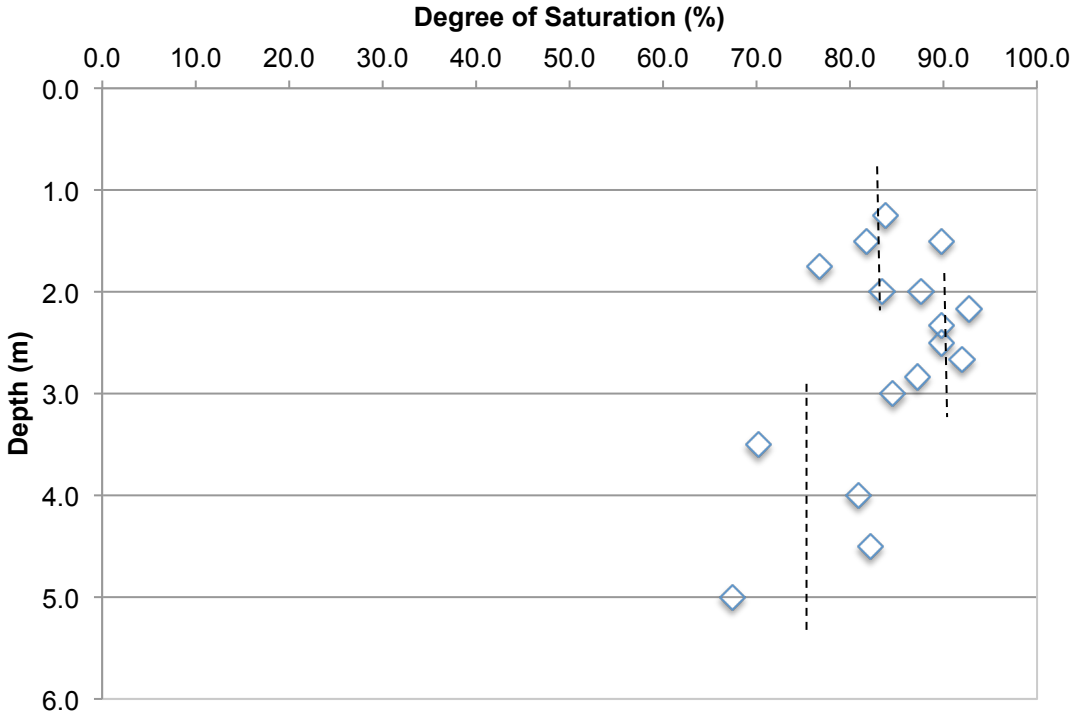

Figure 2.19 Degree of saturation against depth

As the amount of clay material reduces with depth, the values for bulk density seem to increase even with the decrease in water content (lower depth). This condition can be associated with the degree of cementation between the soil particles that is greatly dependant on the degree of weathering. For soil at lower depth, the decomposition process of the parent bedrock was less accelerated by the climate variation and this has preserved a higher degree of cementation between soil particles that is similar to the original structure of the parent rock mass (coarser material). The plot for Atterberg limits parameters also clarifies this suggestion where a variation from a high to low liquid limit values can be seen and these are greatly related to the amount of clay material within the soil. Furthermore, the plot for natural water content is observed to be very close to or less than plastic limit throughout the depth and hence indicating the unsaturated condition of the residual soils (in changing from a solid to a liquid characteristic – solid, semisolid, plastic and liquid - on the basis of water content). The slight decrease in specific gravity is also attributable to the dominant type of soils as shown by the particle size distribution.

From the descriptions made above, it is clear that the variation in index properties for each sample is highly related to the variation in the degree of weathering with depth. A proper and realistic implementation of index properties and classification tests are imperative in order to really understand the variation of these natural characteristics. Without considering the sensitivity possess by the soil during testing, a poor description of soil characteristics can be made and this will lead to false interpretations on how climate change may affect the actual behaviour of the tropical residual soil slope.

2.6 Final Remarks

This chapter aimed to highlight the significance of understanding the engineering geology of residual soils, as the problems related to this type of soils are frequently unforeseen and also difficult to identify during the design stage. At the early part of this chapter, the presentation of the inherent variation of index properties and weathering profile, geological distributions and sampling procedures can be seen, specifically for cases in Malaysia. From this information reported by many researchers in regards to residual soils, it is understandable that extra care should be taken to describe the actual behaviour of these tropical residual soils, especially in correspondence to climate changes.

Research collaboration was established between Durham University, IKRAM and PPj for acquiring undisturbed soil samples from a failed slope located in Precinct 9, Putrajaya. The purpose of the collaboration is to provide advance investigations of the cause of failure, using Durham University's state-of-the-art unsaturated soil testing facilities. The chronology of the incident, topography and geological profile of the slope were presented, as reported by IKRAM. This includes the results of the implemented site investigation programs, which covers the entire section of the slope.

In May 2013, soil sampling works were successfully carried out at the top of the slope. Detailed information in regards to this soil sampling works were presented, including the type of drilling technique and flushing fluid adopted as well as the configuration of equipment utilised. The decision on sampling procedures were made primarily to ensure that the undisturbed soil samples were representative of the area of concern and also not subjected to any irreversible damage either during the sampling process or transportation (e.g. volumetric strains).

A total number of 5 PVC tubes (1m to 5m depth) have been successfully obtained from the sampling process, labelled as MZ1, MZ2, MZ3, MZ4 and MZ1a. The residual soil sample contained in MZ1a was taken from a separate borehole that was off-sett about 0.5m away from the original borehole. Based on observation, it was clear that for samples from MZ1, MZ2 and MZ1a were similar in physical characteristics. The colour of the samples in these tubes was observed to be reddish brown to brownish grey. However, for residual soil samples in MZ3, a variation in

colour from brown to yellowish was seen and this was associated with the variation in degree of weathering for residual soil. Furthermore, MZ4 showed the colour of dark grey with white stripes that was believed to be the underlain bedrock due to its structural rigidity. In addition, there was a recovery ratio less than the upper sample tubes (around 50% rather than 90% as reported in Table 2.5). The sample was also observed to be stiffer than the samples from the upper tubes.

A series of residual soil index and classification tests were also executed in order to classify the materials. For samples near to the ground surface, high natural water content was measured and this was linked with the leaching of minerals in soil (weathering process) that was replaced by water, contributed by climatic events. The weathering process also produced clay-based material (PSD plot) that caused water to be retained instead of flowing down to the lower profile. Both of these soil characteristics reflected to the less bulk density values at this depth. However, as the decomposition process of the parent bedrock was less accelerated by the climate variation for samples at the lower depth, a lower content of clay material within the soil was produced (maintain its original structure of the rock mass). This also caused less voids for water phase (low natural water content). In addition, this condition was explained due to the degree of cementation between particles that was based on the differences in weathering grade. A high to low liquid limit values and constant behaviour of plastic limit shown by the Atterberg limits plot also clarified this suggestion (as they are greatly related to the dominant type of soils shown by the particle size distribution).

Besides that, the variation in index properties of the residual soil samples for each tube also reflected the subsurface profile described by IKRAM (Section 2.3.5). Based on both experiment results and physical observation of each tube, the samples obtained from 1m to 3m (MZ1, MZ1a and MZ2) and the samples from 3m to 4m (MZ3) appear to match the description for residual soil layer (Grade VI) and the highly to completely weathered Schists of Kajang formation (Grade IV to V), shown in Figure 2.9. Whereas, the description for fresh to moderately weathered Schists of Kajang formation (Grade I to III) can be related to the samples obtained from 4m to 5m deep (MZ4). Thus, to make it convenient, these layers will be referred as Layer 1, Layer 2 and Layer 3 in the subsequent chapters.

Overall, it can be concluded that each index property was highly connected to the variation in degree of weathering experienced by the soil. As the weathering grade of the sample increases, less characteristics of its parent rock can be observed, ultimately presenting a clay-based structure or fabric. The heterogeneity of the samples was also one of the factors that contribute to the variation of the soil properties. It is clear that the implementation of a proper and realistic index properties and classification tests for residual soils is highly imperative. A better description of soil characteristics can be made if the sensitivity possessed by the soil was taken into account during testing, The results will also provide better insight on how climate change have influenced its natural characteristics.

Chapter 3
Mechanical behaviour of Tropical Residual Soils

3.1 Introduction

Shear strength is a soil property that describes the mechanical ability of soil to resist shear stress (Karube and Kawai, 2001). For geotechnical problems, such as slopes, an understanding of the changes of shear strength due to climate variations is needed in order to prevent catastrophic slope failure.

To study the actual behaviour of a residual soil slope, a sound understanding of fundamental soil mechanics theoretical concepts is imperative. However, much of classical soil mechanics, predominantly from the study of saturated soils, is only relevant under saturated conditions. In tropical and subtropical environments, the assumption of saturation cannot be made as soils above the water table mainly exist in an unsaturated condition (Toll, 1990).

In the initial part of this chapter, the theoretical background to the strength characteristics of a tropical residual soil and the relation with unsaturated soil concepts will be presented. In the presentation, the definition of suction and its influence on soil shear strength behaviour are discussed. This includes the theoretical background for deriving soil strength parameters to describe the mechanical behaviour of unsaturated residual soil. Then, the presentation of the laboratory results will be reported and discussed towards the end of the chapter.

3.2 Literature Review

3.2.1 Strength characteristics of tropical residual soil slope

The soil strength characteristics of residual soil slopes are mainly governed by the nature of its parent bedrocks; however, they are also very heterogeneous due to the effects of weathering processes. The heterogeneity of this characteristic can be associated with the continuous gradation from highly to slightly weathered composition depending on the extent to which the soil forming processes have advanced (Singh and Huat, 2004). It has been reported in many geotechnical studies that the variation in shear strength for residual soil can be very substantial and is attributed to the high density and cementation between the soil particles (degree of weathering) (e.g. Rahardjo et. al., 1994, Rahardjo et. al., 2003, Toll et. al., 2000, etc.). As a result, Fookes (1997) has outlined some of the main characteristics for shear strength of residual soils, as follows;

1. The existence of bonding between particles derived by chemical composition consequential to the weathering processes.
2. Widely variable void ratio, which is unrelated to stress history.
3. Partial saturation down to a considerable depth.

It is apparent that despite the effect of degree of weathering, the unsaturated soil condition is also considered as one of the important aspects of relevance for residual soils. This is because residual soil generally exists in an unsaturated condition and it has been reported that residual soil slope failures usually occur due to the increase in pore-water pressure (or reduction in matric suctions) within the slope that is caused by rainfall infiltration (Brand, 1981). The pore-water pressure can build up over a number of series of rain storms, eventually culminating in the final triggering rainfall event that leads to failure (Tan et al, 2007). Therefore, it becomes necessary to be fully conversant with the concept of unsaturated soil in order to perform residual soil strength studies (Fredlund and Rahardjo, 1987).

3.2.2 Phases of unsaturated soils

In general, soil comprises 3 phases; solid, water and air phases. The latter two phases fill the spaces (pores) between the soil particles. In a saturated state, the pores are filled with water and no air is present (only 2 phases).

In unsaturated (sometimes called partly saturated) conditions, air is present in the pores and the soil mass now consists of 3 phases. Furthermore, Fredlund and Morgenstern (1977) have also introduced a fourth phase called the air-water interface, due to its unique properties. This air-water interface, also known as the contractile skin, is the natural ability of the water to exert a tensile pull, or surface tension. It has been suggested that the contractile skin can act like a thin rubber membrane pulling soil particles together, leading to volumetric shrinkage with no changes of total stress while the soil specimen undergoes drying (Fredlund and Rahardjo, 1993).

3.2.3 Soil suction

Soil suction can be described as the attraction force exerted by the soil, when being placed in contact with pure water. This degree of attraction will become greater as the soil water evaporates. The theoetical definition for soil suction, or total suction, is made by the sum up of two components which are matric suction and osmotic suction. The expression can be seen in Equation 3.1 (Fredlund and Rahardjo, 1993);

$$\Psi = (u_a - u_w) + \Pi \quad \ldots (3.1)$$

Where; Ψ = total suction;

$(u_a - u_w)$ = matric suction

u_a = pore-air pressure;

u_w = pore-water pressure;

Π = osmotic suction

The matric suction results from the surface tension forces produced at the water and air interfaces within the soil pores and is sometimes referred to as capillarity. This component is dependent on the structure and the amount of water content within a soil. It has been indicated that finer grain size soil can produce

higher values of matric suction and would also increase as the water content within the soil reduces. On the other hand, osmotic suction is due to the effects of dissolved salts in the pore water. The effects of this suction component towards the variation on suction would be greater depending on the concentration of salts in the pore water in the soil relative to the pure water outside (Toll, 2012a). Osmotic suction has negligible effects on shear strength but a very important role in volume change.

In this thesis all suction measurements were done using the application of saturated porous ceramic disc with high air entry value (either in a pressure plate apparatus or using a high suction tensiometer). This means that the pressure difference across the ceramic will be equal to the matric suction since the water on the other side of the ceramic will be of the same composition as the soil water and there will be no osmotic suction component. However, for brevity the term 'suction' only will be used.

3.2.4 Shear strength for unsaturated soil

Shear strength of soil is defined by the magnitude of shear stress that a soil can sustain at failure. Under saturated conditions, the shear strength is contributed by two phase components that are solids and pore-water. For this reason, Terzaghi's law for effective stress, comprising two stress state variables (σ, u_w), can be used to perfectly describe the mechanical behaviour under this state.

In the same way, this principle of stress state variables can still be used to describe the mechanical behaviour of unsaturated soil. However, with the presence of air components in the soil mass, the additional term pore-air pressure, u_a, must be included. Therefore, by extending it from the classical effective stress concept, this additional term has been widely used to produce two combinations of general unsaturated stress state variables, commonly known as net stress, (σ-u_a) and matric-suction, (u_a-u_w) (Fredlund and Morgenstern, 1978).

3.2.5 Constitutive models

There have been a number of constitutive models introduced by researchers in order to explain the shear strength of unsaturated soil. The frameworks, however,

are generally based on two approaches, which are either by combining the contribution by matric suction into an equivalent 'effective' stress approach (Bishop, 1959); or by treating the strength contribution by matric-suction separately, i.e. an independent state variables approach (Fredlund and Morgenstern, 1978).

3.2.5.1 'Effective' stress approach

Bishop (1959) was the first to explain the modification of Terzaghi's effective stress concept through the equivalent 'effective' stress approach. He suggested that the effect of an unsaturated condition in soil could be measured by incorporating a coefficient, χ, into the combination of the stress variables to produce an equivalent 'effective stress'. This basically means that the unsaturated soil shear strength is resolved on the basis of the effective saturated strength parameters cohesion (c'), angle of internal shearing resistance (ϕ') and a single stress variable ('effective stress'). In his equation, he presented the relationship between the effective stress with the net stress state variable and the matric suction as follows:

$$\sigma^* = (\sigma - u_a) + \chi(u_a - u_w) \quad \ldots (3.2)$$

where, σ^* = the effective normal stress

σ = the total stress

u_a = the pore-air pressure

u_w = the pore-water pressure

χ, = an empirical 'effective stress' coefficient

Putting equation 3.2 into the Mohr-Coulomb shear strength equation, it can be rewritten as;

$$\tau = c' + (\sigma - u_a)\tan\phi' + \chi(u_a - u_w)\tan\phi' \quad \ldots (3.3)$$

In his approach, this 'effective stress' coefficient value (χ) was mainly a function of degree of saturation and varied from 0 to 1, representing the condition of dry to fully saturated. Alternatively, Oberg and Sallfors (1997) and Vanapalli et al. (1996) recommended that the degree of saturation (S_r) or the effective degree of saturation (S_e) can also be used as an approximate replacement for χ. This effective

degree of saturation (S_e) is defined as a measure of the degree of saturation, to which the macropores in a dual porosity structure are filled with water while water volume held within micropores remains constant (Fredlund and Rahardjo, 1993).

Up to recent years, there have been many proposed constitutive models that are based on this suggested 'effective strength' approach (Khalili and Khabbaz, 1998). Most of the attempts were mainly focusing to finding the relationship between χ and the degree of saturation (S_r). Nevertheless, Khalili and Khabbaz (1998), suggested a unique relationship between the effective stress parameter χ and the ratio of suction over the air entry value (AEV). As the basis of their model framework, they suggested that effective stress parameter χ should not be treated as a function of degree of saturation but instead a function of suction. This suggestion was made previously by Coleman (1962), of which he indicated that χ is a parameter strongly related to soil structure/fabric, and might not be able to be correlated against a volumetric parameter such as the degree of saturation.

To further explain the Khalili and Khabbaz (1998) model, comparisons were made between the measured (experimental data) and the calculated shear strengths for two laboratory prepared unsaturated soils. The calculated shear strengths were formed based on χ values deduced from equation as follows:

$$\chi = \left[\frac{(u_a - u_w)}{(u_a - u_w)_b}\right]^{-0.55} \quad \ldots(3.4)$$

where, $(u_a\text{-}u_w)$ = matric suction

$(u_a\text{-}u_w)_b$ = Air entry value

This equation of χ was deduced from the graphical assessments on 14 types of different soils published in the literature with 13 of them were naturally occurring soils and one compacted kaolin.

Khalili and Khabbaz (1998) presented the test results in terms of maximum shear strength against matric suction as shown in Figures 3.1a and 3.1b, respectively. The decision of not adopting the general relationship between shear strength against effective mean stress was made due to the assumption that the parameters c' and ϕ' are independent of matric suction ($u_a\text{-}u_w$). This, however, is

not true as there is experimental evidence showing that ϕ' also increases with the increase of suction (Escario and Sáez (1986), Delage et al., 1987, Toll, 2000, Toll et. al., 2008). Nevertheless, the suggested unsaturated soil model is still useful during the condition of low suction (or fairly high degree of saturation) which is associated with less aggregation in the soil fabric (Toll, 2000). Further explanation with regard to this will be given later in this chapter.

Very good agreement can be seen between the measured and the calculated values using the proposed relationship, with less than 5% error in all cases. The deviation point indicated on the both graphs, also show that starting at the Air entry value (AEV), the unsaturated shear strengths for both unsaturated specimens reduces and continuously gives a non-linear relationships (Escario and Sáez, 1986).

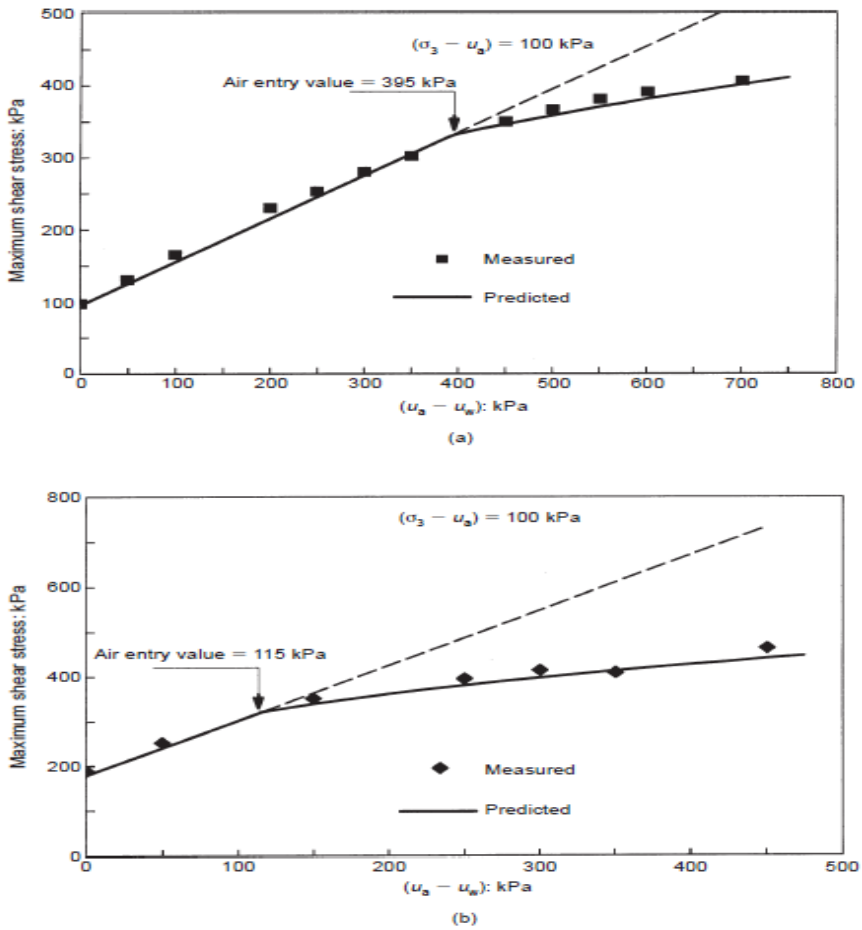

Figure 3.1 Results of measured and predicted shear strength (using Equation 3.3 and Equation 3.4) on unsaturated specimens: (a) compacted kaolin; (b) compacted sand-clay mixture (after Khalili and Khabbaz (1998)).

Although this approach appeared to explain the shear strength behaviour, this single 'effective' stress concept has highlighted several arguments, as it was still incapable of explaining the effects of volume changes due to suction (Burland, 1965). These arguments were made based on the fact that the applied external stress on the boundary of an unsaturated soil element creates quantitatively different ways of pore water movements within the soil skeleton.

It has also been observed that the suction also increased the stabilizing force to resist the shear stress (Wheeler and Karube, 1996). This can be illustrated by the capability of a sand castle to maintain it shape (soil structure) due to the shear strength resistance induced by the suction force (internal tensile force). The outcomes from subsequent studies will show that this volumetric behaviour is not controlled by similar stress component or by any one single stress variable (Fredlund et al., 1978).

3.2.5.2 Independent state variables approach

In relation to the above, Fredlund and Morgenstern (1978) proposed the concept of segregating these two stress states independently, known as the Extended Mohr Coulomb failure surface. This concept was put forward as it was easier to explain the shear strength behaviours contributed by net stress (σ-u_a) and matric suction (u_a-u_w). Equation 3.5 presents the constitutive equation, which is based on independence of the stress state variables.

$$\tau = c' + (\sigma - u_a)\tan\phi^a + (u_a - u_w)\tan\phi^b \quad \ldots (3.5)$$

where, τ = shear strength,

c' = effective cohesion of the soil.

ϕ^a = angle of internal shearing resistance with respect to changes of (σ-u_a)

ϕ^b = angle of internal shearing resistance with respect to changes of (u_a-u_w)

This combination has been found to be the most meaningful combination in engineering practice as it can obviously show the differences contributed by two angles of shearing resistance relating to the two components of stress. Additionally, in many engineering situations, the field pore air pressure u_a is zero, therefore, the two components which are the net stress and matric suction can be simplified into

the general total stress (σ) and negative pore water pressure ($-u_w$), respectively (Fredlund et al., 1978).

In 1986, Escario and Saez showed that the relationship between τ and (u_a-u_w) was non-linear. The finding was then confirmed by Fredlund and Rahardjo (1987) who defined the value for ϕ^b as varying as a function of suction. In this explanation, the variation of ϕ^b is described by having equal value to ϕ' for the condition of suction below air entry value (AEV) but reduces as the suction increases to higher value.

For the strength component by the net stress ($\sigma-u_a$), Fredlund et al. (1978) suggested that ϕ^a could be assumed to be equal to the angle of internal shearing resistance measured in saturated condition ϕ'. The suggested assumption, however, has been brought into question by research done showing that the value of ϕ^a also changes with respect to degree of saturation (Delage et. al., 1987, Toll, 2000, Toll et. al., 2008).

The presentation of the variation on both ϕ^a and ϕ^b with respect to changes in degree of saturation was reported by Toll (1990) and Toll and Ong (2003) on two compacted unsaturated tropical soils which are a lateritic gravel from Kiunyu, Kenya and a residual sandy clay from Jurong, Singapore (Figure 3.2). The tests were performed under constant water content conditions (similar to undrained testing in saturated soils). To describe further, each sample was prepared initially with different water contents and different degrees of saturation (S_r), which then resulted in different measured suction values.

In Toll (1990, 2000), the variation for ϕ^a and ϕ^b has been explained due to the degree of aggregation or 'packet fabric' that occurred based on microscopic observations on the soil structures within the soil element. At lower degree of saturation, the presence of these packet fabrics causes the soil to behave in a coarser fashion than would be justified by the grading (particle size distribution). Due to this, it resulted in an increase of ϕ^a (strength component by the net stress, $\sigma-u_a$).

The variation for the strength component by suction, ϕ^b, however, is due to the withdrawal of the pore-water into packets. As the degree of saturation becomes

lower, it causes ϕ^b to further reduce, which provides less contribution to the overall strength of the soil, especially at very low degree of saturation.

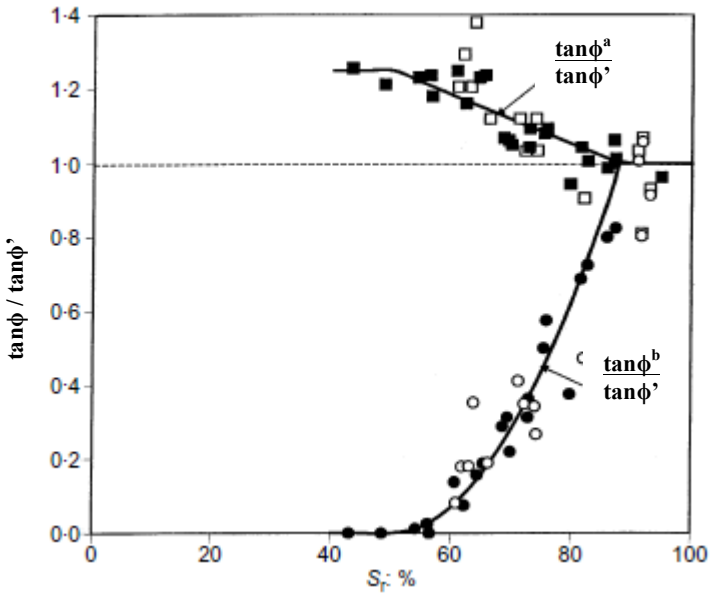

Figure 3.2 Variations of ϕ^a and ϕ^b related to the degree of saturation for two tropical soils [Black symbols for Kiunyu Gravel (after Toll, 1990); Open symbols for Jurong soil (after Toll and Ong, 2003)].

3.2.6 Mechanical testing of unsaturated soils

Various techniques can be used for mechanical testing of unsaturated soils. The details for each technique can be found in the geotechnical literatures, which are axis translation (e.g. Toll, 1990, Wheeler and Sivakumar, 1995), relative humidity (e.g. Oldecop and Alonso, 2000), osmotic (e.g. Dineen and Burland, 1995) and high capacity tensiometer (e.g. Jotisankasa, 2005, Lourenço et al., 2006, Lourenço, 2008). In this chapter, only the two mostly widely used methodologies for triaxial testing are presented, namely: Axis translation technique and using High Capacity (HC) tensiometers.

3.2.6.1 Axis translation technique

The axis translation technique has been one of the most widely used techniques by researchers to study the mechanical behaviour of unsaturated soils. The technique is generally adopted by modifying the saturated triaxial cell system into a system, which capable of controlling independently both air pressure and water pressure. The idea of the system was initially introduced by Bishop and Donald (1961) , which enabled the suction being controlled (or measured) during the whole testing process.

The triaxial testing based upon this axis translation technique can be carried out under constant suction conditions. Using this approach, the desired suction value (u_a-u_w) is obtained by controlling both air pressure (u_a) and water pressure (u_w) applied to the soil sample through a high entry value porous stone. This approach has been adopted for multistage testing so as to imitate the desaturation process occurred in soils starting from a fully saturated state (Gan and Fredlund, 1988, Fredlund and Rahardjo, 1993),. The approach, however, requires long duration for equalisation and furthermore increases the possibility of cavitation occurrences within the porous stone. Alternatively, unsaturated triaxial testing can also be implemented under constant water content conditions. Via this approach, the suction values are measured during the tests by elevating the pore air pressure (u_a), which consequently, elevates the pore water pressure (u_w) to become positive (Toll 1990, Toll and Ong, 2003). The approach (analagous to undrained testing in saturated soils), can measure the suction value (u_a-u_w) using a high air entry porous stone placed at the bottom part of the sample (Hilf, 1956).

Several disadvantages have been pointed out for the use of the axis translation technique due to the dependency of the attainable maximum suction values upon different parts of the triaxial apparatus (i.e. the air entry value of the porous stone and the achievable air pressure). To add further, the concept of having positive pore air pressure has also be seen to be unrealistic as it has been acknowledged that in the field the atmospheric pressure is equal to zero.

3.2.6.2 High capacity tensiometer technique

A tensiometer is a small probe, fitted with a porous stone and a pressure transducer. The main function is to measure the negative pore water pressure in soil relative to the atmospheric pressure. The terminology of “high capacity - HC” essentially marks it out as a different type of tensiometer, which is capable of measuring suctions above the normal cavitation limit of 100 kPa.

There are various types of high capacity tensiometer that have been reported (e.g. Ridley and Burland, 1993, Guan and Fredlund, 1997, Meilani et al., 2002, Chiu et al., 2005, Lourenco et al., 2006 and etc.). These high capacity tensiometers use the same working principle of the design made by Ridley and Burland (1993) at Imperial College London. Although the designs are quite different in types and sizes, the components utilised are still similar, comprising of a High Air Entry Value (HAEV) ceramic disc as a medium between the measuring device and the soil sample, a small water reservoir and an electronic pressure transducer as the measuring device. The measuring range for the maximum suction value is also one the differences observed between each types of tensiometer

The high capacity tensiometer, reported by Lourenço et al. (2006), Lourenço (2008) and Toll et al. (2013), was used in this project. This tensiometer differs from that of Ridley and Burland (1993) particularly in the fabrication process as well as in types and sizes of the components. The schematic of the tensiometer can be seen in Figure 3.3, where the size for the water reservoir is 5 mm^3 in volume and uses a ceramic pressure transducer sealed to a 1.5 MPa high AEV ceramic disc of 10mm thickness, resulting in the dimensions of the device being 35mm by 14mm. Toll et al. (2015) reported that these devices have been used for direct measurement of suction as large as 2000kPa.

To perform suction measurement, the initial procedure of saturating the tensiometer is required. This procedure is done to prevent any air being trapped inside the device. Once fully saturated, the pressures between the ceramic high air entry disc and water reservoir will be equal and the pressure transducer will indicate zero suction value (atmospheric pressure) if placed in free water. Then, the tensiometer will be placed in contact with a soil sample and the water in the high capacity tensiometer will start to be drawn towards the soil until equilibrium is

reached. An increase in suction measurement, shown by the pressure transducer, will be seen until the water in the tensiometer equilibrates with the negative pore water pressure within the soil.

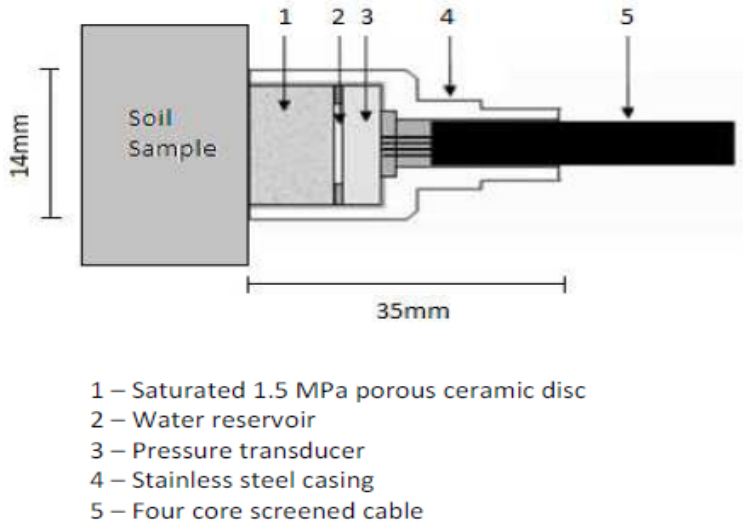

Figure 3.3 Schematic of the Durham University high capacity suction probe (after Lourenco, 2008).

The method of controlling or measuring suction during triaxial test can also be done using tensiometer. For a suction control system, a new development that is an improvement of similar systems reported by Cunningham (2000) and Jotisankasa (2005), has been introduced by Lourenço et al. (2011). The system requires a tensiometer to be fitted through the base pedestal for suction measurement and a diaphragm pump to force air to flow inside a closed loop that runs across the sample and a moisture trap (for sample drying process). The adoption of the moisture trap is to ensure that the relative humidity of the circulating air is kept low as well as to measure the amount of the abstracted water by continuous weighing of the desiccant that is placed inside the moisture trap. For wetting the sample, a controlled injection of water through a solenoid valve connected to a pressurised volume gauge is used. Using this system, the variation of soil water content caused by drying and wetting can be calculated, which is the difference between the amounts of water injected by the volume gauge and that retained by the desiccant.

The system was then being further enhanced by Mendes et al. (2012) with the adoption of a double cell triaxial cell. This is because the traditional method for sample volume change measurement for triaxial test is likely to be affected by problems such as volume variations by the Perspex due to cell volume changing with cell pressure, water absorption, thermal expansion as well as creep of the cell under constant cell pressure. Thus, a double triaxial cell, similar to the Wheeler modified triaxial cell (Wheeler, 1988) but using a glass inner cell wall, was developed by Wykeham Farrance in order to avoid problems of absorption of water by Perspex. With the utilization of this glass inner cell wall, the volumetric measurements of the sample can be carried out as to satisfy the issues of the effects of volume change due to suction. Further information about the application of this modified cell can be seen in Mendes (2011), which was implemented for compacted clay material under constant water content conditions (measured suction).

3.3 Details of Undisturbed Residual Soils Samples for Mechanical tests

A total number of 11 triaxial test samples of residual soil were obtained from the Mazier sampler tubes (described in Chapter 2) for both saturated and unsaturated testing. The details of these samples are summarised and shown in Table 3.1.

Table 3.1 Details of the Undisturbed Triaxial test samples.

Mazier Tube	Depth (m)	Testing type	Number of samples
MZ1	1.0 to 2.0	Saturated	3
MZ2	2.0 to 3.0	Unsaturated	3
MZ3	3.0 to 4.0	Saturated	1
MZ4	4.0 to 5.0	Saturated	2
MZ1a	1.0 to 2.0	Unsaturated	2
	Total		11

It can be seen that an adequate number of triaxial samples have been selected from MZ1 and MZ2 for both saturated and unsaturated testing; as soil samples in both tubes were found to be similar in characteristics to represent the strength for Layer 1 (Figure 2.9 in Chapter 2). For a similar reason, an additional 2 samples were obtained from MZ1a (similar depth with MZ1) with the intention to further investigate the behaviour of residual soils under an unsaturated state. As for soil samples in MZ3 and MZ4 that were observed to have different characteristics and less recovery percentage, only 3 samples managed to be obtained and these have been used for saturated testing to represent the saturated strength parameters for Layer 2.

The dimensions for each sample were set to be 75mm diameter with 150mm in height. The decision to use 75mm as the diameter size for triaxial sample (equivalent to the Mazier sampler tube size) was made essentially to preserve the natural condition of the soils; without having to reduce the size of the samples that

could lead to significant disturbance and deterioration to the soil samples. The equipment used for the preparation of the samples is shown in Figures 3.4a to 3.4c.

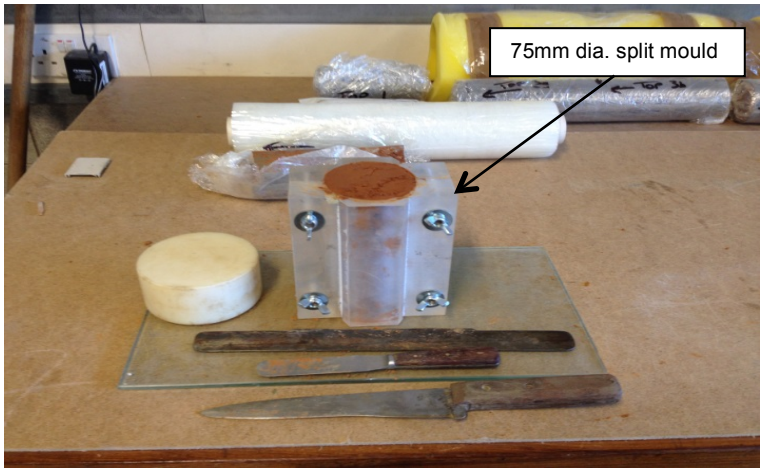

(a)

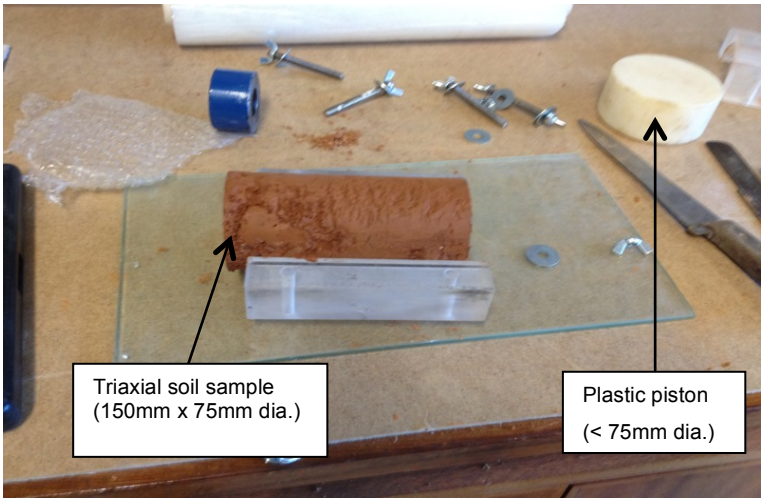

(b)

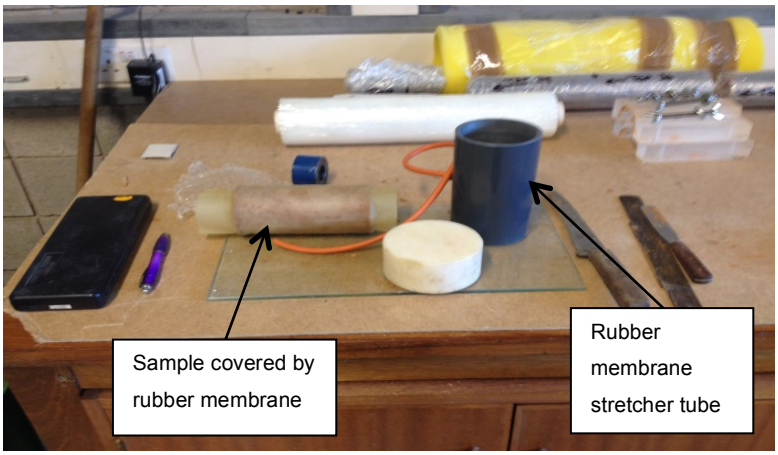

(c)

Figure 3.4 Photos of the process of sample preparations and the utilised equipment.

3.4 Multistage Triaxial Test Programs

The triaxial test system adopted by Mendes (2011), for both saturated and unsaturated soil, was used for the residual soil samples described previously. However, in order to obtain maximum information from the limited number of samples, it has been decided to perform Multistage Triaxial tests for both testing conditions. With these additional stages executed on the samples, multiple strength points could be obtained from one single sample, thus, giving higher degree of accuracy and confidence for the characterisation of strength parameters.

Four confining stages were performed on each sample. After the equalisation procedure for the first confining stage, the recorded maximum deviator stress was carefully observed during the shearing process. It was when the deviator stress reached a constant value, then, the sample was unloaded axially and left for equalisation. Next, the cell pressure was altered for the subsequent confining stage. This procedure was repeated until it reached the final shearing stage when this time the shearing process would be left until the sample reached at least 20% of axial strain.

Among of the difficulties in carrying out multistage triaxial tests is the ability to control the destructurisation effects that can occur within the samples due to the excessive shearing process executed in the earlier stages. This destructurisation effects will alter the structure of the soil particles and cause irreversible damages to the sample. Compliance to a predefined failure criterion during shear is also difficult when applying this method. It requires immediate data reduction in order to define failure. However, it is highly necessary when the soil sample is scarce or nonhomogeneous.

To control the destructurisation effects within sample, experimental investigations were carried out on all the first three triaxial samples from MZ1 (Table 3.2). The confining pressure was varied for each test. The reason behind this was to determine the actual maximum stress value (strength) under every desired confining pressure before applying successive pressures. Furthermore, the final stage confining pressure was set to the same value as the first stage. It was anticipated that if the sample had been destructured, a lower value of strength would be observed. However, as the sample had been subjected to overconsolidation on

unloading for the final stage, it would be expected that the sample would gain in strength, as indicated in Figure 3.5.

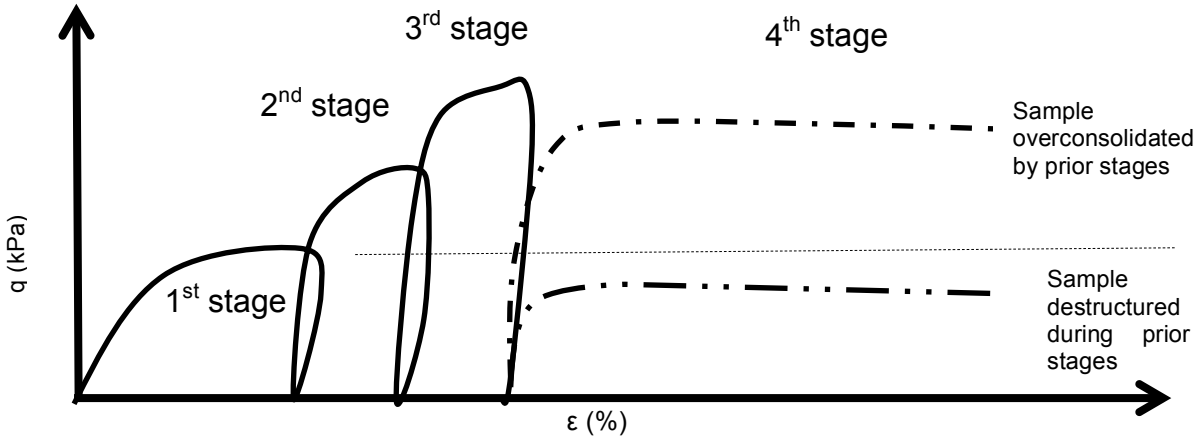

Figure 3.5 Graphical explanation on the effects of destructurisation by prior stages.

For samples from MZ3, MZ4, MZ2 and MZ1a, similar arrangement of confining pressures were applied by increasing the magnitude of the pressures for the initial 3 confining stages prior to shearing. Once the process reached the final confining stage, the magnitude of the confining pressure would be reduced similar to the first stage confining pressure value as explained in the previous paragraph. Full details of the multistage arrangements for both saturated and unsaturated mechanical testing are outlined in Table 3.2 and 3.3, respectively.

Table 3.2 Confining pressures arrangement for Saturated Multistage tests.

Mazier Tube	Sample number	Confining Pressures			
		Stage 1	Stage 2	Stage 3	Stage 4
MZ1	S1	25	50	100	25
	S2	50	100	25	50
	S3	100	25	50	100
MZ3	S1	25	50	100	25
MZ4	S2	25	50	100	25
	S3	25	50	100	25

Table 3.3 Confining pressures arrangement for Unsaturated Multistage tests.

Mazier Tube	Sample number	Confining Pressure			
		Stage 1	Stage 2	Stage 3	Stage 4
MZ2	US1	25	50	100	25
	US2	25	50	100	25
	US3	25	50	100	25
MZ1a	US4	25	50	100	25
	US5	25	50	100	25

3.5 Saturated Soil Tests

3.5.1 Configuration of Triaxial Test System and Procedures

To understand the effects of suction in soils, conventional consolidated triaxial tests on fully saturated samples are required as a reference state for the unsaturated soil testing outputs. The testing was implemented on 6 triaxial samples from MZ1, MZ3 and MZ4 (denoted as MZ1S1, MZ1S2, MZ1S3, MZ3S1, MZ4S2 and MZ4S3).

Due to equipment availability, fabrication of a 75mm diameter size base pedestal and top cap were carried out. These components for triaxial testing were designed with water entry holes to allow drainage of water to flow in and out of the sample during the consolidation process. Full configuration of the triaxial cell is shown in Figure 3.6.

The procedures for the saturated testing essentially consisted of three stages: saturation, consolidation and shearing. In the saturation stage, each soil sample was subjected to a 305 kPa cell pressure together with an elevated back pressure applied to the top and bottom of the sample (300 kPa) in order to saturate the sample, as well as to dissolve air bubbles present in the cell (Figure 3.7). With this slight pressure difference between the cell and the backpressure, the sample was subjected to only small effective stress (5 kPa or less).

Whilst for the process of saturating the sample, the method of measuring B value was used which is the ratio of pore water pressure in response to an increase of cell pressure ($\Delta u/\Delta \sigma_c$). In theory, the B value should be equal to 1 when the sample is fully saturated. The evolution of the B value was calculated by gradually increasing the cell pressure by 100 kPa with all drainage valves linked to the soil samples being closed (undrained conditions). Then, the pore water pressure measurements were taken from the pressure transducers connected to the top cap and base pedestal. It is common to saturate the sample until a B-value of 0.95 is achieved (BS1337, 1990) which for soft clays resembles 99.9% in the degree of saturation (Black and Lee, 1973). Once a satisfactory B-value was achieved (>=0.95), the test would then be subjected to its consolidation.

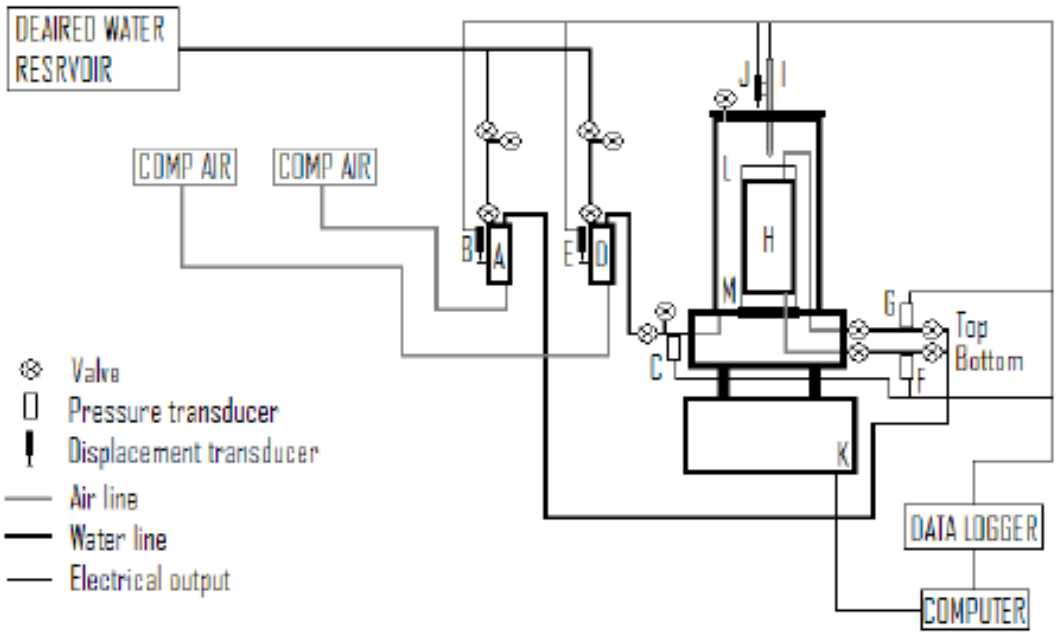

Letter	
A	Volume gauge – sample
B	Volume change transducer – sample
C	Pressure transducer – cell pressure
D	Volume gauge – cell
E	Volume change transducer – cell
F	Pressure transducer – back pressure bottom
G	Pressure transducer – back pressure top
H	Sample
I	Load cell
J	Axial displacement transducer
K	Loading frame
L	Top cap with porous disc
M	Bottom cap with porous disc

Figure 3.6 Configuration of Triaxial testing apparatus for saturated samples (after Mendez, 2011).

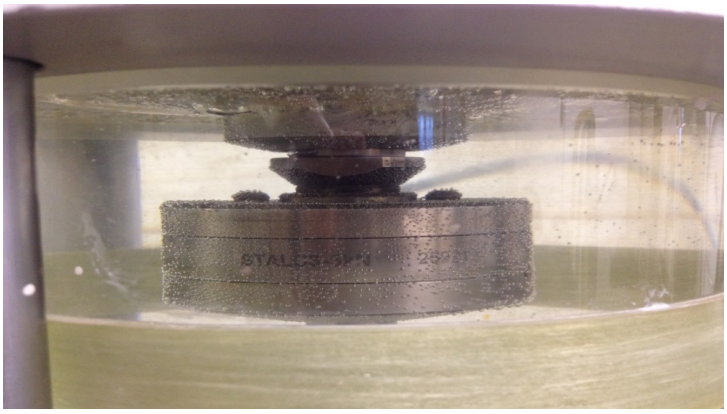

Figure 3.7 Close view of the air bubles present in triaxial cell.

For the consolidation stage, the confining pressure was elevated to the desired value to impose a known effective stress, however, still maintaining the back pressure at 300 kPa. This process was continued until no further significant volume change was recorded in the back pressure volume gauge (0.01cm^3/hr).

Subsequently, the samples were sheared under undrained (CU) conditions. This condition was carried out by closing the both bottom and top drainage lines and the changes in pore water pressure were measured throughout the process. The process for both consolidation and shearing would be repeated for subsequent stages based on the arrangement tabulated in Table 3.2. A strain rate of 0.05mm/min was used throughout the shearing process corresponding to a maximum rate of strain calculated based on the consolidation response during consolidation stage. This estimated strain rate value was adopted considering the presence of fissures and natural cracks within the sample.

3.5.2 Initial Condition of Residual Soil Samples

The initial conditions for each triaxial test samples can be seen in Tables 3.4 and 3.5, respectively. The process of sample classification (to represent Layer 1 and Layer 2) was derived from the soil classification tests results and physical observation presented in Chapter 2. Distinct variations in water content can be seen on each sample of both layers that reflects to the variation in bulk density (ρ_{bulk}), void ratio (e) and degree of saturation (S_r). From observation, the presence of organic materials (i.e tree roots etc.) and fissures were seen clearly and these can be considered as one of the factors causing variations. It has also to be recognised that

all samples were tested in their natural state (undisturbed samples). Therefore, the heterogeneity, of course, is one of the difficulties that need to be faced when testing residual soils.

Table 3.4 Initial conditions for saturated triaxial test samples of Layer 1.

Soil samples	Water Content	Mass	Dimensions				Density		Void Ratio	Degree of Saturation
							Bulk	Dry		
			h	d	A	V	ρ	ρ_{dry}	e	S_r
	%	g	cm	cm	cm^2	cm^3	Mg/cm^3	Mg/cm^3		%
MZ1S1	31.17	1134.85	15.02	7.31	42.01	631.06	1.80	1.37	1.04	83.7
MZ1S2	36.65	1114.30	15.09	7.26	41.34	624.02	1.79	1.31	1.14	89.8
MZ1S3	29.06	1063.80	15.16	7.14	40.00	606.40	1.75	1.36	1.06	76.8

Table 3.5 Initial conditions for saturated triaxial test samples of Layer 2.

Soil samples	Water Content	Mass	Dimensions				Density		Void Ratio	Degree of Saturation
							Bulk	Dry		
			h	d	A	V	ρ	ρ_{dry}	e	S_r
	%	g	cm	cm	cm^2	cm^3	Mg/cm^3	Mg/cm^3		%
MZ3S1	24.23	1112.20	15.07	7.29	41.74	628.84	1.77	1.42	0.967	70.2
MZ4S2	27.51	1150.15	15.09	7.26	41.34	624.02	1.84	1.45	0.937	82.2
MZ4S3	14.32	1217.05	15.16	7.14	40.00	606.40	2.01	1.76	0.595	67.4

3.5.3 Saturated Triaxial Tests Results

To provide clear and precise descriptions for the mechanical behaviour of the residual soils under this condition, the series of the results will be presented based on the characterised subsoil layering in accordance with the previous tables.

3.5.3.1 Layer 1 - Tests Results

During saturation stage, the process of water inflow into the triaxial sample should raise the degree of saturation up to 100%. Throughout this process, it might be assumed that the total volume of the sample would remain the same; therefore, the additional amount of water inflow should be equal to the volume of air within the

samples. However, if the measured amount of water were greater, this indicates that the samples had swelled.

The mass of solids was measured after oven-drying the samples, as the final procedure, in order to back-calculate the actual initial degree of saturation of each sample. The progression can be seen in Table 3.6 that presents the conditions of the soils before and after saturation for samples of layer 1. As expected every sample showed an increase in degree of saturation (higher than 95%) after saturation.

Table 3.6 Sample conditions before and after saturation stage for Layer 1.

Soil samples	M_{dry} (ovendried)	V_s	V_v	Before saturation			After saturation		
				V_w	V_a	S_r	V_{w2}	V_{a2}	S_{r2}
	g	cm^3	cm^3	cm^3	cm^3	%	cm^3	cm^3	%
MZ1S1	865.17	308.99	322.07	269.68	52.39	83.7	309.68	12.39	96.2
MZ1S2	815.44	291.23	332.80	298.86	33.94	89.8	324.36	8.44	97.5
MZ1S3	824.27	294.38	312.02	239.53	72.49	76.8	301.53	10.49	96.6

The conditions of the soils before and after consolidation of each stage are presented in the Table 3.7. From the results, it shows that residual soils decrease in volume when higher effective stress were being imposed, but increased in volume when lower subsequent pressures were applied. These volume changes were recorded directly from the volume gauge that measures the amount of fluid coming in and out of the samples.

The undrained shearing tests were implemented following the consolidation process in each stage. During shearing, both bottom and top drainage lines connected to the sample were closed and the maximum deviator stress (plotted in the stress strain curve) was carefully observed for each stage before progressing to the next stage. For the final shearing stage the test was continued until it reached 20% axial strain. Figure 3.8a, 3.8b and 3.8c present the variation in the deviatoric stress against axial strain for MZ1 saturated samples at different confining pressures used during each stage.

It has been confirmed that every sample did not experience any excessive destructurisations effects as described in Figure 3.5. The deviator stress value (shear strength of the soil) on the final stage for each sample, show higher values compared to the initial stage and increased corresponding to the increase of effective stress. The accumulated strains due to multistage process, however, maintain between 5% to 7% especially for sample MZ1S1 and MZ1S3.

Table 3.7 Sample conditions at the start and end of the constant water compression stage for Layer 1.

Soil samples	Initial Water Content	Stage no	Effective Stress	Consolidation	Volume	Dry Density	Void Ratio	Degree of Saturation
			σ_c		V	ρ_{dry}		S_r
	%		kPa		cm^3	Mg/cm^3	e	%
MZ1S1	31.17	1	25	Initial	631.06	1.371	1.042	96.2
				Final	626.75	1.380	1.028	96.1
		2	50	Initial	626.75	1.380	1.028	96.1
				Final	622.18	1.391	1.014	96.0
		3	100	Initial	622.18	1.391	1.014	96.0
				Final	615.72	1.405	0.993	96.0
		4	25	Initial	615.72	1.405	0.993	96.0
				Final	617.64	1.401	0.999	96.0
MZ1S2	36.65	1	50	Initial	624.02	1.307	1.143	97.5
				Final	617.99	1.319	1.122	97.4
		2	100	Initial	617.99	1.319	1.122	97.4
				Final	611.80	1.333	1.101	97.4
		3	25	Initial	611.80	1.333	1.101	97.4
				Final	613.06	1.330	1.105	97.4
		4	50	Initial	613.06	1.330	1.105	97.4
				Final	612.06	1.332	1.102	97.4
MZ1S3	29.06	1	100	Initial	606.40	1.359	1.060	96.6
				Final	589.96	1.397	1.004	96.5
		2	25	Initial	589.96	1.397	1.004	96.5
				Final	590.50	1.396	1.006	96.5
		3	50	Initial	590.50	1.396	1.006	96.5
				Final	589.14	1.399	1.001	96.4
		4	100	Initial	589.14	1.399	1.001	96.4
				Final	584.38	1.410	0.985	96.4

As all the tests were executed under undrained conditions, the volume of the sample remained constant and variations in pore water pressure were recorded. Figure 3.9a, 3.9b and 3.9c presents the relation between pore water pressure and axial strains throughout shearing stage of each sample for each stage. It is observable that each sample, in each shearing stage, shows a sudden increase in pore water pressure and gradually reduces as axial strain continuously progresses.

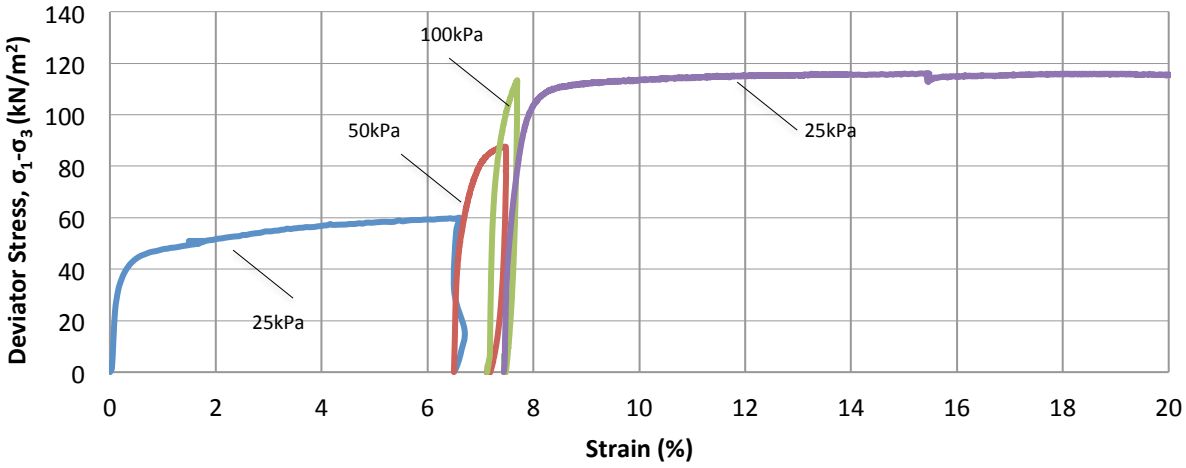

(a)

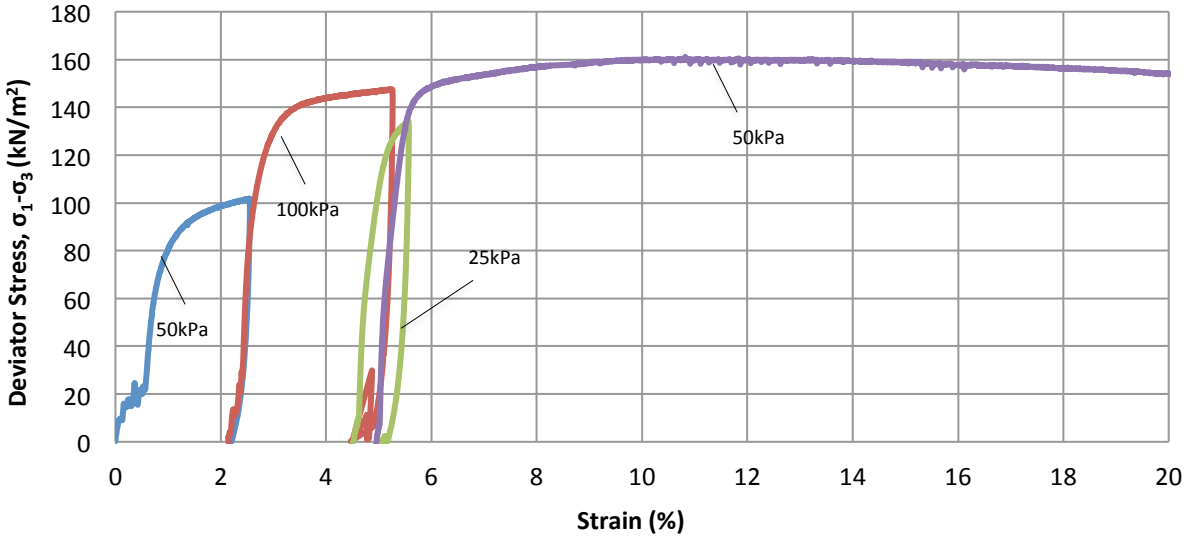

(b)

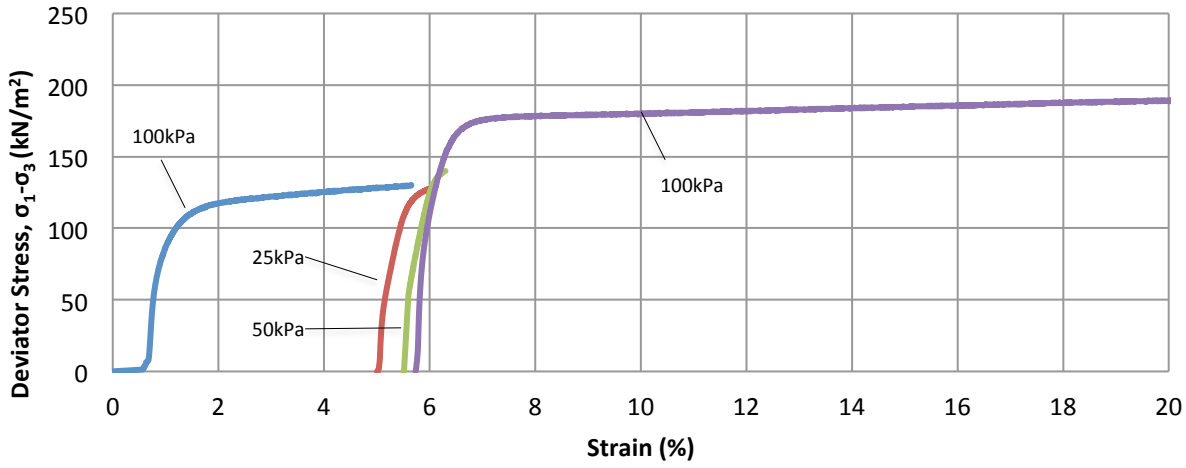

(c)

Figure 3.8 Deviatoric stress stress against axial strain relationships for samples of Layer 1; (a) MZ1S1 (b) MZ1S2 (c) MZ1S3.

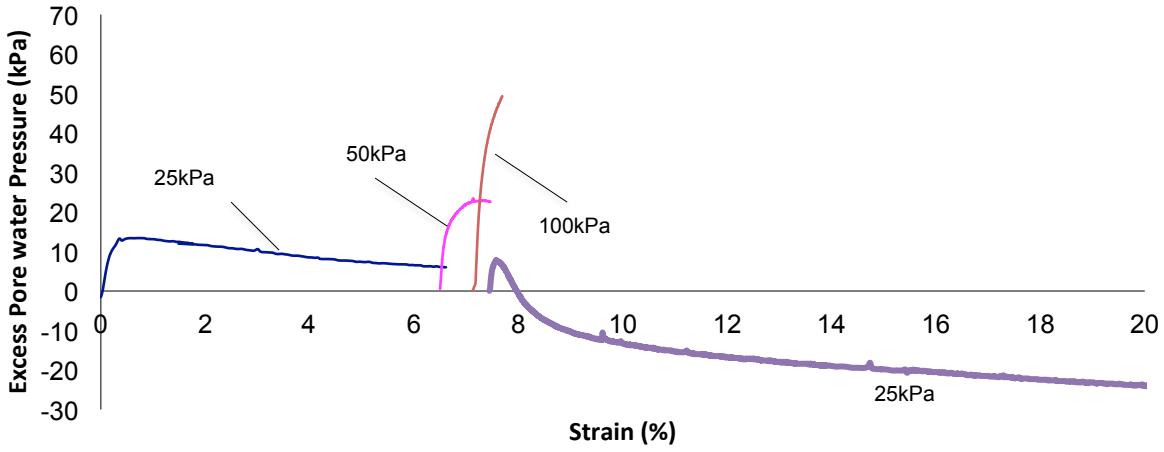

(a)

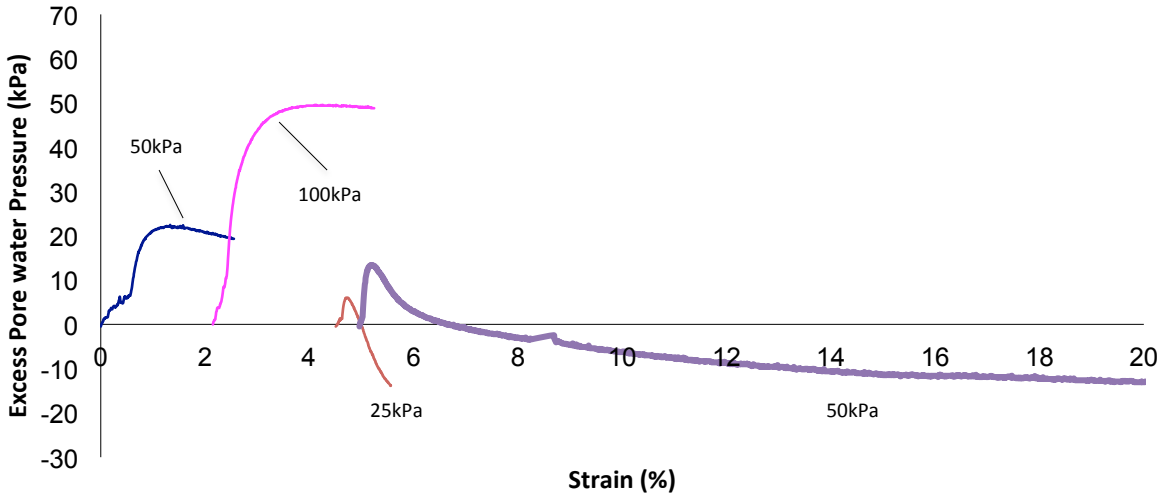

(b)

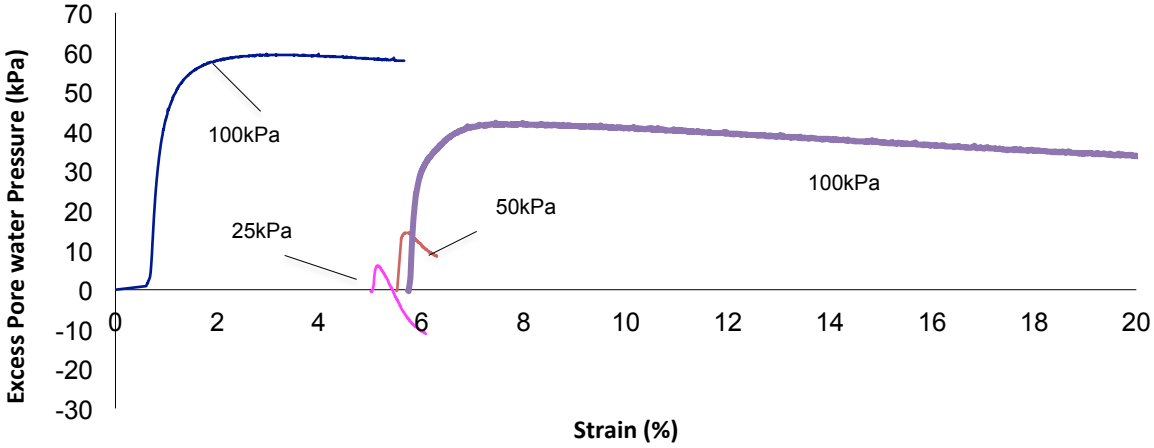

(c)

Figure 3.9 Variation of pore water pressure against axial strain for samples of Layer 1;(a) MZ1S1 (b) MZ1S2 (c) MZ1S3

3.5.3.2 Layer 1 - Critical state limit analysis

It was difficult to determine the critical state points directly from stress strain diagrams as the deviator stress value continued to change after the peak to the end of shearing for MZ1S1 and MZ1S2 (Figure 3.8a and 3.8b) and continuously increasing even at higher strain for MZ1S3 (Figure 3.8c). The relationships between these behaviours with the response of pore-water pressures against axial strain (Figure 3.9a, 3.9b and 3.9c) are also incompatible and consequently make the process of locating the failure points challenging. Therefore, the effective stress paths for each test have been used as alternative. Figure 3.10a, 3.10b and 3.10c present the effective stress paths of each test along with the indication of critical state points.

Based on the data measurements, it is apparent that the critical state only occurs during stage 4 of each sample. For samples MZ1S1 and MZ1S2 (Figure 3.10a and 3.10b), the selection for the critical state points was made based on the observation of a 'discontinuity' in value that can be seen after the maximum deviator stress was reached. At this point, the change in stress value is believed to occur due to strain localisation (i.e. narrow zone of intense shearing strain). On the other hand, the measured deviator stress for sample MZ1S3 (Figure 3.8c) shows inclination in value even at 20% strain. Hence, the maximum deviator stress at the final point of the stage (20% axial strain) was taken as to represent the condition of critical state. The ν against p' plots with the indication of critical state points for each tests are shown in Figure 3.11a, 3.11b and 3.11c.

In order to compare results from each test, it has been decided to carry out normalisation of the stress paths for each sample. Three established approaches have been described by (Atkinson and Bransby, 1978) and Atkinson (1993) for stress path normalisation, which are by using either p'_e, (the equivalent stress on the normal compression line), p'_c, (the equivalent stress on the critical state line) or v_λ, (the equivalent specific volume intercept). However, in consequence to the heterogeneity of the samples (reflected by the differences in initial void ratio for each sample in Table 3.4), none of the approaches was viable. This was due to the difficulty in establishing the unique position of the normal consolidation line (NCL) and the critical state line (CSL) on the ν against p' space.

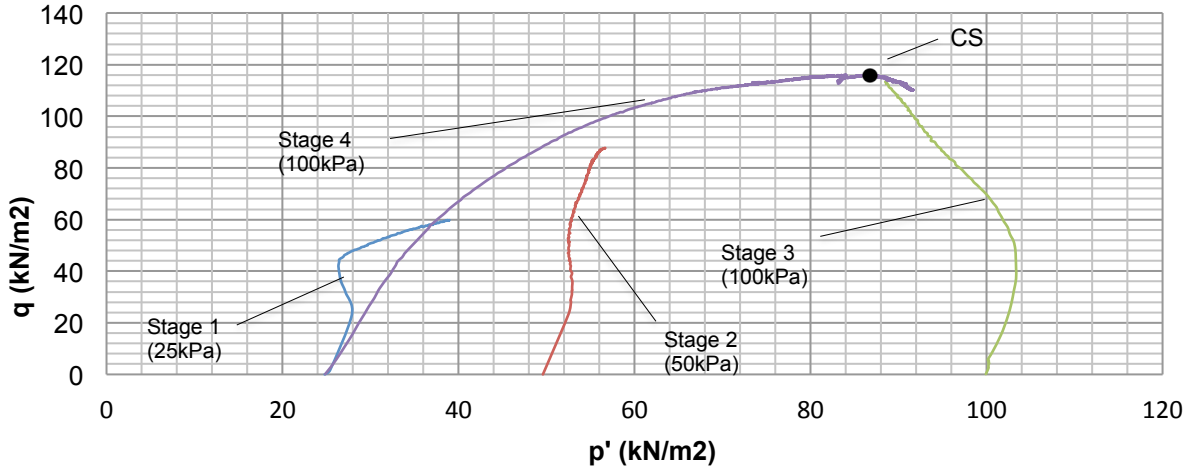

(a)

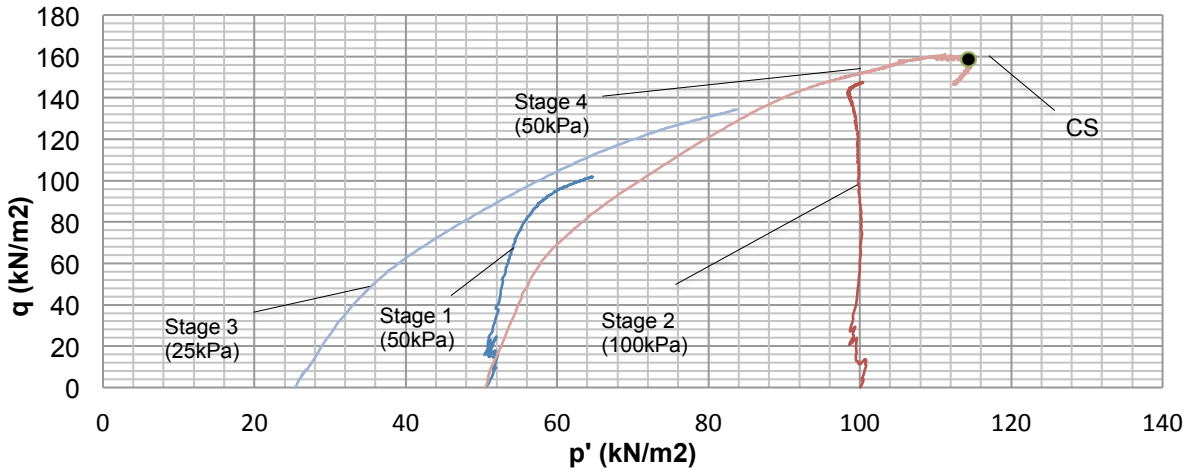

(b)

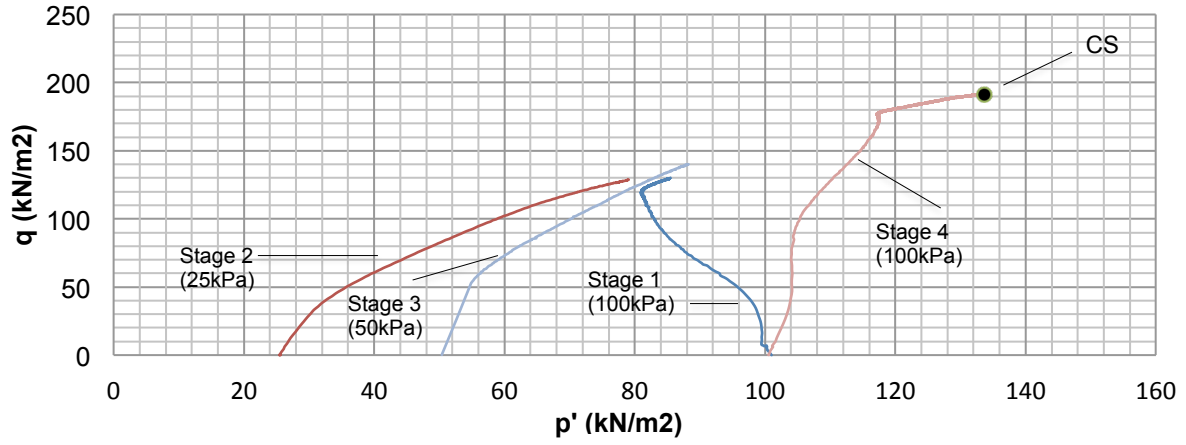

(c)

Figure 3.10 Effective stress paths for samples of Layer 1;

(a) MZ1S1 (b) MZ1S2 (c) MZ1S3

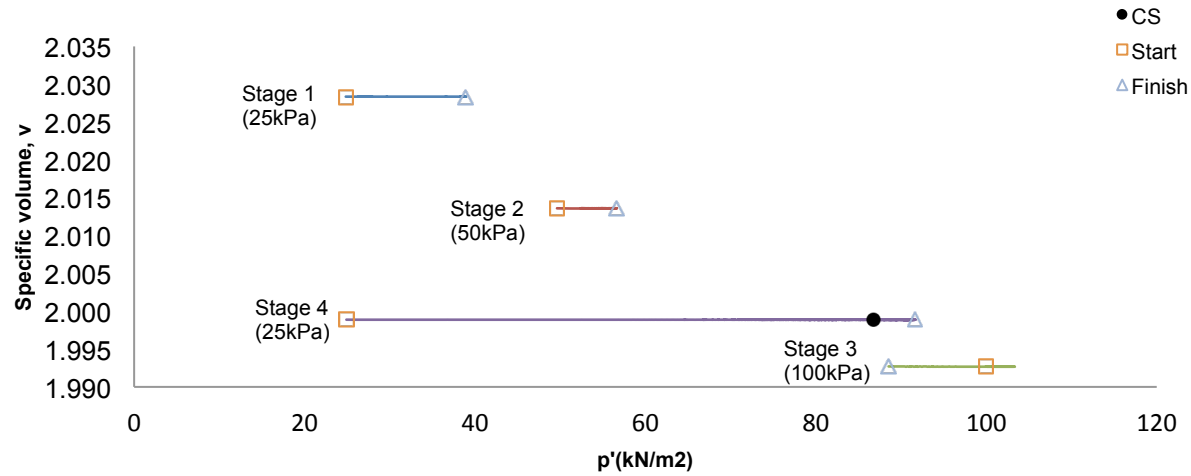

(a)

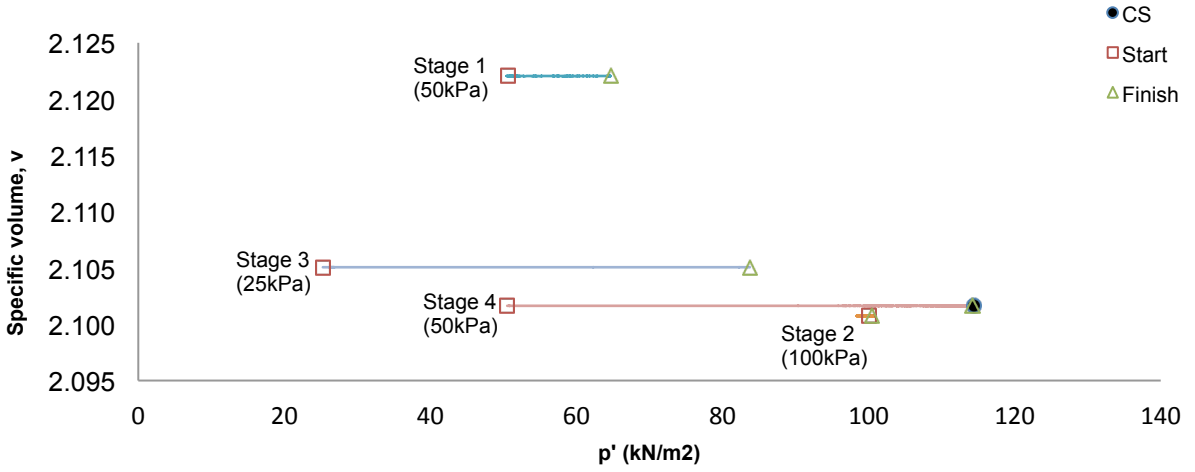

(b)

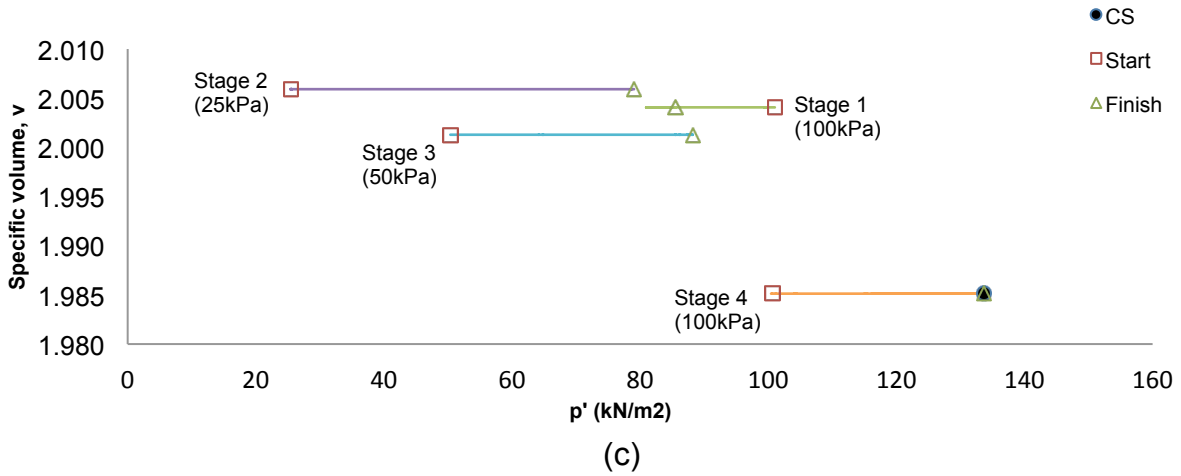

(c)

Figure 3.11 Specific volumes changes with effective stress,p' for samples of Layer 1;

(a) MZ1S1 (b) MZ1S2 (c) MZ1S3

Similar behaviour was also reported by many other researchers in regards to this variation in void ratio (e.g; Konrad, 1990, Yamamuro and Lade, 1998, Mooney et al., 1998, Hosseini et al., 2005, Ali Rahman, 2008). Fourie and Papageorgiou (2001) clarified that the difficulty in defining void ratio is due to errors arising during measurement of samples. The clarification was further agreed by Hosseini et al. (2005) through their description of the variation that was possibly due to error in void ratio calculation or most likely caused by the initial fabric and structure. Consequently, a refinement of the second approach (using p'_c) was also suggested by Hosseini et al. (2005) by describing the critical state as a zone rather than a unique line. By combining all data in one v-p' space plot, the zone with upper and lower bounds can be defined graphically so as to describe the critical state for heterogenous material. The normalisation of the stress path based on the critical state value of p'_c, by definition, should end up with p'/p'_c, =1 and $q/p'_c = M$.

As explained earlier, it was impossible to define a unique critical state line for the studied material; in consequence the p'_c value could not be simply defined for any void ratio for the normalisation of the stress paths. Therefore, a modification based on to the approach introduced by Hosseini et al. (2005) was made by adjusting the critical state value of p'_c for each sample, respectively. The adjustment of p'_c value was basically done by implementing a trial and error procedure for the determination of both λ and Γ parameters. The relationships between critical state value of p'_c, λ and Γ are expressed in Equation 3.6 as follows.

$$p'_c = \exp(\Gamma - v/\lambda) \quad \ldots (3.6)$$

where, Γ = the specific volume at p' = 1.0kPa

λ = slope of the CSL

To explain further, this graphical trial and error procedure was carried out by referring to the normalised stress path produced in q/p'_c against p'/p'_c plots. The procedure should be continued until the maximum point settled upon $p'/p'_c = 1$.

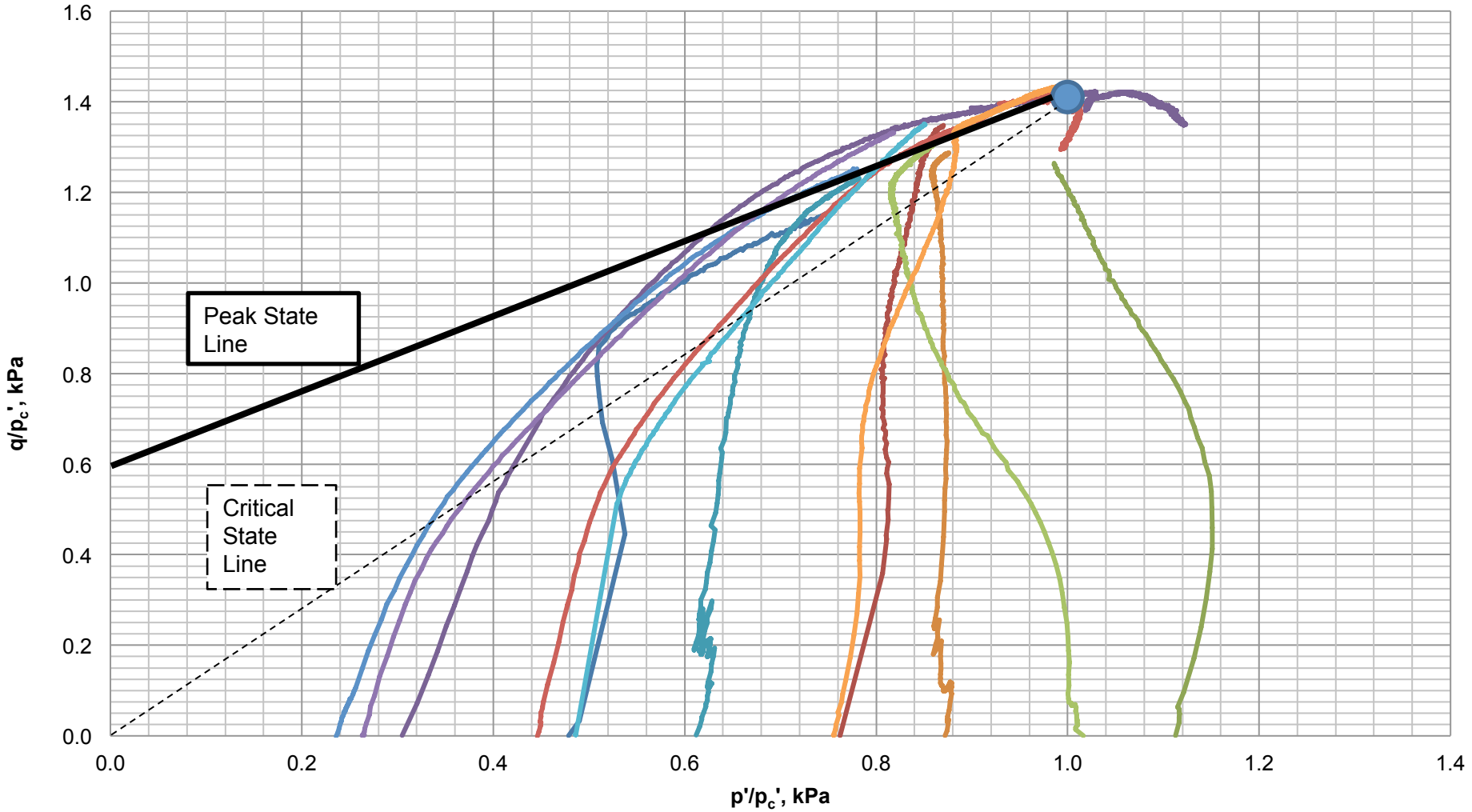

Figure 3.12 Normalised stress paths for the saturated samples of Layer 1.

Figure 3.12 presents the results for the normalised stress path obtained from the multistage tests on all three MZ1 samples. It can be seen that each curve moves towards p'/p'_c equal to 1, giving q/p'_c or M equal to approximately 1.43. A single peak state line has been defined on the graph for the determination of the peak strength. Based on the results, the projection of the peak envelope began at q intercept (in terms of q/p'_c) of 0.6 with gradient equal to 0.83 until it merges with CSL. The summary of the critical state parameters shown in Table 3.8 presents the attained CSL values and peak strength parameters for layer 1 samples.

Table 3.8 Critical state points and peak strength of each saturated test samples of Layer 1.

Sample	Stage	p' kPa	v_f	λ	Γ	M	$Ø_{cr}$ (°)	q_{cr} kPa	H	g_p'	g'	q_p kPa	$Ø_p$ (°)
MZ1S1	1	25	2.028	0.07	2.29	1.43	35	35.75	0.83	0.60	20.75	51.86	21
	2	50	2.014					71.50			39.05	80.55	
	3	100	1.993					143.00			53.87	136.87	
	4	25	1.999					35.75			48.96	69.71	
MZ1S2	1	50	2.122	0.07	2.41			71.50			49.61	91.11	
	2	100	2.101					143.00			68.83	151.83	
	3	25	2.105					35.75			64.40	85.15	
	4	50	2.102					71.50			67.89	109.39	
MZ1S3	1	100	2.004	0.07	2.30			143.00			59.63	142.63	
	2	25	2.006					35.75			57.96	78.71	
	3	50	2.001					71.50			62.24	103.74	
	4	100	1.985					143.00			79.80	162.80	

To justify these parameters, the slope of the critical state lines in the v – lnp' plane are plotted based on these respective λ and Γ parameters values (Figure 3.13). Good agreement can be seen and it shows the CS zone as suggested by Hosseini et al. (2005). The difference between the upper limit and lower limits represents a variation of ±0.1 in terms of specific volume.

Figure 3.14 shows the critical state in a q- p' space. The plotted critical state points exhibit a unique straight line crossing through each failure points on the stress paths, or wet paths moving towards this line, giving a slope of M equal to 1.43. This value is equivalent to a critical state angle of friction, ϕ' of 35°.

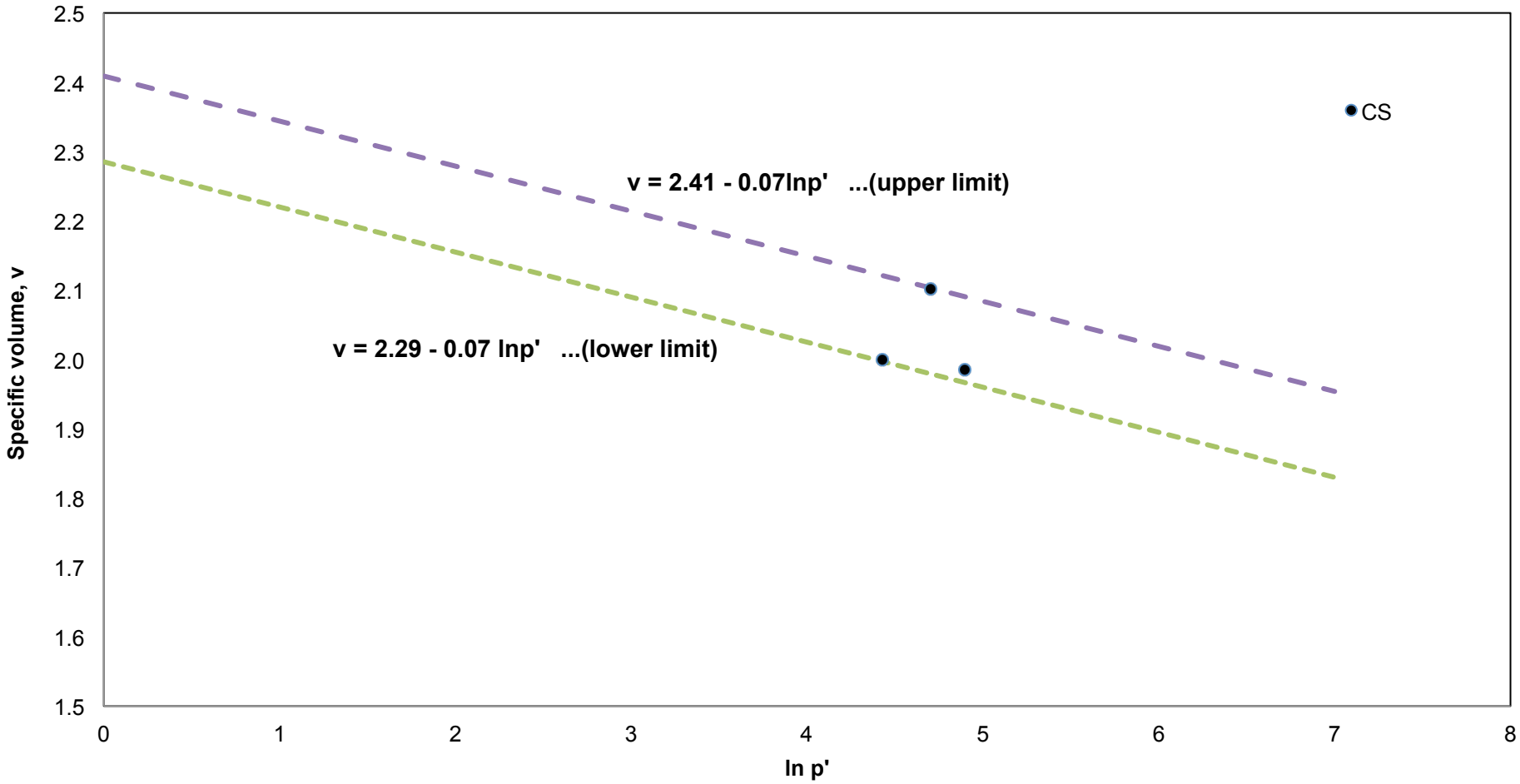

Figure 3.13 Critical state line for the saturated test series in v – lnp' of Layer 1.

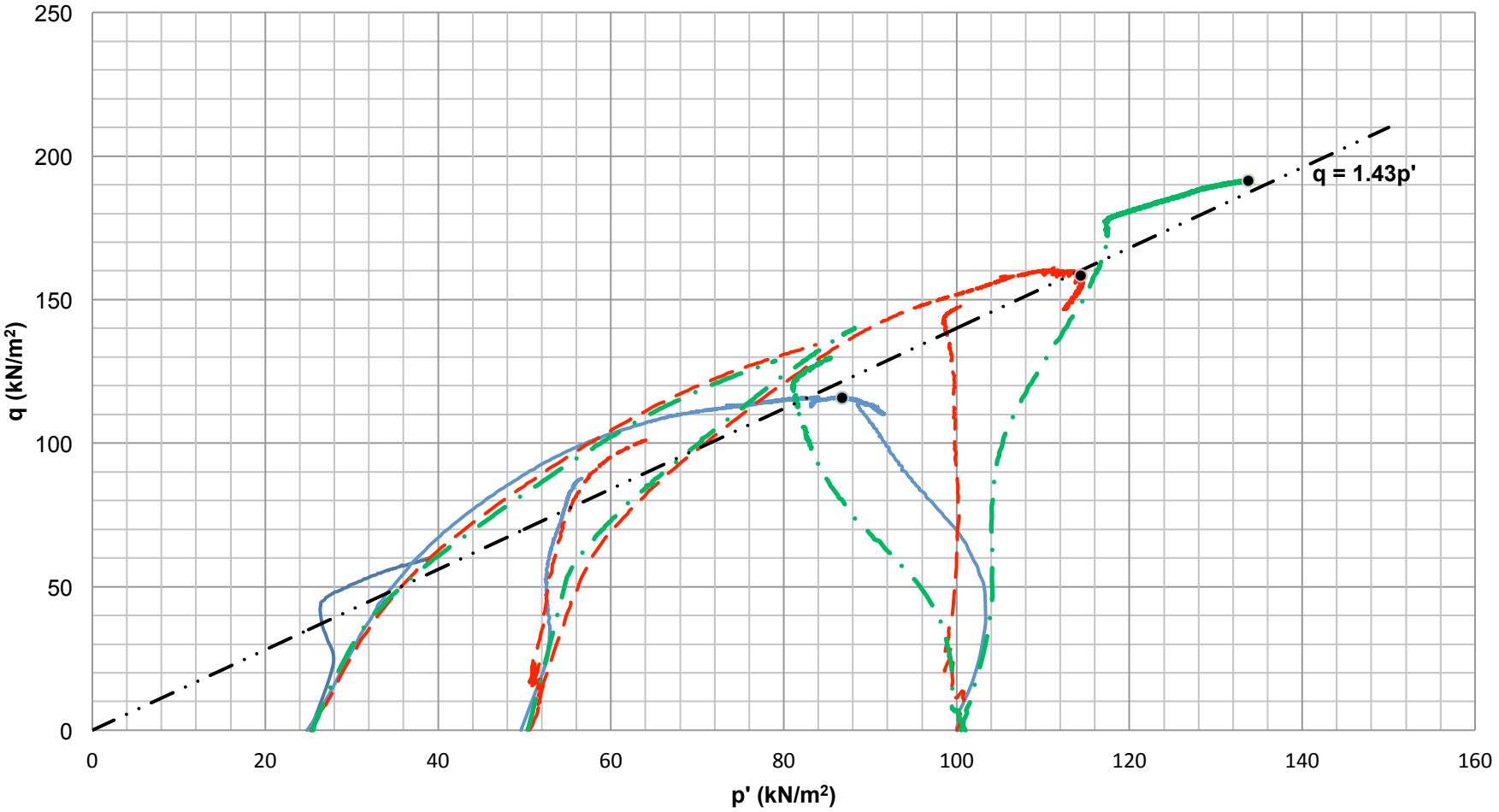

Figure 3.14 Critical state line for the saturated test series in q – p' of Layer 1.

3.5.3.3 Layer 2 - Tests Results

The conditions before and after saturation stage of each sample for layer 2 are shown in Table 3.9. Similarly, the dry mass of solids was measured from the oven-dried samples for the determination of the degree of saturation. From the results, it shows that every sample experienced an increase in degree of saturation (higher than 95%) and reduction in volume of air in consequence of the saturation procedure.

Table 3.9 Sample conditions before and after saturation stage for Layer 2.

Soil samples	M_{dry} (ovendried)	V_s	V_v	Before saturation			After saturation		
				V_w	V_a	S_r	V_{w2}	V_{a2}	S_{r2}
	g	cm^3	cm^3	cm^3	cm^3	%	cm^3	cm^3	%
MZ1S1	895.27	319.74	309.10	216.93	92.18	70.2	301.93	7.18	97.7
MZ1S2	902.01	322.15	301.88	248.14	53.74	82.2	293.14	8.74	97.1
MZ1S3	1064.62	380.22	226.18	152.43	73.75	67.4	221.43	4.75	97.9

A similar multistage triaxial procedure was implemented on the soil samples obtained from MZ3 and MZ4, representing layer 2 of the slope. The arrangement for the process for both consolidation and shearing stages applied to these samples, were 25, 50 and 100 (Table 3.2). It has been observed that the variations in regards to the imposition of different confining pressures in each stage are similar to the preceding tests on layer 1. In Table 3.10, the similarity can be seen by the decrease in volume when samples were consolidated to higher effective stresses and volume increased as lower subsequent pressures being applied.

Figure 3.15a, 3.15b and 3.15c present the changes in the deviatoric stress against axial strain for these second series of saturated tests during each shearing stage. Again, none of the samples seems to experience excessive destructurisation effects as described in Figure 3.5. In general, the deviator stress value (shear strength of the soil) on the final stage for each sample, show higher value compared to initial stage and for stage 2 and 3, increasing corresponding to the increase of effective stresses. The strains per stage due to multistage process vary between 0.5% to 3%.

For sample MZ4S2 (Figure 3.15b), however, the shearing process was ended at a total strain of approximately 7%. The reason for this was because during testing, it was observed that the deviator stress suddenly dropped in value. It has to be noted that natural cracks were seen clearly on the specimen, which can be associated with the failure. Nevertheless, the results for this sample are still comparable for the derivation of strength parameters for Layer 2 as discussed later in the chapter.

Table 3.10 Sample conditions at the start and end of the constant water compression stage for Layer 2.

Soil samples	Initial Water Content	Stage no	Effective Stress	Consolidation	Volume	Dry Density	Void Ratio	Degree of Saturation
			σ_c		V	ρ_{dry}		S_r
	%		kPa		cm^3	Mg/cm^3	e	%
MZ3S1	24.23	1	25	Initial	628.84	1.424	0.967	97.7
				Final	624.53	1.434	0.953	97.6
		2	50	Initial	624.53	1.434	0.953	97.6
				Final	619.96	1.444	0.939	97.6
		3	100	Initial	619.96	1.444	0.939	97.6
				Final	613.50	1.459	0.919	97.6
		4	25	Initial	613.50	1.459	0.919	97.6
				Final	615.42	1.455	0.925	97.6
MZ4S2	27.51	1	25	Initial	624.02	1.445	0.937	97.1
				Final	617.99	1.460	0.918	97.0
		2	50	Initial	617.99	1.460	0.918	97.0
				Final	611.80	1.474	0.899	97.0
		3	100	Initial	611.80	1.474	0.899	97.0
				Final	613.06	1.471	0.903	97.0
		4	25	Initial	613.06	1.471	0.903	97.0
				Final	612.06	1.474	0.900	97.0
MZ4S3	14.3175	1	25	Initial	606.40	1.756	0.595	97.9
				Final	589.96	1.805	0.552	97.7
		2	50	Initial	589.96	1.805	0.552	97.7
				Final	590.50	1.803	0.553	97.7
		3	100	Initial	590.50	1.803	0.553	97.7
				Final	589.14	1.807	0.549	97.7
		4	25	Initial	589.14	1.807	0.549	97.7
				Final	584.38	1.822	0.537	97.7

Figure 3.16a, 3.16b and 3.16c presents the relation between pore water pressure and axial strains during shearing. It is observable that each sample shows a sudden increase in pore water pressure and gradually reduces as axial strain progresses (i.e. dilatant tendency causing pore-water pressures drop).

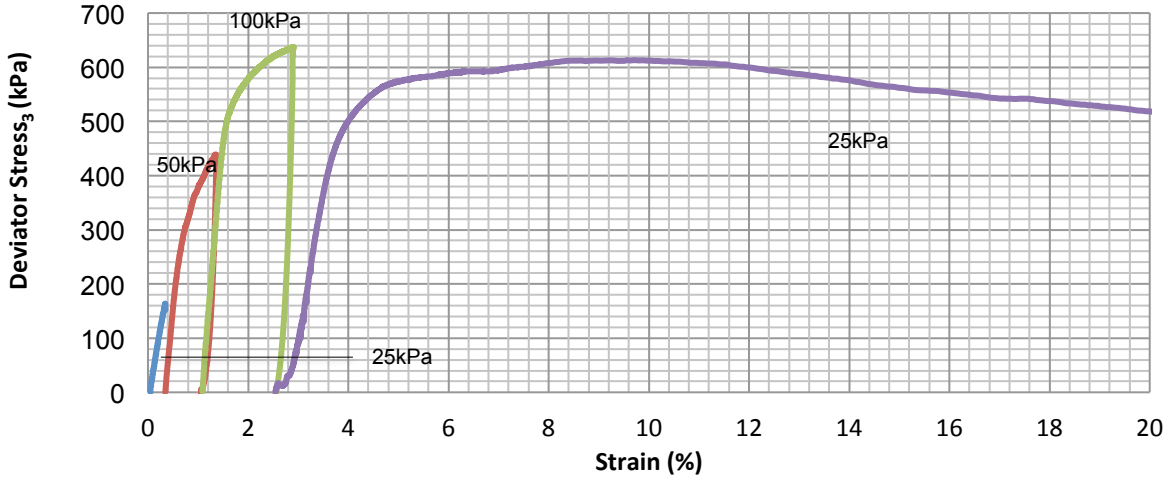

(a)

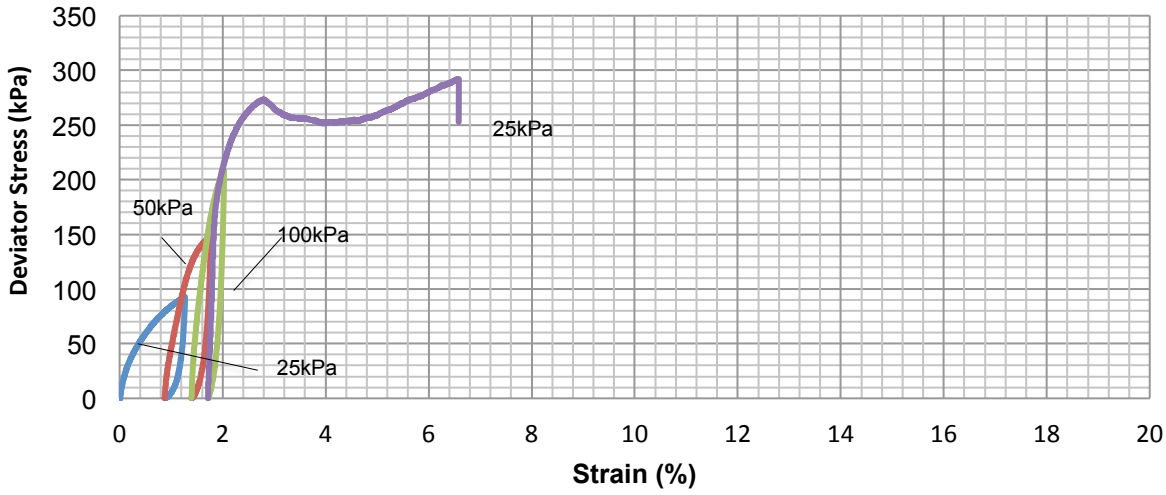

(b)

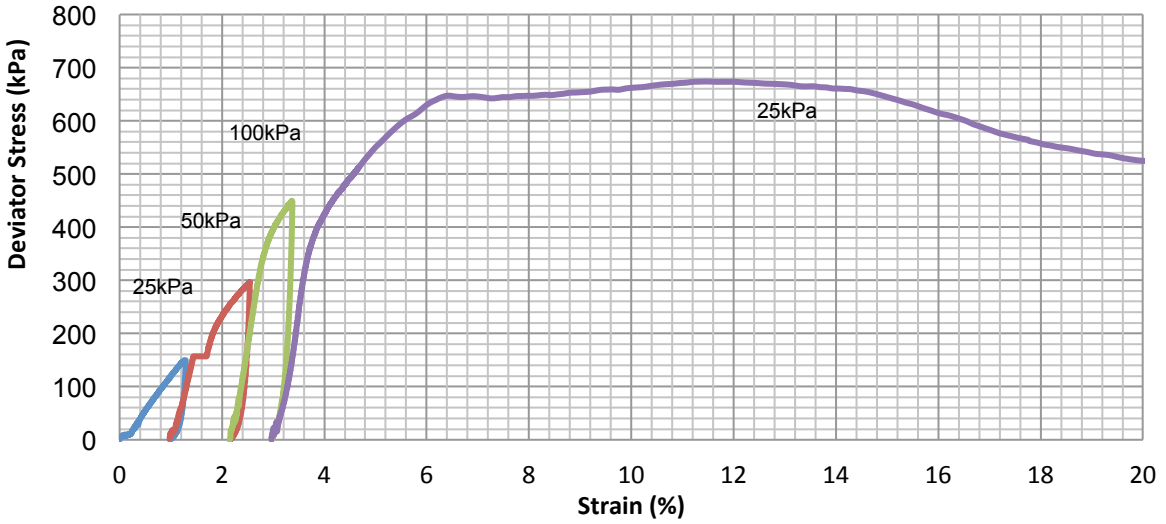

(c)

Figure 3.15 Deviatoric stress against strain for samples of Layer 2

(a) MZ3S1 (b) MZ4S2 (c) MZ4S3

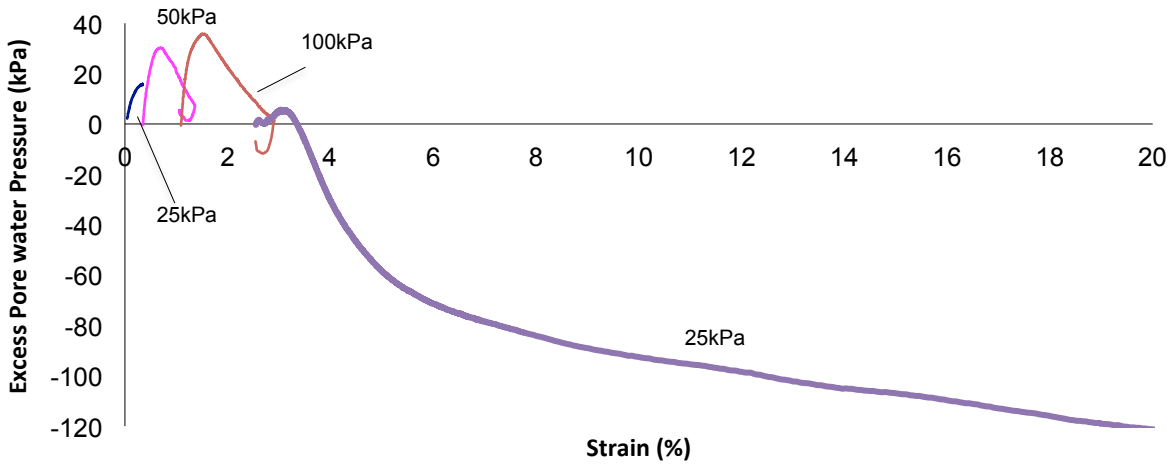

(a)

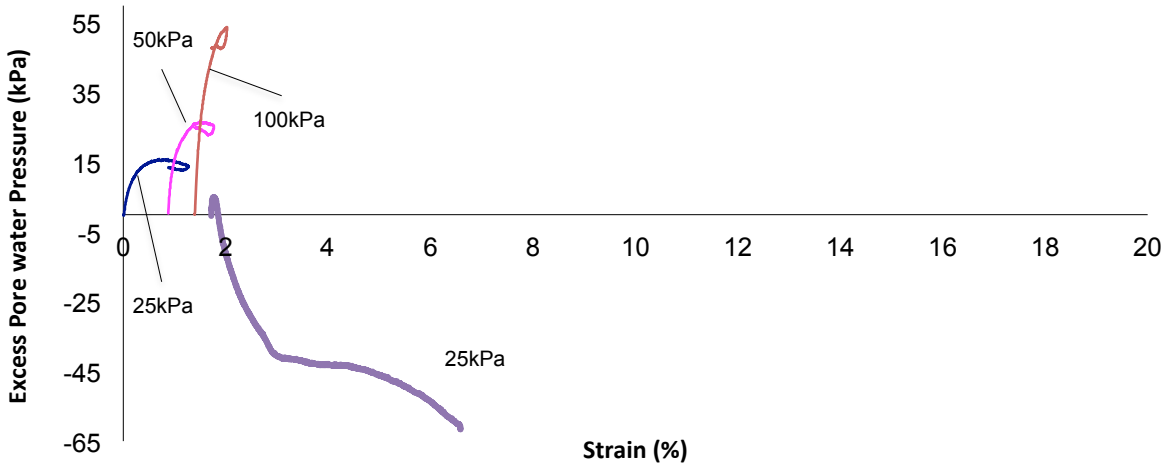

(b)

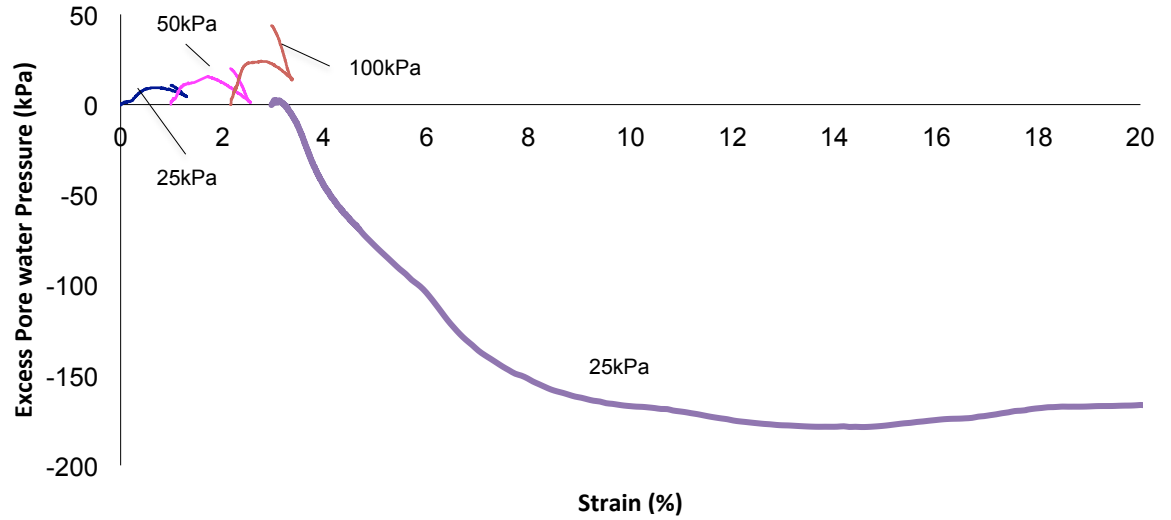

(c)

Figure 3.16 Variation of pore water pressure against strain for samples of Layer 2; (a) MZ3S1 (b) MZ4S2 (c) MZ4S3

3.5.3.4 Layer 2 - Critical state limit analysis

As for the analysis of layer 1, the selection of the critical state points for samples MZ3S1, MZ4S2 and MZ4S3 was made based on the effective stress paths shown in Figure 3.17a, 3.17b and 3.17c. From the graphs, it is apparent that the mean stress value in stage 4 of each sample, started to reduce after the maximum deviator stress value was reached. This stress reduction behaviour is believed to be due to the developments of a shear band within the sample. For comparison, the ν against p' plots with the indication of critical state points for each tests are also shown in Figure 3.18a, 3.18b and 3.18c.

For results comparison of layer 2 with layer 1, the same normalisations of the stress paths technique were carried out. The modified stress normalisation technique using the effective mean stress corresponding to the void ratio on the CSL (full description in 3.5.3.2), was done once more by adjusting the critical state value of p'_c for each sample, respectively. The value of p'_c which was deduced from the relationships with both λ and Γ parameters, expressed in Equation 3.5, once again being calculated using the trial and error procedure for the determination of both critical state parameters for each sample.

Figure 3.19 presents the results of the normalised stress paths for each stage obtained from the second series of saturated tests. From the graph, it is noticeable that only stress path curves for samples MZ4S2 and MZ4S3 present good agreement by curving towards p'/p'_c equal to 1, giving q/p'_c or M equal to approximately 1.60. However, for the stress path curves for sample MZ3S1, a slightly higher q/p'_c or M value of approximately 1.89 was obtained. Similar behaviours also can be seen on the peak strength parameters for each sample. These differences can be justified by the visible dissimilarity in characteristics shown in Figure 2.14 (Chapter 2), which is possibly related to the variation in degree of cementation of the sample (weathering grade).

Table 3.11 presents the summary of the attained CSL values and peak strength parameters for all three samples. Although there is a difference in M value, the obtained CSL parameter values of λ and Γ are seemingly in good agreement with 0.07 as the value for λ and Γ ranges between 1.975 to 2.358.

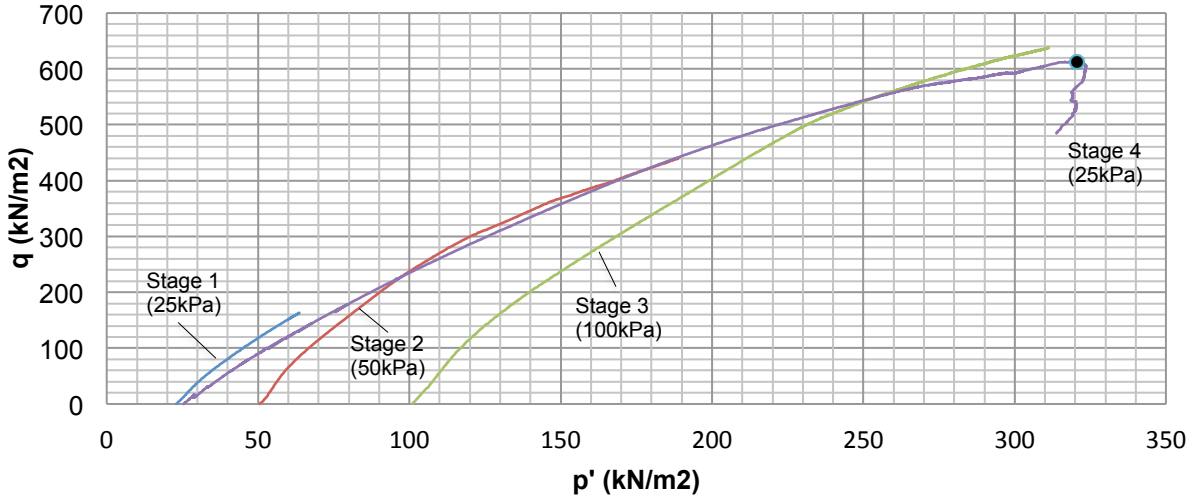

(a)

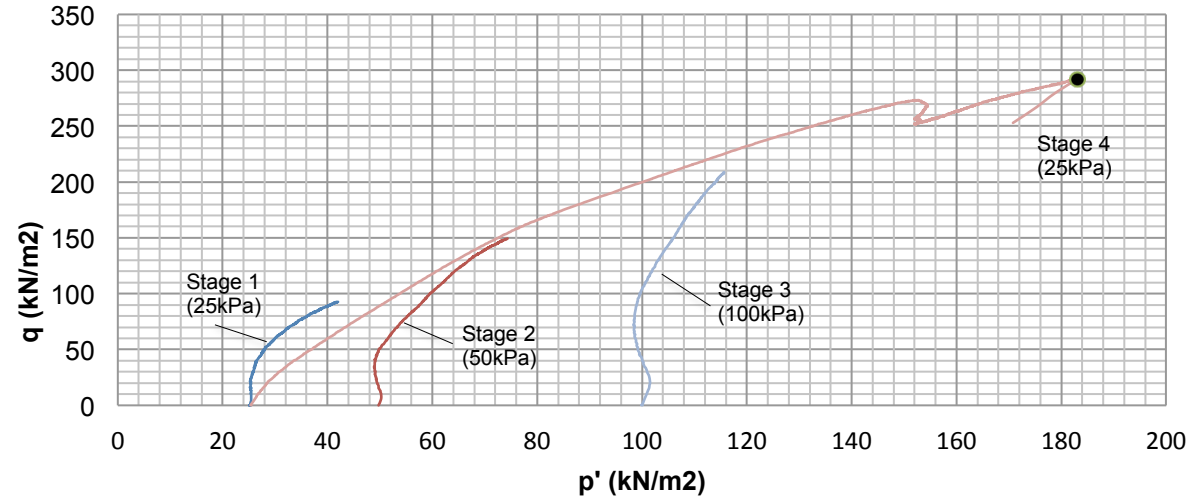

(b)

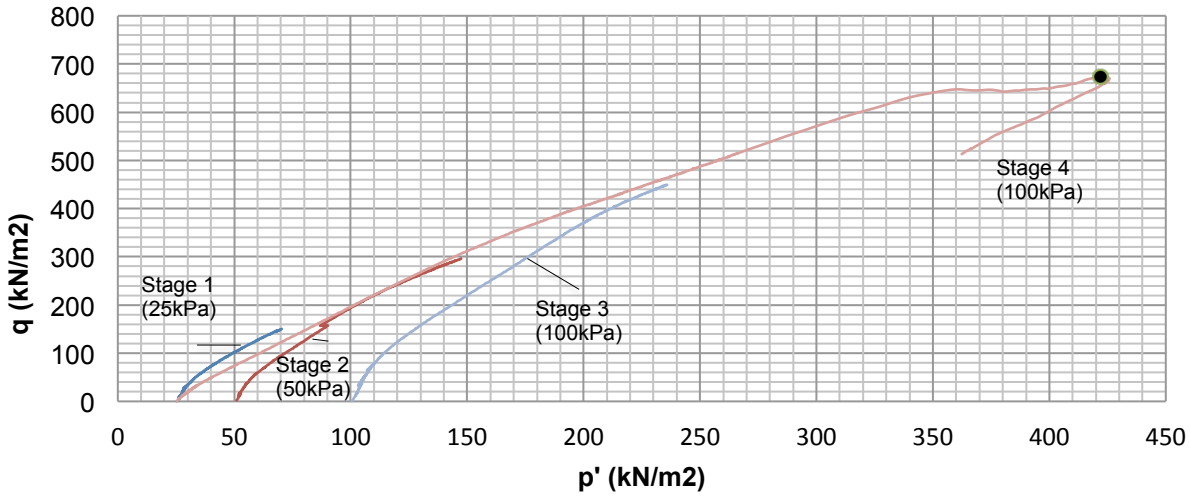

(c)

Figure 3.17 Effective stress paths for samples of Layer 2;
(a) MZ3S1 (b) MZ4S2 (c) MZ4S3

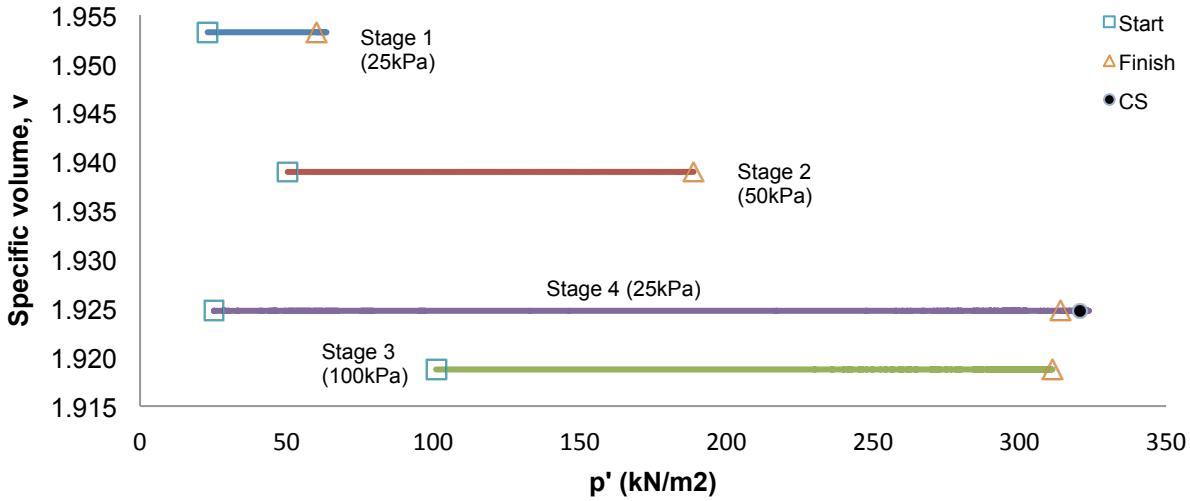

(a)

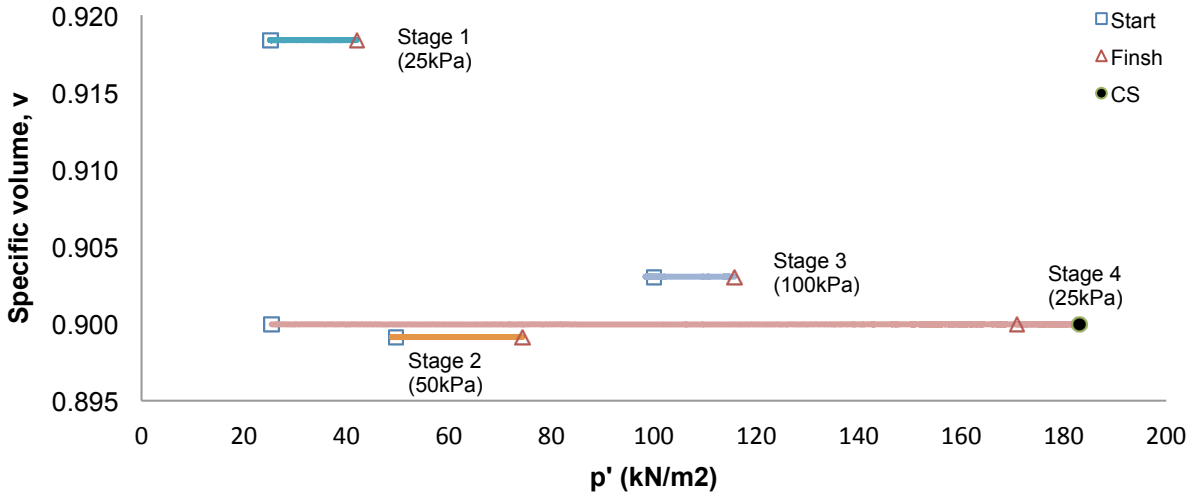

(b)

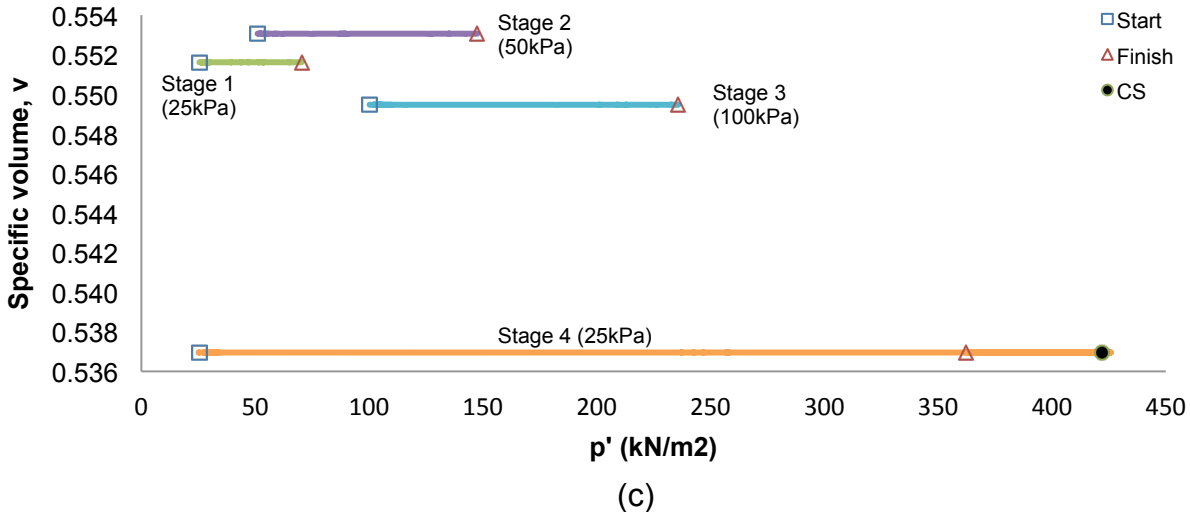

(c)

Figure 3.18 Specific volumes changes with effective stress,p' for samples of Layer 2; (a) MZ3S1 (b) MZ4S2 (c) MZ4S3

Table 3.11 Critical state points of each saturated test samples of Layer 2.

Sample	Stage	p' kPa	v_f	λ	Γ	M	q_{cr} kPa	$\emptyset_{cr}$ (°)	H	g_p' kPa	g' kPa	q_p kPa	$\emptyset_p$ (°)
MZ3S1	1	25	1.953	0.07	2.358	1.89	47.3	46	1.19	0.70	225.53	255.3	30
	2	50	1.939				94.5				276.60	336.1	
	3	100	1.919				189.0				369.16	488.2	
	4	25	1.925				47.3				338.83	368.6	
MZ4S2	1	25	1.918	0.07	2.283	1.60	47.3	39	1.30	0.30	54.87	87.4	32
	2	50	1.899				94.5				72.23	137.2	
	3	100	1.903				189.0				68.31	198.3	
	4	25	1.900				47.3				71.40	103.9	
MZ4S3	1	25	1.552	0.07	1.975		47.3				127.20	159.7	
	2	50	1.553				94.5				124.63	189.6	
	3	100	1.549				189.0				131.18	261.2	
	4	25	1.537				47.3				156.85	189.3	

The slope of the critical state lines in the v – lnp' plane are also plotted based on these respective λ and Γ parameters values (Figure 3.20). The CS zone as suggested by Hosseini et al. (2005) can be justified by the lines indicated by the upper limit and lower limits with a variation of ±0.38 in terms of specific volume.

Figure 3.21 shows the critical state in q- p' space. The plotted critical state points exhibit a unique straight line crossing through each failure point on the stress paths, giving a slope of M equal to 1.60 for both MZ4S2 and MZ4S3 and 1.89 for MZ3S1. These values are equivalent to a critical state angle of friction, ϕ' of 39° and 46°, respectively.

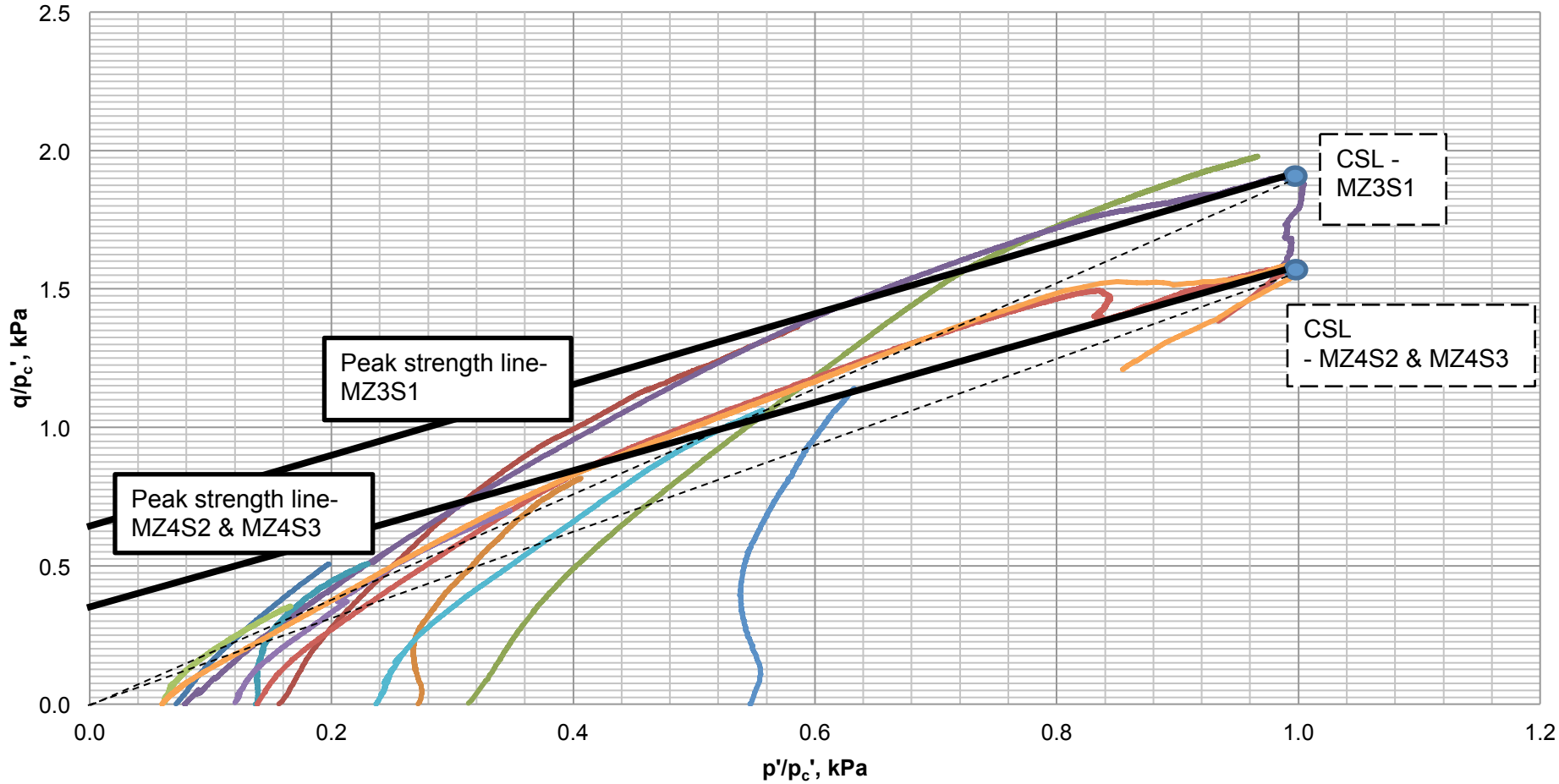

Figure 3.19 Normalised stress paths for the saturated samples of Layer 2.

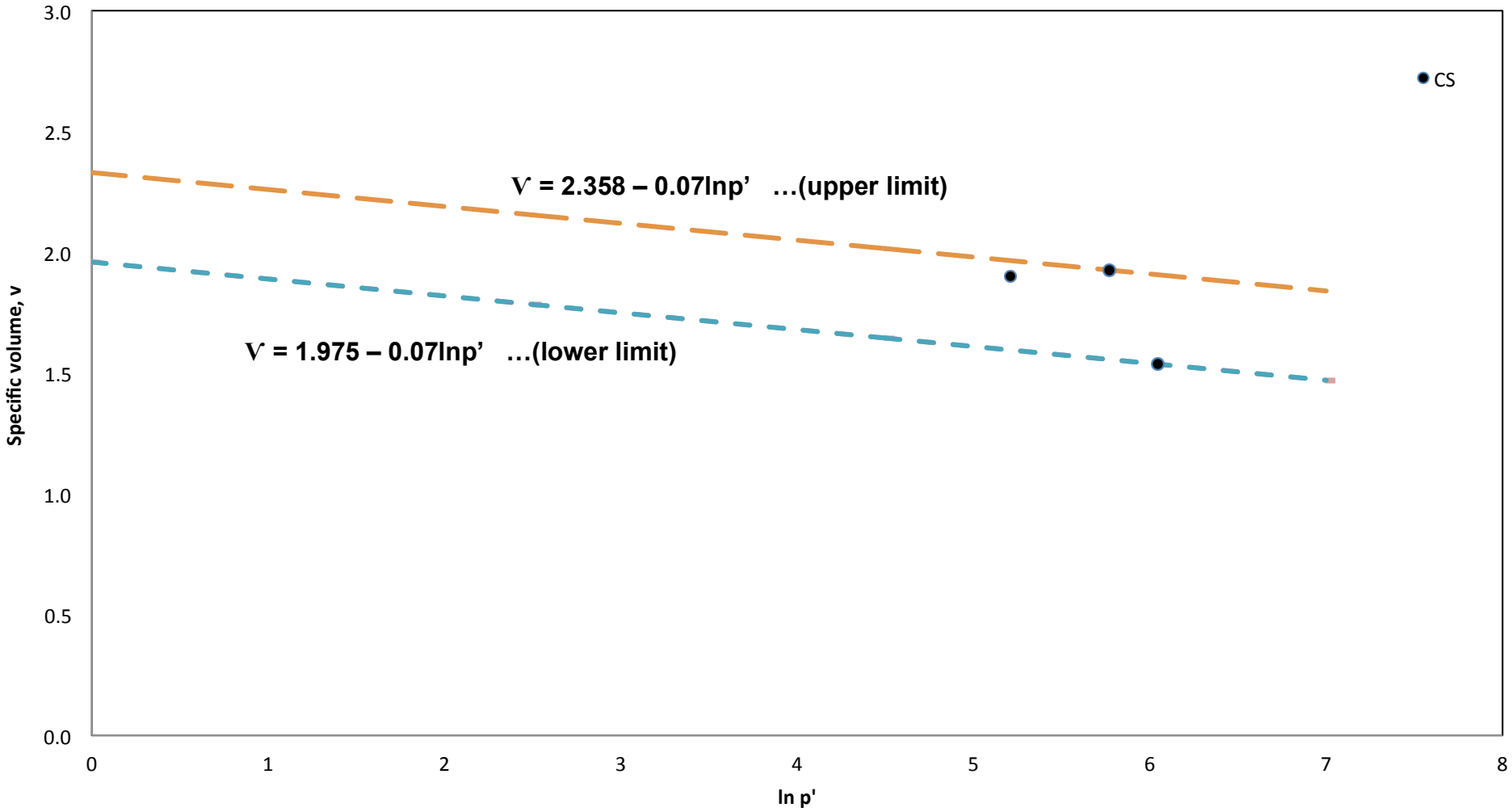

Figure 3.20 Critical state line for the saturated test series in v – lnp' of Layer 2.

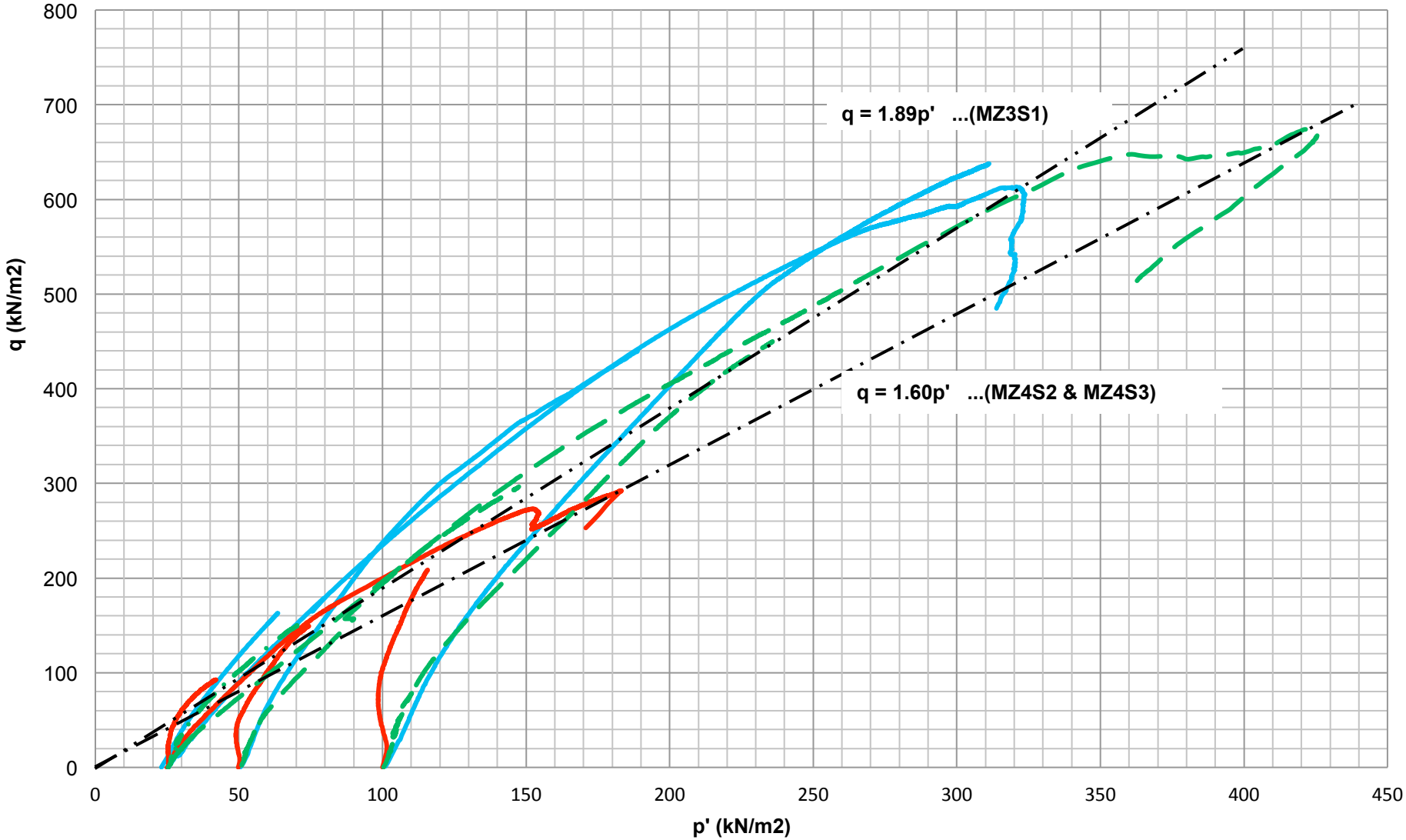

Figure 3.21 Critical state line for the saturated test series in q – p' of Layer 2.

3.6 Unsaturated Soil Tests

3.6.1 Configuration of Triaxial Test System and Procedures

It has been explained in section 3.2.6 that triaxial testing of unsaturated soils can be carried out either under a constant suction condition or a constant water content condition. For a constant suction condition, the test requires a suction control system to maintain the desired suction value applied within the soil. Such tests can be time consuming, as drainage of water is dependent on the permeability function of the soil. Thus, the experiments to understand the mechanical behaviour of residual soils under unsaturated conditions were carried out based on the constant water content concept, where the changes of suction were measured using a high capacity tensiometer fixed in the centre of a customised base pedestal. The concept was preferred to prevent the possibility of the natural packet fabric (soil aggregation) in the soil to be destroyed due to the suction controlled process (if wetted or saturated) and to preserve the 'in situ' condition of the soil (Toll, 1990, 2000). With the water content of the soil fixed as constant, the variation in the suction value was measured by tensiometer during shearing. Full details of the type of tensiometer used in these tests are presented in section 3.2.6.2.

Similar to saturated tests, the constant water content tests (CW) were also performed in a multistage test procedure, with the arrangements of the stages given in Table 3.3. Prior to shearing, samples were subjected to an initial equalisation stage (to measure the initial suction) followed by constant water content compression to impose the required cell pressure. During the equalisation stage each soil sample was subjected to 25 kPa cell pressure together with an elevated air pressure applied at the bottom of the sample (20 kPa). This process was to remove air bubbles within the inner cell (Figure 3.7). The net stress $(\sigma\text{-}u_a)$ was maintained close to zero (5kPa or less). The air pressure imposed on the soil sample was supplied through two air entry holes within the customised 75mm diameter size base pedestal. No drainage was provided by the solid 75mm diameter top cap. The equalisation stage was continued until no further significant volume change was recorded in the volume gauge and the suction measurements were stable.

It has to be noted that CW does not imply constant volume, as samples can still change in volume due to the compressibility of air component when stresses are applied. For that reason, a double cell was utilised, the Wykeham Farrance (WF) double cell triaxial system (Figure 3.22). The WF double cell is similar to Wheeler's modified triaxial cell (Wheeler, 1988), though, it differs in that the interior cell wall was made of glass instead of Perspex. The intention is to prevent any water absorption by the wall of the inner cell. By applying an equal cell pressure inside and outside the inner cell, any error due to expansion of the cell is eliminated; hence, no volume change in the inner cell is caused by cell pressure. Details of the cell components and system calibrations have been reported comprehensively by Mendes (2011) and Mendes et al. (2012). The full configuration of the WF double triaxial cell can be seen in Figure 3.23.

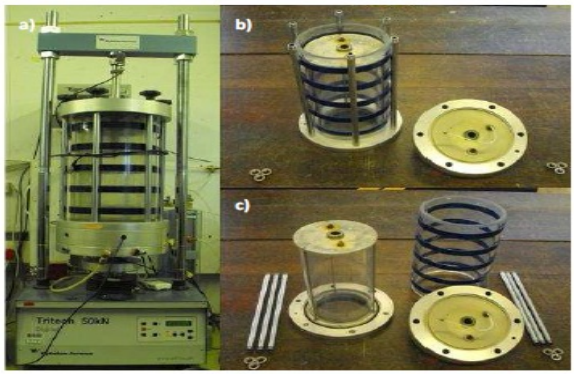

Figure 3.22 Wykeham Farrance double cell triaxial system; (a) fully assembled, (b) without outer cell top cap (c) view of the inner cell (after Mendes, 2011).

After equalisation, the compression stage was started when the confining pressure was elevated to a desired value whilst the elevated air pressure applied to the bottom of the sample was gradually reduced to zero. This sample compression process due to the compressibility or flow of the air component within the soil was continued until no further significant volume change was recorded in the volume gauge for the inner cell. Furthermore, valve 13 in Figure 3.23 would also be opened to atmospheric pressure to prevent any build-up of pore air pressure (maintaining u_a equal to zero). During this process, pore water pressure was monitored using the tensiometer.

Lastly, the samples were sheared and the changes in suction, deviator stress, axial and volume strains were measured throughout the process. The process for both compression and shearing would be repeated based on the stress arrangements tabulated in Table 3.3. A strain rate of 0.02mm/min was used for every shearing process.

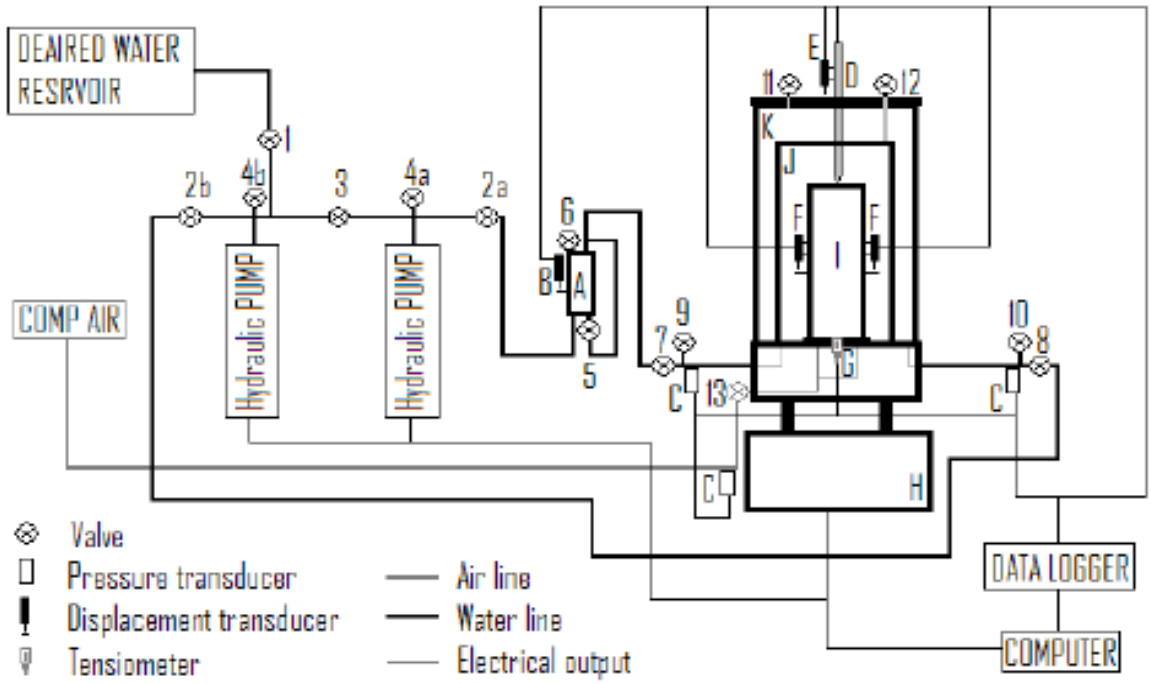

Letter	
A	Volume gauge
B	Volume change transducer
C	Pressure transducer
D	Load cell
E	Axial displacement transducer
F	Mini LVDT
G	Suction probe
H	Loading frame
I	Sample
J	Inner cell
K	Outer cell

Valves	
1	Main deaired water supply
2a	Water supply/pressure line – inner cell
2b	Water supply/pressure line – outer cell
3	Separator valve
4a	Bleed valve – hydraulic pump
4b	Bleed valve – hydraulic pump
5	Overlap – volume gauge
6	Bleed valve – volume gauge
7	Main valve - inner cell
8	Main valve - outer cell
9	Drain valve - inner cell
10	Drain valve - outer cell
11	Bleed valve – outer cell
12	Bleed valve – inner cell
13	Air supply – sample

Figure 3.23 Configuration of constant water content triaxial testing apparatus for unsaturated tests (after Mendes, 2011).

3.6.2 Initial Condition of Residual Soil Samples

The soil classification tests results presented in Chapter 2 show that samples from MZ2 and MZ1a are of similar material to represent Layer 1 (from 1m to 3m depth). In Table 3.12, the variations in water content for both initial and air-dried conditions are shown, as well as the changes in mass and pore-water pressures. The water content measurements were carried out immediately after the sample was prepared (trimmed materials from top and bottom part of the sample) and at the end of the test by oven drying the sheared samples for 24 hour as according to BS1377: 1990 (for back calculation of water content).

The air-drying process was implemented on each sample in order to investigate the effects when the soils become drier (increasing suction). Each sample was left uncovered on the pedestal with an attached high capacity tensiometer touching the bottom part of the sample for the suction measurements. Once the desired suction value was achieved, the volume of the sample would be measured before enclosing it with a rubber membrane.

The dimensions at top, mid and bottom part of the sample were taken manually using a Vernier Caliper for volume measurements for both initial and air-dried conditions. However, the results showed only small change in volume due to the low matric suction values that caused minimal volumetric strain (<0.01%) in the samples. The volume measurements taken after air-drying are presented in Table 3.12 and these were used for the calculations of soil properties tabulated in Table 3.13.

Good agreement can be seen for dry densities and volumetric water content despite the variations in degree of saturation, which is mainly due to water content. The heterogeneity, of course, is also one of the factors causing to the variations in void ratio, in addition to the presence of organic materials (i.e. tree roots etc.) and fissures in the samples.

Table 3.12 Initial conditions for unsaturated triaxial test samples before and after air drying process.

Soil samples	Initial			After Air-dried			Dimensions			
	Water content	Mass	Pore water pressure	Water content	Mass	Pore water pressure	h	d	A	V
	%	g	kPa	%	g	kPa	cm	cm	cm^2	cm^3
MZ2US1	26.0	1232.0	-19	25.4	1229.0	-22	15.05	7.23	41.09	618.23
MZ2US2	26.6	1204.3	-22	25.8	1199.5	-119	15.06	7.21	40.79	614.40
MZ2US3	27.0	1208.5	-35	26.3	1205.3	-49	15.04	7.24	41.22	619.89
MZ1aUS4	30.0	1110.2	-33	28.9	1101.4	-220	15.17	7.14	40.04	607.33
MZ1aUS5	29.4	910.6	-30	28.5	905.4	-155	15.11	6.44	32.57	492.29

Table 3.13 Soil properties at the start of the constant water tests.

Soil samples	Density		Void Ratio	Degree of Saturation	Volumetric Water Content	Matric Suction
	Bulk	Dry				
	ρ	ρ_{dry}		S_r	θ_w	u_a-u_w
	Mg/cm^3	Mg/cm^3	e	%		kPa
MZ2US1	1.99	1.59	0.77	92.7	0.402	22
MZ2US2	1.95	1.55	0.80	89.8	0.400	119
MZ2US3	1.94	1.54	0.82	89.8	0.404	49
MZ1aUS4	1.81	1.41	0.99	81.8	0.407	220
MZ1aUS5	1.84	1.43	0.96	83.4	0.408	155

3.6.3 Constant Water Compression Tests Results

Subsequent to the equilibrium stage was the constant water compression stage (CWC). Each sample would be subjected to isotropic stress in accordance to the stress arrangements shown in Table 3.3.

The results for the CWC stage are presented in Table 3.14a and 3.14b, which show the conditions of each sample at the time of the start and end of each stage. During the first three stages where stresses were increasing (25, 50 and 100kPa), the void space of the sample reduced thus increasing the saturation level. For the fourth stage (where samples were unloaded back to 25kPa), the void space of the sample increased (swelling), causing a reduction in the degree of saturation.

This general tendency during CWC can also be seen in the variation of suction value measured by the high capacity tensiometer. The reduction in volume of the samples caused suctions to decrease, relating to the increase in the degree of saturation under constant water conditions. This reduction of measured suction, however, remained in positive values in each stage (i.e. no positive pore water pressures were generated during compression).

During compression, the volume change for the inner cell was measured. It was assumed that the sample had achieved equilibrium when volumetric changes were almost negligible ($0.01cm^3/hr$), following the procedure described and implemented by Mendes (2011).

Table 3.14a Sample conditions at the start and end of the constant water compression stages.

Soil samples	Initial Water Content	Stage no	Effective Stress	Compression @ Consolidation	Volume	Dry Density	Void Ratio	Degree of Saturation	Volumetric Water Content	Matric Suction
			σ_c		V	ρ_{dry}		S_r	θ_w	u_a-u_w
	%		kPa		cm^3	Mg/cm^3	e	%		kPa
MZ2US1	25.4	1	25	Initial	618.23	1.586	0.766	92.7	0.402	22
				Final	615.95	1.592	0.759	93.5	0.404	18
		2	50	Initial	616.73	1.590	0.761	93.2	0.403	18
				Final	611.93	1.602	0.748	94.9	0.406	16
		3	100	Initial	610.48	1.606	0.743	95.5	0.407	16
				Final	603.88	1.624	0.725	98.0	0.412	15
		4	25	Initial	600.11	1.634	0.714	99.4	0.414	16
				Final	606.65	1.616	0.732	96.9	0.410	15
MZ2US2	25.8	1	25	Initial	614.40	1.552	0.804	89.8	0.400	119
				Final	609.90	1.564	0.791	91.3	0.403	113
		2	50	Initial	608.66	1.567	0.787	91.7	0.404	58
				Final	604.15	1.579	0.774	93.3	0.407	46
		3	100	Initial	603.63	1.580	0.772	93.5	0.407	43
				Final	597.71	1.596	0.755	95.6	0.411	28
		4	25	Initial	595.95	1.600	0.750	96.3	0.413	22
				Final	601.69	1.585	0.767	94.2	0.409	40
MZ2US3	26.3	1	25	Initial	619.89	1.540	0.818	89.8	0.404	49
				Final	614.59	1.553	0.803	91.6	0.408	41
		2	50	Initial	611.31	1.562	0.793	92.7	0.410	31
				Final	605.83	1.576	0.777	94.6	0.414	25
		3	100	Initial	604.67	1.579	0.774	95.0	0.414	24
				Final	598.36	1.595	0.755	97.4	0.419	20
		4	25	Initial	595.92	1.602	0.748	98.3	0.421	15
				Final	602.09	1.586	0.766	96.0	0.416	23

Table 3.14b Sample conditions at the start and end of the constant water compression stages.

Soil samples	Initial Water Content	Stage no	Effective Stress	Compression @ Consolidation	Volume	Dry Density	Void Ratio	Degree of Saturation	Volumetric Water Content	Matric Suction
			σ_c		V	ρ_{dry}		S_r	θ_w	u_a-u_w
	%		kPa		cm^3	Mg/cm^3	e	%		kPa
MZ1aUS4	28.9	1	25	Initial	607.33	1.407	0.990	81.8	0.407	220
				Final	599.53	1.425	0.965	83.9	0.412	216
		2	50	Initial	596.35	1.433	0.954	84.8	0.414	220
				Final	592.78	1.441	0.943	85.9	0.417	175
		3	100	Initial	592.34	1.442	0.941	86.0	0.417	188
				Final	587.57	1.454	0.926	87.5	0.421	120
		4	25	Initial	586.55	1.457	0.922	87.8	0.421	126
				Final	591.10	1.445	0.937	86.4	0.418	165
MZ1aUS5	28.5	1	25	Initial	492.29	1.431	0.956	83.4	0.408	155
				Final	484.58	1.454	0.926	86.2	0.414	153
		2	50	Initial	479.29	1.470	0.905	88.2	0.419	96
				Final	473.84	1.487	0.883	90.4	0.424	70
		3	100	Initial	472.69	1.491	0.878	90.8	0.425	69
				Final	467.17	1.508	0.856	93.2	0.430	35
		4	25	Initial	465.41	1.514	0.850	93.9	0.431	28
				Final	471.12	1.496	0.872	91.5	0.426	75

3.6.4 Shearing Tests Results

The shearing process was carried out following the respective constant water content compression stage, hence; the conditions at which the samples entered the shearing stage correspond to the final values on Tables 3.14a and 3.14b.

The results of the shearing stage for each sample are presented in Figures 3.24 to 3.29. In Figures 3.24, the overall stress-strain relationship for the constant water content tests for each test is shown. It can be seen that the process started with a rapid increase of deviatoric stress over a small range (2 to 3%) of the axial strain, approaching the maximum value, for the initial 3 stages. Then, as the final stage was left until 20% straining, the behaviour post peak was by either a steady or abrupt decline of the deviatoric stress over a short range of axial strain (1 to 5%). After that, the deviatoric stress was maintained at almost a constant level. A similar pattern applies to each test; however, distinct variations in magnitude were produced, with samples with higher initial suction values showing greater strength.

To fully understand the behaviour of the unsaturated samples during shearing stage, the plots for deviatoric stress, pore water pressure and volumetric strains against axial strains have been plotted for each sample, as shown in Figure 3.25, 3.26, 3.27, 3.28 and 3.29. In general, the tendency was similar in all tests. The pore water pressure remained negative, indicating a continuous unsaturated condition throughout each stage.

In the first three stages of each test, as the deviatoric stress progresses towards a maximum value, the pore water pressure increased (but remained negative) and gradually reduced as it reached the peak. The plots for volumetric strains during these stages showed an initial contraction before they started to dilate. For stage 4, similar behaviour can be seen on both pore water pressure and volumetric strains as the stress reached the maximum point. However, after passing the maximum stress, the pore water pressure was maintained at almost a constant level while samples kept on dilating until 20% axial strain. The point of transition from contraction to dilation coincided with the point of decrease in pore water pressure.

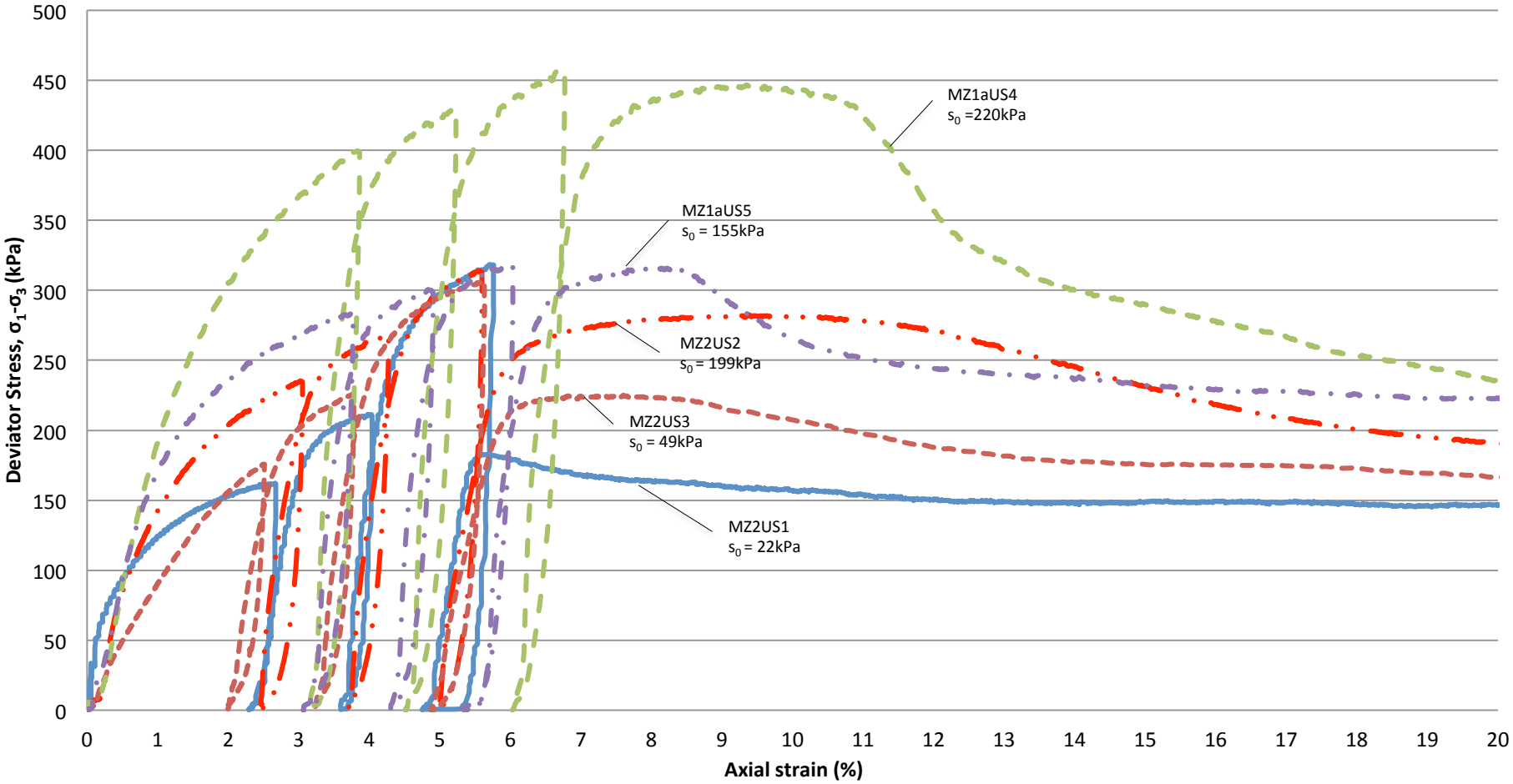

Figure 3.24 Overall deviatoric stress stress against strain relationships for unsaturated samples.

(Suction values, s_0, shown are initial suction in stage 1)

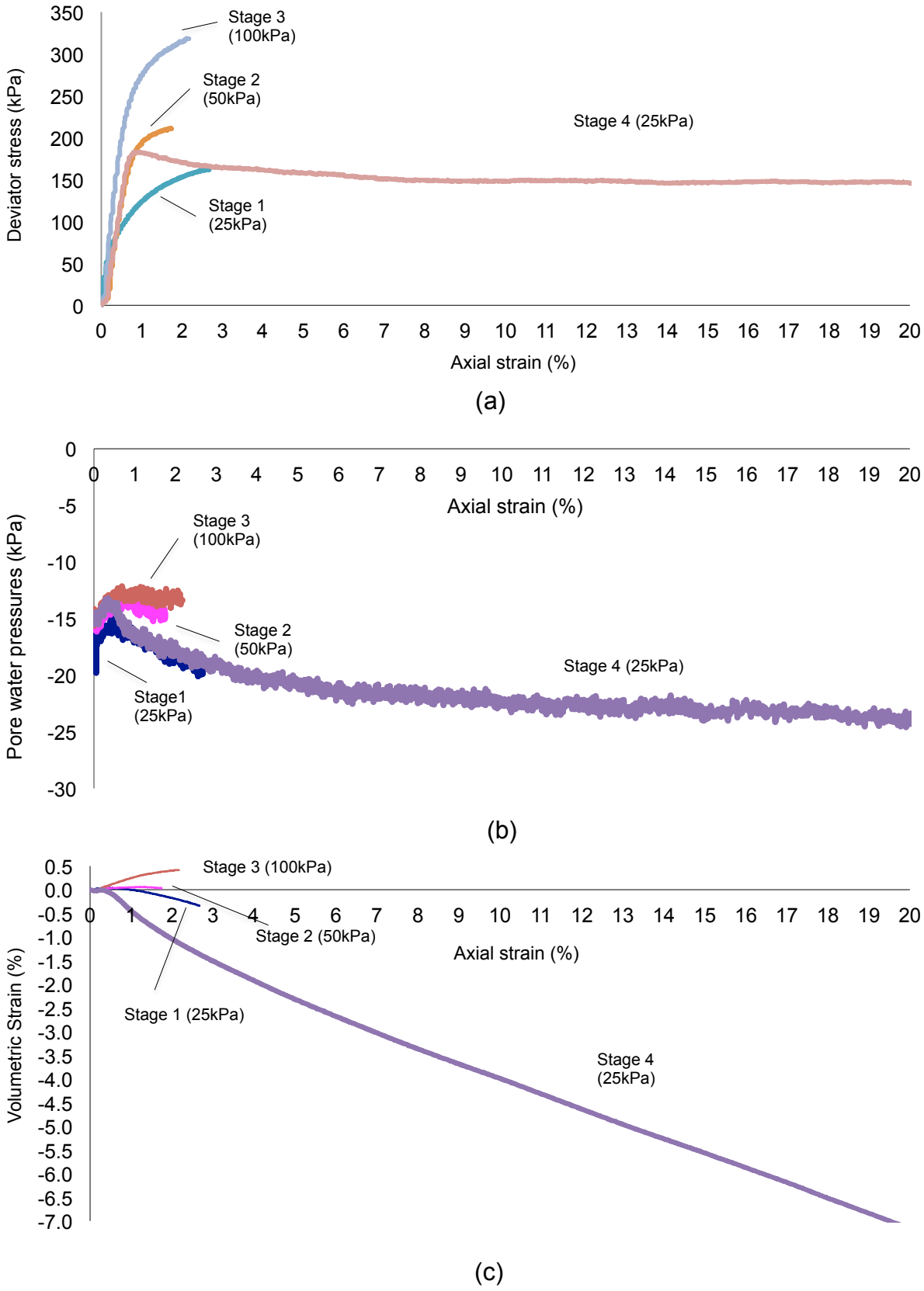

Figure 3.25 Shearing tests results for MZ2US1; (a) Deviatoric stress; (b) pore water pressure; (c) volumetric strains, against axial strains.

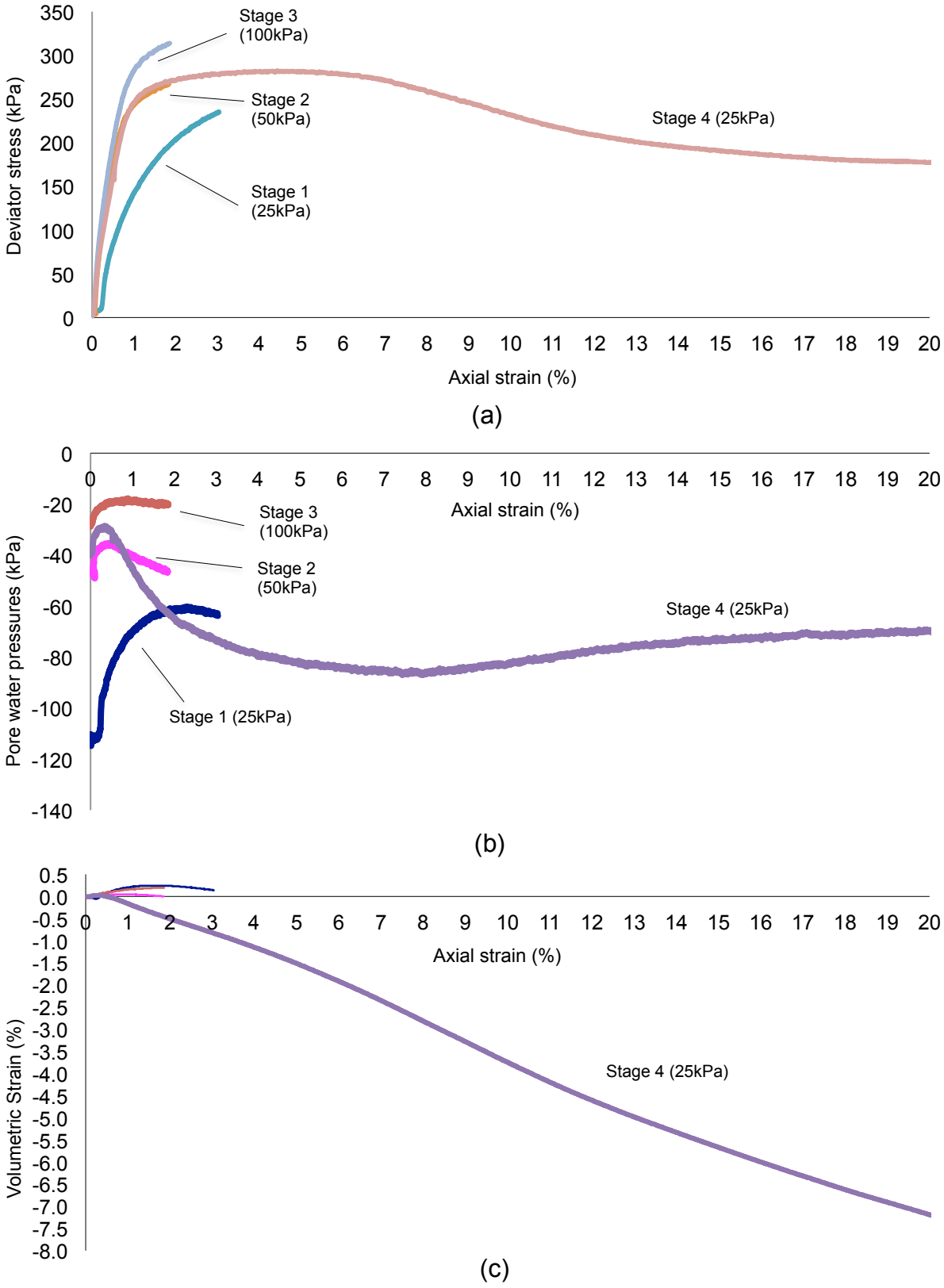

Figure 3.26 Shearing tests results for MZ2US2; (a) Deviatoric stress; (b) pore water pressure; (c) volumetric strains, against axial strains.

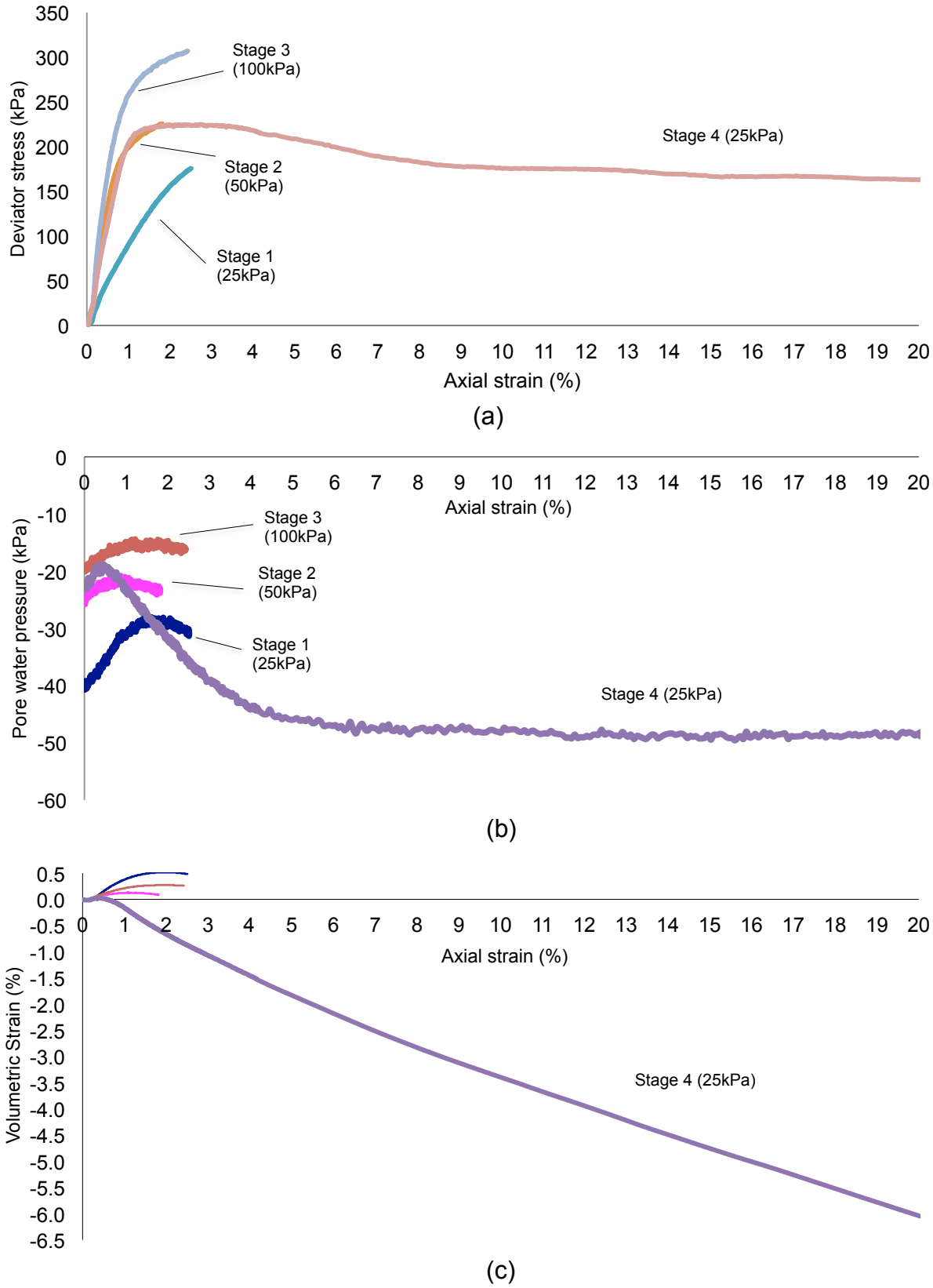

Figure 3.27 Shearing tests results for MZ2US3; (a) Deviatoric stress; (b) pore water pressure; (c) volumetric strains, against axial strains.

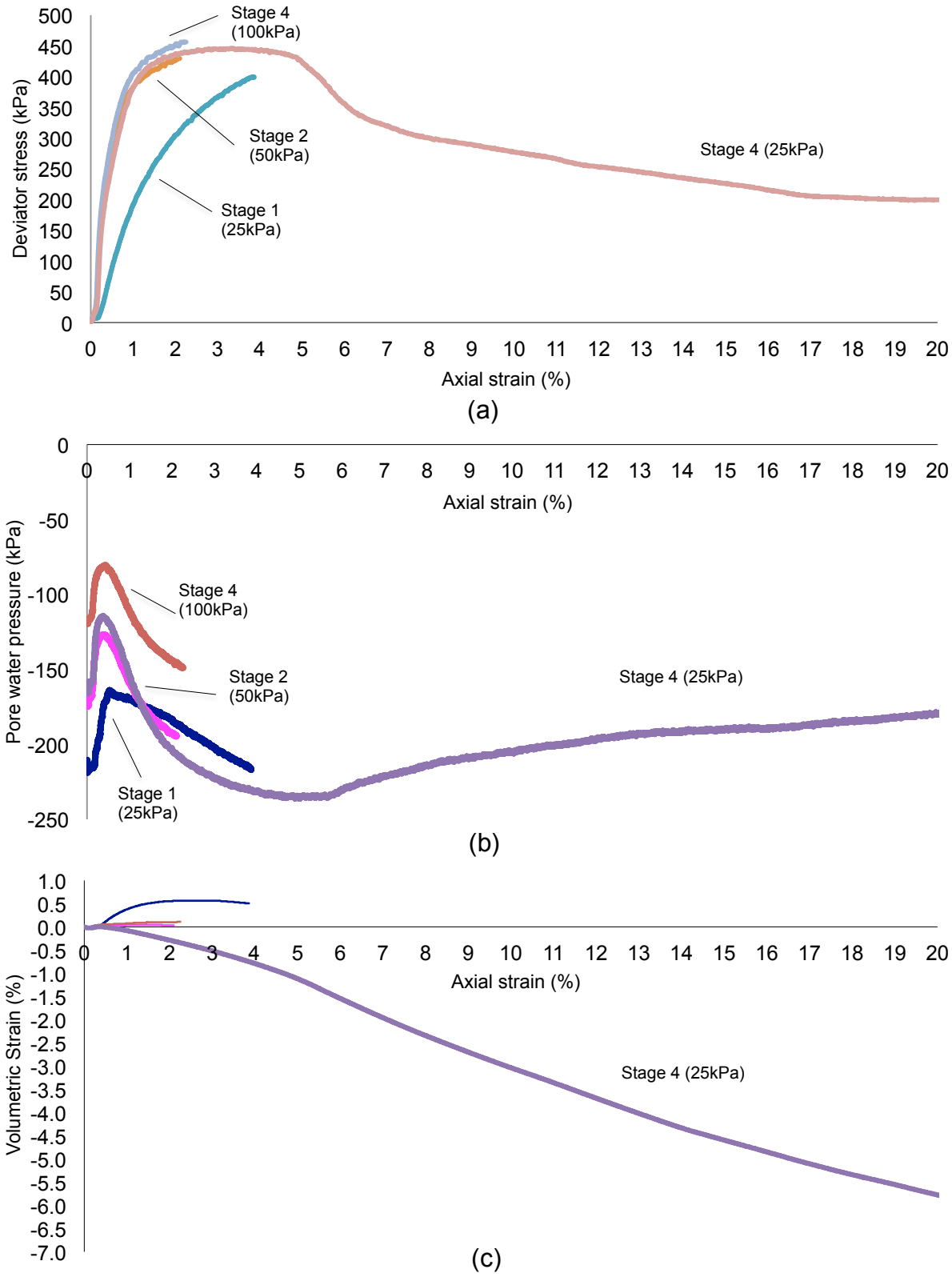

Figure 3.28 Shearing tests results for MZ1aUS4; (a) Deviatoric stress; (b) pore water pressure; (c) volumetric strains, against axial strains.

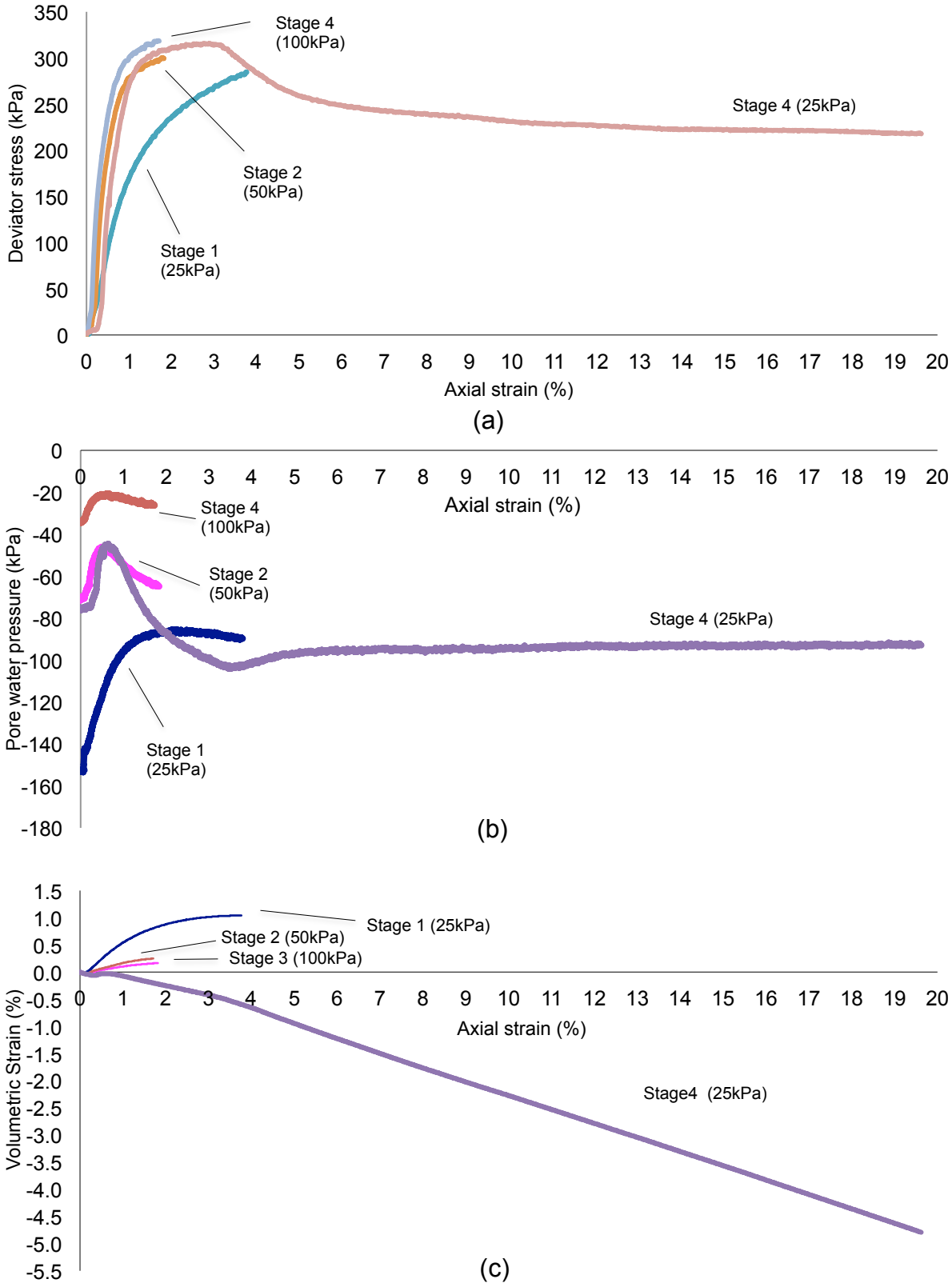

Figure 3.29 Shearing tests results for MZ1aUS5; (a) Deviatoric stress; (b) pore water pressure; (c) volumetric strains, against axial strains.

3.6.5 Critical state limit analysis

The stress strain diagrams from constant water content tests (Figure 3.24) show a range of steady to abrupt declination of the deviator stress values as the samples reach their failure state. Also, shear surfaces could be seen clearly to form within each sample during failure. These indicate that the critical state of the samples can be empirically determined at the point when void ratio changed dramatically due to this change in shearing behaviour. Beyond critical state points, further localisation of strains would be produced as the stress state progresses towards residual state.

In order to compare the results from unsaturated tests against saturated tests, the principle using average skeleton stress assumption (Jommi, 2000) using a "Bishop stress", which incorporates the degree of saturation, has been adopted. This principle can provide a realistic approach for low suction conditions (high degree of saturation – 80% to 100%) of which the air phase is discontinuous (Toll, 1990).

For generalisation, Equation 3.2 will be presented in q-p space. The pore air pressure (u_a) was maintained at zero value at all time, therefore, the equation can be simplified which results in Equation 3.7.

$$p^* = p - S_r(u_w) \quad \ldots (3.7)$$

The results of the critical state points of each sample are presented in Figures 3.30 to 3.34. These critical state points were determined based on the comparison between stress paths (Figure 3.30a, 3.31a, 3.32a, 3.33a and 3.34a) and ν against p* plots (Figure 3.30b, 3.31b, 3.32b, 3.33b and 3.34b), where 'discontinuity' or deviation in value was observed, caused by strain localisation. From the plots, it is clear that as stress progresses, the samples initially contract; however, they then dilate as the stress paths reached a maximum value. This contraction behaviour is more apparent for samples with higher suction value.

The normalisations of the stress paths technique (as applied to saturated tests) were carried out for each constant water content tests results for the determination of λ and Γ. The modified stress normalisation technique using the effective mean stress corresponding to the void ratio on the CSL (full description in section 3.5.3.2), was done by adjusting the critical state value of p'_c for each sample, respectively.

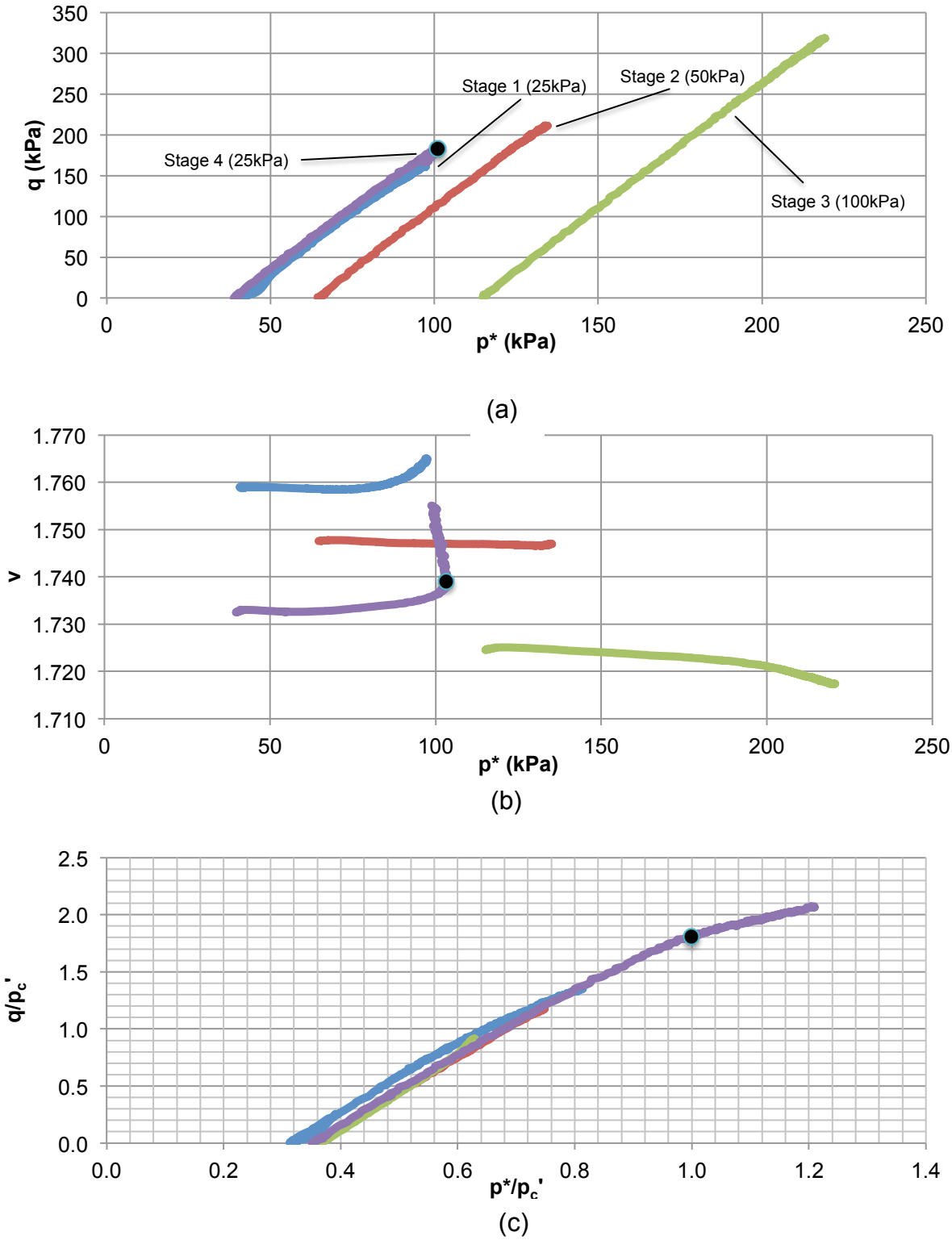

Figure 3.30 Critical state results for MZ2US1; (a) stress paths; (b) specific volume ν against p*; (c) Normalised stress paths.

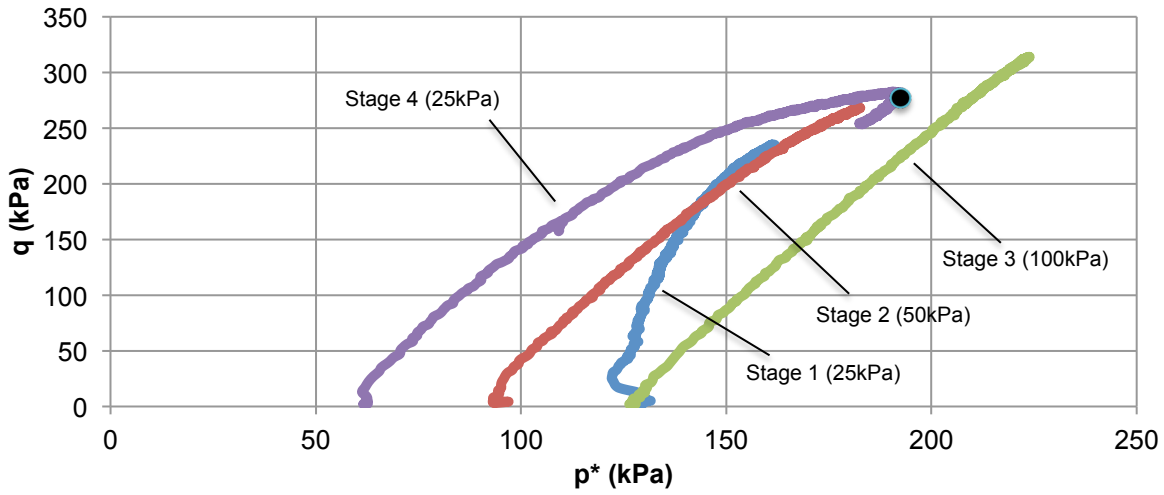

(a)

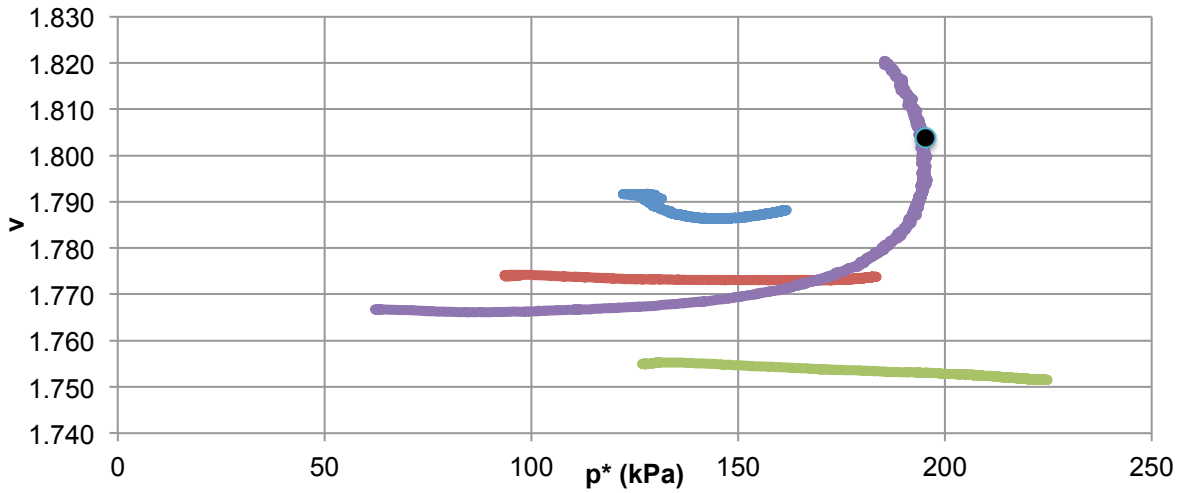

(b)

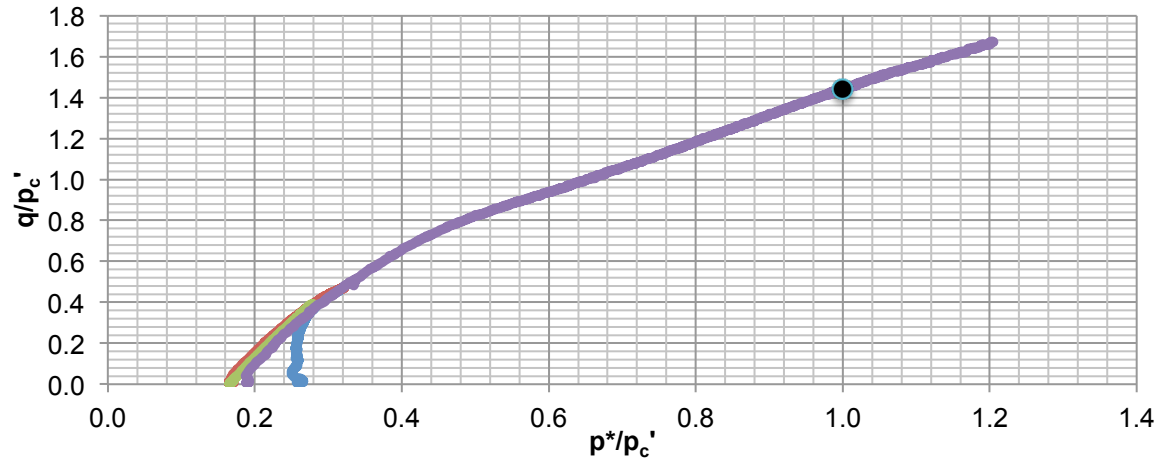

(c)

Figure 3.31 Critical state results for MZ2US2; (a) stress paths; (b) specific volume ν against p*; (c) Normalised stress paths.

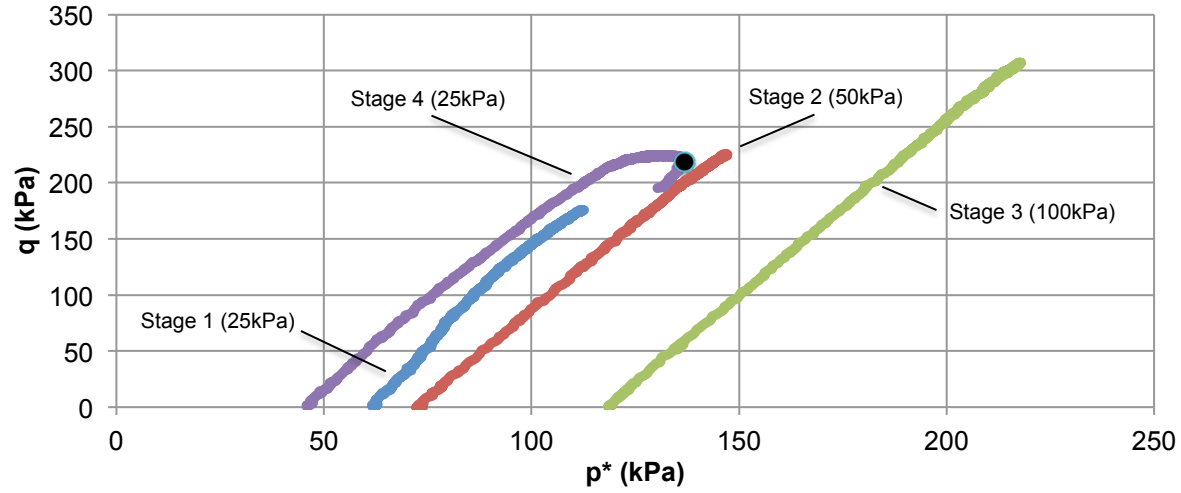

(a)

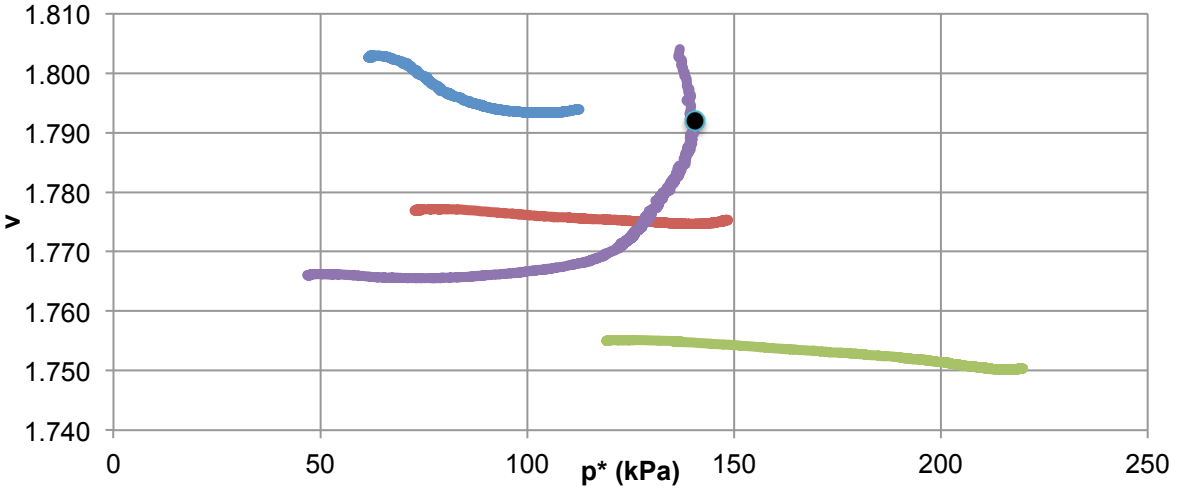

(b)

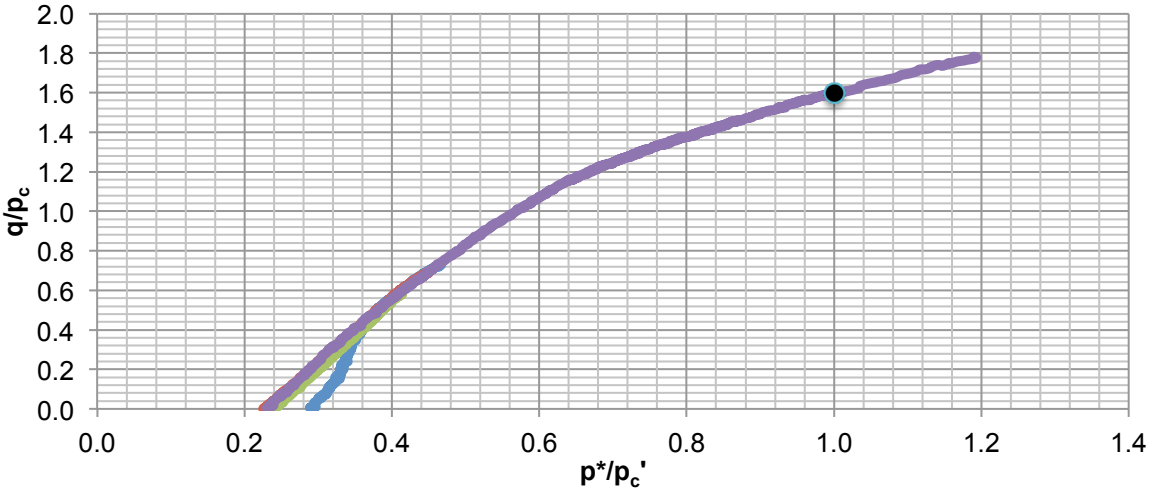

(c)

Figure 3.32 Critical state results for MZ2US3; (a) stress paths; (b) specific volume ν against p*; (c) Normalised stress paths.

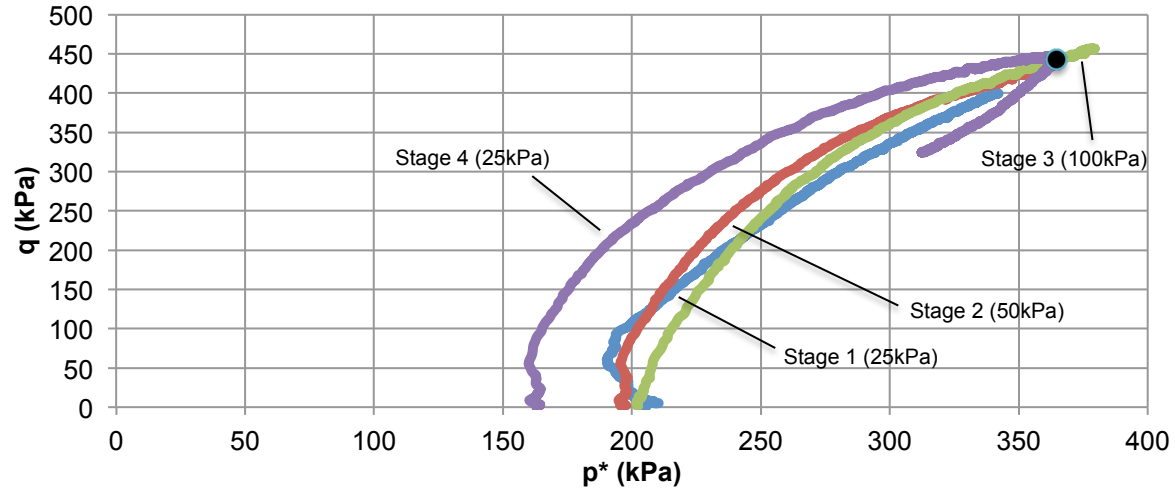

(a)

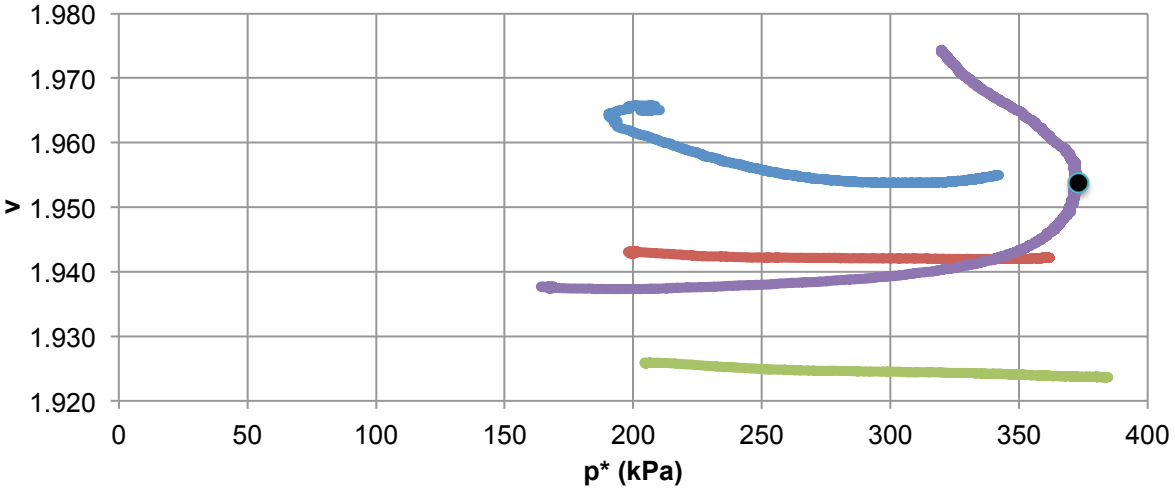

(b)

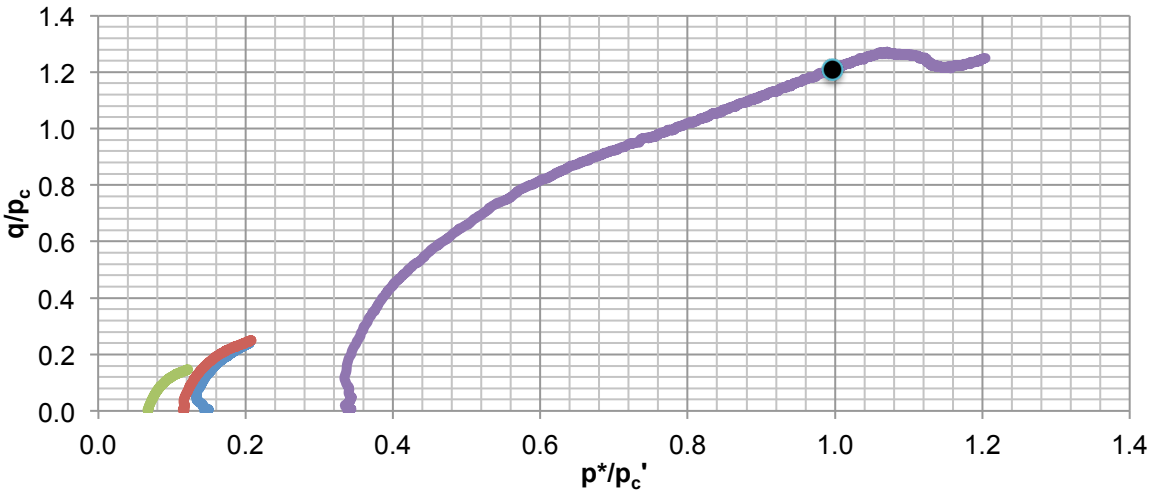

(c)

Figure 3.33 Critical state results for MZ1aUS4; (a) stress paths; (b) specific volume ν against p*; (c) Normalised stress paths.

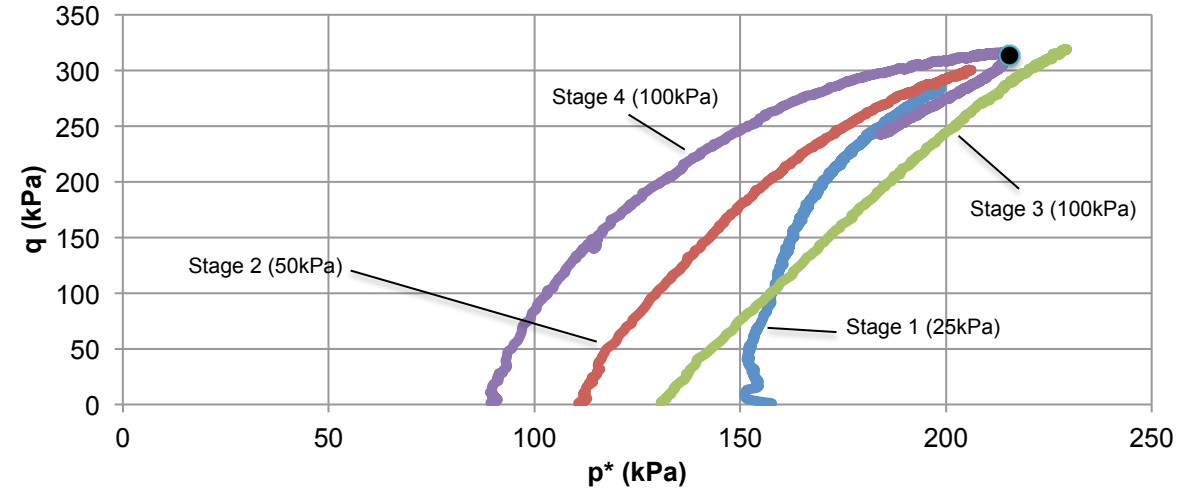

(a)

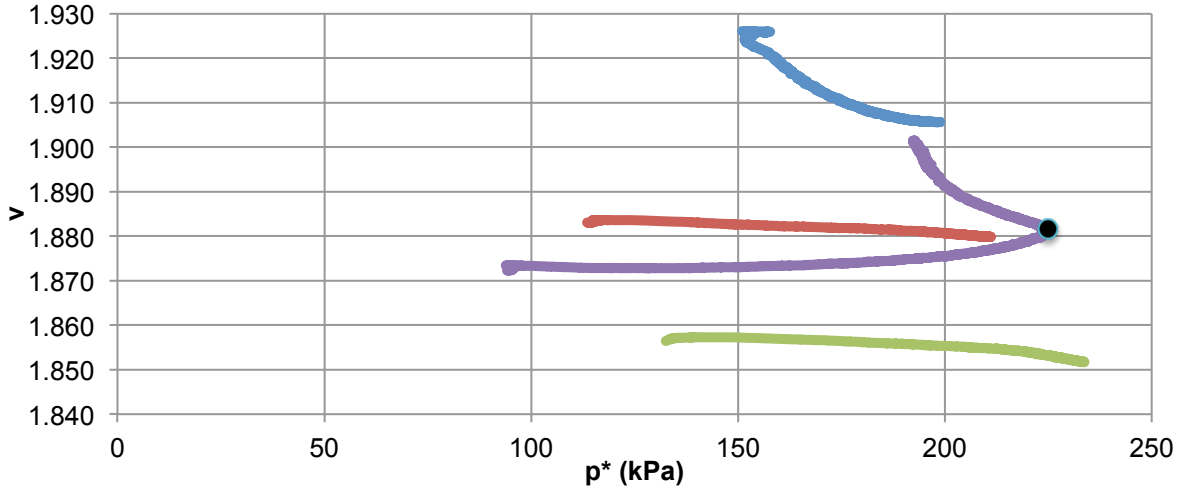

(b)

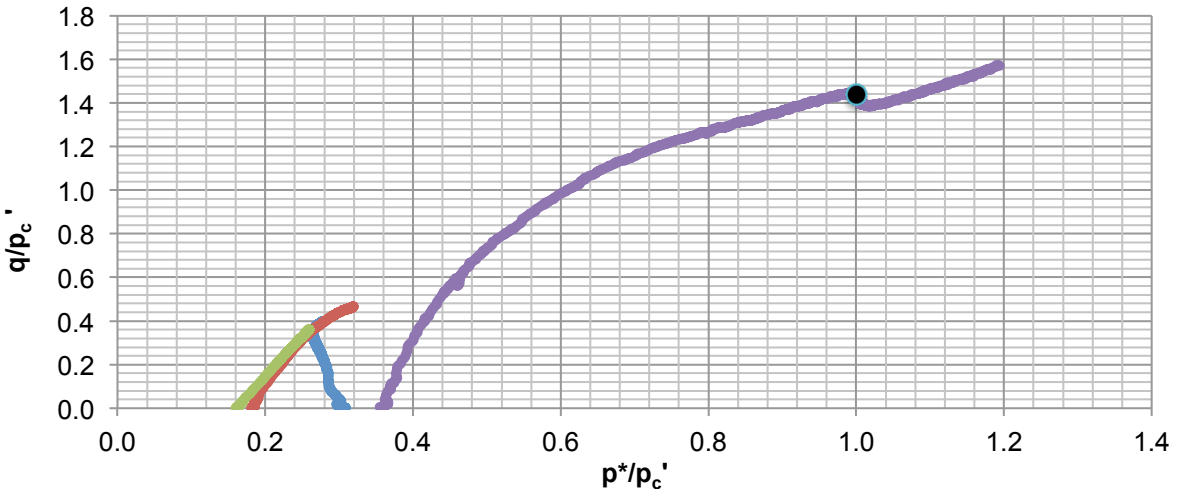

(c)

Figure 3.34 Critical state results for MZ1aUS5; (a) stress paths; (b) specific volume ν against p*; (c) Normalised stress paths.

The adjusted value of p'_c which was deduced from the relationships with both λ and Γ parameters, expressed in Equation 3.6, was calculated using the trial and error procedure for the determination of both critical state parameters of each sample. However, it was found from the normalised stress paths that the plotted curves for each stage did not show any convergence to a single point (as shown by the saturated test results), when a single set of values of λ and Γ parameters were used to represent all samples.

Therefore, for constant water content tests results, the adjustment of p'_c value was done by determining both λ and Γ parameters for every single stage, instead of fixing them for each sample. Figure 3.30c, 3.31c, 3.32c, 3.33c and 3.34c present the results of the normalised stress path obtained from the multistage tests on all samples. It can be seen that the curves of each stage gradually emerge and transcend towards p^*/p'_c equal to 1, though, only curves of stage 4 truly reached the CS condition.

The conditions of the samples at critical state are shown in Table 3.15. Referring to the table, only the outputs from stage 4 of each sample are presented, as it was the only stage that reached the CS condition. For a clearer understanding, all data has also been arranged in the sequence of increasing suction values.

Table 3.15 Critical state points of each unsaturated test samples at stage 4.

Sample	Stage	p^*	q_{cr}	u_a-u_w	v_{start}	v_{final}	λ_{adj}	Γ_{adj}	Sr	M_{p^*}	$\emptyset_{cr}$
		kPa	kPa						%		(°)
MZ2US1	4	103	186.9	16.4	1.73	1.74	0.07	2.064	96.1	1.81	44
MZ2US3	4	141	223.5	44.2	1.77	1.79	0.07	2.139	92.8	1.58	39
MZ2US2	4	195	280.1	85.6	1.77	1.80	0.07	2.173	91.1	1.43	35
MZ1aUS5	4	225	312.6	103.5	1.87	1.88	0.07	2.207	90.5	1.42	35
MZ1aUS4	4	373	449.6	233.5	1.94	1.95	0.07	2.309	84.9	1.21	30

It can be seen that the stress ratio (M_{p^*}) values reduces as the suction values of each sample increases. These values start from as high as 1.81, which is beyond the stress ratio obtained under saturated conditions (M_s = 1.43). In addition, the volumetric CSL values for respective samples are also presented and range between 2.102 to 2.338 for Γ while being fixed at 0.07 for λ. These variations are believed to be due to the heterogeneity of each sample reflected by the differences

in void ratio (or specific volume, as given in Table 3.15). It has to be noted that the degree of saturation (S_r) values also changes with void ratio, but ranges above 85%.

In v–lnp* space (Figure 3.35), most of the critical state points for unsaturated tests fall below the lower limit of the CSL defined from saturated tests. In order to accommodate these points, the CS zone as suggested by Hosseini et. al. (2005) can be justified by moving the lower limit of saturated test down, giving a variation of ±0.308 in terms of specific volume.

The critical state in deviatoric stress (q), against (p*) space, using stress paths, and the critical state points for each unsaturated samples are also presented in Figure 3.36. It has to be noted that the distance between each critical state points is due to the variation in suctions. The plot show that the critical state points for unsaturated samples tend to plot above the critical state line (bilinear line), as defined by the saturated tests, specifically for samples with lower suction values (16.4kPa and 40.6kPa). From the graph, it is clear that the approach of using degree of saturation as the additional parameter, presents a slightly overestimated strength value up to the condition of 100kPa suction (p*=200 kPa) before it starts to provide lower magnitude of strength as suction of the soil increases. The production of non-linear relationships can also be seen from the graph that satisfying the suggestion depicted by Escario and Saez (1986) and Fredlund et al. (1978).

.

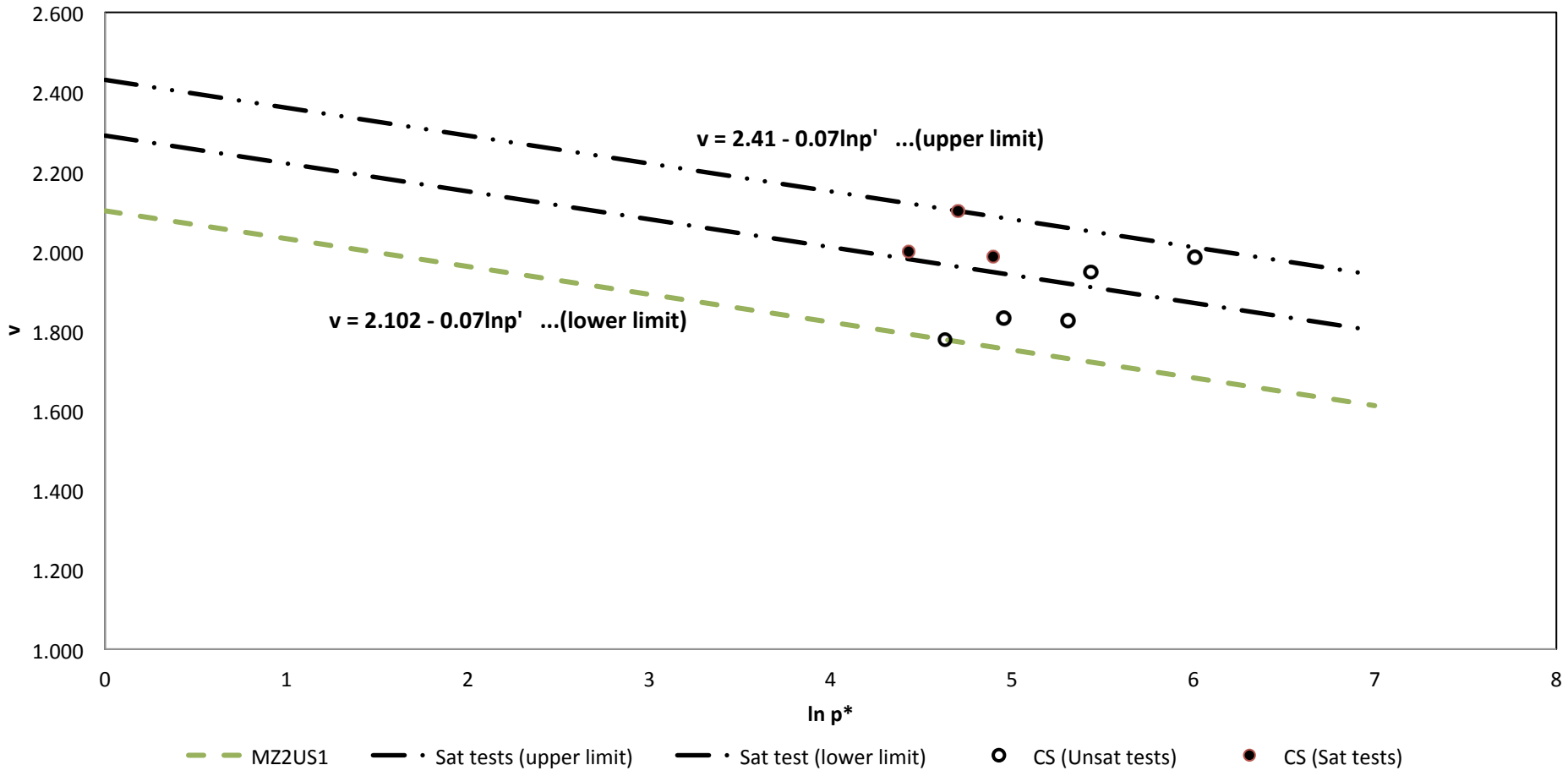

Figure 3.35 Critical state line for the unsaturated test series in v – lnp*.

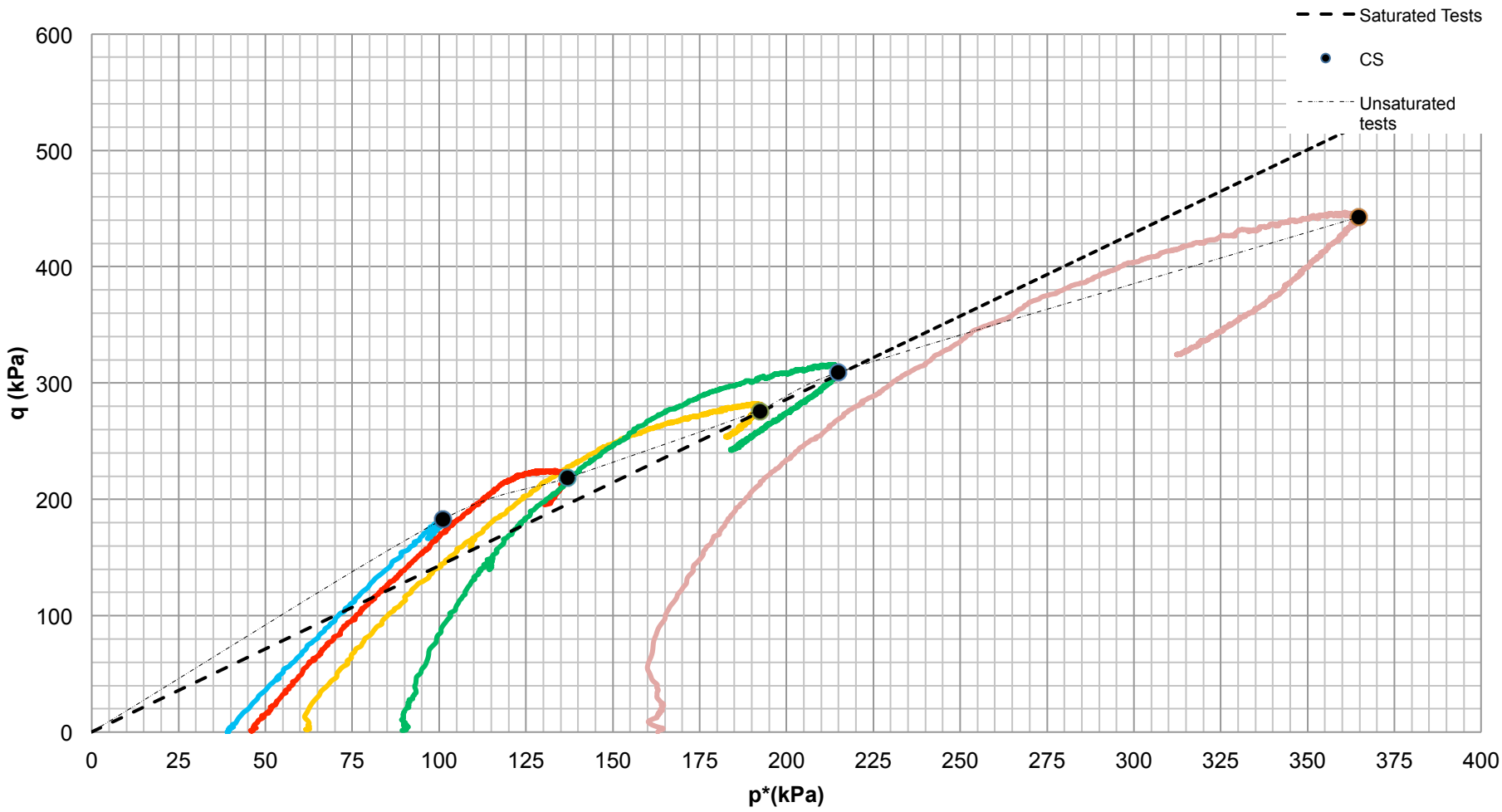

Figure 3.36 Critical state line for the unsaturated test series in q – p*.

3.6.6 Critical state stress ratios (using M_a and M_b)

It has been stated previously that the obtained stress ratio values (M_{p^*}) for samples with lower suctions are higher than the stress ratio under saturated condition (M_s = 1.43). The depiction of these values appears to be in contrast with what might be expected, that is the unsaturated stress ratio of similar materials should be equal or less than the stress ratio value attained under saturated condition (transition of strength from saturated condition to unsaturated condition).

In order to explain this further and to ascertain whether the samples are of similar material, the suggestion to treat the unsaturated strength by segregating it into two stress components, independently, was used for further assessments. For generalisation, the independent stress state variables equation shown as Equation 3.5, shall be best presented in q-p space, as the following.

$$q = M_a(p-u_a) + M_b(u_a-u_w) \quad \ldots (3.8)$$

where, M_a = the net stress ratio

M_b = the suction ratio.

Fredlund et al. (1978) suggested that ϕ^a could be assumed to be equal to ϕ', together with $\phi^b = \phi'$ if the suction was below the AEV. This would imply M_a=M_b=M_s in q-p space.

A recalculation of q was implemented using Equation 3.8 for each CS point, following the suggestion made above (M_a=M_b=M_s). The procedure were carried out to investigate the differences in strength between the actual q (test data) and the calculated q, with regard to changes in suctions. The presentations of the calculations are as shown in Table 3.16.

Table 3.16 Calculation of q with M_a and M_b equal to M_s and the differences with actual q.

Stage	q	p-u_a	u_a-u_w	Sr	M_a=M_s	M_b=M_s	Net Stress	Suction	q_{cal}	q-$q_{cal.}$
	kPa	kPa	kPa	%			kPa	kPa	kPa	kPa
4	186.9	87.4	16.4	96.1	1.43	1.43	125.0	23.5	148.5	38.4
4	223.5	99.6	44.2	92.8	1.43	1.43	142.4	63.1	205.6	17.9
4	280.1	118.5	85.6	91.1	1.43	1.43	169.4	122.5	291.9	-11.8
4	312.6	129.3	103.5	90.5	1.43	1.43	184.9	148.0	332.9	-20.3
4	449.6	174.9	233.5	84.9	1.43	1.43	250.2	333.9	584.1	-134.5

In the table, the amount of strength contributed by the net stress component (p-u_a) and suction have been calculated and shown for each sample, respectively. With the combination of strengths from these two components, the differences between the actual q and the calculated q can be resolved. It can be seen that the influence of suction has caused some considerable differences in strength, as the value gets higher.

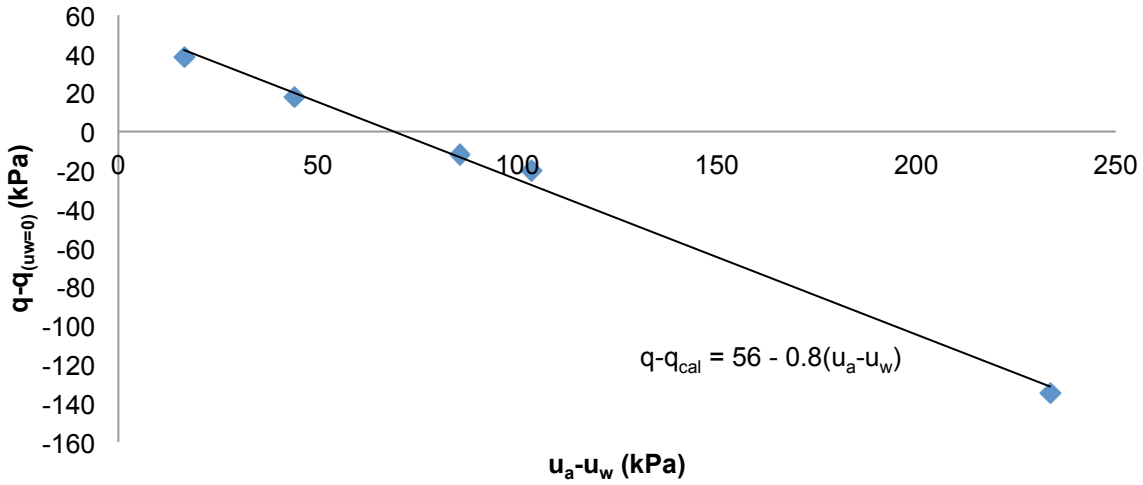

Figure 3.37 Differences in strength between the calculated q and actual q. against suction

A plot of the differences in strength against suction is presented in Figure 3.37. It can be seen that suction has significantly influenced the strength of the samples through a linear declination with average gradient of 0.8. It can be assumed

that this suction influence is due to variation in M_b (as the parameter that relates to suction). Therefore, by incorporating this 0.8 value as the amount of reduction for M_b, the reduction of M_b due to suction can be calculated.

For the value of M_a, it has been proven that this net stress ratio also changes (Delage et. al., 1987, Toll, 2000, Toll et. al., 2008). Hence, a recalculation of M_a was carried out for each CS points by applying the new M_b value (deduced from the regression measurements) into Equation 3.8. The value of M_a was determined so that the difference in strength for both actual and calculated q is equal to zero. The summary of the variations of M_a and M_b can be seen in Table 3.17.

Table 3.17 Calculation of q with the variation of M_a and M_b; to achieve equilibrium with actual q.

Stage	q	$p-u_a$	u_a-u_w	Sr	M_a	M_b	Net Stress	Suction	q_{cal}	$q-q_{cal.}$
	kPa	kPa	kPa	%			kPa	kPa	kPa	kPa
4	186.9	87.4	16.4	96.1	1.92	1.14	168.2	18.8	186.9	0
4	223.5	99.6	44.2	92.8	1.84	0.92	183.1	40.4	223.5	0
4	280.1	118.5	85.6	91.1	1.84	0.73	217.4	62.7	280.1	0
4	312.6	129.3	103.5	90.5	1.95	0.59	252.0	60.6	312.6	0
4	449.6	174.9	233.5	84.9	1.94	0.47	340.1	109.4	449.6	0

The values for M_a (relates to net stress) appear to increase as M_b (relates to suction) reduces towards zero. To explore the effect, the variation on M_a and M_b with suction have also been plotted and presented in Figure 3.38. The graph shows that the total stress contribution represented by M_a does not remain constant, but in fact increases as the suction increases. The explanation for the variation of M_a and M_b can be related to the effect of the degree of aggregations or packet fabric that occur at microscopic scale within the soil (Toll 1990, 2000). As the suction increases, the groups of particles held together within soil (packet fabric) would be induced to create a higher degree of aggregation, behaving like a coarser material and contributes to the increase in M_a. The reduction of M_b, however, is due to the decease of degree of saturation (volumetric water content) within the sample,

caused by the withdrawal of the pore-water into packets. This strength component provides even less contribution to the overall strength of the samples as the soil gets drier.

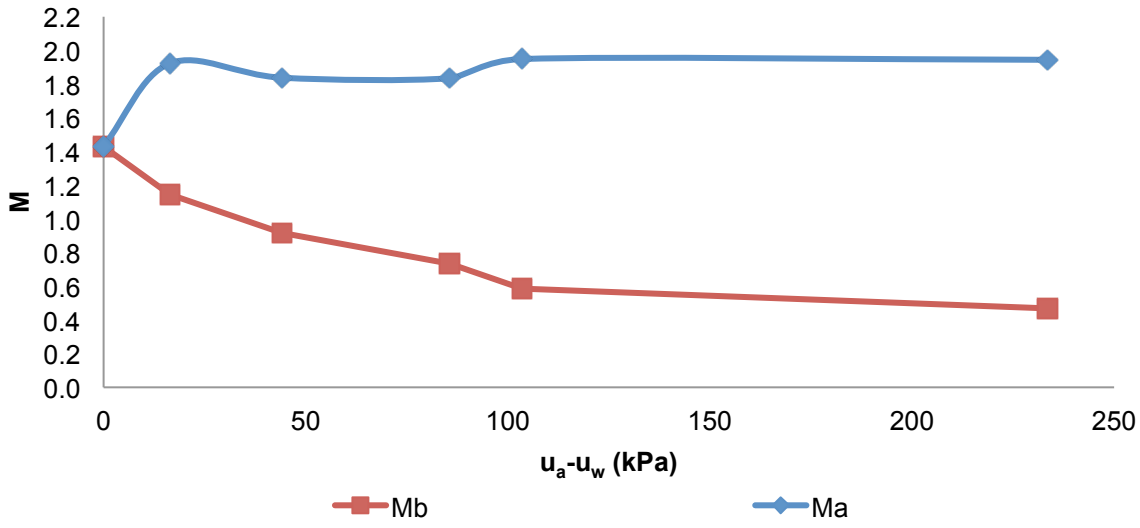

Figure 3.38 Variations of M_a and M_b against suction.

However, Toll (2000) has presented the relationship between the variations of both stress ratios with the degree of saturation and defined the volumetric parameter as the controlling factor. Thus, in Figure 3.39, the relations with the degree of saturation are also presented for comparison.

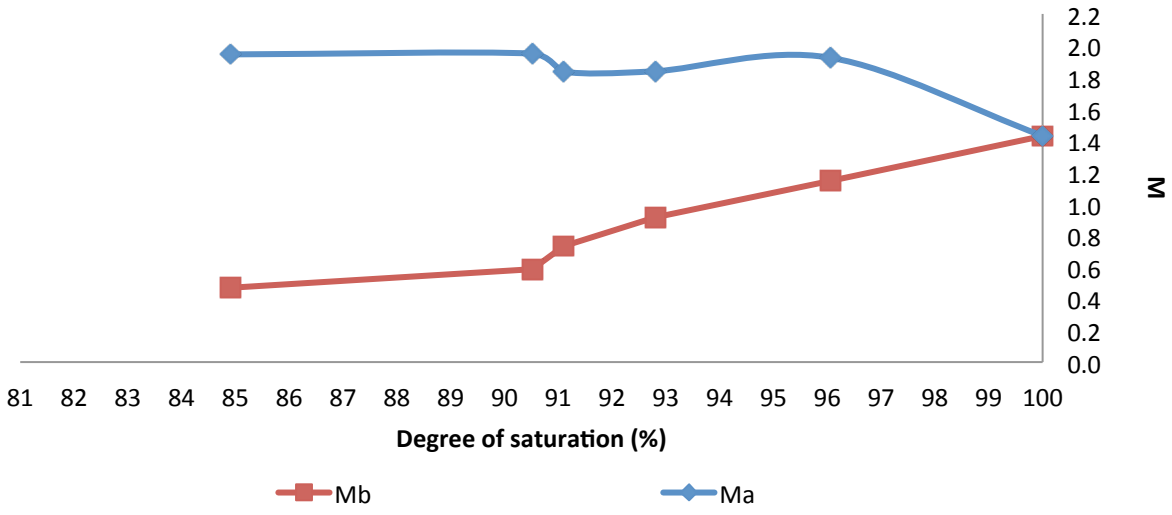

Figure 3.39 Variations of M_a and M_b against the degree of saturation.

A similar trend can be seen for the relationship of both stress ratios against the degree of saturation. The value of M_b for each constant water content tests sample tends to decrease and M_a increases up to the value equal to 1.94, as the degree of saturation of the soil reduces.

3.6.7 Critical state stress ratios (using M_s and M_b)

In the Extended Mohr-Coulomb formulation by Fredlund et. al. (1978), the angle of friction for net stress was identified as ϕ^{α} and was later assumed to be equal to ϕ'. The expression of the concept can be seen in Equation 3.9, using the q-p space.

$$q = q_i + M_s(p\text{-}u_a) + M_b(u_a\text{-}u_w) \quad \ldots (3.9)$$

The interpretations of the results, by fixing M_a (ϕ^{α}) equal to M_s (ϕ'), were interpreted based upon the graphical method reported by Ho and Fredlund (1982). They suggested that the term q_i (intercept point at q) is similar to the cohesion (c') in the Mohr Coulomb equation. Thus, in the paper, the suction term in the shear strength equation $(M_b(u_a\text{-}u_w))$ for an unsaturated soil could be considered as contributing to the total cohesion (denoted as C in the paper) of the soil. The total cohesion of each sample is then plotted against suction to obtain the gradient of the plots that represents (M_b). To represent this total cohesion in q-p space, the expression shall be presented as the following.

$$q_i^* = q_i + M_b(u_a\text{-}u_w) \quad \ldots(3.10)$$

Substituting into Equation 3.9,

$$q = q_i^* + M_s(p\text{-}u_a) \quad \ldots(3.11)$$

By using this equation 3.10, the calculation to derive both stress ratios can be implemented separately. Table 3.18 presents the total value of q_i^* (suction related strength component plus cohesion) for each sample. It can be seen that the q_i^* values gradually increase corresponding to the changes in suction. Using these results, the graph for q against $p\text{-}u_a$ can be plotted (Figure 3.40). From the graph, it shows that each line is parallel, reflecting a gradient equal to M_s.

Table 3.18 Calculation of q by segragating the total stress contributions and q_i* (total cohesion).

Sample	Stage	q	p-ua	ua-uw	M_s	Net Stress	q_i*	q_{cal}	$q-q_{cal.}$
		kPa	kPa	kPa		kPa	kPa	kPa	kPa
MZ2US1	4	186.9	87.4	16.4	1.43	125.0	61.9	186.9	0.0
MZ2US3	4	223.5	99.6	44.2	1.43	142.4	81.0	223.5	0.0
MZ2US2	4	280.1	118.5	85.6	1.43	169.4	110.7	280.1	0.0
MZ1aUS5	4	312.6	129.3	103.5	1.43	184.9	127.7	312.6	0.0
MZ1aUS4	4	449.6	174.9	233.5	1.43	250.2	199.4	449.6	0.0

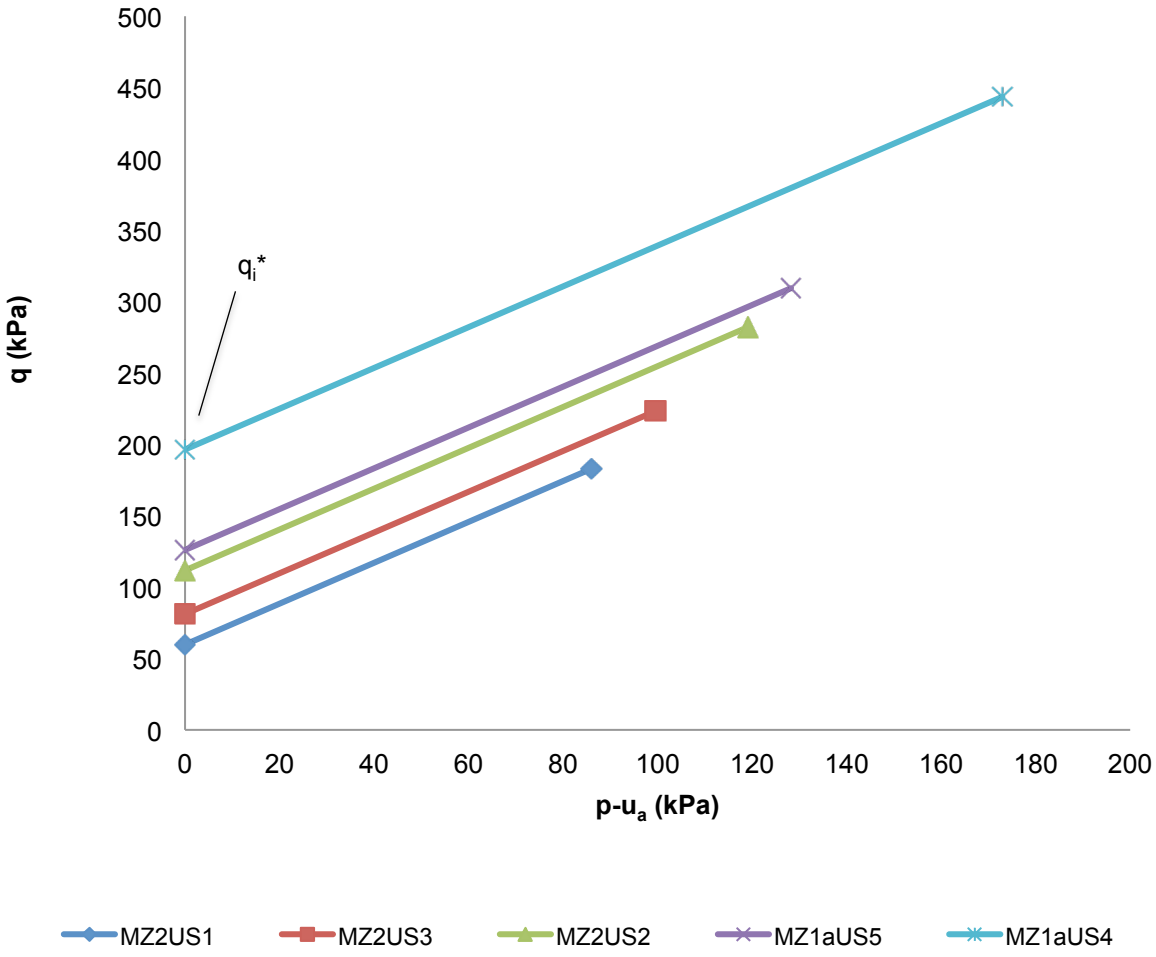

Figure 3.40 Graphical analysis of total cohesion in q against p-u_a.

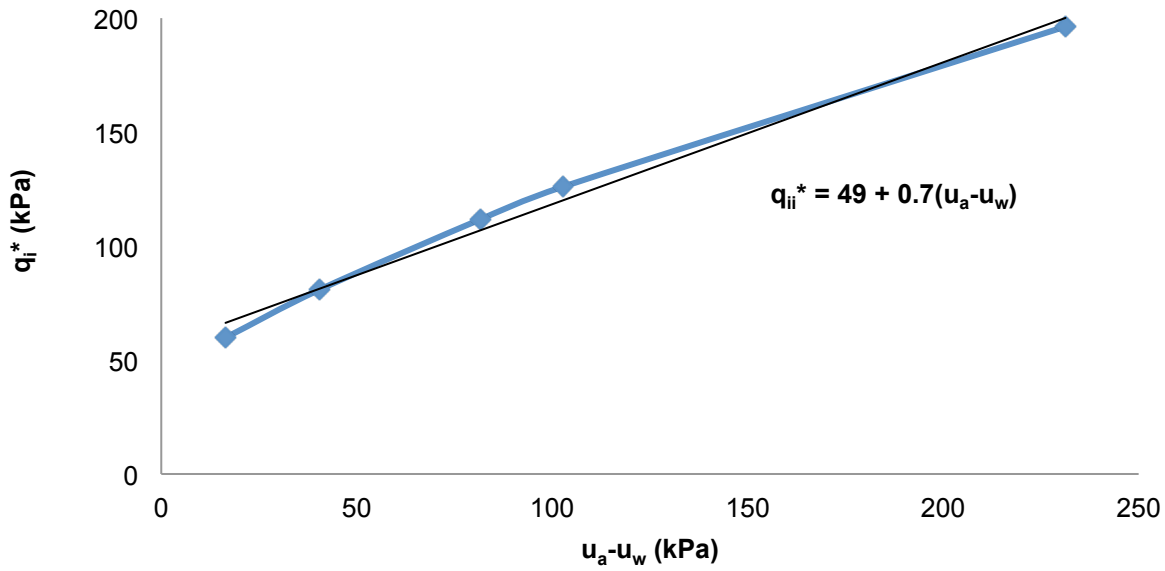

Figure 3.41 The graphical interpretation of the relationships between total cohesion with suction.

The q_i^* (when $p-u_a$ is equal to zero) of the various suctions were then plotted against suction for the determination of stress ratio M_b. It is shown in Figure 3.41, where an almost linear relationship can be seen between both parameters with average gradient of the slope equal to 0.7. This graphically obtained gradient shall be used as a conservative estimate for the representation of M_b.

Table 3.19 Calculation of q with the M_a equal to Ms and M_b equal to 0.7; to achieve equilibrium with actual q.

Sample	Stage	q	p-ua	ua-uw	M_s	M_b	Net Stress	Suction	q_i	q_{cal}	$q-q_{cal.}$
		kPa	kPa	kPa			kPa	kPa	kPa	kPa	kPa
MZ2US1	4	186.9	87.4	16.4	1.43	0.70	125.0	11.5	50.4	186.9	0
MZ2US3	4	223.5	99.6	44.2	1.43	0.70	142.4	30.9	50.1	223.5	0
MZ2US2	4	280.1	118.5	85.6	1.43	0.70	169.4	59.9	50.7	280.1	0
MZ1aUS5	4	312.6	129.3	103.5	1.43	0.70	184.9	72.4	55.3	312.6	0
MZ1aUS4	4	449.6	174.9	233.5	1.43	0.70	250.2	163.5	35.9	449.6	0

Table 3.19 presents the recalculated q based on M_b equal to 0.7 and M_a equal to M_s (1.43). In order to achieve zero differences in strength (between the calculated q and the actual q), an average of 49kPa additional strength value was needed for each sample. The additional strength, denoted as q_i, can be clarified as similar to the extra strength contributed by the total stress, due to the degree of aggregations or packet fabric that occurred as suction increases.

3.7 Final remarks

This chapter has presented the attempts to describe the mechanical behaviour of the tropical residual soils, obtained from the slope in Precinct 9, Putrajaya, Malaysia. The testing programme involved a series of multistage saturated tests (for layer 1 and layer 2) and a series of multistage unsaturated constant water content triaxial tests (layer 1).

In the early part of this chapter, the presentation of the theoretical background relevant for the characteristics of residual soils and the derivation of soil strength parameters from different unsaturated constitutive soil models were explained. Then, the detailed descriptions of the undisturbed tropical residual soil triaxial samples were discussed. A total number of 11 triaxial test samples were prepared for both saturated and unsaturated testing.

A detailed description of the multistage testing procedures, for both saturated and unsaturated soils testing were presented. It was decided to perform Multistage Triaxial testing in order to improve the degree of confidence for the characterisation of strength parameters by obtaining multiple strength points. The procedure consisted of a total number of 4 confining pressures to be performed in one single test. These confining stages were implemented prior to shearing. The shearing was stopped when the deviator stress reached a constant strength value before proceeding to the next stage. However, in the final shearing stage, the process was continued until 20% strain was achieved.

The saturated tests were carried out on a total of 6 triaxial samples from MZ1, MZ3 and MZ4 that represent layer 1 and layer 2. During the saturation stage, the

process of water inflow into the triaxial sample raised the degree of saturation up to approximately 100% (higher than 95%). Then the process was followed up with the consolidation stage. The results for the conditions before and after consolidation of each stage showed that the sample decreased in volume when higher confining pressures were imposed and increased in volume when lower subsequent pressures were applied. This volumetric change was due to the amount of fluid coming in and out of the sample.

Undrained shearing tests were implemented following the consolidation process in each stage. None of the sample was observed to have experienced any excessive destructurisations effects. This was because in the final shearing stage for each sample (carried out at the same stress level as the first stage), the deviator stresses showed higher values compared to initial stages and increased in correspondence to the increase of confining pressures.

The determination of the critical state points for the saturated samples of both layers was made based on the effective stress paths produced from each test (q-p' plot). The selection for the critical state points was made based on the observation of a 'discontinuity' in volumetric behaviour that could be seen after the maximum deviator stress was reached. For the case where the measured deviator stress showed a continuous inclination up to 20% strain, the final point of the final stage (20% axial strain) was taken to represent the condition of critical state.

The unique position of the critical state line (CSL) on the ν against p' space was determined based on the suggestion made by Hosseini et al. (2005) that described the critical state as a zone rather than a unique line. This was due to the difficulty in defining void ratio that was caused by the inevitable errors during measurement of samples and also the heterogeneity of the sample. The normalisation of the stress path based on the critical state value of p'_c, were adjusted by implementing trial and error procedure on λ and Γ parameters value until the curve end up with p'/p'_c, =1 and $q/p'_c = M$. Using these parameters for the production of v-p' space plot, the zone with upper and lower bounds can be defined graphically to describe the critical state for the results of both layers. The results for the normalised stress paths obtained from the multistage saturated tests for layer 1 showed critical state stress ratio (M_s) equal to approximately 1.43. However, for the

case of layer 2, two stress ratio values were obtained that were equal to 1.6 and 1.89. These differences were justified due to the visible dissimilarity in characteristics and related to the variation in degree of cementation of the sample (weathering grade).

For the case of unsaturated soil strength, a series of multistage constant water content tests were carried out on 5 residual soil samples with 5 different initial suctions (4 of the samples were dried before testing). This concept was preferred in order to prevent the possibility of the natural packet fabric (soil aggregation) in the soil to be destroyed due to the suction controlled process (if wetted or saturated) and to preserve the 'in situ' condition of the soil. The changes of suction during test were measured using a high capacity tensiometer fixed in the centre of a customised base pedestal. Prior to shearing, samples were subjected to an initial equalisation stage (to measure the initial suction) followed by constant water content compression to impose the required cell pressure. These tests were executed by a sequence of confining pressures (25, 50, 100 and 25kPa) for the determination of critical state parameters. During testing, the samples were connected to atmospheric pressure to prevent any build-up of pore air pressure (maintaining u_a equal to zero).

Overall, the results showed that the obtained stress ratio values (M_{p^*}), calculated based on the "Bishop stress" concept, for samples with lower suctions were higher than the stress ratio under saturated condition (M_s = 1.43). These appeared to be in contrast with the actual situation of soil drying and seemed to imply that the samples might be of different material, thus giving higher M_{p^*}. However, it was felt that that the use of a single stress state parameter with degree of saturation (S_r) as the additional parameter was insufficient to explain the unsaturated behaviour. However, it can provide a realistic approach at low suction conditions (high degree of saturation) when the air phase is discontinuous.

To explain these characteristics, a recalculation of q was implemented for each CS points; by assuming that the suction values have not reached the AEV (M_a=M_b=M_s). The procedure was adopted to investigate the differences in strength between the actual q and the calculated q, in regards to changes in suctions. Regressions of M_b due to suction were calculated based on the graphically obtained values. By applying these new M_b values, the determination of M_a could be acquired.

The values for M_a appeared to increase as M_b reduces towards zero. This suggested that the net stress contribution represented by M_a did not remain constant, but in fact increased as the suction increases. The effect of the degree of aggregations or packet fabric that occurred in microscopic scale within the soil element, as reported by Toll 1990; 2000, can explain these stress ratio variations. As the suction increases, higher degrees of aggregation will be produced, resulting in samples behaving in a manner similar to a coarser material with the increase in M_a. The reductions of M_b, however, are due to the decease of degree of saturation (volumetric water content) within the sample. It was due to the withdrawal of the pore-water into packets which in consequence, produces less contribution of suction to the overall strength of the samples.

Further assessments have also been implemented to determine the critical state parameters based on the Extended Mohr Coulomb model (in q-p space). The interpretations of the results based on the assumption of having M_a as equal to M_s have also been implemented. The total cohesion (additional strength component contributed by suction and effective cohesion) has been plotted against suction and shows an almost linear relationship with average gradient of the slope equal to 0.7. This gradient was used as a conservative estimate for the representation of M_b. However, by validating the calculated strength value with the actual value, an average of 49kPa additional strength value was needed by each sample in order to equal the actual strength value. These variations of additional strength are attributable to the effects of degree of aggregations or packet fabric that occurred within the soil as the suction increases.

In conclusion, suction and soil structure plays an important role in the variation of the mechanical behaviour of tropical residual soils. Evidence showed that the soil strength was not only related to the degree of weathering but also to the suction. The additional strength associated with the effects of degree of aggregation or packet fabric occurred during drying (suction increases) can be used to explain how a tropical residual soil slope sustains its stability during the dry season. The deterioration towards failure, however, will be accelerated by infiltration that causes rapid soil strength degradation.

Chapter 4
Hydrological behaviour of Tropical Residual Soils

4.1 Introduction

In tropical regions, soils located above the groundwater table such as residual soils are generally unsaturated and possess negative pore-water pressures (suction). Due to climate variations, suctions are induced by the process of evapotranspiration that often exceeds infiltration, especially for locations where the groundwater tables are deep. The prolonged evapotranspiration creates soil-water deficits.

To describe the hydrological behaviour of tropical residual soils, the application of unsaturated soil concepts is essential. Using this concept, the role of suction in influencing the movement of water within soil and the relationships with soil water content, can be assessed. It has been acknowledged that this unsaturated condition is present in most engineered earth structures, especially tropical residual soil slopes.

In the initial part of this chapter, the theoretical background to the Soil water retention curve and the relation with drying and wetting process will be presented. Then, it carries on with the description of hydrological testing procedures to obtain a Soil Water Retention Curve (SWRC). The SWRC is also used in deriving the permeability function. The results for saturated permeability tests, SWRCs using different suction measurement techniques and the estimated permeability function will be shown and discussed towards the end of the chapter.

4.2 Literature review

4.2.1 Soil water retention curve (SWRC)

To explain the effect of suction in unsaturated soil concepts, the determination of a soil property to describe its ability to attract and retain water is essential. This hydrological relationship is normally clarified based upon graphical approach, defined as the Soil Water Retention Curve (SWRC) (sometimes also know as the Soil Water Characteristic Curve, SWCC). The curve represents the relationships between water content and suction, and can be presented in various terms such as gravimetric water content, w, volumetric water content, θ or even degree of saturation, S_r (Fredlund and Rahardjo, 1993). These terms are closely related as presented in Equation 4.1.

$$\theta = \frac{w.G_s}{1+e} = \frac{S_r.e}{1+e} \quad \text{... (4.1)}$$

Where: θ = volumetric water content
w = gravimetric water content
Sr = degree of saturation
Gs = specific gravity of the soil
e = void ratio

However, Toll et al. (2015) has commented that the use of 'characteristic' in the SWCC term is unsuitable as the water retention behaviour varies with other factors, such as the void ratio, thus, the term Soil Water Retention Curve (SWRC) is preferred.

By using SWRC, various properties such as shear strength, permeability and thermal coefficient under unsaturated conditions can be estimated (Brooks & Corey, 1964; van Genuchten, 1980, Vanapalli et al., 1996). The continuous relationship between water content and suction can be explained through the process of soil drying or wetting. The pattern of the curve is typically in S-shaped (sigmoidal curve) and is highly dependent on the type of soil, soil structure or fabric and mineralogy (Fredlund and Xing, 1994). An example of a typical behaviour of a SWRC following a

(primary) drying process can be seen in Figure 4.1 (Vanapalli et. al., 1999), in which three different parts can be distinguished.

4.2.1.1 Primary drying curve

At the first part of the curve, when the soil is subjected to drying from its saturated state (slurry condition), the SWRC will maintain a degree of saturation close to 100% before it starts to curve down at a limiting value of suction called the air entry value (AEV). During this stage, known as the Boundary effect zone, the condition of soil pores remain saturated with water under tension. Then, once the AEV is reached, the bulk water starts to be pulled from the largest pores and air starts to enter, eventually forming a continuous linkage of air-filled pores within the soil.

In this transition zone, the water content of the soil will continously reduce as finer pores progressively desaturate until a residual degree of saturation is reached. Beyond this zone, i.e. the residual zone of saturation, most of the soil water will only be concentrated at the interparticle contacts. The water evaporation process reduces during this condition and causes the curve to flatten (the turning point is defined as residual suction). However, for finer material such as clayey soils, it may involve water adsorption that will produce a continous process of soil water reduction even within the residual zone.

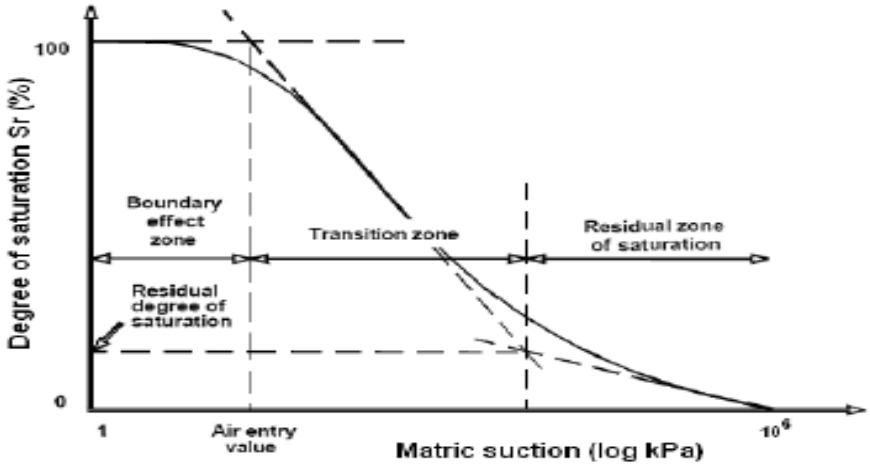

Figure 4.1 An example of a typical behaviour of a SWRC following a (primary) drying process. (after Vanapalli et al., 1999)

The SWRC is also dependent on the particle size distribution of the soil (Fredlund and Rahardjo, 1993). For clay soil, the air entry value is higher and the slope of the curve in the transition zone is much flatter as compared to the coarser material. Figure 4.2 presents the typical SWRC for a clay, silt and sand (Li and Standing, 2014).

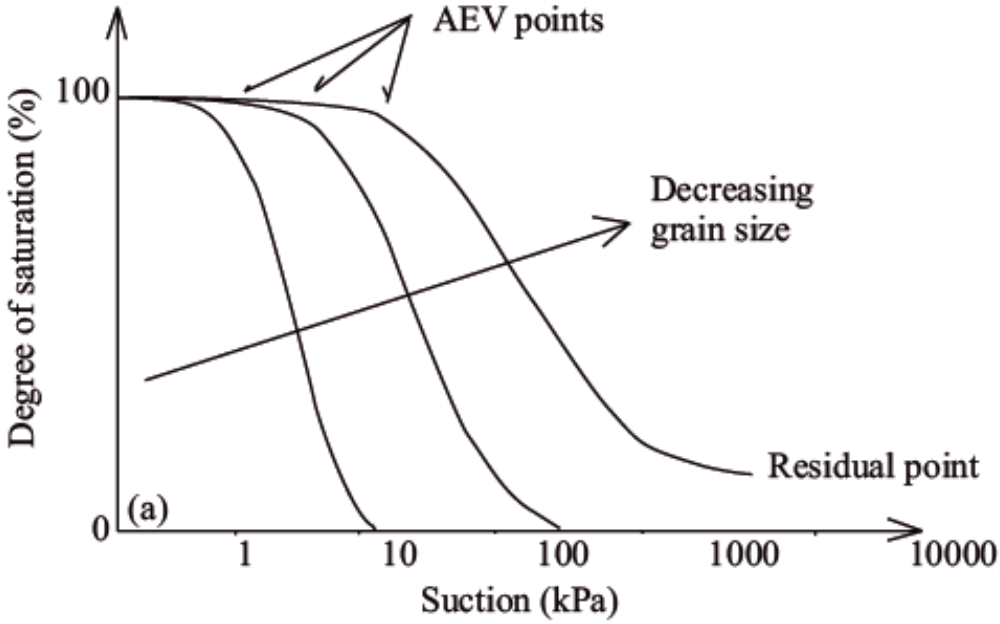

Figure 4.2 The typical SWRC for various soil grading (after Li and Standing, 2014)

4.2.1.2 Primary wetting curve

For the case of soil wetting from its residual water content state, the production of a wetting curve will show a different path compared to the drying curve. This hysteretic behaviour, as illustrated in Figure 4.3, is commonly attributed to hydraulic hysteresis (Croney, 1952). From the graph, it can be seen that a significant increase in water content will occur at a particular value of suction known as the water entry value (Wang et al., 2000). Starting at this point, more water will start to fill in the pores and simultaneously reducing the suction towards zero. However, it has to be recognised that the attained final water content (suction equal to zero) may be lower than the initial saturated value. This difference is explainable either due to the effects of pore entrapment within the soil, or as a result of irrecoverable shrinkage of the soil (Toll, 2012a).

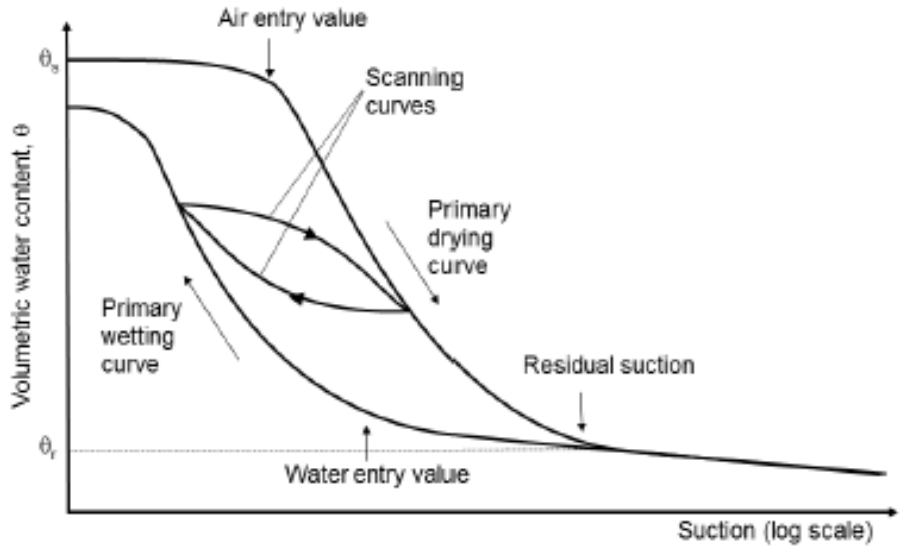

Figure 4.3 Hysteretic characteristics of SWRC (after Toll, 2012a)

The process to define the primary wetting curve of a soil has been found to be difficult, as the soil needs to be dried completely or at least have reached its residual water content state. Without achieving this condition, the obtained SWRC from a wetting process may not be defined as the primary wetting curve but instead an ascending scanning curve. For this reason, it has been suggested that in order to obtain the main wetting curve, suction measurements are required to be conducted to suctions as high as possible (Lourenço, 2008). A comparison between both primary wetting and scanning curves can be seen in Figure 4.4, where Ho et al. (2007) have presented the SWRCs for both primary drying and wetting for decomposed granite at different stress levels. From the graph, it is apparent that the results for the sample at 30kPa stress level (CDG_30_a) have produced drying and wetting lines that coincide at higher suctions (upper curve). In this case, the obtained wetting curve is acceptable (Lourenço, 2008). However, the curve for zero stress (CDG_0_a) shows different drying and wetting paths at high suction, suggesting that residual suction has not been reached and the wetting curve is a scanning curve.

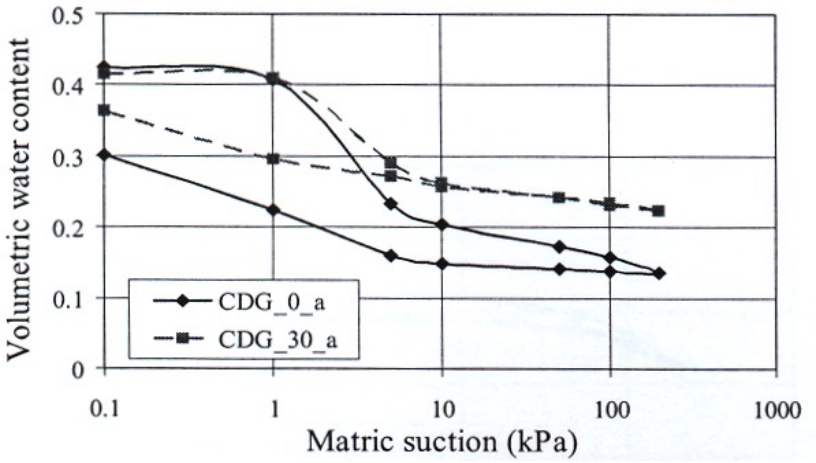

Figure 4.4 SWRCs in decomposed granite at different stress levels (0kPa for the bottom curve and 30kPa for the upper curve); the upper SWRC closes at lower suctions suggesting that the wetting curve is the main wetting and not a scanning curve (after Ho et al., 2007)

4.2.1.3 Scanning curve

A soil may not follow a continuous path from a totally dried or totally wetted state. For a situation where the drying or wetting process is reversed during its primary drying or wetting, a flatter intermediate curve will be produced and will eventually converge with one of the primary paths of the SWRC. This ascending or descending curve is generally known as scanning curve. Detailed illustrations of these behaviour can be seen in Figure 4.5.

Different types of scanning curves have been distinguished between ascending and descending curves, and within them are (1) crossing, (2) converging, and (3) returning scanning curves (Figure 4.5). Converging and crossing scanning curves are common while returning curves are rare. Each type of curve is related to the pore network openings/constrictions produced during drying or wetting (Tompsett et al., 2005, Ravikovitch and Neimark, 2002).

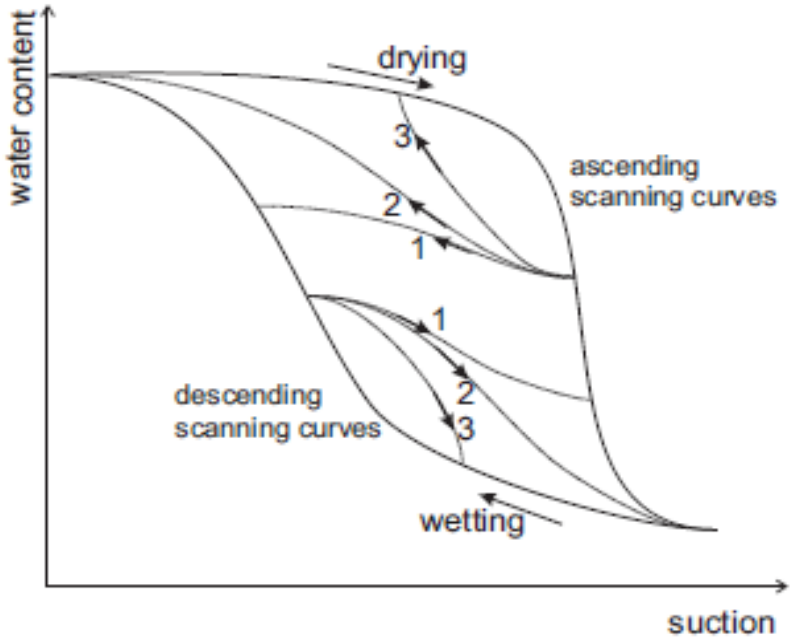

Figure 4.5 Scanning curves from the main drying and wetting curves; 1 – crossing, 2 – converging, 3 – returning (after Tompsett et al., 2005, Ravikovitch and Neimark, 2002)

4.2.2 SWRC determination method

Various techniques can be used to determine SWRC. The details for each technique can be found in the geotechnical literature (e.g. Fredlund and Rahardjo, 1993, Ridley and Burland, 1993, Rahardjo and Leong, 2006, Bulut and Leong, 2008, Lourenco, 2008, Toll et. al., 2013, Toll et. al., 2015 among others). Similar to the concept used for triaxial test, these techniques can be implemented for suction measurement and control, and generally differentiated based upon its suction range and equilibration time. In this chapter, only two methodologies (used to produce this research) are presented, which are the pressure plate (axis translation technique) and High Capacity (HC) tensiometer (direct suction measurement technique).

4.2.2.1 Pressure plate (axis translation technique)

Equipment and procedures

The pressure plate technique is one of the most commonly used techniques to produce SWRCs due to its simple concept for imposing suction to the soil sample. The concept, also known as 'axis translation', is implemented by elevating the pore air pressure (u_a) in order to make the pore water pressure (u_w) to become positive

(Hilf, 1956). To perform this technique, both u_a and u_w must be controlled respectively, throughout the experiment, for the production of the desired suction that is defined by the difference between these pressures.

A pressure plate apparatus essentially consists of a pressure chamber (enclosing cell) that is equipped with a saturated high air entry value (HAEV) ceramic disc. The prior saturation process on the HAEV ceramic disc is essential to prevent air entry through the disc. The maximum suction imposable on the sample is dependent on the AEV of the HAEV porous ceramic disc. Once the air pressure on ceramic disc reaches the maximum value (AEV), air entry occurs (when air starts to flow through the HAEV porous ceramic disc) and this would interrupt the measured back pressure (pore water pressure) and lead to incorrect suction measurements. AEVs for high air-entry ceramic discs are genrally available up to a maximum of about 1500kPa.

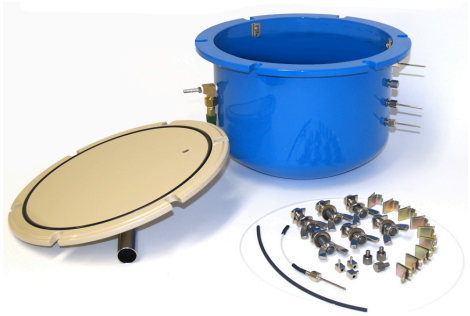

Figure 4.6 5-bar pressure plate apparatus (manufactured by Soil Moisture Corp.).

To initiate a test, the cell top is held down with quick release bolts and a rubber seal. Air pressure is gradually applied in the cell to values above atmospheric pressure. During this process, the pore water pressure will be controlled by the back pressure and it is normally maintained at atmospheric pressure. The soil sample will then be left for equalisation as the water pressure in the sample equilibrates with the water pressure below the plate. This process will be carried out until no further flow of water from the sample is observed using a graduated burette. Lastly, the sample

will then be removed from the chamber and weighed to obtain the gravimetric water content measurement.

For the production of SWRC, the previous process will be repeated by imposing different values of suction (increasing the pore air pressure). Once the final suction stage is completed, the back calculated water content measurement is carried out by oven-drying the sample in order to obtain the actual sample water content.

Vaquero (2007) has introduced a different configuration for this technique by using 4 independent porous discs (100mm in diameter) of the same AEV value (1500kPa). By using this modified configuration which is available in Durham University, multiple sample testing can be implemented at the same time. Further modification has been made, where the measurement of the outflow of water from the sample is replaced by independent volume gauges (rather than burettes), attached to each porous disc (Figure 4.7).

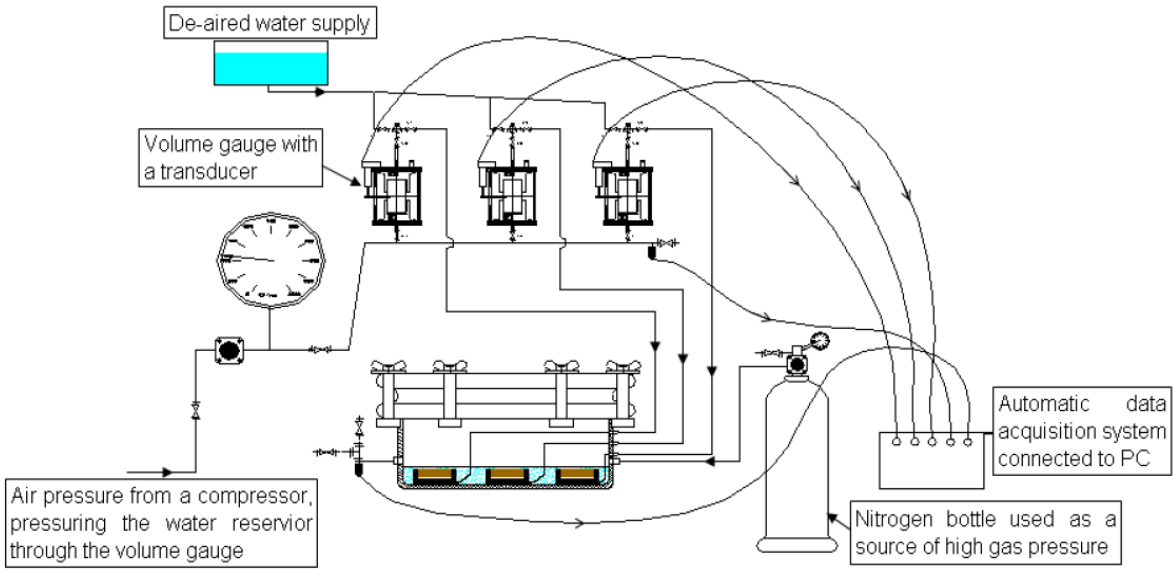

Figure 4.7 Setup of the pressure plate apparatus (after Vaquero 2007).

Reliability Review

The drawbacks of SWRCs produced by the pressure plate technique have been reported in many literatures, especially with regard to its data accuracy. Most of these problems are associated with the lack of soil-plate contact, imperfect sealing of the pressure chamber and the exchange of water vapor between the soil and the air in the chamber (Wang and Benson, 2004). These errors may lead to incorrect estimation of the water volumes exchanged by the soil, thus, affecting suction equalisation and producing erroneous suction measurements (Campbell, 1988, Madsen et al., 1986).

Furthermore, the hydraulic conductivity of a soil can also hinder full equalisation of a sample. Gee et al. (2002) has reported numerical simulations of how sample equilibrium is affected by both soil and ceramic hydraulic conductivity. The study indicates that long time lapses are necessary for coarse grained soils (sands and gravels) to achieve equilibrium because of the very low soil water conductivity at low degree of saturation. These problems are also shown to depend on the dimensions of the sample (i.e. height). Besides that, Cresswell et al. (2008) investigated the data accuracy of pressure plate measurements for suction values of 0.5 and 1.5 MPa, and discovered that the contact loss problems are also due to soil shrinkage.

The comparison between axis translation (pressure plate test) and direct measurement technique (tensiometer test) has been reported by Toll et al. (2013) based on a small number of measurements by Lourenço (2008) and Tarantino et al. (2011). From the study, it showed that the axis translation tests show higher gravimetric water contents than those measured by natural drying using direct measurements. These differences in water content were described to be due to the fact that the pressure plate test prevents cavitation from occurring within the soil and desaturation only occurs by air entry from the sample boundaries. The results also showed that the desaturation process for tensiometer test occurs at lower suctions than the pressure plate tests, since the water contents are lower. However, the trends for SWRC plotted in terms of degree of saturation present different results, with pressure plate tests desaturating at lower suctions than tensiometer tests (Toll et. al., 2015). Such differences were explained as being due to different volumetric responses; with pressure plate tests showing different shrinkage paths that resulted

in less volume change. Therefore, it is important to obtain volumetric measurements as part of the determination of the soil water retention curves, especially by implementing continuous volume change readings that is unlikely to be carried out using axis translation technique.

Nevertheless, despite its well-known drawbacks, the pressure plate extractor is still considered as one of the most convenient piece of equipment for the determination of water retention properties of unsaturated soils. Further research efforts are essential to limit these drawbacks and to suggest possible improvements in order to increase its data reliability (Bittelli and Flury, 2009).

4.2.2.2 High Capacity (HC) tensiometer (direct suction measurement technique)

Equipment and procedures

To determine the SWRC using this technique, the combination of high suction tensiometers for suction measurement and an electronic balance to record water content is used (Cunningham, 2000, Boso et al., 2003, Toker et al., 2004, Lourenço et. al., 2007, Lourenço, 2008, Toll et. al., 2013, 2015). This technique can be done either by drying continuously while exposed to the atmosphere (continuous procedure) or by drying in stages (stage procedure). The technique can also be used for wetting, where water is added in a slow, controlled way. In the stage procedure, the specimen is sealed and allowed to equalise internally after each period of drying or wetting (Toll et al, 2015).

A number of studies have been made for the comparison between both procedures (Boso et al., 2003, Cunningham, 2000, Lourenço et. al., 2007, Li and Standing 2014). Boso et al. (2003) and Cunningham (2000) have highlighted that the evaporation rate had little or no influence on the resulting soil water retention curve obtained by the continuous procedure. The studies, that were carried out on samples of reconstituted clayey silt and reconstituted silty clay, also indicate that there is no difference observed between the SWRCs using these two procedures. However, for test implemented on granular material, Li and Standing (2014) have emphasized the importance of controlling temperature and humidity that will influence the SWRC of the sample. It is suggested that ambient conditions around the test set up should be

kept stable as possible during the process of developing SWRCs. Thus, the continuous method apparatus was set up within an insulated chamber (with wooden walls) in order to minimise additional evaporation effects.

Lourenço et al. (2007) reported that the SWRCs obtained by continuous drying showed higher suctions (by as much as 200kPa) than the SWRCs obtained by stage drying at the same water content (equivalent to higher water contents at the same suction). These results were initially described by the lack of suction equalization throughout the sample due to:

i. The fast evaporation rate controlled by the low relative humidity inside the laboratory.
ii. The limited surface area of the sample exposed to the atmosphere.
iii. The fact that the measurements of suction were conducted on the exposed sample surface.
iv. Possible additional errors introduced by the experimental set-up (e.g. errors in the measurement of the sample mass due to the weight and stiffness of the tensiometer cable).

Reliability Review

The main disadvantages of the high capacity tensiometer, in general, are cavitation and zero suction value (Mendes, 2011). When the device is used for a long period in the negative pressure range, a drift in zero suction value can be observed. Although for certain types of tensiometer, the variations may be small (i.e. ranging up to 5 kPa for high capacity tensiometers developed at Durham University, as reported by Lourenço et al. (2006), Lourenco (2008) and Toll et al. (2013)); this can induce some errors, when working in the small suction range unless the zero value is checked regularly.

The advantages on using high capacity tensiometer are mainly in its practicality to implement direct measurement of suction of a soil due to the small size of the equipment and quick measurement. Its ability to permit the process of natural drying without any imposition of air pressure, either during continuous or stage procedure testing, is also one of the important factors that makes it more relevant

than any other equipment. For this reason, cavitation can take place naturally within the soil and this reflects in a greater replication of soil natural behaviour (Toll et. al, 2013). Furthermore, a continuous volume measurement can also be made with the continuous procedure, which would provide greater accuracy for the representation of SWRC behaviour (Toll et. al., 2015). In addition, both continuous and stage approaches have also been found to be quicker than the traditional methods (e.g. pressure plate) for obtaining SWRCs (Lourenço, 2008).

4.2.3 Permeability function

Another soil property that is equally important, when dealing with unsaturated soil, is the permeability function. In general, the soil permeability (hydraulic conductivity) is defined by the ability of the soil to transmit water throughout its pores. When the soil pores are completely filled with water, in a saturated condition, continuous channels of groundwater flow are expected. However, when there is existence of air in soil pores, associated with an unsaturated condition, the permeability of the soil will reduce. This means that the soil permeability is greatly dependant on the water content of the soil (i.e. Degree of Saturation or Volumetric water content). This also explains why that the soil permeability is not constant under unsaturated conditions (Fredlund et al., 1994).

The permeability function of a soil is normally expressed by the relationship between the coefficient of water permeability against matric suction. Under unsaturated conditions, the correlation between these two hydraulic properties will produce a non-linear function but eventually approaching constant permeability value as it reaches the saturated state. The methods of deriving the permeability function of a soil can be implemented either by direct measurement by laboratory works and field measurement, or by numerical estimation from water retention data (SWRC). The direct measurement methods are practically more expensive and time consuming (van Genuchten et. al., 1991, Leong and Rahardjo, 1997, Toll et. al., 2014). Due to these reasons, the difficulty in predicting the unsaturated hydraulic conductivity is often overcome by adopting the commonly used integration functions, which are based on soil-water retention data. These estimation methods predict the shape of the function relative to the saturated permeability value which is more easily obtained.

There are three methods to produce the permeability function using SWRC, which are; (i) empirical; (ii) macroscopic and (iii) statistical. For the empirical method, the unsaturated permeability is expressed as a function of saturated permeability with either the volumetric water content or the matric suction (Frendlund and Rahardjo, 1993). The correlations between these parameters are controlled by the adoption of certain fitting parameters introduced in each equation. These parameters are mostly determined from a curve fit of the direct measurement of permeability test data but some researchers have attempted to define some of these constants (e.g. Wind, 1955). Nevertheless, the permeability function by this method is less suitable particularly for problems involving a wide range of degree of saturation change (dry to fully saturated conditions).

On the other hand, the permeability function using macroscopic method is developed by the assumption of similarity between laminar flow (microscopic level) to flow in porous media (macroscopic level). Based on this assumption, the average macroscopic flow variables (e.g flow velocity, hydraulic gradient, permeability, and hydraulic radius) can be used as to interrelate with the microscopic flow behaviour within the soil. The direct analogy between these variables with the corresponding variables for a soil-water-air system is generally presented in term of degree of saturation. Although the method is based on fundamental physical laws, the inability to incorporate the effects of pore size distribution can cause difficulties to replicate the actual soil systems (Brooks and Corey, 1964).

As a result, the subsequent alternative to predict the permeability function is now based on the use of the so-called statistical method. This method is developed based upon three assumptions (Mualem, 1986), which are;

i. The soil pores are interconnected and distributed randomly in the soil;
i. The Hagen-Poiseuille equation is used to estimate the permeability of a pore channel and the total permeability is determined by integration over the contributions from the filled pores.
ii. The SWRC function is analogous to the pore size distribution function.

The method is the most popular because it includes the influence of pore-size distribution on the soil suction and permeability (e.g. Green and Corey, 1971, Fredlund et. al., 1994, Van Genuchten, 1980). Also, SWRC data can be directly

used due to the relationship with the volumetric water content for the development of the permeability function for unsaturated soils. Among the various available models produced from this method is the model introduced by van Genuchten (1980). The model can be considered as the most widely adopted and has even been included as a standard function in a number of geotechnical engineering software packages available in the market. The model proposed the following closed form equation to describe the hydraulic conductivity of a soil as a function of matric suction:

$$k_w = k_s . \frac{\left[1-\left(a\psi^{(n-1)}\right)\left(1+(a\psi^n)^{-m}\right)\right]^2}{\left[\left((1+a\psi)^n\right)^{\frac{m}{2}}\right]} \quad \ldots(4.2)$$

Where, k_s = saturated hydraulic conductivity

ψ = required suction range

a, m, n = SWRC curve fitting parameters; which, $m = 1 - \frac{1}{n}$ … (4.3)

From Equation 4.2, the hydraulic conductivity function of a soil can be estimated once the saturated conductivity and the two curve fitting parameters, a and n are known. These fitting parameters can be estimated graphically based on the SWRC, expressed in terms of the volumetric water content of the soil.

4.3 Details of Undisturbed Residual Soil Samples for Hydrological tests

A total number of 13 samples of residual soil were obtained from the Mazier sampler tubes (described in Chapter 2) for both permeability and SWRC hydrological testing. The details of these samples are summarised and shown in Table 4.1.

Table 4.1 Details of the undisturbed permeability and SWRC hydrological tests specimens.

Layer	Mazier Tube	Depth (m)	Testing type	Number of samples
1	MZ1	1.0 to 2.0	Permeability	3
			SWRC	1
	MZ2	2.0 to 3.0	SWRC	3
2	MZ3	3.0 to 4.0	Permeability	1
			SWRC	1
	MZ4	4.0 to 5.0	Permeability	2
Total				13

It can be seen that adequate number of samples have been selected from each tube in order to define the permeability and SWRC of layer 1 and layer 2 (Figure 2.9 in Chapter 2). MZ1 and MZ2 were found to be similar in characteristics to represent the properties for Layer 1, thus, 3 samples were prepared for permeability tests (denoted as MZ1S1, MZ1S2 and MZ1S3). A similar total number of specimens were also prepared from MZ3 and MZ4 for the determination of permeability of layer 2 (denoted as MZ3S1, MZ4S2 and MZ4S3). The specimens used for determination of permeability were those later used for triaxial testing. Permeability was carried out as part of the saturation procedure, prior to strength testing. The dimensions for each sample were 75mm diameter with 150mm in height and further details on the initial conditions of each sample are presented in Table 3.4 and Table 3.5 in Chapter 3.

For soil water retention behaviour; a total number of 5 samples were successfully prepared from MZ1, MZ2 and MZ3 for the determination of SWRC of each layer (denoted as MZ1S1, MZ2S1, MZ2S2, MZ2S3 and MZ3S1). However, due

to less recovery obtained in MZ3 and MZ4, only 1 specimen would be selected for SWRC of Layer 2. The dimensions for each sample for the SWRC test were 70mm diameter with 20mm in height. The equipment used for the preparation of the samples is shown in Figures 4.8.

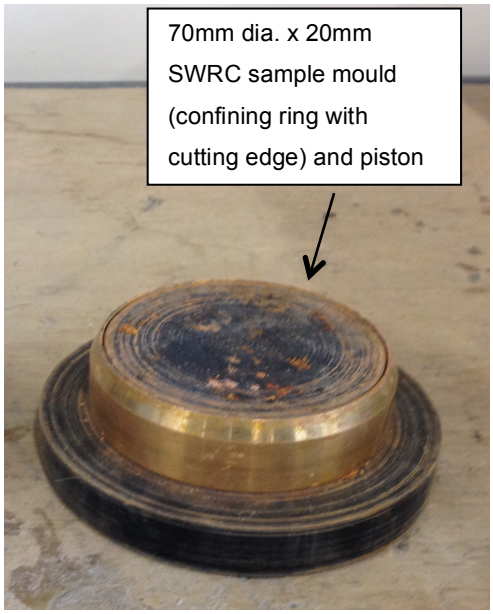

Figure 4.8 Photos of the process of SWRC sample preparations and the utilised equipment.

4.4 Saturated Permeability Tests (k_{sat})

4.4.1 Test procedures

The procedure outlined in Clause 6 of BS1337 (1990) was adopted for the permeability testing on the samples described previously. This procedure has been described to be suitable for low and intermediate permeability soils (i.e. clays and silts) and hence relevant for residual soils. The procedure is executed by imposing the sample in the triaxial apparatus with a known condition of effective stress under the application of a backpressure, and a constant hydraulic gradient is applied across it i.e. a constant head test (Head, 1998). The coefficient of permeability at saturation, k_{sat}, was then determined by measuring the volume of water passing through the sample (downwards).

The permeability test was carried out on each sample after the equalisation procedure of the first confining stage (Multistage triaxial tests). At this point, the back pressure system at the top of the sample was increased to 320kPa (while bottom pressure was maintained at 300kPa), to give a pressure difference up to 20kPa between top and bottom of the sample. The main purpose of this procedure was to initiate downward flow within the specimen (Head, 1998). During this stage, the readings of the volume gauges connected to the top and bottom of the sample were recorded and plotted against time. These data measurements were implemented by using a real-time data acquisition system (TRIAX), developed by Toll (1999). The procedure was continued until the two plots were linear and relatively parallel (top and bottom volume gauge readings against time), which indicate that a steady state has been reached. Finally, the test was stopped by reducing the top pressure down to the value equal to the pressure at the bottom of the sample before the line was closed and was left for further consolidation. Further details of the configuration of Triaxial testing apparatus can be seen in Figure 3.6, in Chapter 3.

4.4.2 Results

The recorded cumulative flow (volume gauge readings) against time for each sample, defined for layer 1 and 2, are presented in Figures 4.9 and 4.10. From the

plots, it can be seen that linear relationship was achieved by both volume gauges connected to the top and bottom of the sample.

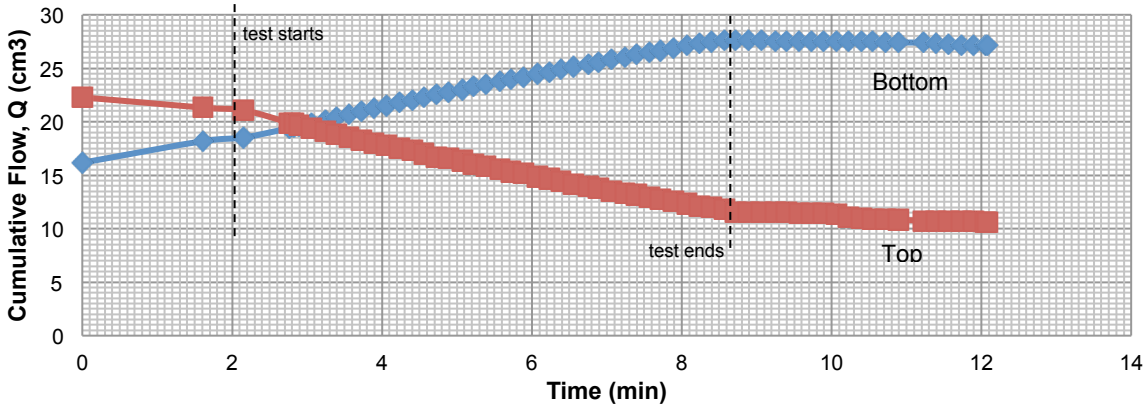

(a) Test 1 (MZ1S1)

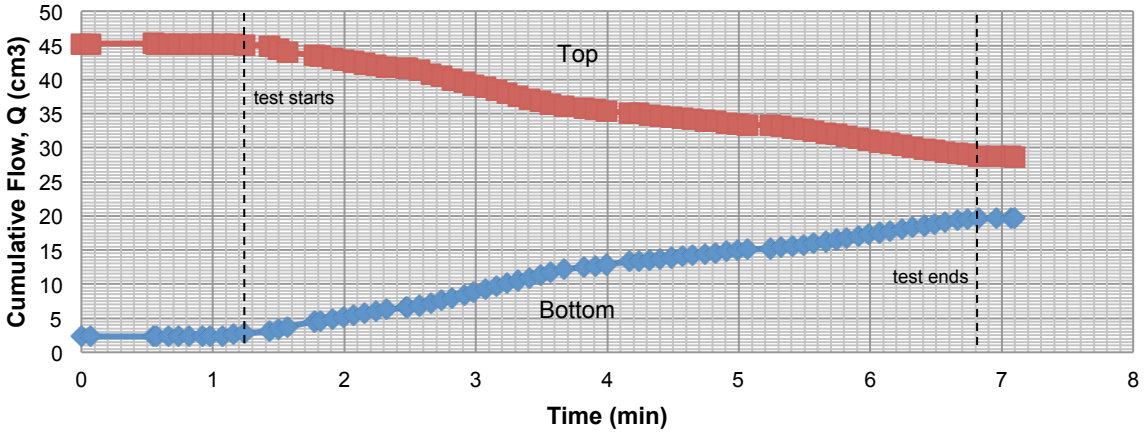

(b) Test 2 (MZ1S2)

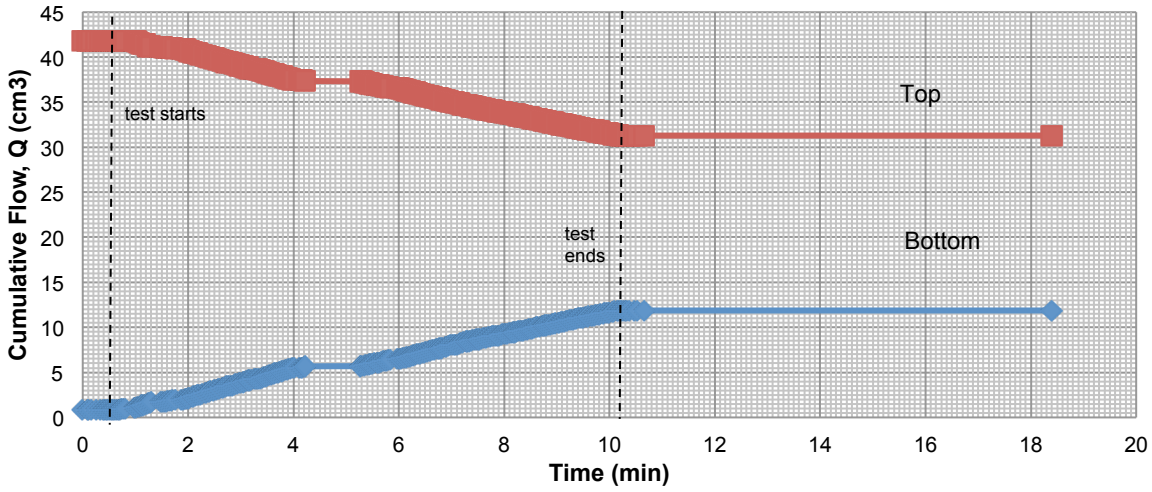

(c) Test 3 (MZ1S3)

Figure 4.9 The recorded cumulative flow (volume gauge readings) against time for specimens of layer 1.

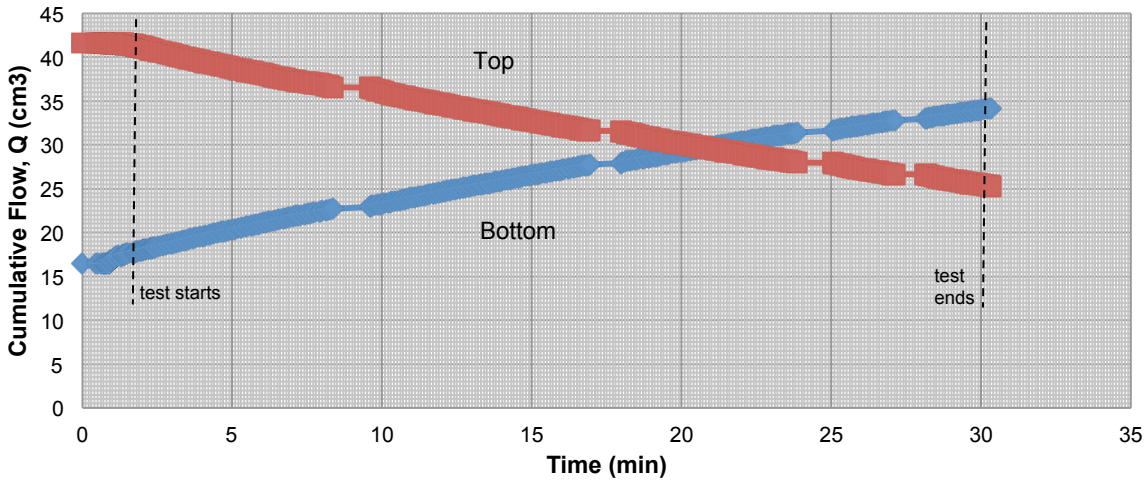

(a) Test 1 (MZ3S1)

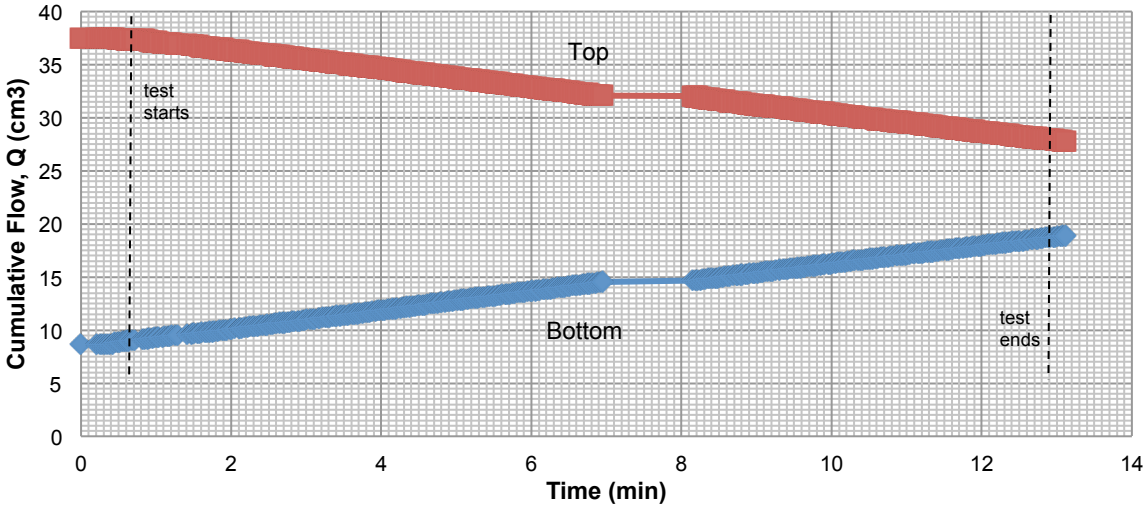

(b) Test 2 (MZ4S2)

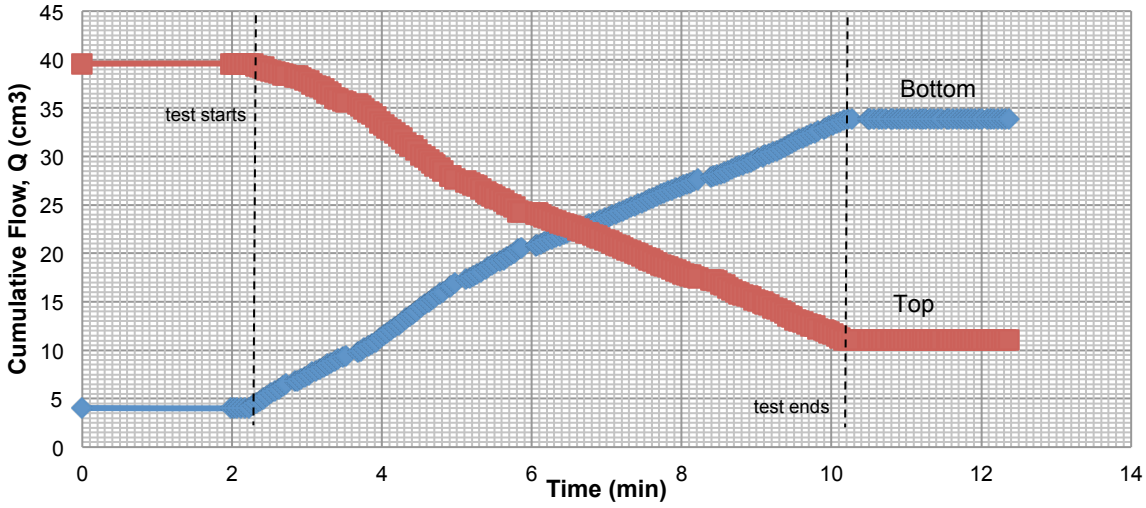

(c) Test 3 (MZ4S3)

Figure 4.10 The recorded cumulative flow (volume gauge readings) against time for specimens of layer 2.

Using these data, the mean rate of flow (q) was calculated, which is represented by the slope of the graph. Whilst, the hydraulic gradient value of each test was calculated using Equation 4.4.

$$i = \frac{\Delta p \times 1000}{9.81 \times H} \quad \ldots (4.4)$$

Where, Δp = Top and bottom pressure difference (kPa).

H = Height of the specimen (mm).

Subsequently, the permeability of the soil for each layer was determined and this was done based on the expression shown in Equation 4.5.

$$k_{sat} = \frac{q}{A \times i \times 60} \quad \ldots (4.5)$$

q = The mean rate of flow (ml/min).

A = Cross-sectional area of the specimen (mm^2).

i = Hydraulic gradient

Table 4.2a and 4.2b present the overall results of the permeability tests, calculated for both layers. The results show that the permeability of the specimens of layer 1 ranges from 3.96×10^{-7} m/s to 1.31×10^{-6} m/s (with average of 8.33×10^{-7}), while, for samples of layer 2 ranges between 2.40×10^{-7} m/s to 1.26×10^{-6} m/s (with average of 6.98×10^{-7}). An average value of 8×10^{-7} m/s has been adopted to represent the saturated coefficient of permeability for both layer 1 and 2.

Table 4.2a Details of the overall results of the permeability tests for layer 1.

Depth (m)	Test No.	Specimen	Confining Pressure (kPa)	Pressure Difference (kPa)	Sample Cross Section Area (mm^2)	Hydraulic Gradient, i	Flow rate, q (cm^3/min)	Permeability, k_v (m/s)
1 to 2	1	MZ1S1	25	20.6	4299.07	13.80	1.41	3.96E-07
	2	MZ1S2	50	22.4	4218.01	14.94	4.95	13.08E-07
	3	MZ1S3	100	9.9	4084.80	6.60	1.29	7.95E-07

Table 4.2b Details of the overall results of the permeability tests for layer 2.

Depth (m)	Test No.	Specimen	Confining Pressure (kPa)	Pressure Difference (kPa)	Sample Cross Section Area (mm^2)	Hydraulic Gradient, i	Flow rate, q (cm^3/min)	Permeability, k_v (m/s)
3 to 5	1	MZ3S1	25	20.4	3663.40	12.50	0.66	2.40E-07
	2	MZ4S2	50	10.4	3854.07	6.60	0.91	5.95E-07
	3	MZ4S3	100	20.4	3588.77	12.41	3.36	12.58E-07

4.5 Soil Water Retention Curve tests

It has been discussed earlier that SWRCs present hysteric behaviour. This means that the representation of the data depends on the path chosen to obtain the curve, which is either through the process of soil drying or wetting. To acquire the primary drying curve, the requirement to fully saturate the sample is essential. Without adhering to this condition, the curve may not be defined as primary drying curve (as the sample is not dried from a slurry condition) but instead a scanning curve, representing a state between the primary drying curve and primary wetting curve.

However, for the case of the residual soil samples, this sample saturation procedure can lead to the possibility of altering the natural fabric of the soil (e.g. natural geometrical arrangement of particles within a soil). According to Toll (1990, 2000), the effect of fabric on the behaviour of unsaturated soils can be of great significance as it may cause differences in characteristics. Therefore, in order to minimise the possibilities of disturbance to these specimens, it was decided to implement the drying process from the initial natural conditions.

The axis translation technique using pressure plate apparatus and direct suction measurement technique using high capacity tensiometer for both continous and stage methods were adopted in these drying tests. The specimens were then rewetted (except for specimens tested using the continuous method) for the derivation of wetting curves as well as scanning curves.

4.5.1 Initial condition of residual soil specimens

The initial conditions for each SWRC samples are presented in Tables 4.3. Distinct variations in water content can be seen for each sample that reflect the variation in bulk density (ρ_{bulk}), void ratio (e) and degree of saturation (S_r). Similar to the samples prepared for the mechanical tests, the presence of organic materials (i.e tree roots etc.) and fissures were seen and these can be considered as one of the factors causing variations.

Table 4.3 Details of the initial conditions for each SWRC samples

Soil Specimens	Water Content	Mass	Dimensions				Density		Void Ratio	Degree of Saturation	Volumetric W.C.	SWRC method
							Bulk	Dry				
			h	d	A	V	ρ	ρ_{dry}		S_r		
	%	g	cm	cm	cm^2	cm^3	Mg/cm^3	Mg/cm^3	e	%	Θ_w	
MZ1S1	33.9	142.2	2.06	6.99	38.35	78.96	1.80	1.35	1.08	87.8	0.46	P.Plate
MZ2S1	26.7	157.3	2.09	7.00	38.48	80.36	1.96	1.54	0.81	92.0	0.41	P.Plate
MZ2S2	28.7	151.5	2.07	7.05	39.04	80.81	1.88	1.46	0.92	87.2	0.42	Tensio - Stg
MZ2S3	29.0	154.0	2.04	7.03	38.82	79.25	1.94	1.51	0.86	94.6	0.44	Tensio - Cont
MZ3S1	24.0	153.2	2.04	7.10	39.59	80.77	1.90	1.53	0.83	80.9	0.37	Tensio - Cont

4.5.2 Test procedures

4.5.2.1 Pressure plate

The pressure plate apparatus system introduced by Vaquero (2007) was used on samples MZ1S1 and MZ2S1. As indicated in Section 4.2.4.1, the system allows independent multi sample testing (up to four soil samples) by the utilisation of four porous discs plate with 1.5MPa AEV that are connected to four independent volume gauges. Also, to impose higher air pressure within the cell (more than 1000kPa), a gas supply by nitrogen bottles can be used as an alternative to the conventional laboratory air compressor.

It was important to ensure that the ceramic discs were completely saturated before testing. This procedure was required for the removal of all trapped air bubbles within the ceramic discs that could affect the reliability of the suction measurements. To implement this procedure, the plates were submerged within deaired water inside the cell, up to approximately 2cm above its surface. Then, the cell top was tightly fastened and an air pressure of 20kPa was applied in order to push water through. The air pressure was increased gradually in steps until the volume gauge reading became constant, which means no air bubbles were present inside the cell.

Once the ceramic discs were fully saturated, the excess water inside the cell was drained out down to the level slightly below the top edge of the ceramic plates. This was carried out in order to humidify the air inside the cell and to avoid excess drying of the specimens. The samples were then placed on the saturated porous

ceramic plates and the cell was tightly covered using the cell top. This time the air pressure was increased to 270kPa, with a constant 250kPa backpressure beneath the plate to impose the initial desired value of 20kPa matric suction on the specimens (the difference between air and water pressure). The application of backpressure was made to prevent dissolved air coming out of solution.

During this stage, the readings of the volume gauges connected to the ceramic discs would show the volume of water flowing in or out of the specimen as the suction was changed. Similarly, these data measurements were implemented by using a real-time data acquisition system (TRIAX), developed by Toll (1999). The equalisation of a soil sample was assumed to be reached when the volume change read by the gauge was less than 0.35cc/day, as implemented by Mendes (2011). After equalization, the samples were taken out of the cell and the weight was measured to the nearest 0.01g as well as dimensions with an accuracy of 0.01mm using Vernier callipers. These procedures were repeated until highest suction imposed was 1163kPa, using an air pressure of 1400kPa and a water pressure of 237kPa. Then, the wetting procedure was carried out by gradual reducing the air pressure (but maintained 250kPa back pressure) until suction was equal to 10kPa.

4.5.2.2 High capacity tensiometer – Stage procedure

The stage procedure developed by Lourenço et. al. (2007) for tensiometer SWRC test was used for sample MZ2S2. This procedure required the specimen to be sealed and allowed to equalise internally after each period of drying or wetting. The suction measurement was taken at the bottom of the sample on a PVC pedestal designed with an O-ring to hold the tensiometer so that the specimen rested on it by its own weight (Figure 4.11).

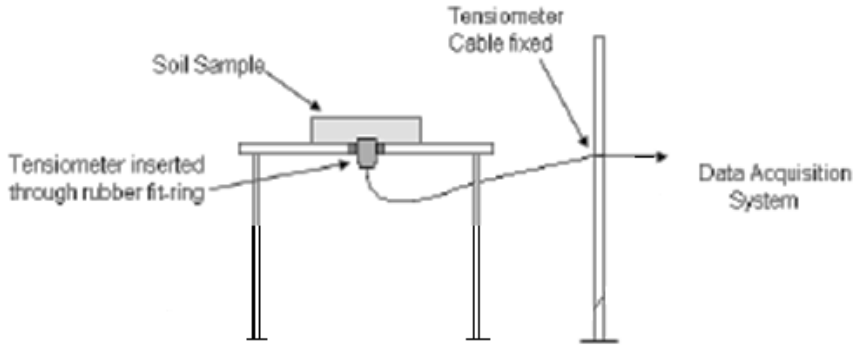

Figure 4.11 Configuration of high capacity tensiometer – stage procedure test .

The drying wetting procedures were defined by achieving the target mass calculated according to Equation 4.6.

$$m_{final} = \frac{m_{initial}+(1+w_{final})}{(1+w_{initial})} \quad \ldots (4.6)$$

Where m_{final}= the targeted mass after drying or wetting procedure.

$m_{initial}$= the initial mass of the specimen

w_{final} = the desired water content for SWRC

$w_{initial}$ = the initial water content of the specimen

Based on this targeted mass value, the sample was air dried in a controlled way using an electronic balance (Figure 4.12). Then, the sample was sealed using cling film and placed inside a container to allow equalisation for a period of at least 24 hours. After equalisation, a suction measurement was taken at the bottom of the specimen and volumetric measurements were obtained by measuring the sample diameter and height using a Vernier calliper. This procedure was repeated for successive different water contents until suction measurement was as high as 590kPa. At this suction, the condition of the sample was observed to be considerably dry and this has caused difficulty in getting a perfect contact between both soil and tensiometer surfaces. By further forcing the tensiometer into the soil, it would cause additional disturbance to be experienced. Therefore, the wetting procedure was subsequently performed.

In the wetting procedure, a few small drops of water were placed on top of the sample using a syringe (Figure 4.12). This was done slowly until the targeted mass was achieved. After that, the sample was once again sealed and left for equalization period (at least 24 hour). These procedures were carried out in a temperature control room to prevent rapid evaporation of the specimen. 3 cycles of drying and wetting procedures were implemented using this procedure in order to study the characteristic of scanning curves for residual soil.

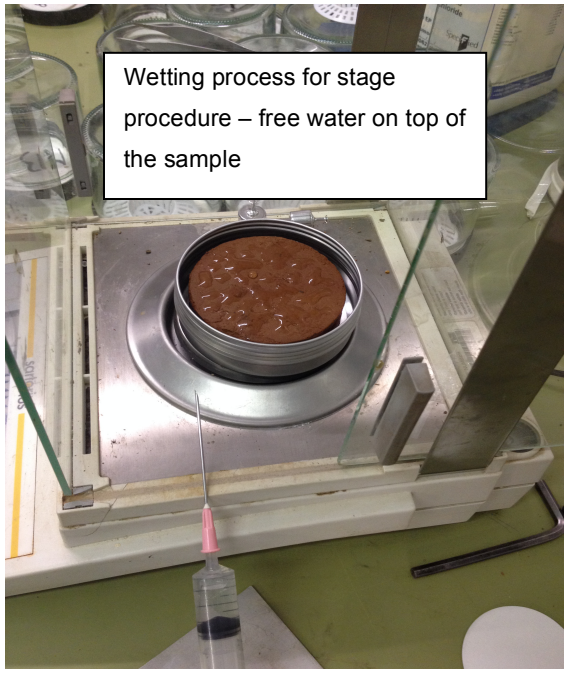

Figure 4.12 Photos of drying and wetting process for SWRC test using high capacity tensiometer (stage procedure).

4.5.2.3 High capacity tensiometer –Continous procedure

The tensiometer SWRC test for samples MZ2S3 and MZ3S1 were carried out using the modified version by Noguchi et al. (2012) and Liu et al. (2016) on the test procedure developed by Lourenço et al. (2007). Using this modification, it allows continuous measurements of water content, suction and volume change to be made while the sample was being air-dried. The apparatus was made up of a PVC frame (shown in Figure 4.13) and placed on an electronic balance to determine the change in sample weight and hence water content. The apparatus consists of 6 displacement transducers that were attached to the sample through the four outside beams of a PVC frame to measure radial displacement and two more through the upper beam to measure axial displacement.

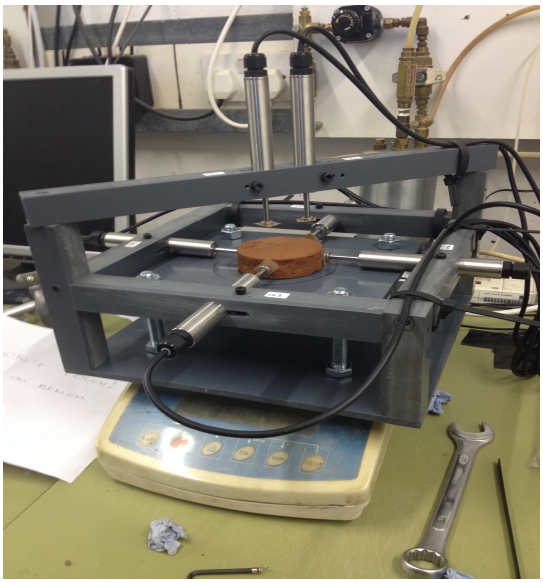

Figure 4.13 View of equipment for SWRC test using using high capacity tensiometer (continous procedure).

For the suction measurements, a tensiometer was fitted through a hole in the support plate, with a tight fitting rubber O-ring to secure it in place. All the cables of the transducers and the tensiometer were fixed and connected to a real-time data acquisition system (Toll, 1999). A retort stand was used to minimize the influence of cable stiffness on the mass measurement (Lourenco, 2008). It has been reported by Liu et al. (2016) that the apparent mass change due to the cables was less than 0.25g. This assembly was also set up in a laboratory room with a controlled temperature of approximately 20°C.

4.5.3 Results

4.5.3.1 Initial drying curve

The initial drying SWRCs of each test (pressure plate, stage drying and continuous drying tests) have been compiled and plotted as gravimetric water content, volumetric water content and degree of saturation against suction. These tests were performed from each sample's natural state so as to study its genuine response during drying. These plots are presented in Figure 4.14, 4.15 and 4.16.

In Figure 4.14, it can be seen that the variation for each test is highly related to the location of each samples within the ground profile, which reflects the variation in degree of weathering (varying gravimetric water content). Despite the reasonable agreement exhibited by the tests implemented on samples obtained from MZ2 (variation in water content - less than 2%), samples MZ1S1 and MZ3S1 show different trends. For sample MZ1S1, the water content variation (up to 6% higher than specimens from MZ2) can be linked to the depth of the sample that is closer to the ground surface, where a more porous structure (void ratio 1.08, Table 3.4) causes more water to be retained, giving higher gravimetric water content. The rate of desaturation (the slope of transition zone), however, is relatively similar to the tests of samples from MZ2 as both tubes are of similar material. Whereas, MZ3S1 is different due to the higher fraction of coarser material (approximately 27% of sand material as shown in Figure 2.17 in Chapter 2), reflected from a lower degree of weathering. This explains the differences on the position of the plots as well as gradient of the curve (steeper slope).

It has been mentioned earlier that volumetric measurements were made throughout each test. This was done to capture the effect of volume change (shrinkage) during the desaturation process. In Figure 4.15, the presentation of SWRC using volumetric water content is presented based on the relationship between the changes in water content and dry density of each specimen during drying. From the plots, better agreement can be seen for every sample obtained from MZ1 and MZ2 due to the similarity in initial volumetric water content (0.41 to 0.46) for layer 1. The dissimilarity shown by SWRC of MZ3S1 further supports the

observation that the specimen for Layer 2 is of different material to the Layer 1 material.

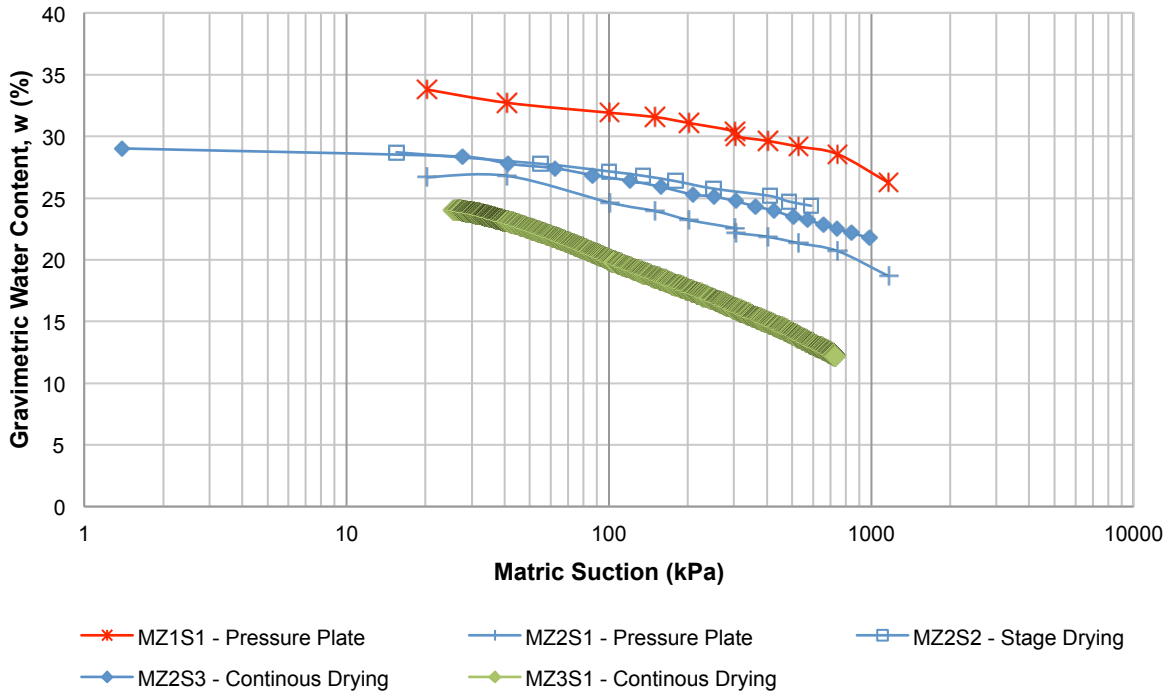

Figure 4.14 Initial drying SWRCs - gravimetric water content against suction

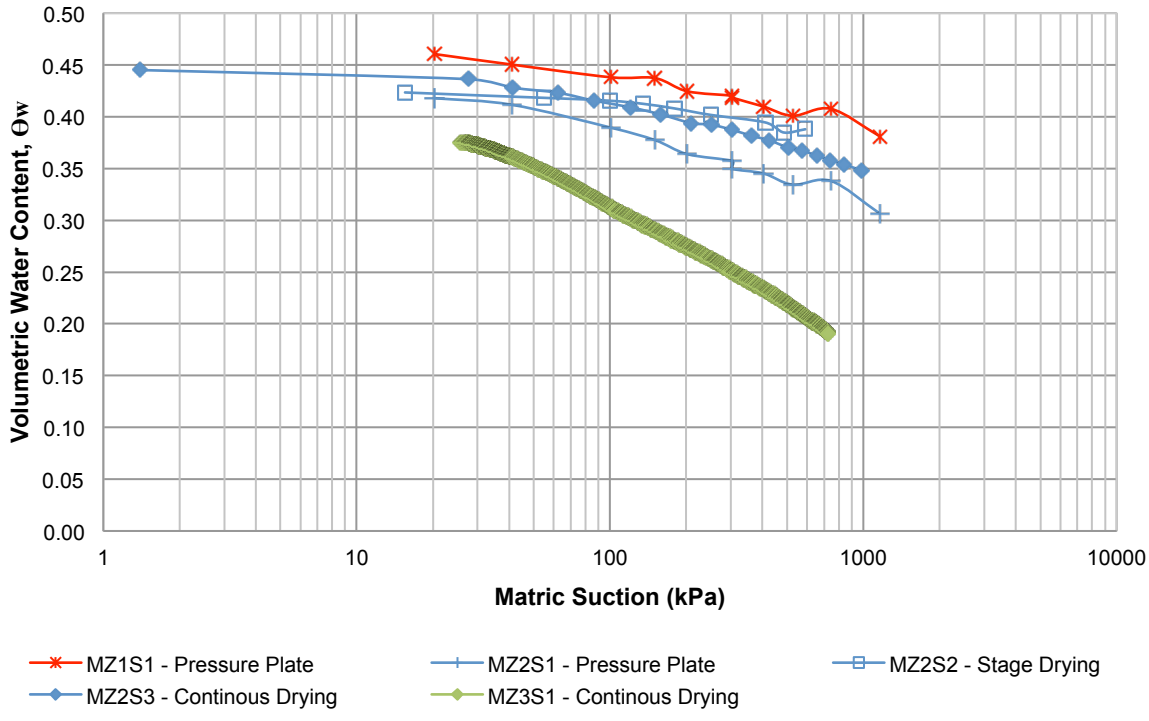

Figure 4.15 Initial drying SWRCs - volumetric water content against suction

The presentation of SWRCs in terms of degree of saturation is shown in Figure 4.16. From the plot, it can be seen that MZ1S1 presents a S_r at the bottom of the range for samples obtained from MZ2, even though the gravimetric water content was higher. As indicated previously, the porous structure has caused a high void ratio, thus, giving less degree of saturation even with higher water content. This probably reflects a higher degree of weathering for a layer closer to the ground surface.

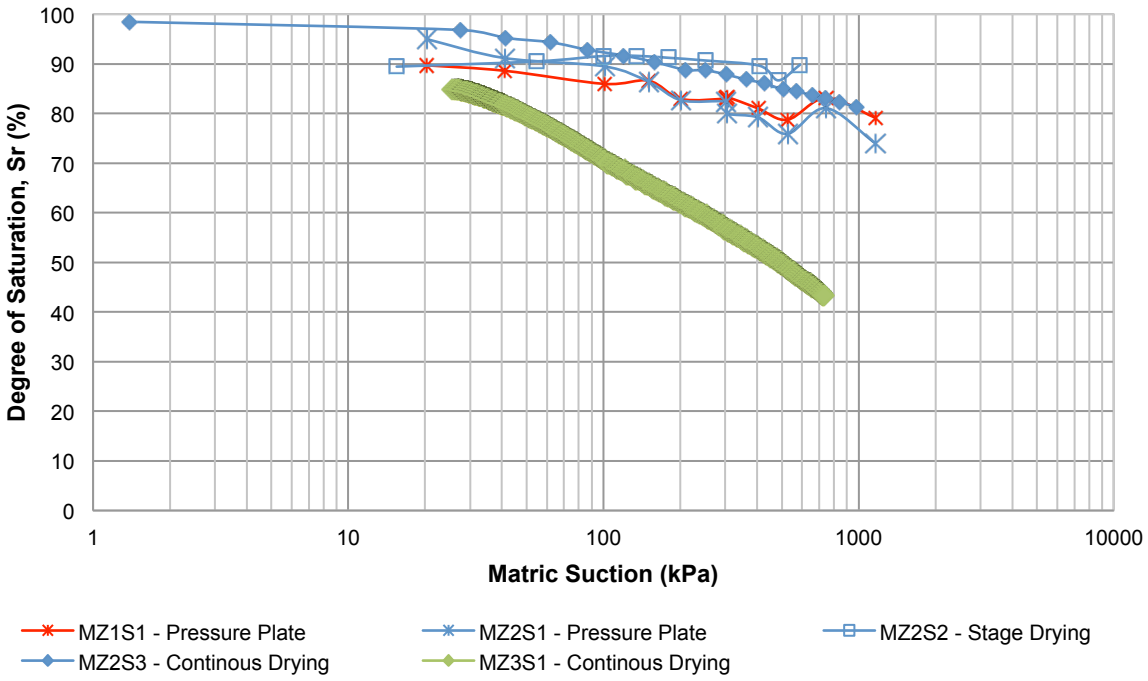

Figure 4.16 Initial drying SWRCs – degree of saturation against suction

To further describe the characteristics of each curve, the comparison between AEV for each SWRC plotted using volumetric water content and degree of saturation (Figure 4.15 and 4.16) is presented in Table 4.4. These AEVs were numerically obtained from the estimation of curve fitting parameters (i.e. 'a', 'n', 'm', if expressed in terms of volumetric water content; or 'g_a', 'g_n', 'g_l', if expressed in terms of degree of saturation) using the RETC code (van Genuchten et al., 1991). The code defines the parameter 'a' or 'g_a' to be related to the inverse of the AEV and is represented by the unit of pressure head. Thus, a conversion into SI unit of kPa is required and this can be done, using Equation 4.7. A fixed relationship has been assumed between

the 'n' and 'm' or 'g_n' and 'g_l' parameters as shown in Equation 4.3 (Mualem 1986) and these represent the gradient and the asymmetry of the curve.

$$AEV = \frac{a^{-1}}{0.102} \quad \ldots (4.7)$$

Table 4.4 The estimated curve fitting parameters ('a', 'n', 'm' and 'g_a', 'g_n', 'g_l') using the RETC code (van Genuchten et al., 1991) and the AEV for initial drying SWRCs of each test

Soil Specimens	van Genuchten parameters						Air entry value (AEV)		SWRC method
	using volumetric water content, θ_w			using degree of saturation, S_r			θ_w	S_r	
	a	m	n	g_a	g_l	g_n	kPa	kPa	
MZ1S1	0.132	0.062	1.066	0.858	0.034	1.035	75	11	P.Plate
MZ2S1	0.204	0.092	1.102	0.581	0.064	1.069	48	17	P.Plate
MZ2S2	0.040	0.078	1.084	0.004	0.426	1.741	248	2770	Tensio - Stg
MZ2S3	0.131	0.084	1.091	0.133	0.061	1.066	75	74	Tensio - Cont
MZ3S1	0.164	0.219	1.280	0.167	0.217	1.278	60	59	Tensio - Cont

It has to be noted that the AEV for both hydrological terms should be similar, if the weight and volume measurements truly represent the actual behaviour of the soil. Any mistakes carried out during testing will provide variation to these soil properties as they are highly related to volumetric measurement, especially the degree of saturation. From Table 4.4, it appears that only tests using the continuous procedure (MZ2S3 and MZ3S1) provide similarity of AEV values, with 1kPa difference. The magnitude, however, is slightly higher for MZ2S3 (75kPa) as compared to MZ3S1 (60kPa). This is attributable to the suggestion described for clayey soil in which the air entry value should be higher than a coarser material (Fredlund and Rahardjo, 1993). Moreover, the differences of 'n', 'm' and 'g_n', 'g_l' reflect the variation in gradient of both curves in the transition zone that further support the differences in material distribution of Layer 1 and Layer 2. The value of 'n' or 'g_n' for Layer 1 is 1.066 to 1.102 but Layer 2 shows a steeper slope with 'n' or 'g_n' equal to 1.280.

However, a huge variation of AEV for both hydrological terms can be seen for the tests using pressure plate and stage procedure. These differences are within

31kPa and 2522kPa and particularly higher for the results from SWRC of MZ2S2 (stage method). The most likely reason is due to the disturbance experienced by the samples during the handling for weight and volume measurements. Also, it can be seen that only the stage method gives AEV using S_r as a higher value than the AEV using volumetric water content. This is attributable to the fact that diameter/height readings are not repeatable due to the difficulties to obtain measurements at the same part of the sample using a Vernier calliper. In addition, the procedure of measuring the suction for the stage method, by forcing the tensiometer into the soil, could also be one of the factor that causes additional volume changes to the sample as a small depression could be seen to occur at the bottom of the specimen, which grew in size with the sequence of measurements (Figure 4.17).

Figure 4.17 A small depression formed by pressing in the tensiometer that grew in size with the sequence of suction measurements

Despite these differences, the results for the parameters 'n' and 'm' for each sample using pressure plate and stage procedure (MZ1S1, MZ2S1 and MZ2S2) seem to show a reasonable agreement with the parameters obtained for MZ2S3 (continuous method). For the SWRCs in terms of volumetric water content, the value of parameter 'm' ranges from 0.062 to 0.084, while 1.066 to 1.091 for the parameter 'n'. This provides further evidence that these samples are of similar material (Layer 1). Whereas, for the SWRCs in terms of degree of saturation, the results from stage method show differently, with a flatter curve as compared to the rest (Figure 4.16). As discussed earlier, this is due to erroneous volume measurements.

To further compare the differences between each test method, the data is plotted as conventional shrinkage curves in the form of void ratio against gravimetric water content (Figure 4.18). From the plots, it is apparent that the continuous method

(MZ2S3 and MZ3S1) gives better explanation of volume changes of the soil by the smooth deviation of shrinkage behaviour. The data fluctuation on the volume changes by the rest of the tests (pressure plate and stage method) can be associated with the disturbance experienced by the samples during testing.

Despite that each sample was dried from its natural condition to minimise the possibilities of disturbance, the trends for each curve, however, seem to move away from the saturation line, which demonstrates less shrinkage behaviour. For sample MZ2S2 (stage method), the gradient of the curve seems to be steeper than the rest of the tests and this is due to the additional disturbance imposed on the sample for suction measurement as well as the unrepeatable diameter/height measuring points for volume measurement. MZ3S1 does not show much change on volume. This can be associated with the low degree of weathering through the preservation of its parent bedrock original behaviour (high degree of cementation between soil particles) and higher fraction of coarser material. Overall, these results signify the importance of continuous measurements of water content, suction and volume change for the determination of SWRC. Its requirement is even greater, especially when dealing with tropical residual soil that is well known of its heterogeneous characteristics.

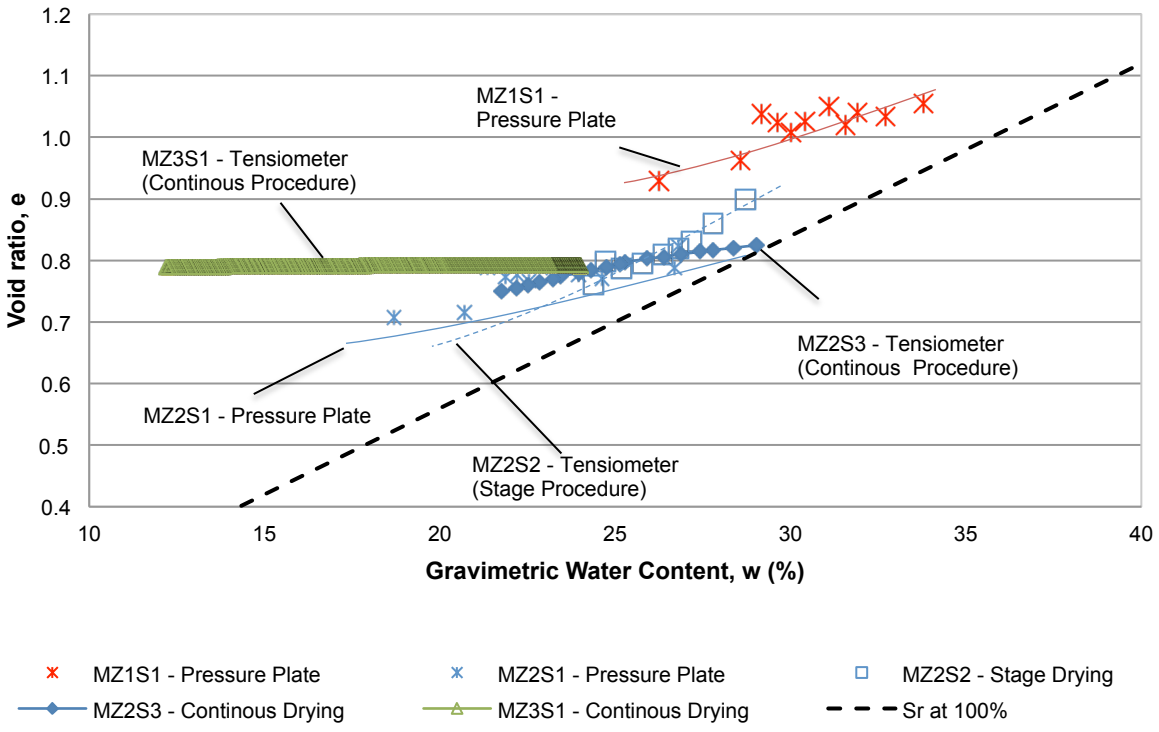

Figure 4.18 Conventional shrinkage curves - void ratio against gravimetric water content

4.5.3.2 Wetting curve

Wetting procedures were conducted for sample MZ1S1, MZ2S1 and MZ2S2 using pressure plate and tensiometer-stage procedure. The results are shown in Figure 4.19, 4.20, 4.21, and are plotted in terms of gravimetric water content, volumetric water content and degree of saturation versus suction. Based on these plots, it is clear that all figures show hysteresis of the gravimetric and volumetric water content and degree of saturation component with the wetting path positioned below the drying path. However, these wetting curves cannot be taken as the primary wetting curves because each test was conducted only for suction measurement as high as 1163kPa for pressure plate and 590kPa for stage method. These highest suction values are still considerably lower than those needed in order to confirm that each sample has been dried completely or at least have reached its residual water content state (Lourenço, 2008). Without further data measurements at higher suctions, the assessment whether drying and wetting lines have coincided at higher suctions cannot be made, suggesting that these wetting curves are the scanning curves (Ho et. al., 2007).

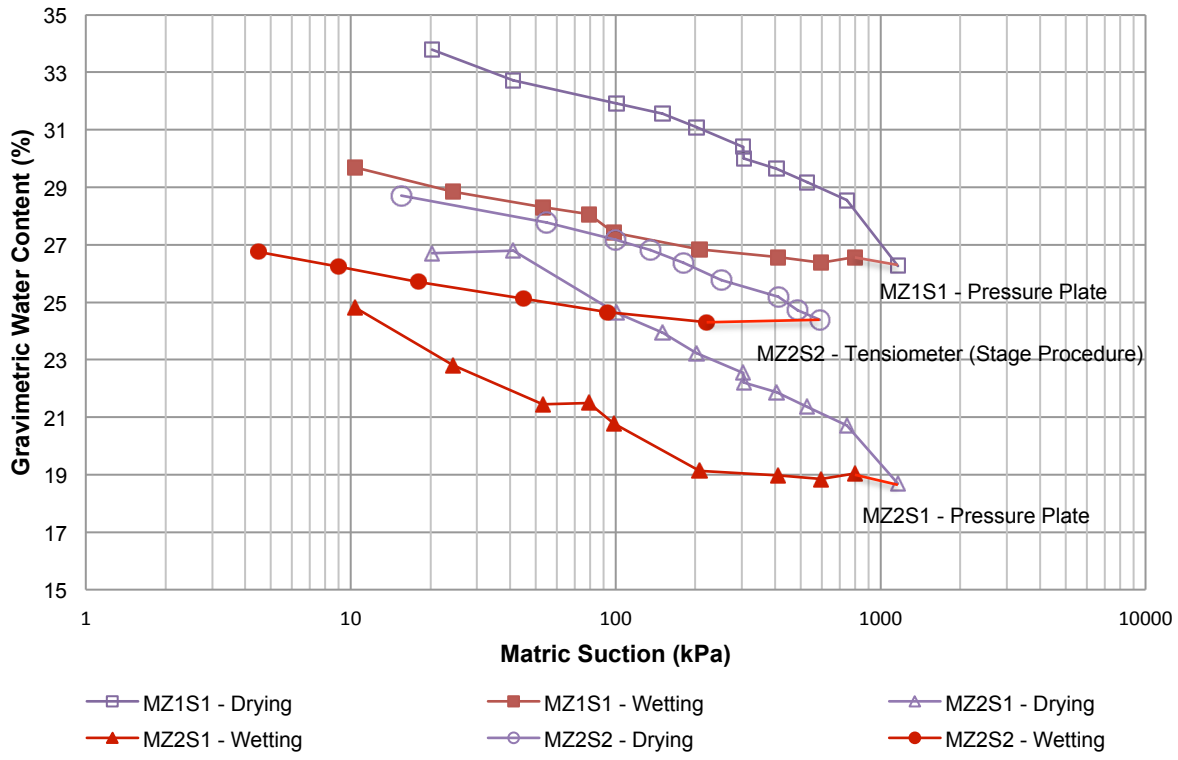

Figure 4.19 Drying and wetting curves - gravimetric water content against suction

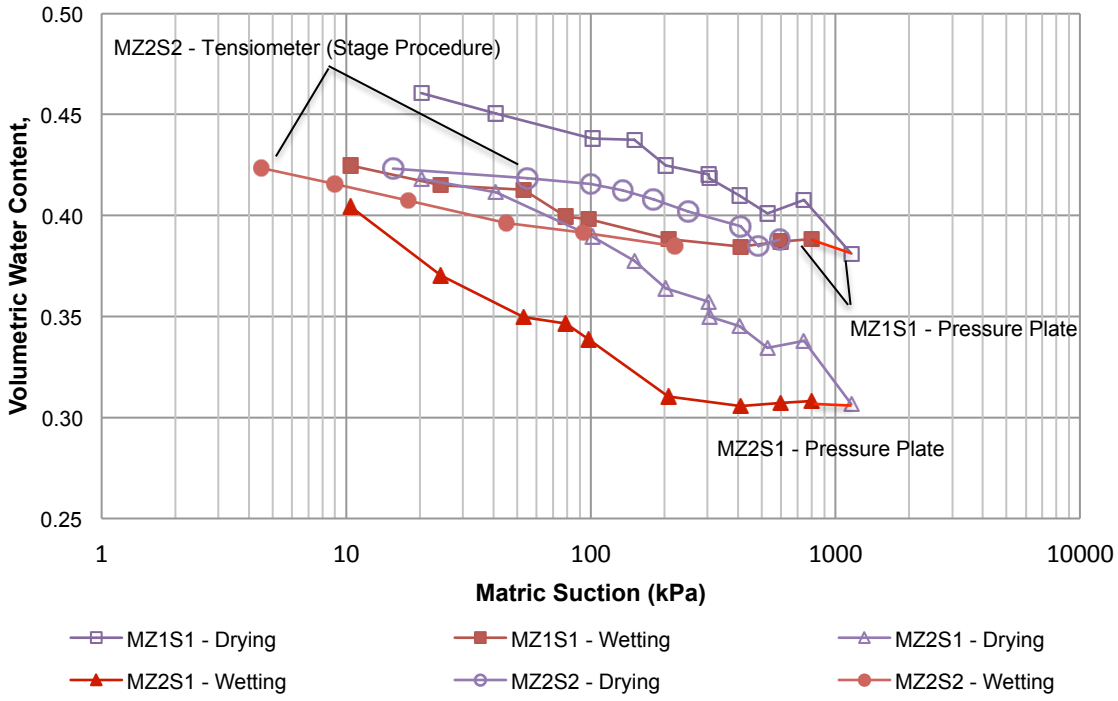

Figure 4.20 Drying and wetting curves - volumetric water content against suction

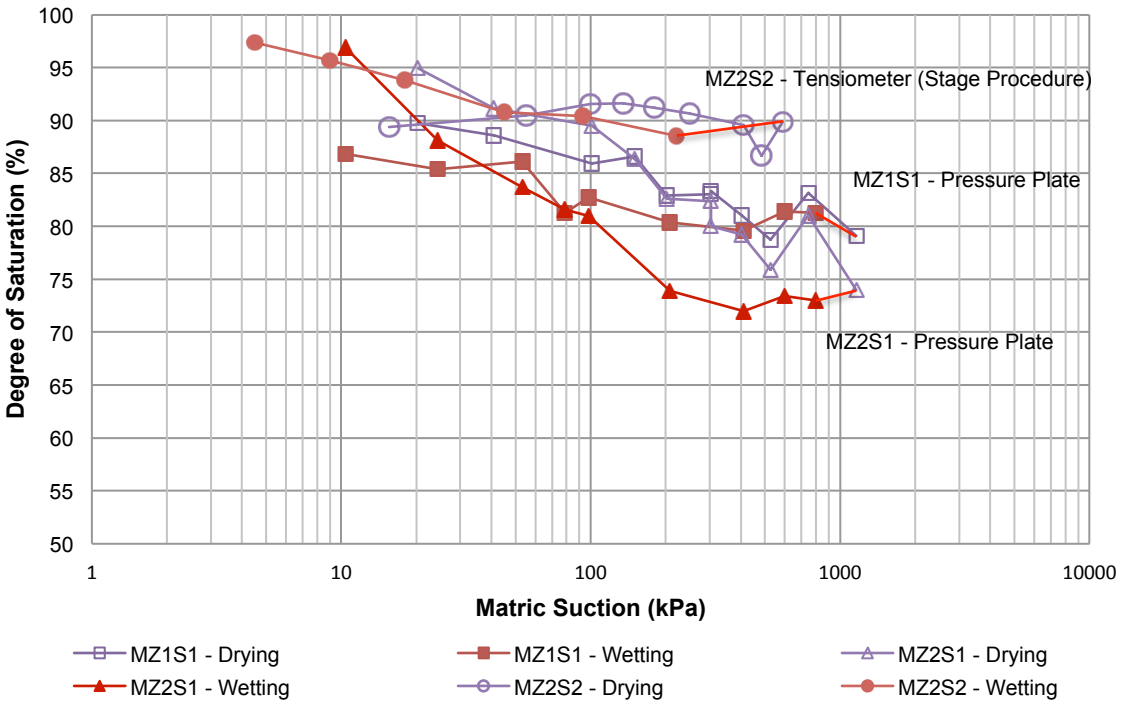

Figure 4.21 Drying and wetting curves –degree of saturation against suction

Good agreement can be seen from the plots between drying and wetting curves at low suction; with gravimetric water content gives differences between 2% to 4% and volumetric water content between 0.01 to 0.05. However, the degree of saturation data should be considered with care since the volume measurements are not accurate enough. From Figure 4.21, it can be seen that there are slight differences in S_r values for each drying and wetting curves that is approximately 4%. The plot for MZ2S2 (stage method) presents a higher degree of saturation for wetting curve at low suction and this further supports the explanation of additional disturbance experienced by the soil, as discussed in the previous section.

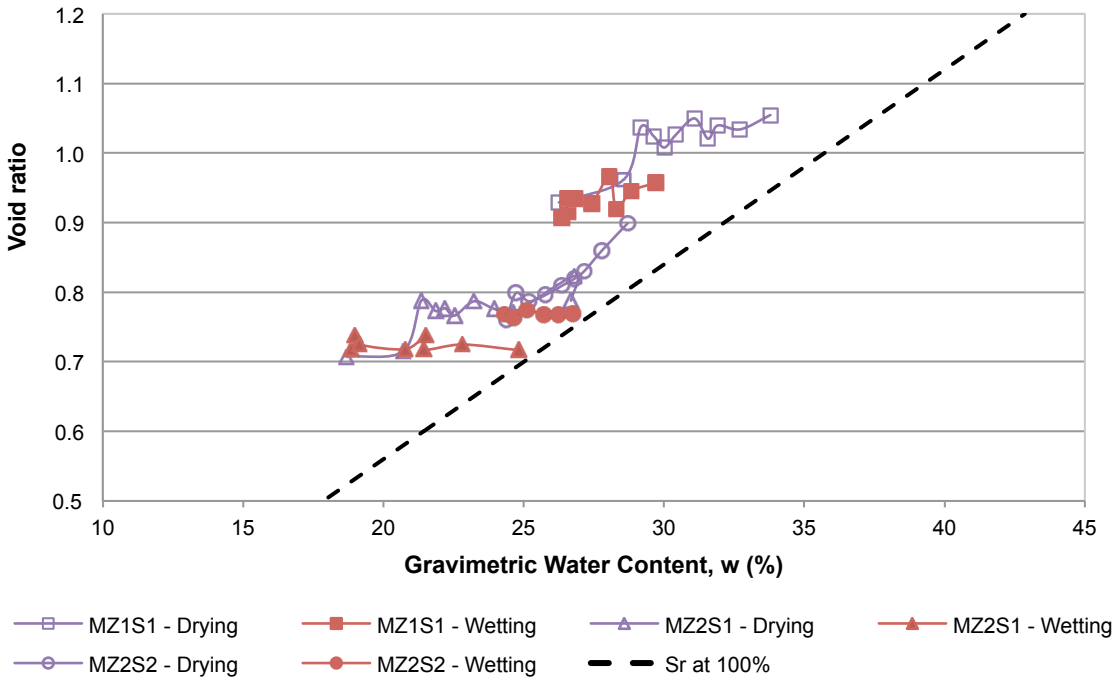

Figure 4.22 Conventional shrinkage curves - void ratio against gravimetric water content

The drying-wetting curves of each test were further analysed by comparing the results using the shrinkage curves (now swelling curves for wetting paths), as shown in Figure 4.22. It is clear that during the wetting process, less changes in volume occurred for each sample with each line showing an almost direct path towards the saturation line. This behaviour can be associated with a stiffer “elastic” response, reflecting an unloading response of the soil.

For sample MZ2S2, an additional drying procedure was performed in order to study the effect of wetting and drying sequences. However, in order to ignore the effects of erroneous volume measurements, only the plot using gravimetric water content is presented. From Figure 4.23, it can be seen that the curve exhibits a converging behaviour towards the final suction value measured for the initial drying curve. Also, the second drying curve shows only slight differences of 1% in gravimetric water content as compared to the curve produced by the precedent wetting procedure. This can be related to the pore network openings/constrictions behaviour that was due to the trapped air bubbles within the soil, produced during wetting procedure. Nevertheless, hysteresis is also clearly visible in the second drying curve with its position located slightly above the wetting cycle.

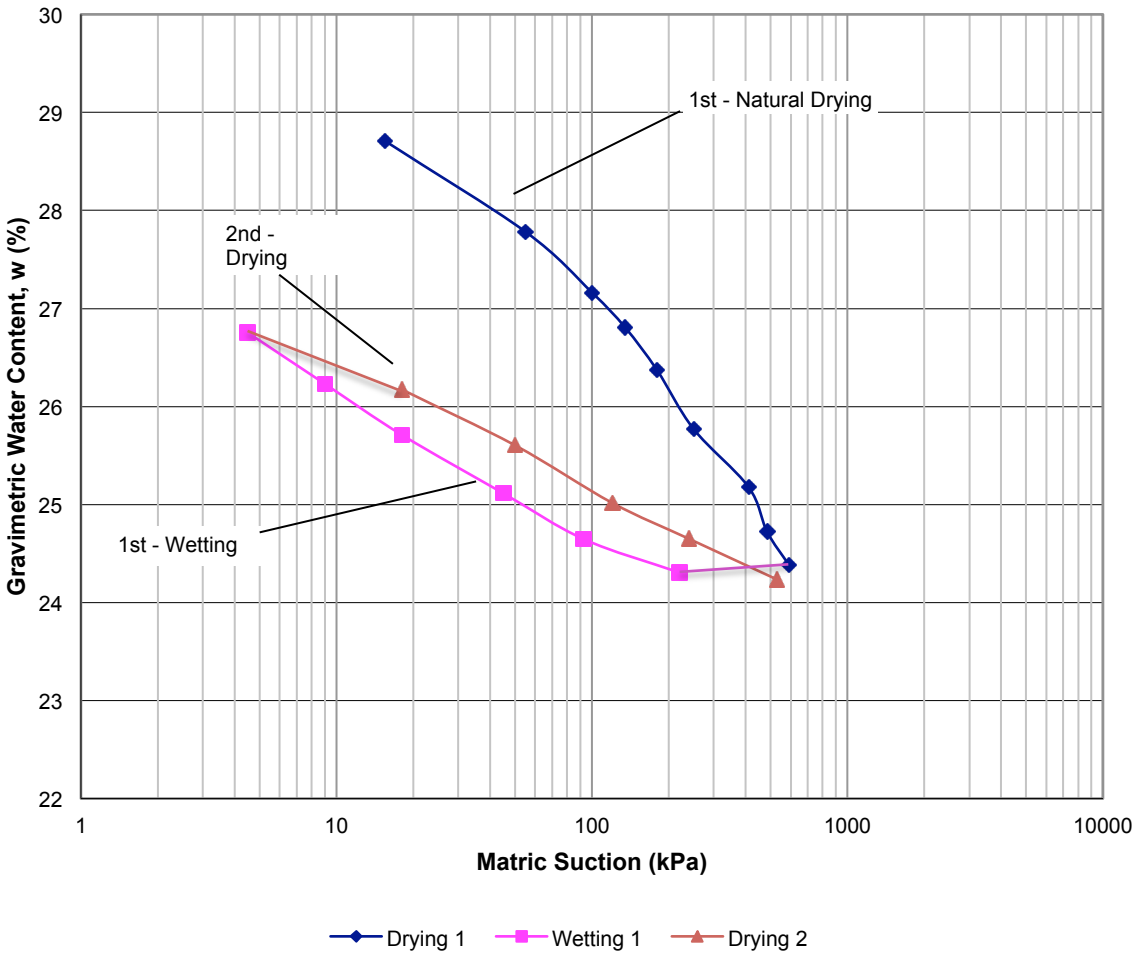

Figure 4.23 Cycles of drying and wetting - gravimetric water content against suction

4.5.3.3 Permeability Function

A comparison of the permeability function using two different statistical model equations has been made. These functions were estimated based on the SWRC data obtained from sample MZ2S3 (volumetric water content plot) and were produced numerically using SEEP/W software application. The software calculates the value of 'a', 'n' and 'm' of the measured SWRC data points using a fitting algorithm that is based on two closed form functions proposed by van Genuchten (1980) and Fredlund and Xing (1994). With these 2 sets of curve-fitting parameters, the estimation of both van Genuchten (1980) and Fredlund et al. (1994) permeability functions were carried out together with 8×10^{-7}m/s as the saturated permeability. This saturated permeability value is the average value from the permeability test results obtained from samples of layer 1.

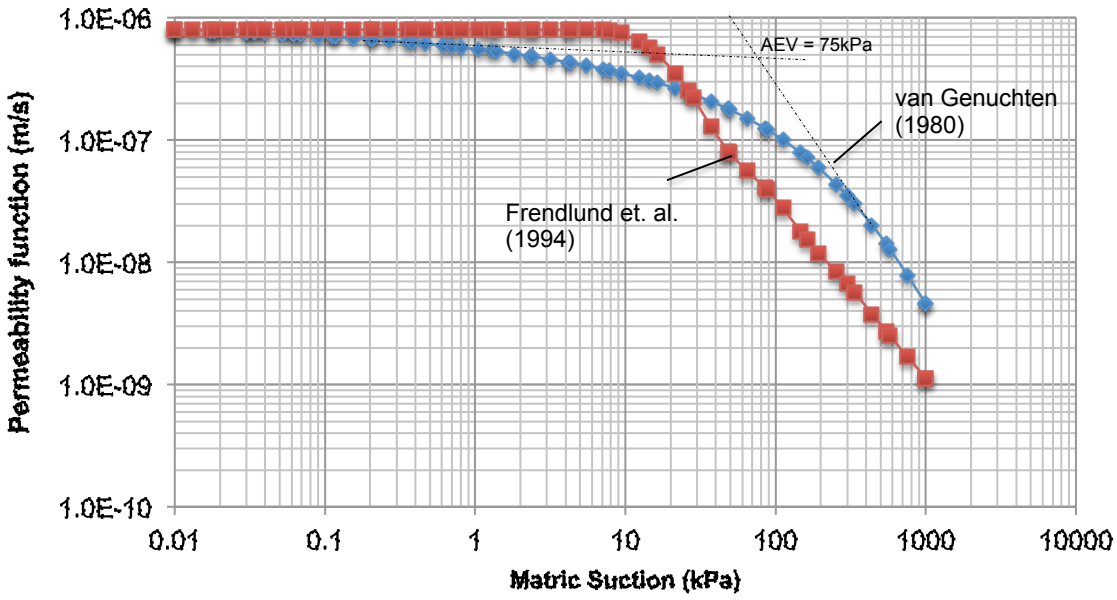

Figure 4.24 Estimated permeability functions using van Genuchten (1980) and Frendlund et al. (1994) method.

It can be seen from Figure 4.24 that there is a difference in pattern between the shapes of the curves calculated from both methods. The variations in permeability by van Genuchten (1980) seem to occur for matric suction as low as

1kPa, with AEV at approximately 75kPa. This value is equal to the AEV calculated from the SWRC using the RETC code.

However, for the permeability function based on Fredlund et al (1994), the changes can be clearly seen to take place when the matric suction reached 10kPa The plot also suggests the AEV to be approximately equal to 10kPa. As SEEP/W does not provide the 'a', 'n' and 'm' of the measured SWRC data points based on Fredlund and Xing (1994) equation, it is difficult to define the AEV of the curve. Nevertheless, it is obvious that the gradient of the curves by both methods appear to be different, with Fredlund et al. (1994) giving an apparent linear relationships as compared to van Genuchten (1980). The difference is also visible at a suction equal to 1000kPa, by approximately half order of magnitude. This indicates the danger in using such expressions without an experimental confirmation of their validity (Karthikeyan et. al., 2008).

4.6 Final Remarks

In the initial part of this chapter, the role of suction in influencing the movement of water within the slope and the relationships with soil water content were discussed. This was followed by the detailed descriptions of different hydrological testing procedures for the production of SWRC using different suction measurement techniques.

A total number of 13 specimens of residual soil specimens were tested for the derivation of both permeability and SWRC properties of layer 1 (1m to 3m) and layer 2 (3m to 5m). The permeability tests were carried out on triaxial specimens after the equalisation procedure of the first confining stage (Multistage triaxial tests) using the constant head test concept. The results showed that the permeability of the specimens of layer 1 ranges from 3.96×10^{-7} m/s to 1.31×10^{-6} m/s, while, for specimens of layer 2 ranges between 2.40×10^{-7} m/s to 1.26×10^{-6} m/s. An average value of 8×10^{-7} m/s was adopted to represent the saturated coefficient of permeability for both layer 1 and 2.

For the SWRC tests, the axis translation technique using pressure plate apparatus and direct suction measurement technique using high capacity tensiometer for both continous and stage methods were adopted. Due to the reasonably high degree of saturation represented by each specimen, it was decided to implement the drying process from its natural conditions. This procedure was also executed to minimise the possibilities of disturbance and change of fabric in these specimens.

The initial drying SWRCs of each test were plotted as gravimetric water content, volumetric water content and degree of saturation against suction. The gravimetric water content results showed that the variation for each test is related to the location of each specimen within the ground profile (varying gravimetric water content). For depths closer to the ground surface, the more porous structure produced by weathering process gives a higher void ratio, allowing more water to be retained, giving higher gravimetric water content. The rate of desaturation (slope of SWRC), however, was relatively similar for specimens from MZ1 and MZ2. This confirmed that soil samples from both tubes were of similar material. The argument was strengthened by the results plotted using volumetric measurements and degree of saturation data, which showed close agreement when plotted as volumetric water content. On the other hand, specimen MZ3S1 was different due to the higher fraction of coarser material (approximately 27% of sand material). This explained the differences in the position of the plots as well as gradient of the curve (steeper slope). The dissimilarity shown by SWRC of MZ3S1 confirmed that the specimen was of different material than the rest, representing a different layer.

For the study of the differences between each test method, the comparison between AEV for each SWRC plotted using volumetric water content and degree of saturation was presented in Table 4.4. These AEVs were numerically obtained from the estimation of curve fitting parameters (i.e. 'a', 'n' and 'm') using the RETC code. The results showed that only tests using continuous procedure gave similarity of AEV, with 1kPa difference. The magnitude was slightly higher for MZ2S3 as compared to MZ3S1. This further strengthened the differences in material distribution of Layer 1 and Layer 2.

A huge variation of AEV for both hydrological terms (volumetric water content or degree of saturation) can be seen for the tests using pressure plate and stage procedure. This was believed due to the disturbance experienced by the samples during the handling for weight and volume measurements. The difficulty to obtain measurements at the same part of the sample using a vernier calliper was also indicated as one of the factor causing the variations. The procedure of forcing the tensiometer into the soil for suction measurement in stage method, was also linked to the additional volume changes to the sample as a small depression could be seen to occur at the bottom of the specimen.

The conventional shrinkage curves were also used to further compare the differences by each test. The results showed that the continuous method (MZ2S3) exhibited a smooth representation of shrinkage behaviour as compared to the rest of the tests. The trend for each curve also seemed to move away from the saturation line, demonstrating less shrinkage behaviour. However, sample MZ3S1 did not show much change in volume and this was due to high degree of cementation between soil particles and higher fraction of coarser material. In general, the results showed the importance of continuous measurements of water content, suction and volume change for the determination of SWRC.

In addition, wetting procedures were also conducted using pressure plate and tensiometer-stage procedure for specimens MZ1S1, MZ2S1 and MZ2S2. These wetting curves were defined as the scanning curves as the highest suction values were insufficient in order to confirm that each sample have been dried completely or at least have reached its residual water content state. However, the results exhibited a similar trend based on hysteretic behaviour with the wetting path positioned below the drying path. Furthermore, for specimen MZ2S2, an additional drying procedure was performed for the study of the effect of wetting and drying sequences. The curve exhibited a converging behaviour towards the final suction value measured for the initial drying curve. Only slight difference of 1% in gravimetric water content was observed as compared to the curve produced by precedent wetting procedure. The shrinkage (and swelling) curve plot showed a stiff swelling response indicative of elastic behaviour.

Lastly, a comparison study of permeability function using 2 different statistical model equations has been made. These permeability functions were estimated based on the SWRC data obtained from specimen MZ2S3 using two closed form functions proposed by van Genuchten (1980) and Fredlund et al (1994). The results showed obvious differences in pattern between the shapes of the curves calculated from both methods; van Genuchten (1980) exhibited a curve deviation at matric suction as low as 1kPa and AEV at approximately 75kPa; and Fredlund et al (1994) presented sharp changes when the matric suction reached 10kPa.

In conclusion, the results have highlighted the importance of continuous measurements of water content, suction and volume change for the determination of SWRC. The danger in using any hydrological expressions without an experimental confirmation of their validity is also essential, as it will provide false information in geotechnical design. The requirement is even greater, especially when dealing with tropical residual soil that is well known for its heterogeneous characteristics.

Chapter 5
Numerical Modelling of Tropical Residual Soil Slope

5.1 Introduction

In the introduction chapter, it has been recognised that rainfall is one of the most common triggering factors to cause slope failures. The effect of such climatic events on slope stability is by the process of rainwater infiltration, which creates increases in pore-water pressure (or reduction in matric suctions) within the slope (Brand, 1981). To assess this variation in pore-water pressure, the implementation of seepage analyses with rainfall as a surface boundary condition is essential.

The analysis of seepage conditions of a tropical residual soils slope can be executed using the finite element method (numerical modelling). By adopting this method, the mechanism of rainwater infiltration and the influence of soil properties on the changes of flow of water within the slope can be modelled. The stability of the slope can then be analysed based on the results of a seepage analysis.

It is crucial that the stability assessment for an unsaturated soil slope is determined by taking into consideration the characteristics of the soil and not only climatic information. Thus, this chapter presents the numerical modelling of slope stability analysis by coupling the equations for the flow (hydrological) and deformation (mechanical) assessments. The analyses were carried out for two different tropical residual soils slopes; (i) a reanalysis of a previous numerical study reported by Tsaparas and Toll (2002) and (ii) back analysis of a slope failure that occurred in Precinct 9, Putrajaya.

5.2 Literature review

5.2.1 Slope failures of tropical residual soils slope

Residual soil slope failures are generally reported to be caused by high precipitation (heavy rainfalls). These incidents were observed to occur on both natural and engineered slopes, with the latter presenting the higher frequency of failure (Liew, 2004). In most of the reports, the slopes were described to have remained stable for a long time but then failed, either during and after prolonged and heavy rainstorms (Brand, 1984, Toll, 2001).

Previous studies have reported that residual soil slope failures are normally shallow (Krahn et al., 1989, Day and Axten, 1989, Toll, 2001, Tan et al., 2007). This is due to the fact that infiltration of rainwater only creates changes in pore water pressure down to limited depths, near to the ground surface. This effect (due to advancement of a wetting front) is common, however, if left exposed to a wet climate for a long period of time, the infiltrations would proceed to deeper depth and eventually lead to deep seated instability (Macari et al., 1992, Fourie, 1996, Gasmo et al., 1999, Deutcher et al., 2000, Low et al., 2000, Dykes and Thornes, 2000). Furthermore, for cases of residual soil slopes with very permeable soil characteristics, the exposure to certain rainfall patterns would produce a great magnitude of slope failures (Lumb, 1975).

The occurrences of rainfall-induced slope failures are very common in Malaysia with higher frequency especially during the monsoon seasons (Low et al., 2012). Some of these disastrous incidents have resulted in not only extensive damage to properties but also loss of lives. Ooi (2004) in his special lecture on Earthwork Practice in Malaysia, has presented the case histories of major landslides occurred in Malaysia (Table 5.1). Referring to his findings, it is apparent that the cause of these major slope failure events is highly related to long periods of continuous or intense rainfall that is believed to be linked to climate change. The paper also highlighted the importance of risk assessment in engineering design with the utilisation of comprehensive numerical investigations to estimate and prevent any sort of disaster to the completed works.

Table 5.1 Case histories of (after Ooi, 2004)

Date	Location	Landslide Details
January 1971	Bukit Gasing, Petaling Jaya	Gasing Height Development. Perimeter drains collapsed during one week of incessant rain. Tipped-fill Flow slide damaged two Government Quarters completely. The slope reconstructed with proper compaction and quarters rebuilt.
September 1988	Ulu Kelang, Ampang Jaya	Slope failure due to excavating neighbouring land during prolonged period of incessant rain. Damage to bungalow and swimming pool
December 1993	Ulu Kelang, Ampang Jaya	Collapse of Block I of Highland Towers on December 11, 1993 during prolonged period of incessant rain. 48 people were killed.
June 1995	Genting, Selangor	Debris flow, Genting Highlands on June 30, 1995 caused closure of Kuala Lumpur – Karak Highway 20 people were killed 23 people injured Economic losses, destruction of several vehicles, destruction of roadway and disruption of traffic.
May 1999	Ulu Kelang, Ampang Jaya	Bukit Antarabangsa filled slope failure during prolonged period of incessant rain. Access road to Bukit Antarabangsa cut-off. Residents of the area were evacuated. No loss of lives but economic loss and anxieties. Rehabilitation by installation of horizontal drainage system.
November 2002	Ulu Kelang, Ampang Jaya	Landslide occurred at 6.00am during prolonged period of incessant rain. Landslide buried the bungalow at the foothill and eight people were killed.
November 2003	Bukit Lanjan, NKVE	Rockslide occurred during prolonged period of incessant rain. Rockslide caused closure of NKVE Highway at Bukit Lanjan for six months. Rock slope stabilised and slided materials were blasted and removed.
May 2006	Taman Zooview, Ulu Kelang, Ampang Jaya	Massive landslide of an old tipped-fill slope with terrace houses on top of the slope. Continuous heavy rainfall in the month of April and May 2006 before the landslide. Long houses at the bottom of the slope demolished by the landslide materials and four persons in the long houses were killed. Residents of the terrace houses on top of the slope evacuated. Local authority directed slope rehabilitation by the Developer for the bottom of the slope.

Moreover, Liew (2004) has presented four case histories of landslides consisting of three cut slopes and one fill slope with underlying formations of weathered soils derived from igneous rocks and meta-sedimentary formations. The forensic investigation consisted of detailed topography survey, subsurface investigation, laboratory testing, instrumentation scheme for slip surface detection, groundwater regime establishment and back-analyses using finite element method Despite the many uncertainties in identifying and establishing the weak structure, subsoil variation and adverse groundwater level due to the natural heterogeneity of tropical residual soils, it was concluded that the major cause to slope failures are mainly related to prolonged and heavy rainfall. This conclusion was proven based on the recorded rainfall data spanning over the period from before the incident till the end of the investigation. In addition, the needs of more research works and practical design approaches for slope design were also suggested in order to mitigate the risk of failure as minimal as possible.

5.2.2 The effects of rainfall on tropical residual soils slope

There is much evidence in the geotechnical literature to demonstrate the statistical correlation between rainfall against the stability of residual soils slope. For residual soil slopes in Hong Kong, Brand (1984) suggested that rainfall intensities of 70mm/h and above can be used as a good indication of the possibility to trigger slope failures. This empirical correlation was later proven by Premchitt et al. (1994) through the study of a 20-year review of slope failures occurred in Hong Kong.

Another major factor that has been reported to contribute to slope failure is the effects of antecedent rainfall (i.e. the rainfall in the days leading up to the event) (Lumb, 1975, Wolle and Hachichi, 1989, McDonell, 1990, Wei et al., 1991, Rahardjo et al., 1998, Toll, 2001, Rahardjo et al., 2001). This factor; also can be expressed as the initial condition prior to the major rainfall event, essentially contributes to the increase in moisture content within the slope which would eventually culminate in the final triggering rainfall event that precipitates a failure. However, for slope failure cases in Hong Kong, Brand (1984) has indicated that the controlling parameters for rainfall-induced slope failures are generally governed by the peak hour rainfall and the total 24-hour rainfall intensities. Thus, the contribution of antecedent rainfall is

indicated to be less significant. This is likely to be due to the permeable nature of many Hong Kong soils.

To further explain the effects of rainfall on slope stability of tropical residual soil slope in the South East Asia region, an empirical study was done by Toll (2001). In his paper, correlation was established based on the observations of past minor and major slope failures occurred in Singapore, as reported by various researchers (Chatterjea, 1989, Wei et al., 1991, Li, 1995, Tan et al., 1988, Pitts, 1985, Yang and Tang, 1997). The data were analysed against the quantified data of 5-day and 15-day period of antecedent rainfall. Figure 5.1 and 5.2 present the plots for each case, respectively.

From the plots, the author suggested that a total rainfall of 100 mm within a six-day period is sufficient to trigger minor slope failures. This indication of slope failures by total rainfall is made based on the outcome of the plots that presents the occurrences of failures corresponding to the daily and antecedent rainfall conditions. It was also indicated that major slope failures may occur after a 24-hour rainfall of over 110mm. The diagonal line shown in Figure 5.1 provides further justification on this finding. The condition for major landslides has also been described; however, the result was explained to be less conclusive due to limited data obtained for 15-day antecedent rainfall. Nevertheless, a line for total rainfall of 320 mm is believed to be relevant to represent a lower bound for each major case in both figures.

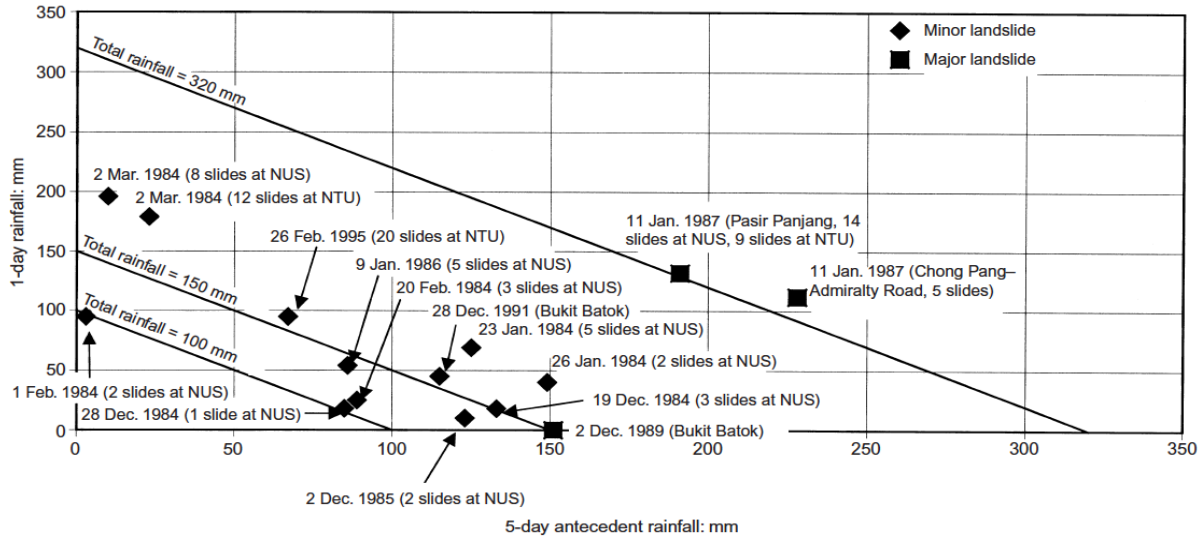

Figure 5.1 Five-day antecedent rainfall for landslides in Singapore (after Toll, 2001)

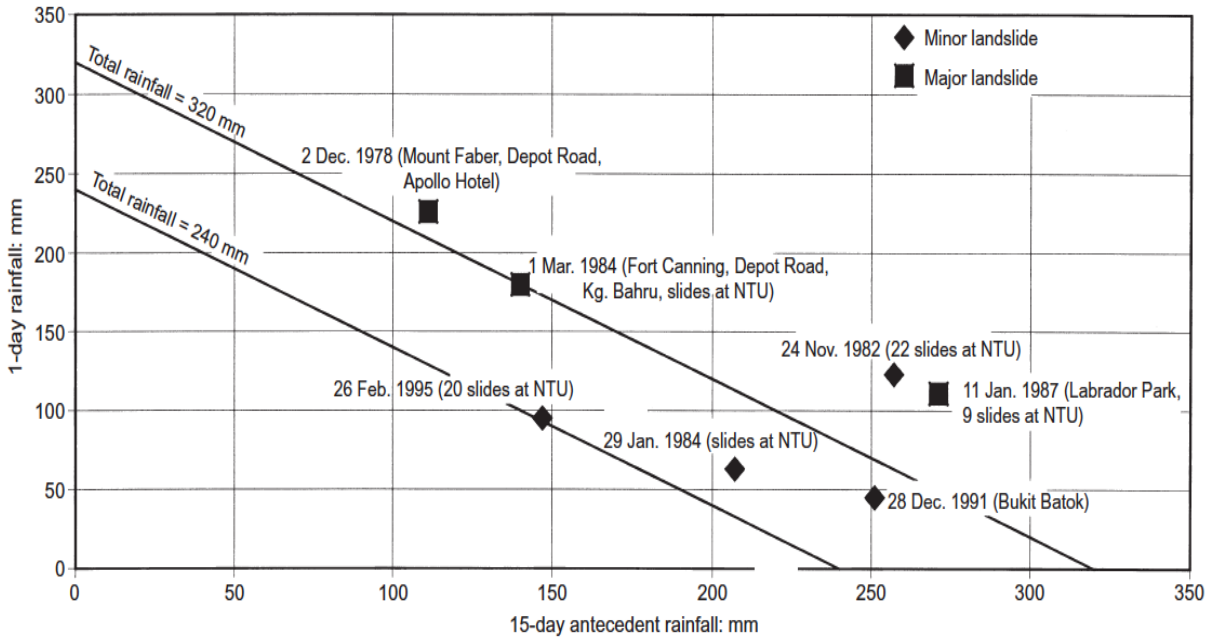

Figure 5.2 15-day antecedent rainfall for landslides in Singapore (after Toll, 2001)

5.2.3 Numerical modelling of unsaturated residual soil slopes

The adoption of numerical modelling using finite element method for slope assessments has becoming more important due to its ability to describe the infiltration mechanism within slopes (Tsaparas, 2002). Using this technique, the justification of the influence of soil properties upon changes of rainwater flow within the slope, can be defined clearly. Its necessity is even more significant for the cases of complex slope problems that could not be explained using conventional techniques.

It is common for finite element analyses for stability assessments to calculate the flow (hydrological) and deformation (mechanical) assessments in two separate analyses (Md. Rahim and Toll, 2014). The hydrological analyses (seepage analyses) are carried out under transient conditions to exhibit the effects of rainfall infiltration of the changes on pore-water pressure as well as the progression of a perched water table (Leach and Herbert, 1982). Throughout the analyses, factors such as, the rainfall intensities, ground water table, soil permeability and the type of vegetation at the surfaces of the slope must be taken into consideration in order to emulate the

actual behaviour of the slope. Then, based on these calculated seepage conditions, the stability analyses (mechanical analyses) are implemented.

5.2.3.1 Numerical modelling of the hydrological behaviour

There is a large volume of published studies that describe the application of numerical modelling on the study of infiltration process and its influences upon the seepage conditions of an unsaturated slope (Tsaparas, 2002). Among the first to illustrate this effect was Hodge and Freeze (1977) via a study using a steady state analysis with a finite element model. However, it was discovered later that the variation in the seepage conditions within a slope during infiltration can occur rapidly, thus, transient analysis is considered to be more relevant (Leach and Herbert, 1982).

Leach and Herbert (1982) implemented a preliminary analysis using finite-difference model (FDM) and concluded that the numerical model tended to overestimate the head at a particular point, in comparison to the available field data. Furthermore, the magnitude of error from the outputs, was also observed to decrease with depth. Thus, it is suggested to decrease the mesh dimensions near the ground surface, where rapid changes in head occur.

The incorporation of the evaporation and evapotranspiration effects at the ground surface are often excluded from analyses, as the modelling is very difficult to handle (Tsaparas, 2002). In actuality, this complex drying process, that is a function of the water content and negative pore-water pressure, is highly dependent to the soil type (Wilson et al., 1995). Gasmo et al. (2000) attempted to model evaporation by defining the surface boundary with a negative flux. However, it was found that the reduction of negative pore-water pressures at the ground surface was too rapid compared to the available field data.

Another critical issue when analysing the seepage condition of a slope is the modelling of surface desiccation and vegetation effects. These effects are important as they influence the pore-water pressure distribution developed near the ground surface (Hodge and Freeze, 1977). If the ground surface of a slope is covered by grass, small pathways or fissures would be created in the soil which produce a significantly higher permeability value compared to the larger depths (Anderson et

al., 1996). Hence, it is essential to define a representative layer with high permeability value near the ground surface (surface desiccated zone). Tsaparas and Toll (2002) found that the near surface permeability values needed to correctly predict infiltration rates in numerical models, were two orders of magnitude higher than values measured in the field. This condition was used in their numerical model analyses by the introduction of 0.25m thick soil layer, defined at the ground surface.

The effect of the soil-water retention curve hysteresis has also been studied for the simulation of seepage behaviour within a slope. Vargas et al. (1990) have highlighted the difficulties in modelling this criterion due to the changing process of wetting to drying soil water retention curves at the end of a rainfall event. In theory, the wetting process may still be continuing at larger depths and this would produce possible numerical instabilities within the analyses. For that reason, the authors adopted only the wetting soil water retention curve in their numerical assessments. A similar issue was also reported by Tsaparas (2002) from the attempts to incorporate the draining process into seepage analyses. The idea was to predict a realistic decrease of the pore-water pressures during periods of no rainfall that would be comparable to the field observations. As a result, the adoption of drying phase of the soil water characteristic curve was only defined for dry periods that were longer than 12 hours.

5.2.3.2 Numerical modeling of the mechanical behaviour

The evaluation of the mechanical behaviour of a slope is generally associated with the investigation of the potential failure mechanisms (stability assessments). This is because, generally only ultimate limit states (failure conditions) are of concerned for slope stability assessment and the linear elastic-perfectly plastic Mohr Coulomb constitutive model is normally employed. The relationship between rainfall and slope failures can be described due to the loss of negative pore-water pressures (caused by infiltration) that decreases the shear strength of the soil below the mobilised shear strength along the potential slip surface (Brand, 1981). Vargas et al. (1990) explained that the decrease of the suction would result in a decrease in the strength of the soil, resulting in instability and shallow superficial slides. The instability may also be identified due to the development of positive pore-water pressures at the toe of the slope.

To link the effect of infiltration on the stability of a tropical residual soil slope, the application of unsaturated soil concepts is essential. The traditional limit equilibrium method with the incorporation of the Extended Mohr Coulomb concept ($\emptyset^b$) can be used to identify the mobilised shear strength (τ_m) at the base of each slice in an analysis (Figure 5.1).

$$\tau_m = \frac{b}{FOS}[c' + (\sigma - u_a)\tan\emptyset' + (u_a - u_w)\tan\emptyset^b] \quad \cdots(5.1)$$

Where, b = the width of each slice.

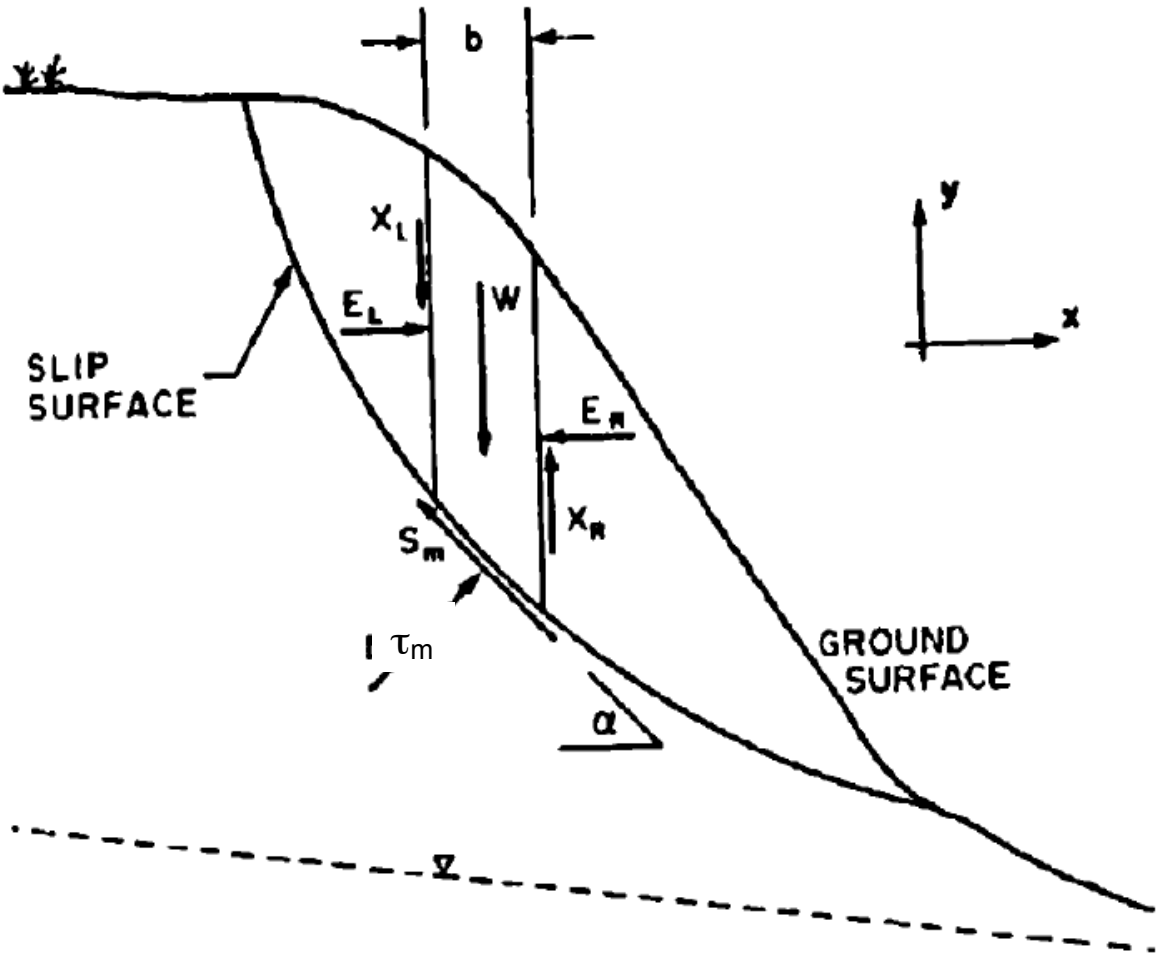

Figure 5.3 Forces acting on each slice of the slope for limit equilibrium analysis of slope stability (Tsaparas, 2002)

Fredlund and Barbour (1992) expressed the moment equilibrium factor of safety $(FOS)_m$ and force equilibrium factor of safety $(FOS)_f$ as the following.

$$(\mathrm{FOS})_{\mathrm{m}} = \frac{\sum\left[c'.b.R+\left(N-u_w.b\frac{\tan\emptyset^b}{\tan\emptyset^{'}}\right)R.tan\,\emptyset^{'}\right]}{\sum W.x-\sum N.f} \quad \cdots(5.2)$$

$$(\mathrm{FOS})_{\mathrm{f}} = \frac{\sum\left[c'.b.\cos\alpha+\left(N-u_w.b\frac{\tan\emptyset^b}{\tan\emptyset'}\right)tan\,\emptyset'\cos\alpha\right]}{\sum N.\sin\alpha} \quad \cdots(5.3)$$

Where, u_a = atmospheric pressure (0 kPa)

W = total weight of each slice

α = the inclination of the base of the slice.

N = the normal force acting at the base of each slice

R = the radius of the potential slip surface,

x = the horizontal distance from center of each slice to the center of moments

f = the offset distance from the force to the center of moments.

Another alternative approach to calculate the stability of a slope is by adopting the shear strength reduction concept (SSR) using the finite element method. The principle of SSR is justified by the simultaneous reduction of $\emptyset_r$ and c_r in small increments until a failure mechanism is created (Matsui and San, 1988). This stability assessment method that is available in many finite element codes produces the concurrent reduction factor for the two shear strength parameters and ultimately represents it as the factor of safety for the slope. For further justification, the formulation of deriving the factor of safety (FOS) is presented as the following.

$$\mathrm{FOS} = \frac{\tan\emptyset}{\tan\emptyset_r} = \frac{c}{c_r} \quad \ldots(5.4)$$

Where, $\emptyset_r$ and c_r = shear strength parameters at failure.

5.2.3.3 Fully coupled hydro-mechanical slope assessment

The interrelation of hydraulic and mechanical behaviour in unsaturated soils is a subject of great interest in geotechnical engineering practice (Khalili et al., 2008). This is because, in actuality, both these aspects are highly interlinked especially during infiltration. The characteristics of water flow, changes of pore-water pressure, and shear strength of soils are the main parameters associated with the flux boundary condition at the soil-atmosphere interface (Hamdhan and Schweiger, 2011).

Hamdhan and Schweiger, (2011) presented the evaluation of the effects of hydraulic characteristics of soils (hydraulic conductivity and initial degree of saturation) and rainfall in slope stability calculations that were carried out using the finite element method. The analyses were performed by simultaneously computing the deformation and groundwater flow with time dependent boundary conditions. This computation is based on the concept introduced by Bishop (1959), where “effective” stress in unsaturated soils is used to represent the hydro-mechanical coupling effects (Equation 4.1).

To further justify the concept, it was suggested by Oberg and Sallfors (1997) and Vanapalli et al. (1996) that the factor χ can approximately be replaced by the degree of saturation or the effective degree of saturation. According to the authors, the shear strength of unsaturated soils is observed to be strongly related to the amount of water in voids of soils (i.e. degree of saturation), reflected by the variation of the matric suction. Figure 5.4a and 5.4b present the relationship between the factor χ and degree of saturation based on experimental data gathered from various researchers (Vanapalli et. al., 1996).

In summary, the coupled analyses can present the influence of rainfall on the distribution of negative pore water pressures (suction) and hence slope stability. It can be concluded that the stability of a slope decreases during infiltration and therefore the Factor of Safety (FOS) of the slope is reduced (Figure 5.5). This reduction of FOS is even greater for soil with high permeability compared to the low permeability soil. Different soil water retention curves are also one of the key factors to affect FOS of the slope.

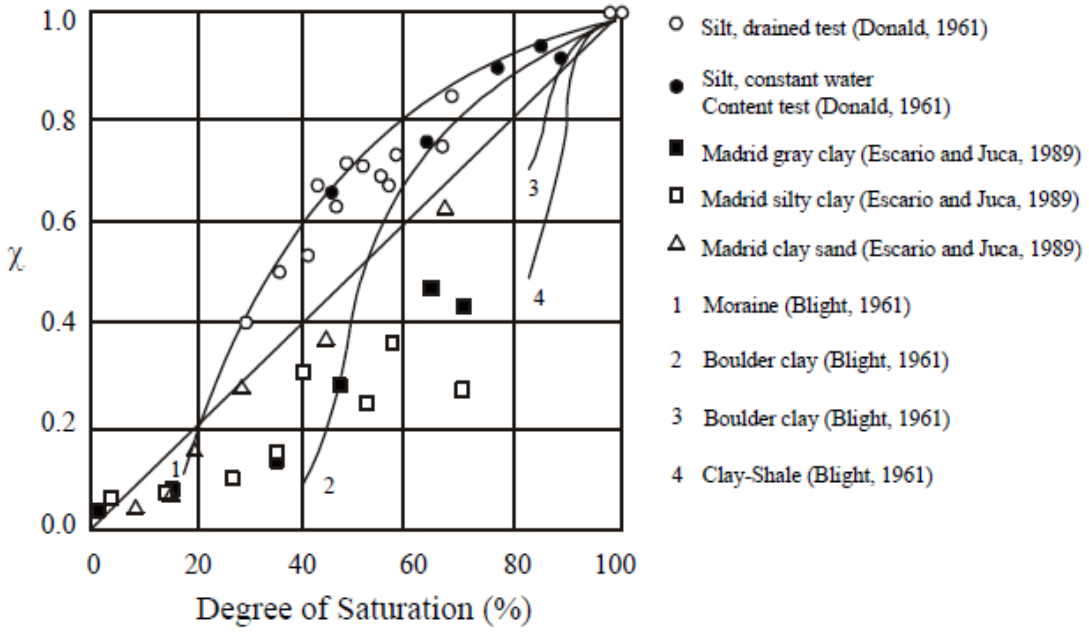

(a)

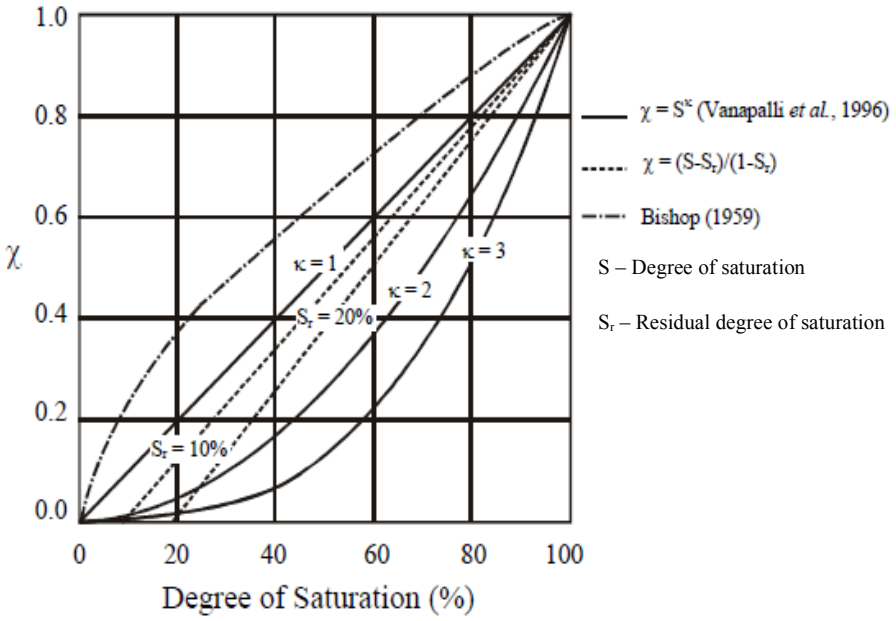

(b)

Figure 5.4 χ and S_r relationship (after Vanapalli et. al., 1996)

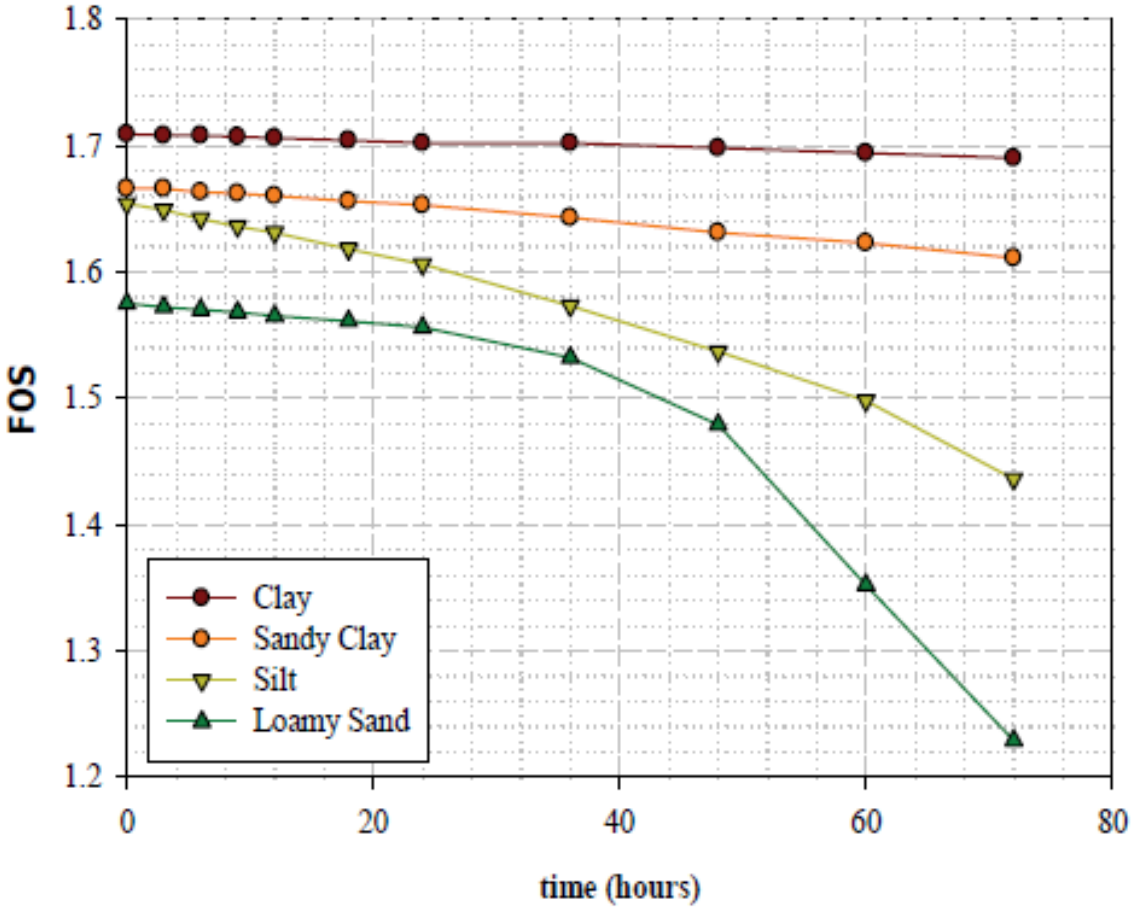

Figure 5.5 Change of FOS with time for unsaturated soil slope during a period of rainfall (after Hamdhan and Schweiger, 2011) .

5.3 Fully Coupled Hydro-Mechanical Analyses of Infiltration and Matric Suctions within a Tropical Residual Soil Slope in Singapore

A reanalysis of a previous numerical study reported by Tsaparas and Toll (2002), was carried out using a hydro-mechanical coupled model (using PLAXIS 2D) with time dependent boundary conditions (Md. Rahim and Toll, 2014). PLAXIS 2D is a two dimensional finite element commercial program developed for analysis of deformation, stability and groundwater flow in geotechnical engineering. The program incorporates models for both saturated and unsaturated conditions, using van Genuchten (1980) relations between suction head, degree of saturation and permeability (Brinkgreve et al., 2010). PLAXIS 2D version 2012 was used for this research.

The research slope analysed by Tsaparas and Toll (2002) was an instrumented tropical residual soil slope located on the campus of Nanyang Technological University (NTU), Singapore (called NTU-ANX). The earlier numerical investigation of the slope was done by adopting an uncoupled flow analysis using SEEP/W and SLOPE/W software (GeoSlope International, 2007) and was validated against field monitoring data obtained for the slope. The monitoring equipment installed consisted of runoff data and pore-water pressure changes that were measured at several depths and locations on the slope. This section provides a comparative study between the stability assessments of the coupled and uncoupled analyses.

5.3.1 Unsaturated soil hydrological model

As described in Chapter 4, the hydraulic parameters for the unsaturated zone (above the groundwater table) are defined by the Soil Water Retention curve (SWRC) that is the relationship between the water content and suction for the soil. In this study, the van Genuchten (1980) model was used that provides a set of closed-form equations of hydraulic characteristics of unsaturated soils. The implementation uses a model that relates the degree of saturation to suction.

$$S(\emptyset_p) = S_{res} + (S_{sat} - S_{res})\left[1 + \left(g_a|\emptyset_p|^{g_n}\right)^{g_l}\right] \quad \ldots(5.4)$$

Where $\emptyset_p$ = suction head (m);

S_{res} = degree of saturation at residual state;

S_{sat} = degree of saturation at saturated state;

g_a, g_n, g_l = fitting parameters in the van Genuchten equation (equivalent to 'a', 'n', 'm')

And it is assumed that:

$$g_l = 1 - \frac{1}{g_n} \quad \ldots(5.5)$$

For the derivation of the permeability function, the model calculates the relative permeability $k_{rel}(S)$, and this is based on the effective degree of saturation (S_e) as described in Equation 5.6.

$$s_e = \frac{S - S_{res}}{S_{sat} - S_{res}} \quad \ldots(5.6)$$

The relative permeability $k_{rel}(S)$ can be expressed as follows (Galavi, 2010):

$$k_{rel}(S) = (S_e)^{g_l} \left\{ 1 - \left[1 - S_e^{\left(\frac{g_n}{g_n - 1}\right)} \right]^{\left(\frac{g_n - 1}{g_n}\right)} \right\}^2 \quad \ldots(5.7)$$

5.3.2 Unsaturated soil mechanics model

In the Plaxis analysis, the concept introduced by Bishop (1959) for "effective" stress in unsaturated soils is used for coupled analyses which is available under Advanced mode in Plaxis 2D (using $\chi = S_r$). However, it has to be recognised that this simple concept of "effective stress" in unsaturated soils is not valid for all ranges of degree of saturation. It should not be seen as a true effective stress that controls all aspects of soil behaviour, as would be the case for saturated soils (Gens, 2010). Nevertheless, the concept should provide a realistic approach at high degrees of saturation when the air phase is discontinuous. For stability assessment, the principle of the shear strength reduction method (SSR) is used for the calculation of factor of safety (FOS).

For stability analysis using the uncoupled SLOPE/W model (using the traditional limit equilibrium method), the Extended Mohr Coulomb concept incorporating $\emptyset^b$ is used to identify the mobilised shear strength (τ_m) at the base of

each slice in the analysis. Further details of both approaches can be seen in Chapter 3 and section 3.2.5.

5.3.3 Review of the instrumented tropical residual soil slope

The slope at NTU-ANX is described by Tsaparas et al. (2003). It has a gradient of 27°. It is located in residual slope formed by the Jurong sedimentary rock formation, the main geological formation normally encountered in the west of Singapore. Pitts (1984) and Rahardjo et al. (2000) reported that there is significant depth of residual soil at this location and the level of the groundwater table is deep, ranging between 15m to 17m deep.

In the year 2000, the NTU-ANX slope was instrumented with three rows of tensiometers to measure pore-water pressures at selected depths, a rainfall gauge, a device for runoff measurements, a piezometer and a rainfall simulator. Full descriptions of the instrumentation can be found in Tsaparas (2002) and Tsaparas et al. (2003).

5.3.4 Review of tropical residual soil properties for NTU-ANX site

The site investigation report indicates that the sub-profile for NTU-ANX consists of two main residual soil layers; with the depth for upper layer, extends to 10m deep (Rahardjo et al., 2000). This layer 1, identified as silty to sandy clay with 58% of fines and moderate plasticity material, is underlain by soil layer 2; classified as clayey silt with siltstone and sandstone fragments. This layer has 32% fines and the interface inclination between the two layers is parallel to the slope gradient.

A saturated coefficient of permeability of (k_{sat}) 6×10^{-7} m/s, obtained by Guelph permeameter, was used to represent the permeability value for both layer 1 and 2. It was reported that seepage conditions of the slope are only affected at depths close to the ground surface, giving the hydrological properties of Layer 2 to be less important. It should be noted that Tsaparas and Toll (2002) noted discrepancies in their initial numerical assessments and the observed pore water pressures, which gave lower results compared to observed values in the field. Hence, a 0.25m thick layer with a permeability value of 5×10^{-5} m/s was defined at the ground surface to model the effects of grass covering and surface desiccation.

Figure 5.6 shows the data points and fitted SWRC (wetting and drying curve) of a soil sample retrieved from the NTU-ANX slope. These data points were obtained from a laboratory test using a pressure plate and fitting curves were produced numerically using the RETC code (van Genuchten et al., 1991). Figure 5.6 shows that the saturated volumetric water content (θ_{sat}) is 0.53 and the volumetric water content reduces to 0.38 after the imposition of 200kPa of suction. The derivation of the predicted permeability functions were then produced based upon these SWRCs and shown in Figure 5.7. This were originally derived by Tsaparas and Toll (2002) using the Green and Corey (1971) approach. However, as Plaxis only provides van Genuchten's (1980) equation for the permeability function, the curves created by Tsaparas and Toll (2002) were refitted to gain the van Genuchten parameters.

The strength parameters for NTU-ANX were measured by Gasmo et al. (1999) for Layer 1 and Layer 2, respectively. The parameters were obtained through laboratory triaxial tests, providing the value of $\emptyset^b$ for the slope stability assessments considering unsaturated soil concepts. Table 5.2a and 5.2b present the summary of hydrological and mechanical properties used in both coupled and uncoupled analyses.

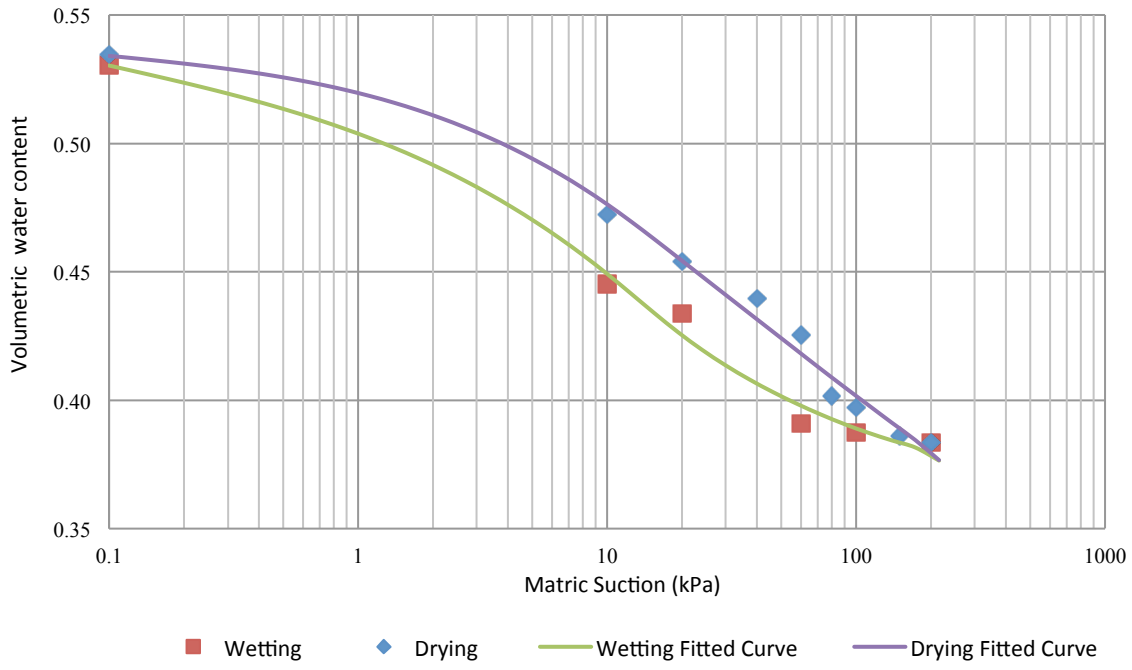

Figure 5.6 Soil Water Retention Curve for NTU-ANX fitted using van Genuchten (1980).

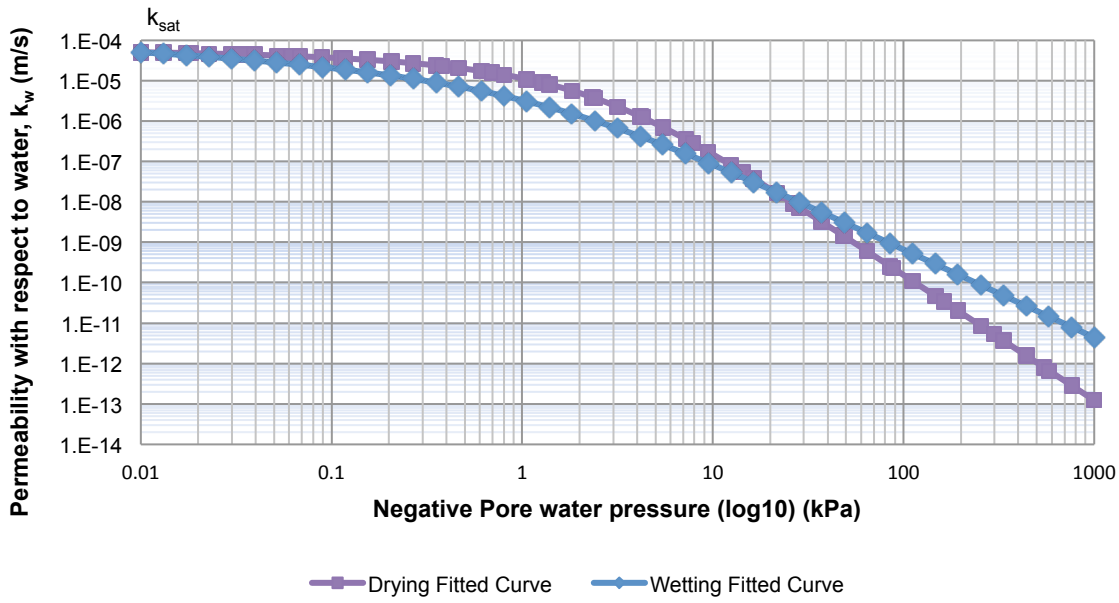

Figure 5.7 Permeability Functions for NTU-ANX using van Genuchten (1980).

Table 5.2a The summary of hyrdrological parameters for each soil layer of the NTU-ANX slope.

Soil Layer	Description	Densities		k_{sat} (m/s)	van Genuchten parameters					
					wetting			drying		
		γ_{sat} (kN/m^3)	γ_{unsat} (kN/m^3)		a	m	n	a	m	n
1	Grass &surface dessication	20	19	$5x10^{-5}$	3.361	0.319	1.47	3.304	0.075	1.081
2	Silty to sandy CLAY	20	19	$6x10^{-7}$	3.361	0.319	1.47	3.304	0.075	1.081
3	clayey SILT with siltstone and sandstone	20	19	$6x10^{-8}$	3.361	0.319	1.47	3.304	0.075	1.081

Table 5.2b The summary of strength parameters for each soil layer of the NTU-ANX slope.

Soil Layer	Description	c'	ϕ'	ϕ_b	E'	v
		kPa	°	°	kPa	
1	Grass &surface dessication	1.2	30	30	1000	0.33
2	Silty to sandy CLAY	1.2	30	30	1000	0.33
3	clayey SILT with siltstone and sandstone fragments	1.4	31	31	1000	0.33

5.3.5 Description of the numerical models

5.3.5.1 Model Geometry, Mesh Discretisation and Boundary Conditions

The model geometry shown in Figure 5.8 illustrates the complete figure of the slope with the inclination of 27° (approximately 2H: 1V). The distances of the boundary of the mesh (side edges) to the slope are set to be equal to 3 times of the height of the slope (3H). This is to ensure the possible position of the analysed slip failure to be within the model geometry.

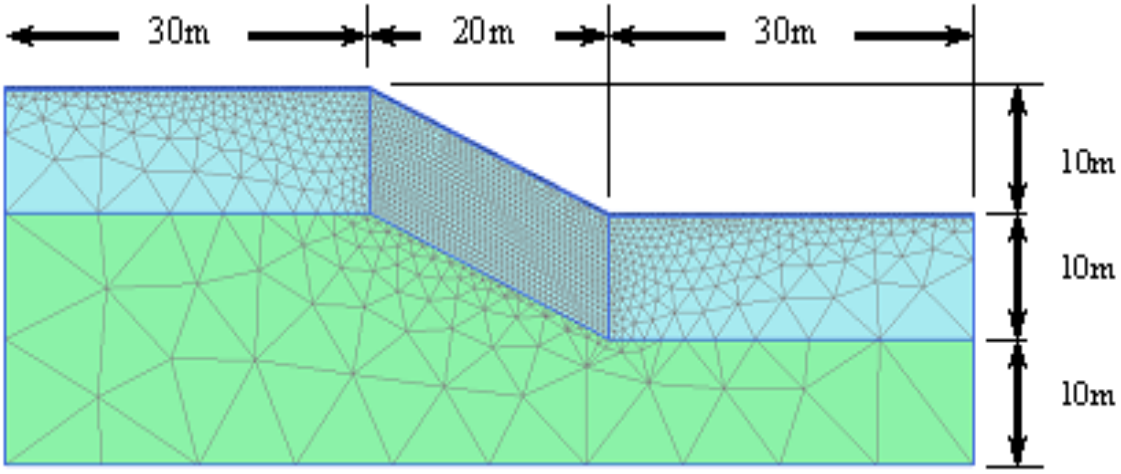

Figure 5.8 Geometry and finite element mesh of the slope.

Several series of mesh refinement procedures were carried out in order to capture the region with the largest displacement on the slope. This procedure was targeted to prevent possible numerical instabilities. The finest mesh was defined for the region below the slope surface and this gave an overall number of 3300 15-noded triangular elements (Figure 5.8).

Standard fixities were set at the boundaries of the slope model to restrict any lateral movements for side edges and both vertical and horizontal movements at the base.

For hydraulic boundaries, two recorded natural rainfall events, taken from 23rd March to 25th March 2000 (88 hours), were modelled as a unit flux boundary (q) along the ground surface (Figure 5.9). As 'ponding' effects are assumed unrealistic to occur on the slope surface, the minimum and the maximum pore pressure head

(options introduced for rainfall hydraulic boundary in Plaxis), were set to be -0.001m ($Ø_{min}$) and 0.001m ($Ø_{max}$). This means that water can only flow on the surface with a maximum height of 1 mm. The left and right boundaries of the model were also assumed to be impervious for drainage. The groundwater table was set at 17m below the slope surface with inclination of 10° as to match with the analysis made by Tsaparas and Toll (2012). The flow boundaries are illustrated in Figure 5.10.

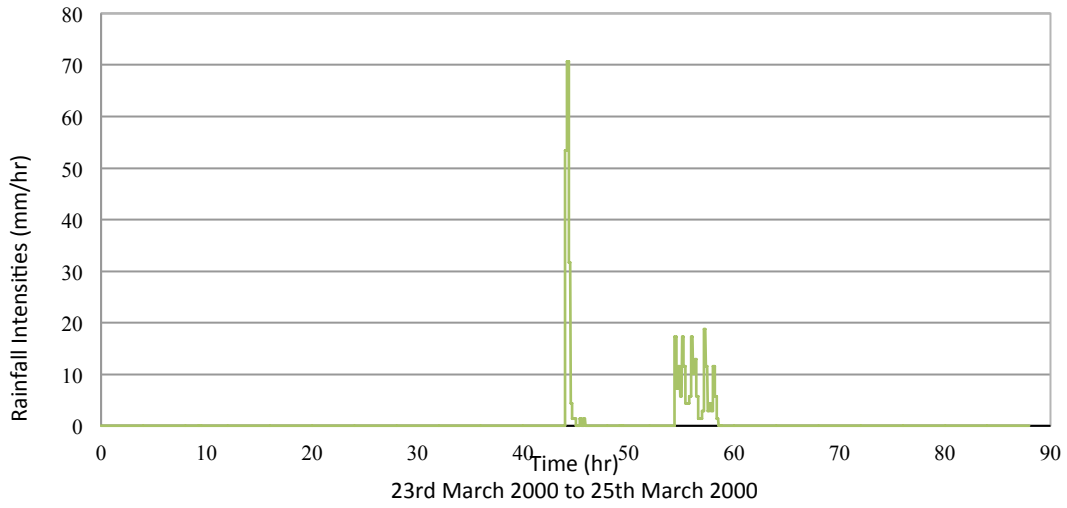

Figure 5.9 Rainfall intensities from 23rd March to 25th March 2000

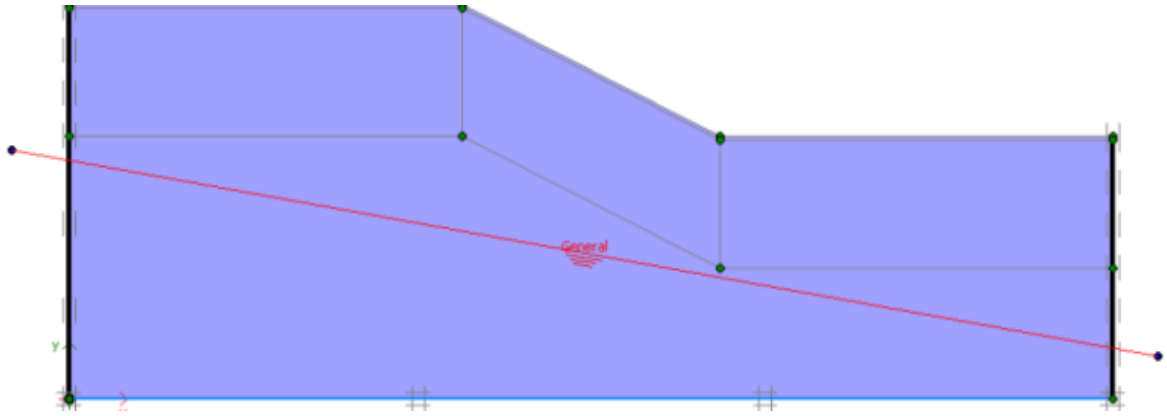

Figure 5.10 Illustration of hydraulic boundaries in Plaxis

5.3.5.2 Initial Condition

The initial pore water pressures were set corresponding to the value of -3kPa obtained by tensiometers measurements on 22nd March 2000. This chosen value

was described by Tsaparas and Toll (2012) as the pore water pressure value at 0.5m depth after a 2-day period of no rainfall occurrence.

5.3.5.3 Transient Analyses Calculation Procedures

The adoption of finite element method for geotechnical analyses is generally associated with the assessments of stresses and deformations. This means that elasto-plastic behaviour can be modelled by means of critical state parameters, enabling soil displacements up to failure to be modelled (Potts and Zdravkovic, 2001).

In Plaxis, the transient analysis for the determination of elasto-plastic behaviour due to variation of groundwater flow is conducted by applying the Consolidation Total Pore Pressure (Consolidation-TPP) calculation option. The rainfall flux was modelled through 35 sequential phases that were defined for the characterisation of wetting and drying cycles, in accordance with the rainfall data (Figure 5.9). Under this option, each phase will calculate the degree of plastic behaviour using the combination of deformation and ground water flow equations that is based on Biot's theory of consolidation (Biot, 1941). However, for the case of slope stability assessment; where consolidation is not an issue, a default value of 10^{15} was used for the parameter, c_k, that represents the change in permeability of the soil due to consolidation. With this value applied into Equation 5.7, it prevents any consolidation effect to be considered during calculation.

$$\left(\frac{K}{K_0}\right) = 10^{\left(\Delta e / c_k\right)} \qquad \ldots(5.7)$$

Where, Δe = the change in void ratio

K = the permeability value in the calculation

K_0 = the input permeability value

Nevertheless, although the consolidation effect is neglected, the application of elastic modulus and Poisson's ratio are still required for the calculation of elastic behaviour. The adoption of these elastic parameters as soil properties in the analyses will reduce the computational time, as the automatic time stepping procedure for transient analysis is highly dependent on the soil stiffness modulus.

The calculation of safety factor of a slope (FOS), however, is not affected by the magnitude of Young's modulus used. This is because for stability assessment of a slope, only ultimate limit states (failure conditions) is of concern. Hence, elastic modulus (E) of 1000kPa and 0.33 for Poisson's ratio (v) were defined for both layers in order to fulfil this finite element method requirement.

As for the stability assessments for the uncoupled model, the seepage outputs presented by Tsaparas and Toll (2002) at a similar time as the coupled model were selected which were then incorporated into SLOPE/W adopting the limit equilibrium method.

5.3.6 Results

Figure 5.11 shows a comparison of both the coupled (Plaxis) and uncoupled (SEEP/W) analyses against the field data at 0.5m depth. Reasonable agreement can be seen between the two models, although neither captures exactly the magnitude of the observed field response. However, the models do explain the trends in fluctuations of pore-water pressures during rainfall; the curves show agreement with inclinations and declinations at the right time periods during and after rainfall events. This shows that the solutions are comparable for subsequent assessments.

For consistency with the analysis of Tsaparas and Toll (2002), the initial suction at the beginning of the analysis was set at 3kPa. As can be seen in Figure 5.11, the measured suction was about 1kPa, and if this starting value was adopted, the magnitude of the results would compare closely with the field observation.

Figure 5.12 presents the correlation between mobilised shear strength (τ_m) against the variations of pore-water pressure induced by rainfall. As anticipated, that the τ_m value decreases during both rainfall events as the increase in pore-water pressure consequently produces reduction in suction, weakening the soil.

It is interesting to note that during wetting a sharp increase in pore water pressure occurs that results in a rapid drop in mobilised shear strength (Figure 5.12). However, during the drying period following a rain storm, the pore water pressures drop much more slowly, so the resulting strength increase takes place quite gradually. Figure 5.13 shows a similar picture for degree of saturation, with rapid changes during wetting but taking longer to recover during drying.

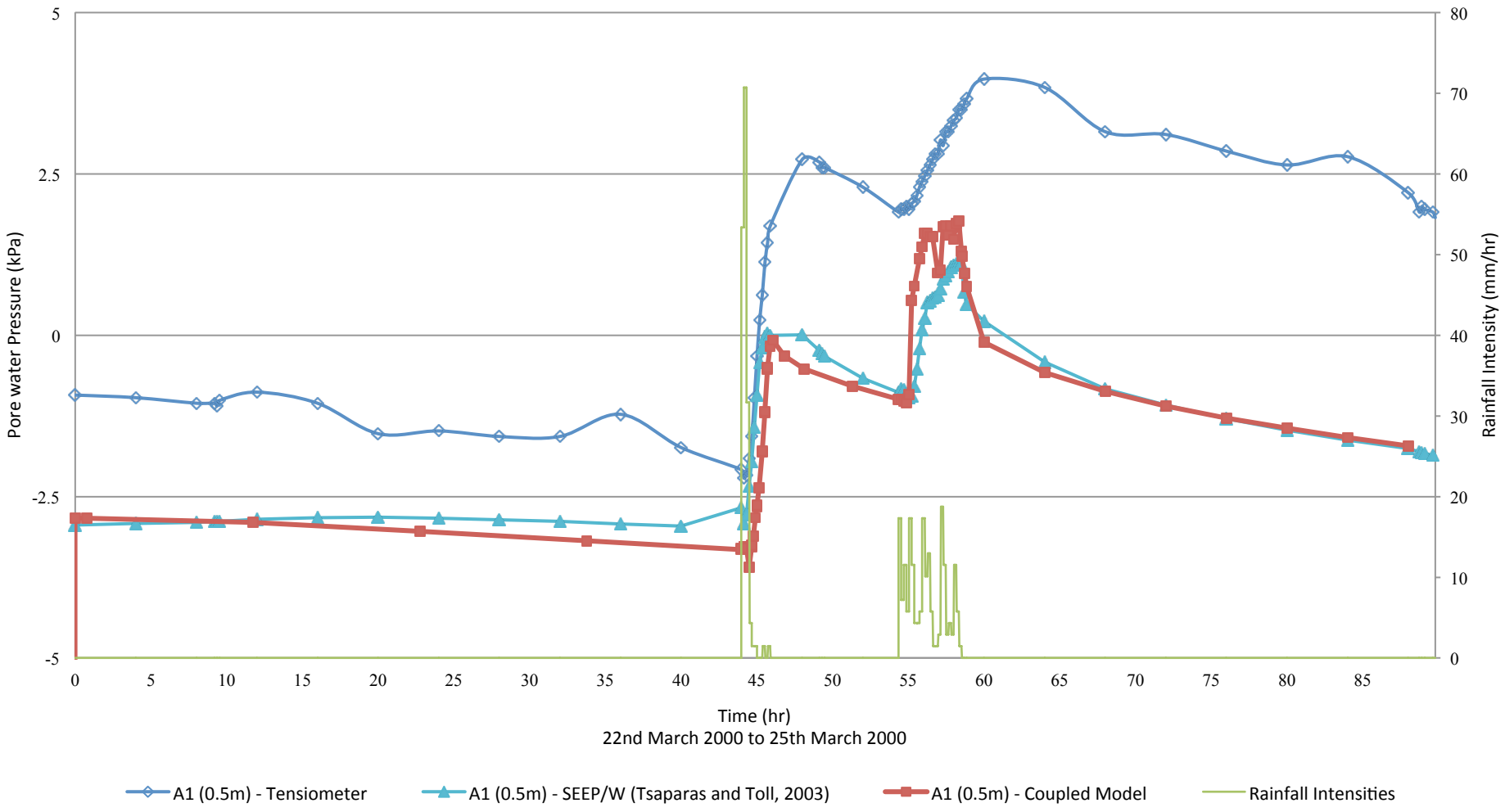

Figure 5.11 Pore water pressure variations at 0.5m against time of NTU-ANX from 23rd March to 25th March 2000

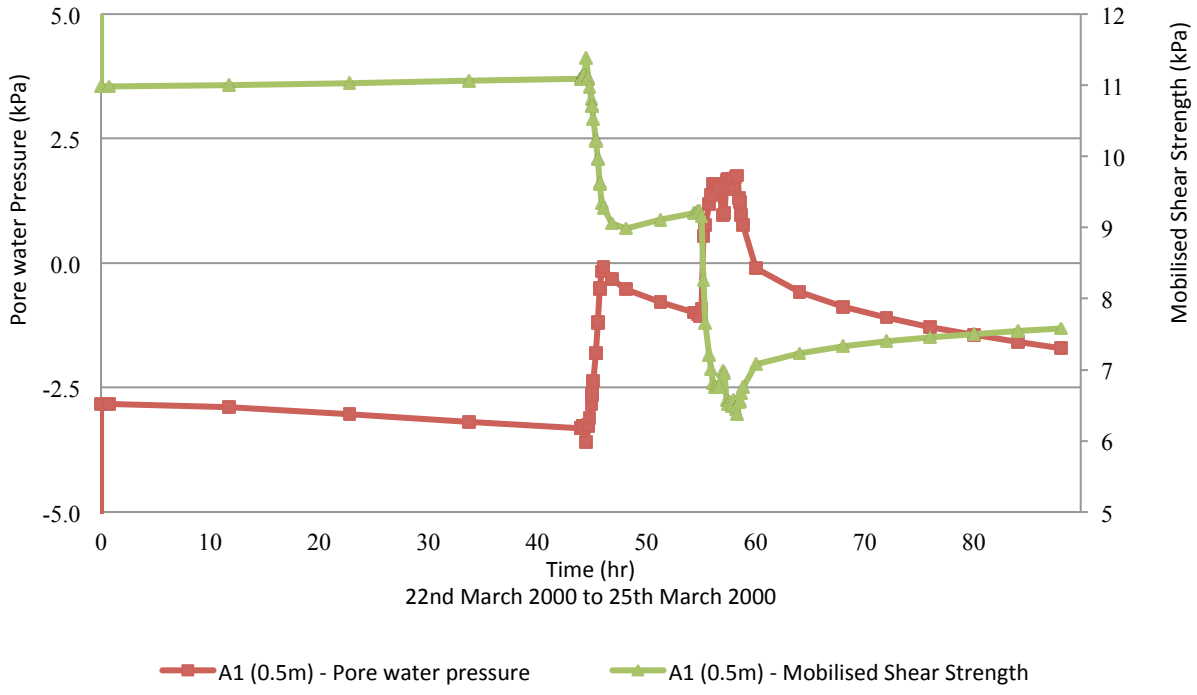

Figure 5.12 Pore water pressure and Mobilised shear strength at 0.5m of NTU-ANX from 23rd March to 25th March 2000.

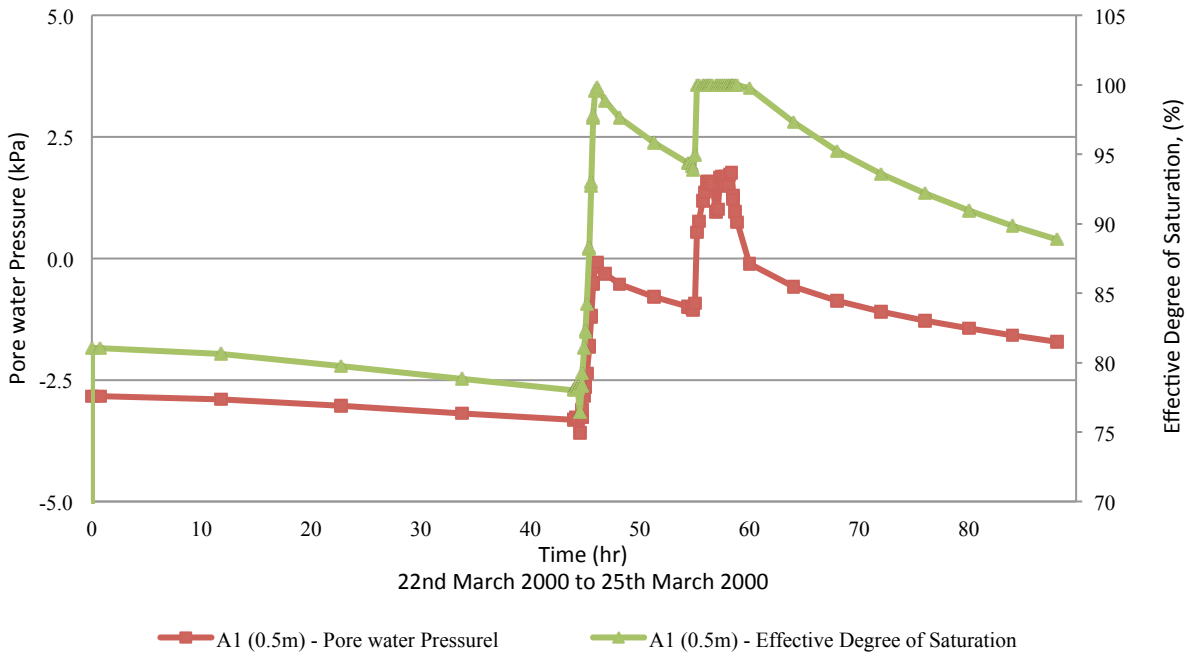

Figure 5.13 Pore water pressure and Degree of Saturation at 0.5m of NTU-ANX from 23rd March to 25th March 2000.

This obviously shows how a series of regular rain storms with short periods of drying in between can cause a 'ratcheting' effect, with rapid loss of strength during each period of rain that is not recovered during the intermediate drying periods.

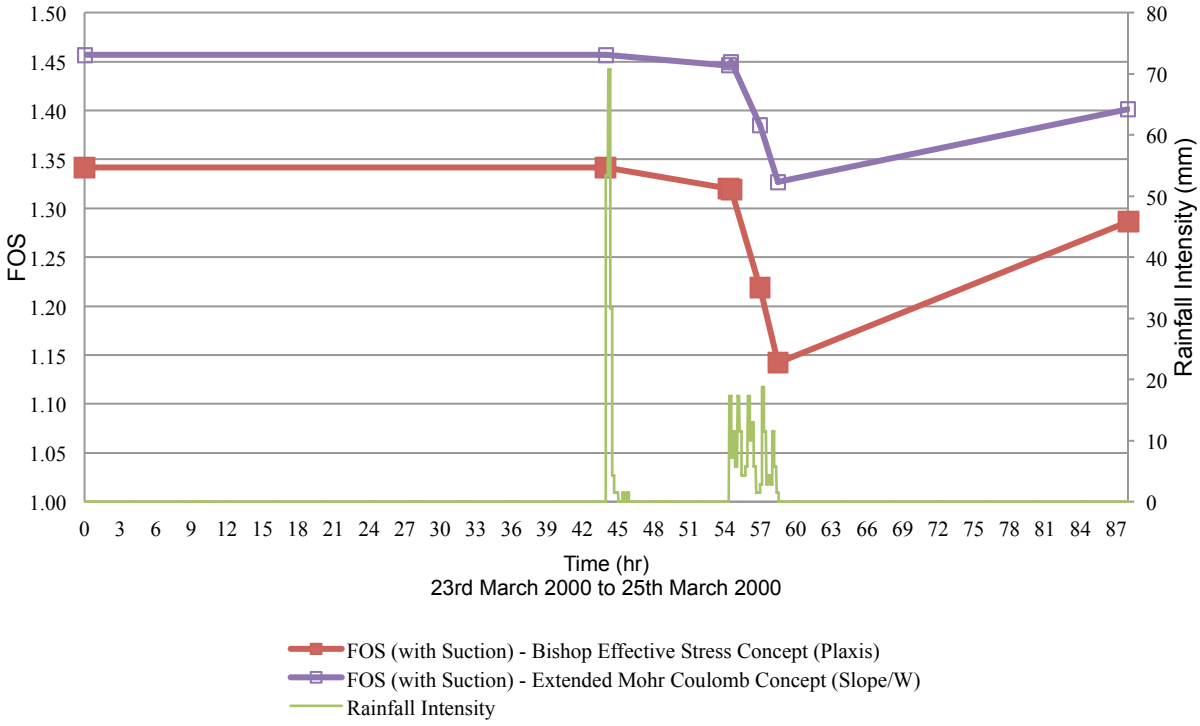

Figure 5.14 Factor of Safety value against time from 23rd March to 25th March 2000.

The comparison between the stability assessments between the SLOPE/W uncoupled model and the Plaxis coupled model is shown in Figure 5.14. From the graph, it can be seen than the Factor of safety (FOS) of the slope is slightly higher for the uncoupled analyses compared to the results for the latter. Although there is this difference in magnitude of FOS, which will be due to the difference in approach of SSR and Limit equilibrium methods, the trends of the curves show a very similar shape as both FOS decline and rise up during and after rainfall infiltration. This implies that the adoption of the unsaturated concept for slope stability assessment is highly significant in order to mitigate the risk of failure, especially for slopes in tropical regions.

5.4 Back Analysis of Tropical Residual Soil Slope Failure in Putrajaya, Malaysia.

A back analysis of a slope failure that occurred in 2007 in Precinct 9, Putrajaya has been carried out by similarly adopting the hydro-mechanical coupled model using Plaxis 2D. Two-dimensional (2D) stability analysis (plane-strain condition) was adopted to model the slope, in order to obtain conservative factor of safety that may represent the failure due to the triggering factor of rainfall. Also, from the detailed site investigations data provided by IKRAM, it showed that the failed slope section was critical, with the thickness of residual soils layer of approximately 10m deep (see Chapter 2, Figure 2.9).

The objectives of this numerical analysis are to investigate the possible cause of the slope failure, as well as to further understand the effect of the infiltration mechanism on the strength behaviour of the slope prior to failure. The numerical modelling works were executed based on the details of the tropical residual soil slope outlined in Chapter 2, Chapter 3 and Chapter 4. These details which consist of groundwater table, slope geometry, hydrological and mechanical properties are used together with time dependent boundary conditions (rainfall data) in order to emulate the behaviour of the slope before failure. It was anticipated that the slope should produce FOS higher than 1 prior to the failure incident and gradually decreasing towards less than unity (FOS $\leq$ 1) due to the triggering factor of rainfall.

5.4.1 Review of the tropical residual soil slope

The slope was reported to be a combination of a cut slope with gradient of 27° (1H: 2V) and natural slope with less than 27° gradients that continues from the cut slope top edge up to a road that leads to a 36 million-litre water tank at the hilltop (see Chapter 2). The subsurface profile of the slope is defined to be consisting of Residual soils layer (Grade VI) and highly to completely weathered Schists of Kajang formation (Grade IV to V), ranges between 1m to 10m deep. The bedrock is categorised as fresh to moderately weathered Schists of Kajang formation (Grade I to III). Furthermore, the monitoring data that were collected after the failure incident showed that the groundwater level within the failed slope was high, ranging from ground surface (toe) to 5m below ground level (crest). Further details can be seen

from Figure 2.9 (Chapter 2) which presents the simplified geometry of the slope together with the generalised subsoil profile and hydrological condition of the failed slope.

5.4.2 Review of tropical residual soil properties

A series of laboratory tests has been carried out for the determination of hydrological and mechanical properties of the tropical residual soil slope (Chapter 3 and Chapter 4). These tests were executed on undisturbed samples to obtain the actual characteristics of the soils that are representative of the in situ conditions. For this reason, the results from the tests were used in this numerical modelling assessment that is described in the following section.

5.4.2.1 Hydrological properties

A saturated coefficient of permeability of (k_{sat}) 8×10^{-7} m/s was used to represent the permeability value for both layer 1 and 2. This chosen value is the average value of permeability from the permeability tests results, implemented on saturated triaxial samples of both layers (see Chapter 4). Considering the apparent heterogeneity that is generally characterised for tropical residual soil, the adoption of the same permeability for both layers may seem questionable. With the inherent variation of degree of weathering in subsoil profile, the permeability value might be expected to be lower in magnitude for residual soils of low weathering grade. However, this was not found to be the case in the laboratory investigation. Therefore, the value is still relevant to represent layer 2,

For the unsaturated soil condition, the soil water retention curve of MZ2S3 sample (expressed in terms of degree of saturation) obtained from the test using continuous drying procedure was used in the analysis (Figure 5.15). The decision to use this curve is due to the reliability of the results based on testing procedure that does not require any imposition of air pressure and hence allowing the soil specimen to dry naturally. Besides that, this procedure also demands minimal handling for water content and volume measurements through the utilisation of an electronic balance to record the change in sample weight and 6 displacement transducers that were attached to the sample. The fitting curves were produced numerically using RETC code (van Genuchten, 1991) and the permeability function is produced by PLAXIS 2D based on the van Genuchten (1990) approach (Figure 5.16).

The incorporation of the soil-water retention curve hysteresis (drying and wetting curves) and evaporation effects were not included in the numerical assessment. This is due to the fact that there was not any field monitoring works for this site that would have been used for validation of pore water pressure changes. Besides that, the wetting curves (SWRC) shown in Chapter 4 were conducted using testing procedures that required the samples to be removed for weight and volume measurements. This implies that the specimens might have experienced disturbance and hence not fully representative to the actual characteristics of the soil layer. The modelling of evaporation is also very difficult to handle (Tsaparas, 2002). In actuality, this complex drying process is highly dependent to the soil type and there was not any laboratory works that have been done for the acquisition of this parameter (Wilson et al., 1995). Previous research done by Gasmo et al. (2000) also shows that the modelling of evaporation cannot be simply defined by using a negative flux boundary condition. Therefore, the application of evaporation is neglected.

The effect of surface desiccated layer was initially considered in the analysis. However, it was observed that high numbers of plastic points seemed to occur at the toe of the slope when the application of a 0.25m thick top soil layer with 2 orders of magnitude higher was made in the model. This has caused numerical instabilities in the analysis and required the program to end the iteration as the number of tolerated error has exceeded the specified limit error. Other factor is believed due to the shallow location of groundwater level (especially at the toe of the slope) that is defined based on the actual data obtained after the sliding incident (causing unrealistically high concentration of plastic points at toe of the slope).

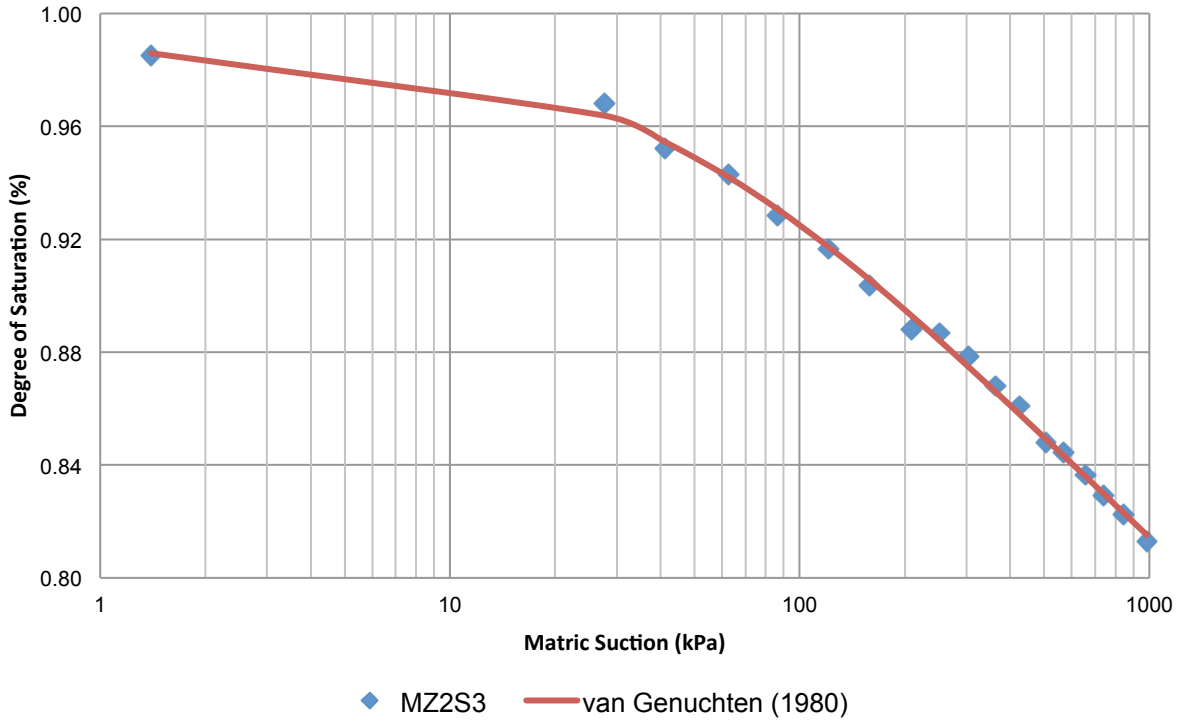

Figure 5.15 Soil Water Retention Curve for Precinct 9 slope using van Genuchten (1980)

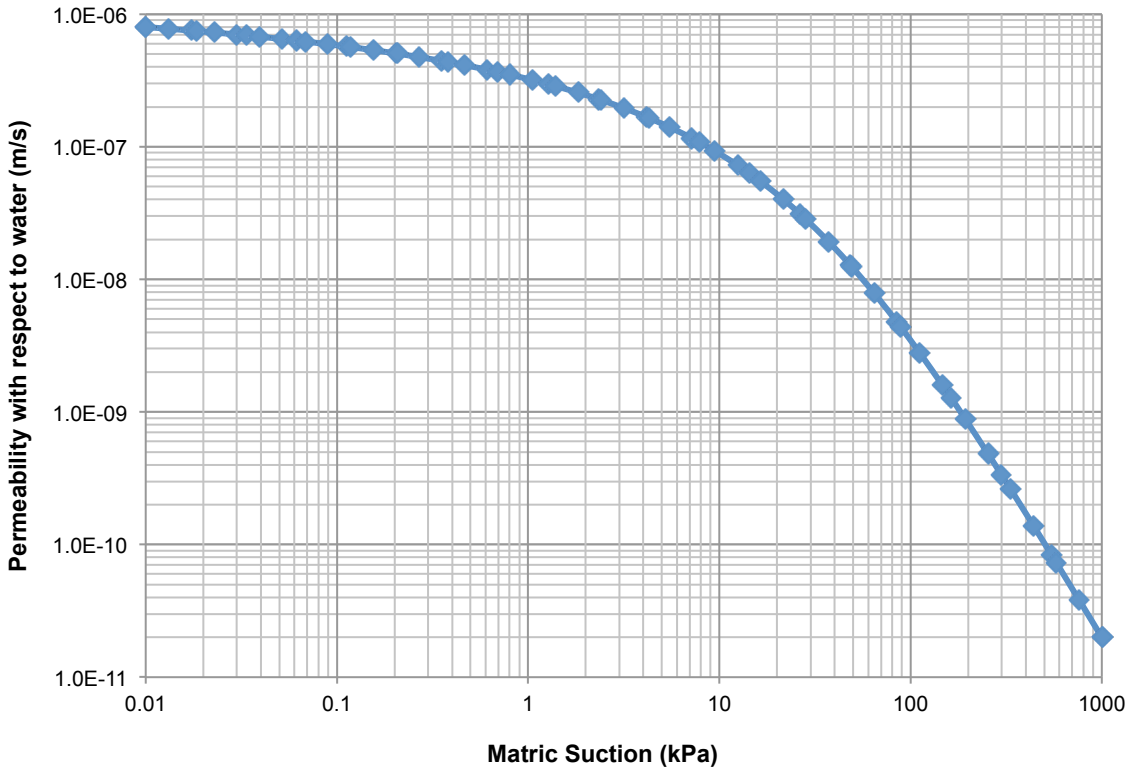

Figure 5.16 Permeability Functions for Precinct 9 slope using van Genuchten (1980)

5.4.2.2 Mechanical properties

It has been presented in Chapter 4 that the critical state stress ratio values, M_{p^*} (based on Bishop stress using S_r) for samples with lower suctions are higher than the stress ratio under saturated condition (M_s = 1.43). These observations related to the effects of degree of aggregations or packet fabric, seem to suggest the application of additional strength using 'cohesion' in order to perfectly model the strength of the residual soil under unsaturated condition (Figure 3.36 in Chapter 3). This introduction of 'cohesion' is also necessary to prevent the possibility of shallow stability failure (surface failure) to be included in the stability calculation due to low strength value at slope surface when cohesion is set to zero.

However, it has to be noted that the application would also lead to the overestimation of soil strength once the degree of saturation reaches 100% (saturated condition). This scenario is likely to happen at the region near to the ground surface as well as the groundwater level. Thus, it was decided to define a 1kPa 'cohesion' with saturated stress ratio (M = 1.43) to avoid any overestimation in strength and shallow slope failure. This stress ratio is equivalent to angle of shearing resistance of 35°. As for layer 2 and the underlying bedrock that are mostly located below the groundwater table, an angle of shearing resistance value of 42° was used for both layers. This value is the average friction angle calculated for layer 2, shown in Chapter 4.

For the purpose of calculation of elastic behaviour using finite element method, the application of elastic modulus and Poisson's ratio is necessary. Although it will not affect the calculation of factor of safety (as stability is related to the strength characteristics), the computational time during transient analysis can be significantly reduced. Thus, an elastic modulus (E) of 1000kPa and 0.33 for Poisson's ratio (v) were defined for all layers in order to fulfil this finite element method requirement.

Table 5.3a and 5.3b present the summary of the hydrological and mechanical properties used in the analysis.

Table 5.3a The summary of hyrdrological parameters for each soil layer of the Precinct 9 slope.

Soil Layer	Description	Grade	Densities		k_{sat} (m/s)	van Genuchten parameters		
			γ_{sat} (kN/m^3)	γ_{unsat} (kN/m^3)		g_a	g_l	g_n
1	Residual soils	VI	18	18	$8x10^{-7}$	0.13	0.084	1.092
2	Highly to completely weathered Schists	IV to V	20	20	$8x10^{-7}$	0.13	0.084	1.092
3	Fresh to moderately weathered Schists	VI	20	20	Non porous			

Table 5.3b The summary of strength parameters for each soil layer of the Precinct 9 slope.

Soil Layer	Description	Grade	c'	ϕ'	E'	ν'
			kPa	°	kPa	
1	Residual soils	VI	1	35	1000	0.33
2	Highly to completely weathered Schists	IV to V	0	42	1000	0.33
3	Fresh to moderately weathered Schists	VI	0	42	1000	0.33

5.4.3 Description of the numerical models

5.4.3.1 Model Geometry, Mesh Discretisation and Boundary Conditions

The model geometry shown in Figure 5.17 illustrates the complete figure of the cut slope prior to failure; with the inclination of 27° (approximately 2H: 1V) and consists of 2 layers of soil that is underlain by the bedrock. Standard fixities were set at the boundaries of the slope model to restrict any lateral movements for side edges and both vertical and horizontal movements at the base.

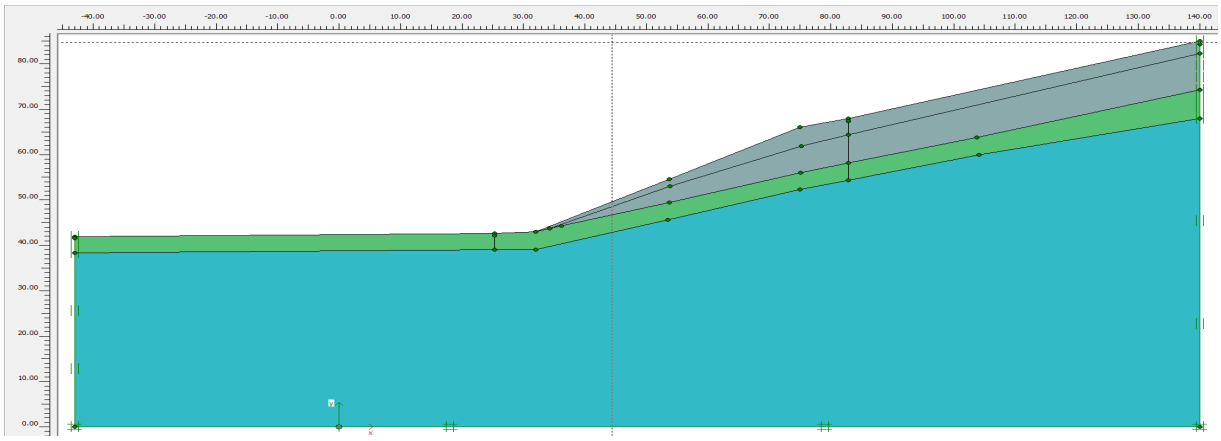

Figure 5.17 Geometry of the slope.

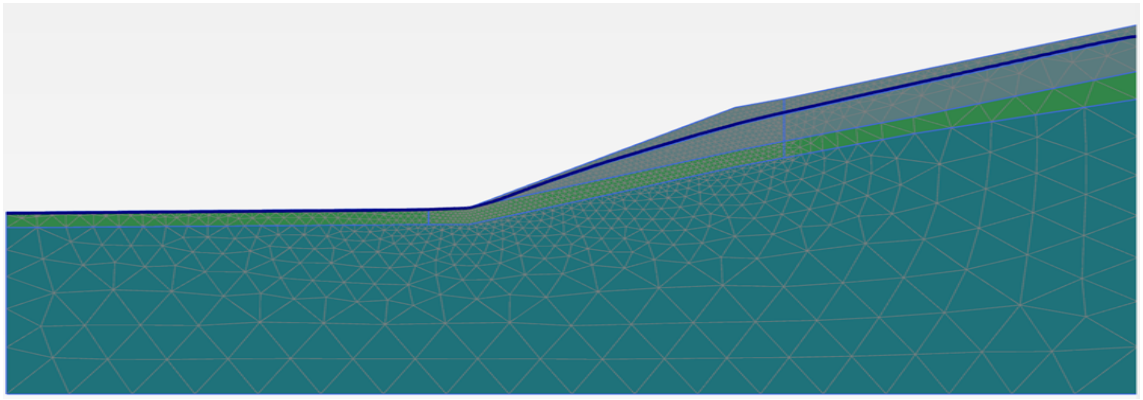

Figure 5.18 Finite element mesh of the slope.

Similar to previous slope assessment, several series of mesh refinement procedures were carried out in order to capture the region with the largest displacement on the slope. This procedure was targeted to prevent possible numerical instabilities. The finest mesh was defined for the region below the slope

surface and this gave an overall number of 2996 15-noded triangular elements (Figure 5.18).

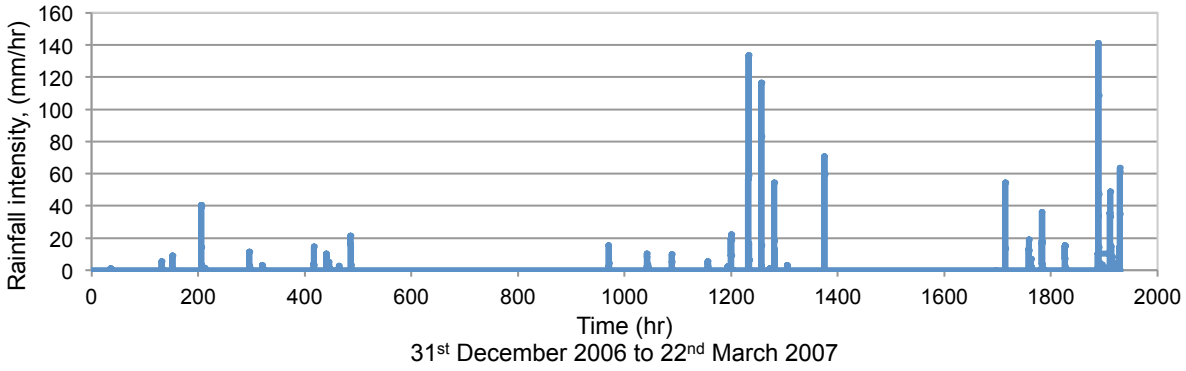

Figure 5.19 Rainfall intensities from 31st December till 22nd March 2007

For hydraulic boundaries, the recorded natural rainfall events, taken from 31st December 2006 till the day of slope failure that was at 4.30am, 22nd March 2007 (1940.25 hours), were modelled as a unit flux boundary (q) along the ground surface (Figure 5.19). This gave a total number of 67 phases for the simulation of the wetting and drying cycles for the transient analysis. This rainfall data was obtained from a nearby rain gauge station located at Precinct 2 (Coordinates: 2° 55'44", 101° 41' 38"). The data was provided by the Department of Drainage and Irrigation of Malaysia (DID).

The minimum and the maximum pore pressure head (options introduced for rainfall hydraulic boundary in Plaxis), were set to be -0.001m ($Ø_{min}$) and 0.001m ($Ø_{max}$). This is to ensure that no 'ponding' effect is allowed to occur on the slope surface. This means that water can only flow on the surface with a maximum height of 1mm. The left and right boundaries of the model were set as groundwater head conditions where the magnitude is determined by the vertical distance between the boundary node and the water level. The groundwater table was set in accordance to the actual data obtained from piezometers reading after the sliding incident, as described in Chapter 2 (0m at the toe and 5m at the crest)

5.4.3.2 Initial Condition

It was difficult to define the initial pore water pressures of the slope. This is due to the limited data that could be used to validate the variation of pore water

pressures within analysis. However, it was decided that a constant pore-water pressure with depth, equal to -5kPa should be set as the initial pore water pressures. This value was defined with the intention to produce a very low pore-water pressure profile before the imposition of the long period of wetting and drying conditions (approximately 3 months duration) until the incident took place. The initial conditions will be important, as the 3 months of imposing real conditions will ensure appropriate values of pore-water pressure will be established.

5.4.4 Results

Figure 5.20 presents the results of pore-water pressures changes against time for node locations at mid slope. The results are compared for the points at 0.1m, 0.25m, 0.5m, 1.0m and 1.5m deep from the ground surface. From the plots, it can be seen that by the first rainfall event at 35.5h, the initial assumed pore water pressures of 5kPa have differentiated for each depth, with positive pore water pressures (~2kPa) at 1.5m depth and negative values (~-10kPa) near the surface (0.1m depth). The trends in fluctuation of pore-water pressures induced by rainfall are similar to the previous assessment for the NTU-ANX slope, where the curves show inclinations and declinations at the right time periods during and after rainfall events. However, the distinction is observed to be less obvious at greater depths within the slope model. This scenario can be explained due to the restriction of the amount of water flowing into the soil, caused by the lower permeability with respect to water (permeability function). At the time of failure, the pore water pressures for each depth exhibit an increase in value due to greater infiltration.

The comparison of the pore-water pressure profiles at mid slope after each series of rainfall and drying events is presented in Figure 5.21. During infiltrations, the development of wetting front can be seen to form at depth close to the ground surface, where a large change in pore-water pressures is calculated. This effect, however, gradually disappears during drying periods due to the localised seepage movement towards the ground water table. This means that only smaller amount of water are flowing towards deeper in the slope and hence the negative pore water pressures at large depth are not highly affected.

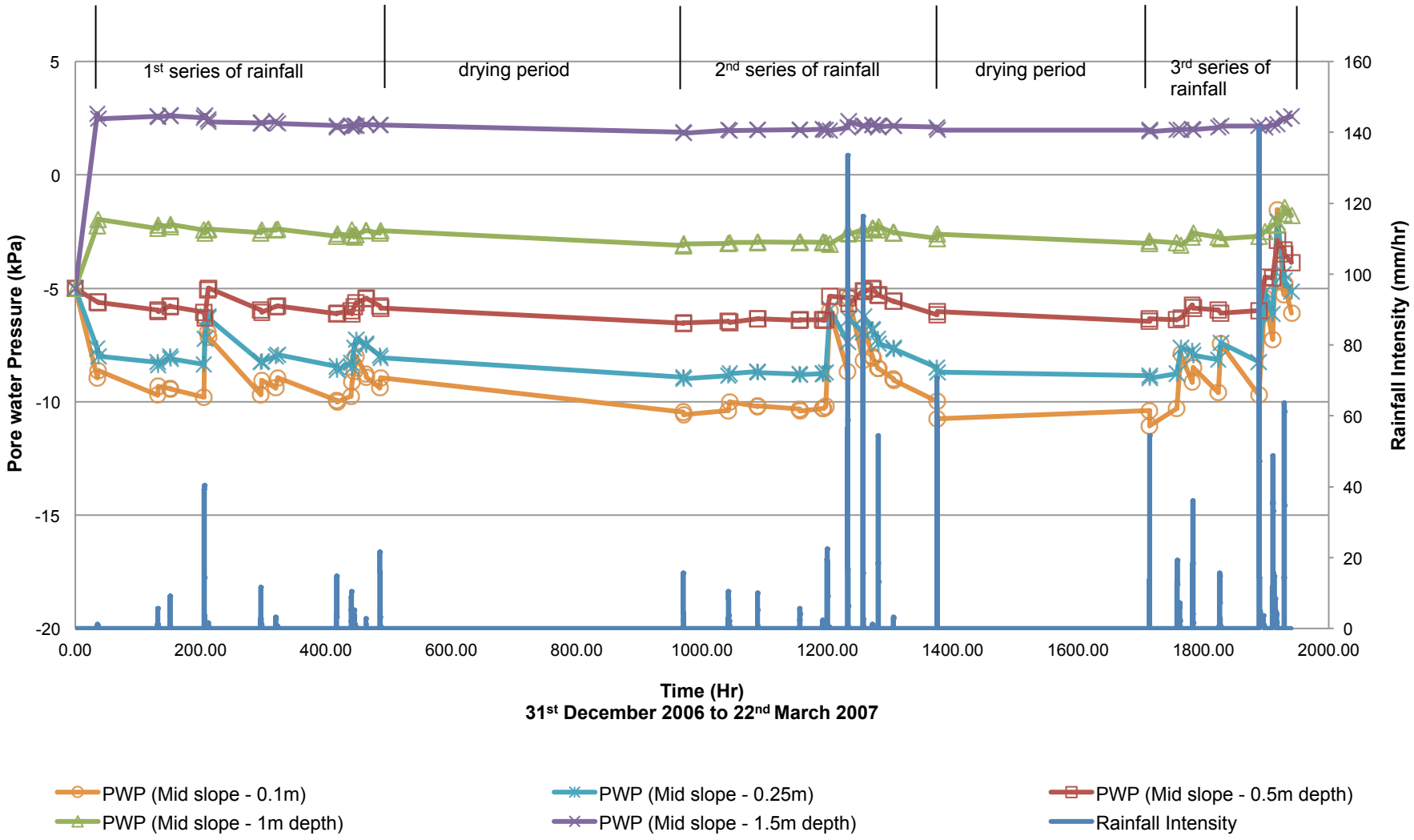

Figure 5.20 Pore water pressure variations against time of Precinct 9 slope: at 0.1m, 0.25m, 0.5m, 1.0m and 1.5m from ground surface (Mid slope)

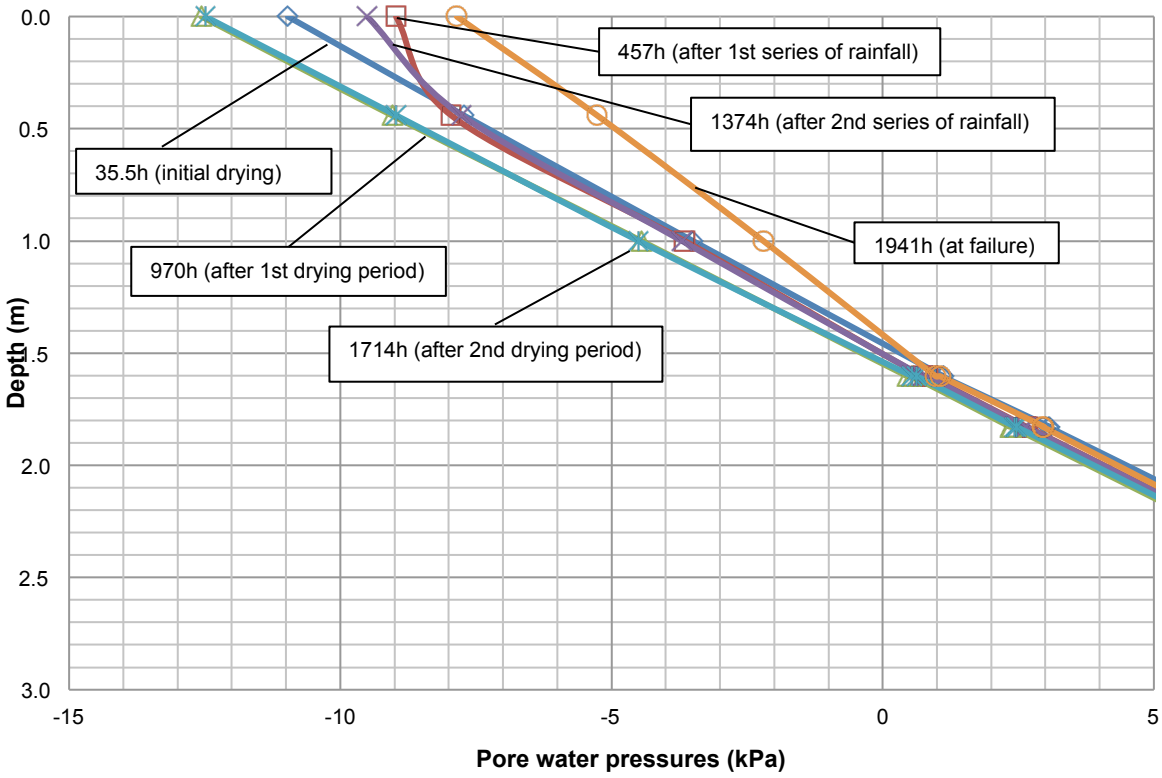

Figure 5.21 Comparison of the pore-water pressure profiles at mid slope after each series of rainfall and drying events until the time of failure.

The plots also indicate a rise in ground water table after the occurrences of each series of rainfall event. This scenario is reflected through the position of the curve at pore water pressure equal to 0kPa, which varies between 1.4m and 1.6m deep. The increase of unsaturated zone soil moisture due to the localised seepage towards groundwater level has caused to the elevation of groundwater position and this creates a transition zone that is commonly known as capillary fringe. However, once the adjustment process of pore water pressure to form hydrostatic equilibrium with the groundwater table is done (after long drying periods), the groundwater table is drawn back to a lower depth and presents the hydrostatic suction profile. Nevertheless, with the exceptionally high rainfall event occurred in 21st March 2007, a greater infiltration has been produced and this reflects to the highest elevation of ground water table that eventually triggered the failure.

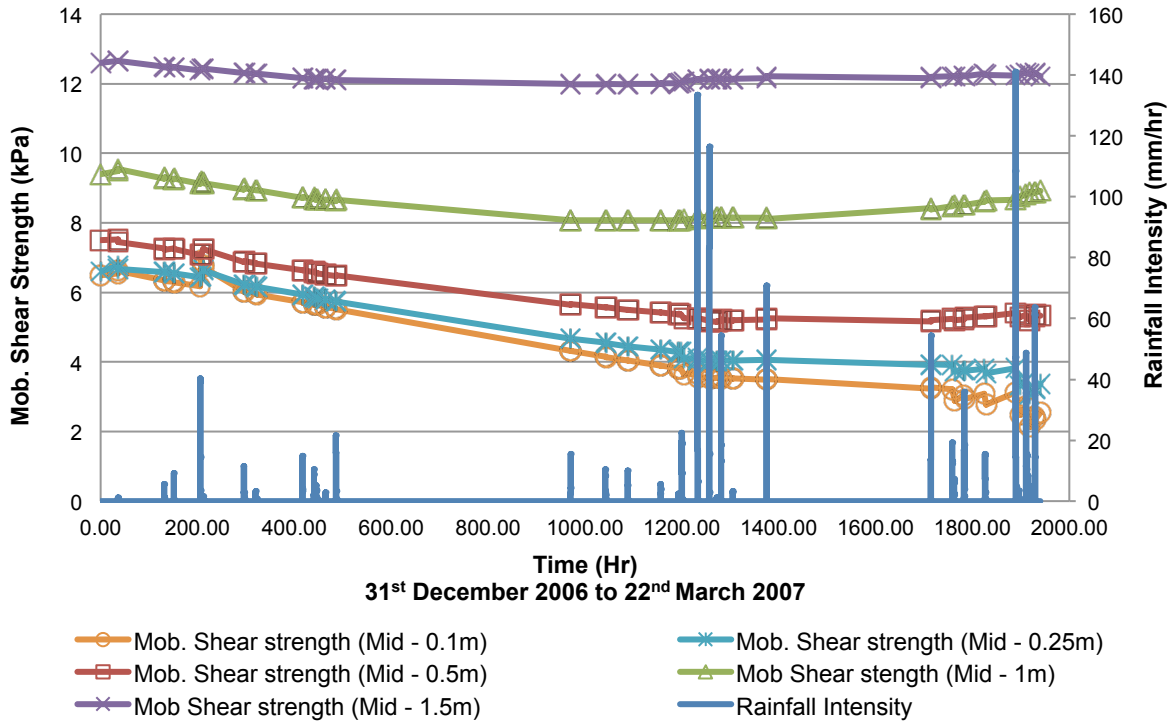

Figure 5.22 Pore water pressure and Mobilised shear strength comparison : at 0.1m, 0.25m, 0.5m, 1.0m and 1.5m from ground surface (Mid slope)

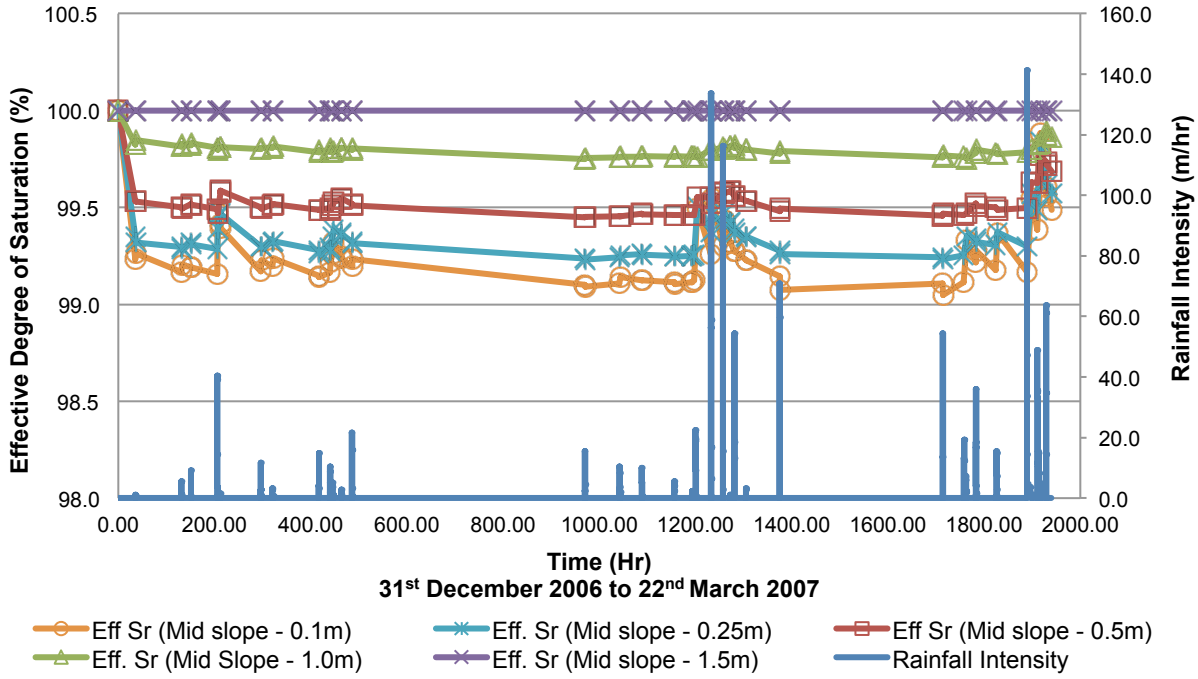

Figure 5.23 Pore water pressure and Degree of Saturation comparison : at 0.1m, 0.25m, 0.5m, 1.0m and 1.5m from ground surface (Mid slope)

Figure 5.22 presents the correlation between mobilised shear strength (τ_m) against the variations of pore-water pressure induced by rainfall. As anticipated, the τ_m value decreases during rainfall events as the increase in pore-water pressure consequently produces reduction in suction, weakening the soil. The reduction in strength is observed to be even greater for soil near to ground surface due to the build-up of a wetting front.

Similar 'ratcheting effect' on soil strength can also be seen from the plot in Figure 5.22. This rapid loss of strength during each period of rain, which is not recovered during the intermediate drying periods, is more apparent for the depth near to the ground surface. Figure 5.23 shows a similar illustration for degree of saturation, with rapid changes during wetting but taking longer to recover during drying.

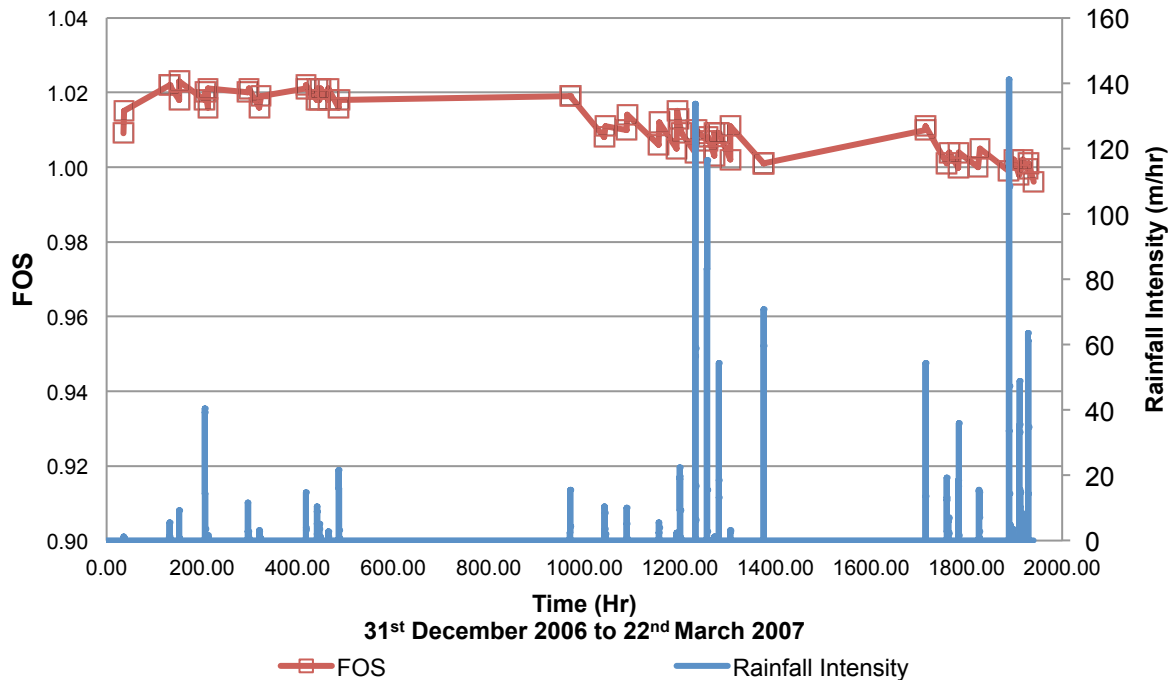

Figure 5.24 Factor of Safety value against time from 31st December till 22nd March 2007

The most striking result to emerge from the output is the variation of slope stability against time, shown in Figure 5.24. From the graph, it can be seen that the curve for Factor of safety (FOS) of the slope generally shows a decline during and rise up after rainfall infiltration. Although the difference in magnitude between the

maximum FOS and FOS at failure (FOS<1) is quite minimal (approximately 0.03), the overall trend of the curve, however, does show a gradual declination before it was triggered to failure due to the intense rainfall event on 21st March 2007. These rainfall events that occurred prior to the landslide incident caused a rise of groundwater table, thus, weakened the soil. (It has to be noted that the incident took place at around 4:30am on the 22nd March 2007, with no rain reported. This delay in instability can be related to the adjustment process of pore water pressure to form hydrostatic equilibrium with the groundwater table).

To justify this further, the plot of daily rainfall for entire 2007 is shown in Figure 5.25. Through the plot, it is clear that the amount of rainfall is exceptionally high during the two days the before incident with total amount of 140mm on the 20th and 60mm on 21st March 2007. This suggests that the slope was fairly stable before the incident took place but eventually prompted a failure due to these very extreme amounts of rainwater infiltration. Figure 5.26 presents the position of the slip failure with estimated incremental displacements contour, based on the outputs of SSR calculation. Figure 5.27 shows the location of the calculated plastic points at the time of failure. These indicate a zone of failure, reaching approximately 15m in height from the toe of the slope that is similar to the real case as reported by IKRAM, shown in Chapter 2.

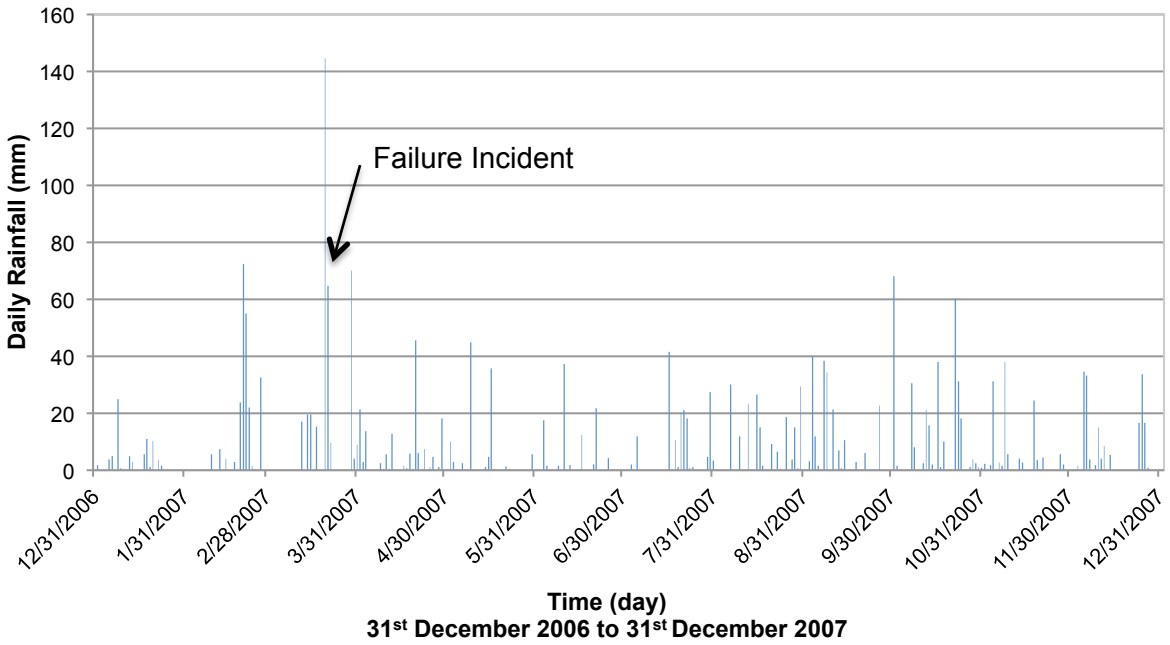

Figure 5.25 The distribution of daily rainfall for entire 2007

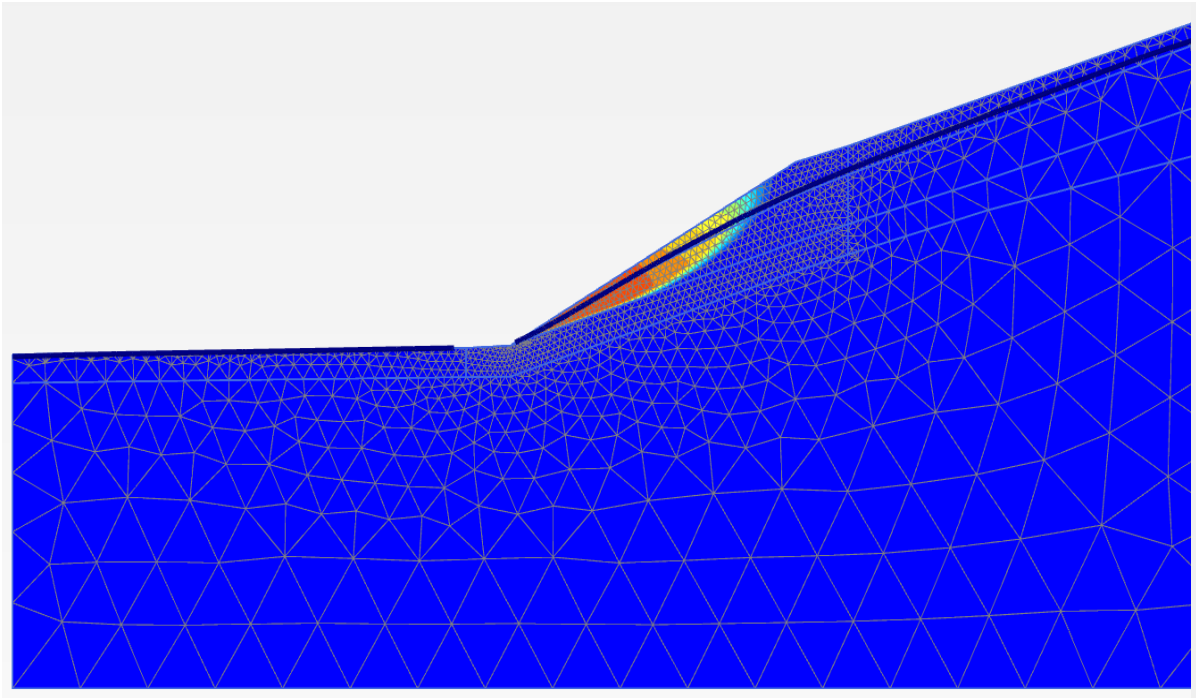

Figure 5.26 The position of the slip surface with contour of incremental displacements at failure

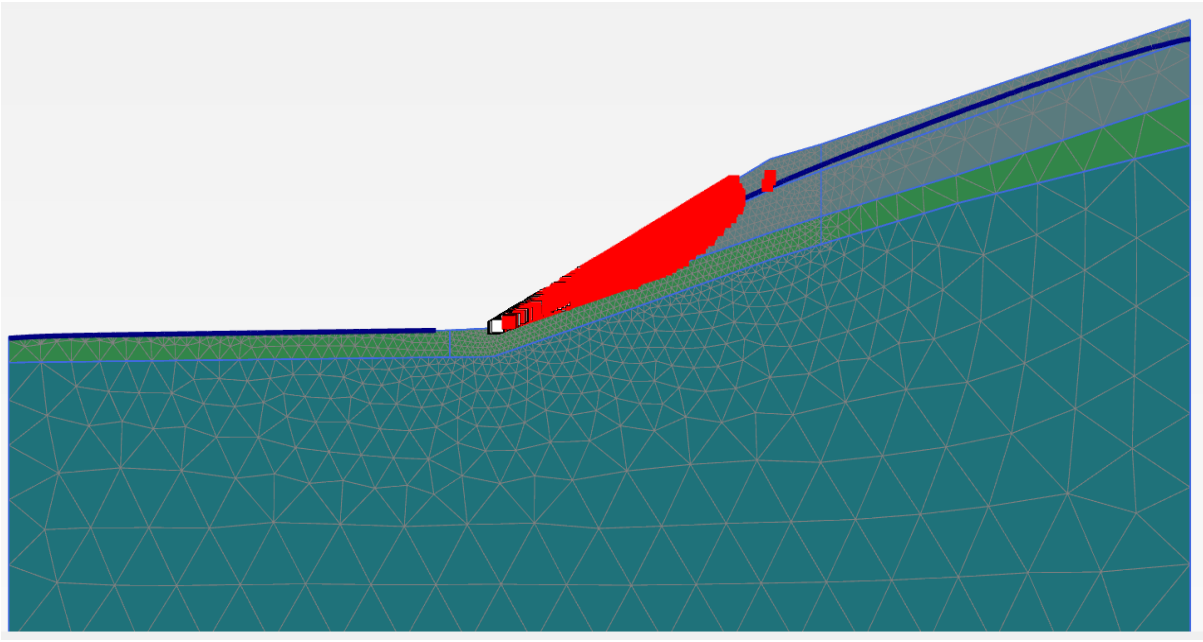

Figure 5.27 The position of the calculated plastic points at failure

5.4.5 Progressive Slope Failure

Referring back to the previous assessment, it is clear that the slope had experiencing a strain softening effect (in terms of shear strength); caused by the rainfall infiltration before the eventual collapse mechanism occurred. This strain-softening behaviour of the soil causes unstable forces to propagate as a progressive failure surface in the slope. However, the progressive slope failure theory suggests that in most cases, the mobilisation of shear strength along slip failure is non-uniformly distributed between the strength at peak state and ultimate state (or critical state) (Potts and Zdravkovic, 2001). At collapse, this failure surface will consist of a part that has lost its post-peak strength (ultimate state) and a part that has not yet fully deteriorated (peak state).

Therefore, a sensitivity analysis using the peak strength parameters for the mechanical properties of the layer 1 is made in order to further investigate its effect towards the stability of the slope. Figure 5.28 presents the plot for q against p' which indicates the peak state line and critical state line of layer 1. The productions of these lines are based on the laboratory tests results presented for sample MZ1S1, MZ1S2 and MZ1S3 (Chapter 4).

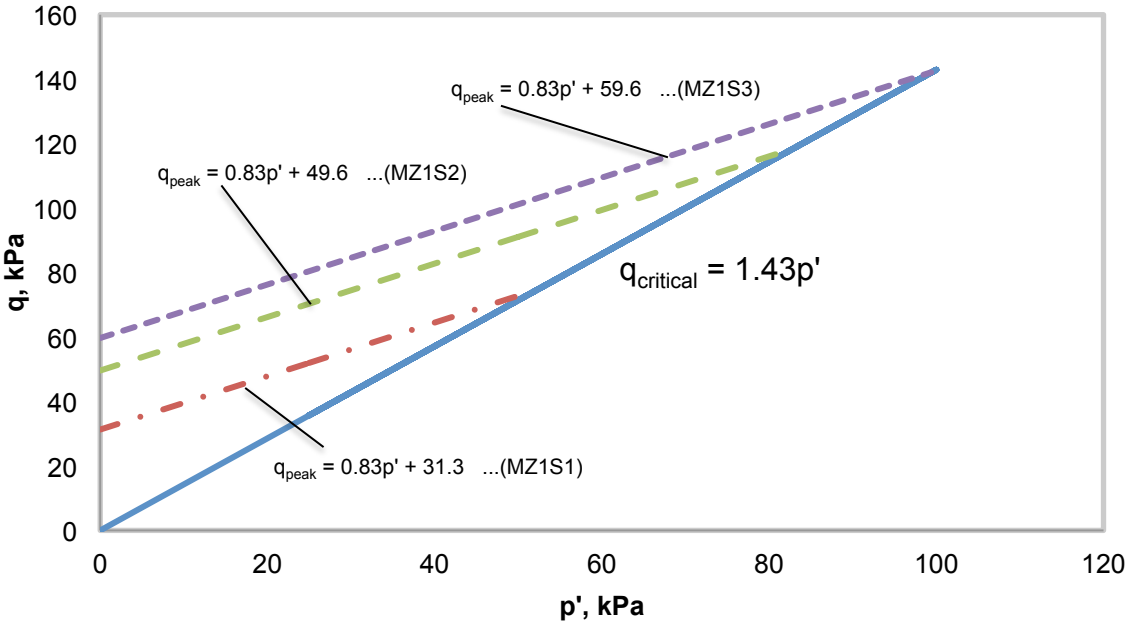

Figure 5.28 The plots for q against p' for samples MZ1S1, MZ2S2 and MZ1S3 of layer 1

A single stress ratio of 0.83 has been obtained to represent the peak state, equivalent to 21° as an angle of shearing resistance. The cohesion, however, are varies between 31.3kPa to 59.6kPa and this is due to the differences in initial void ratio for each sample. Thus, a lower bound value of 32kPa was taken as the cohesion at peak state.

5.4.5.1 FOS comparison assessment

Figure 5.29 presents the comparison for FOS for both analyses using critical state and peak state strength parameters, respectively. From the plots, it is apparent that the trend for FOS using peak strength does not explain the inclinations and declinations of FOS that match with the fluctuations of pore-water pressures, caused by rainfall. However, there is a clear trend of decreasing towards FOS equal to 1 as the analysis continues towards the time of failure.

o explain this further, the outputs of incremental displacements estimated based on SSR calculation are used. The magnitude of these displacement results is not relevant (as a simple Mohr Coulomb model with an estimated Young's modulus was used to calculate the displacements), however, the illustration of the displacement concentration area can be used to provide insight for this scenario. Figure 5.30a, 5.30b, 5.30c, 5.30d, 5.30e, 5.30f and 5.30g present the condition of incremental displacements and variation of pore-water pressure for initial condition, the conditions before and at the end of all three series of rainfall events as well as at failure.

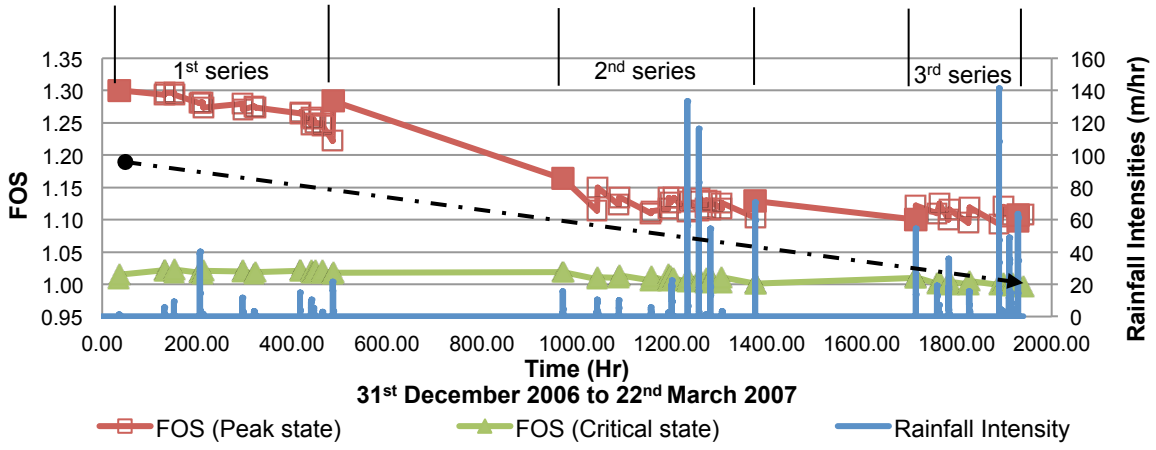

Figure 5.29 The comparison for FOS for both analyses using critical state and peak state strength parameters

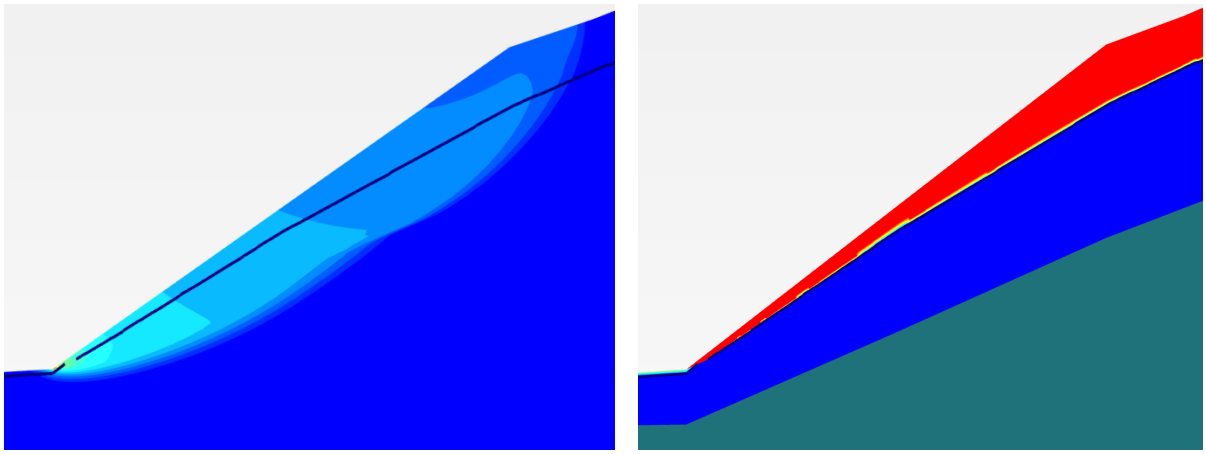

(a) initial condition

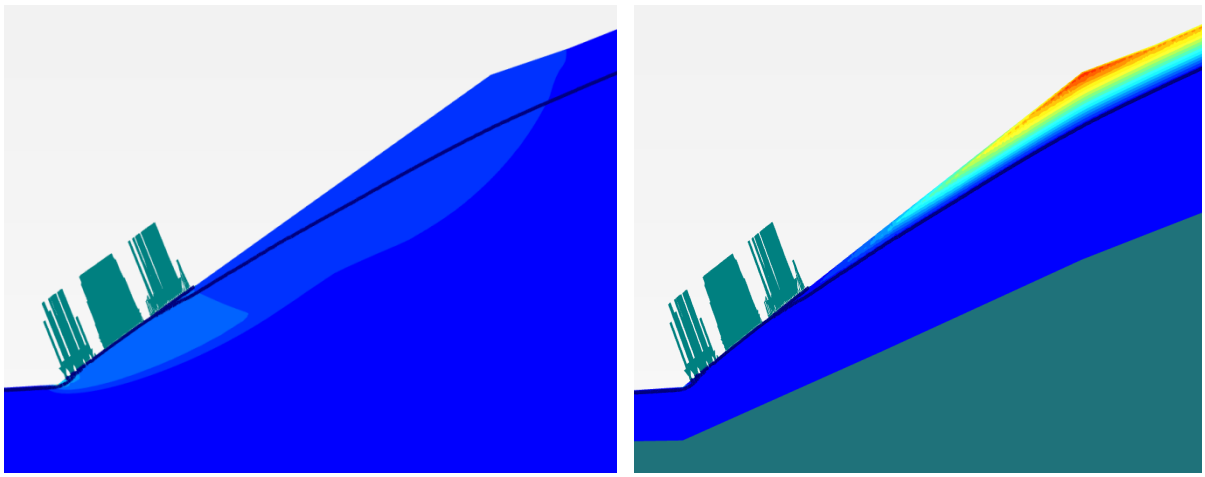

(b)at the end of 1st series of rainfall

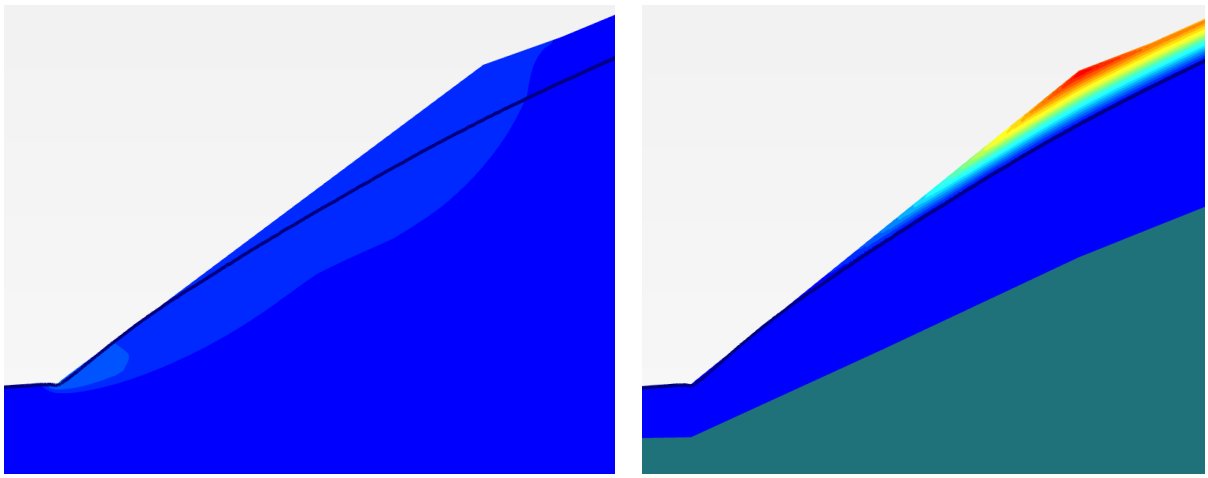

(c) before 2nd series of rainfall

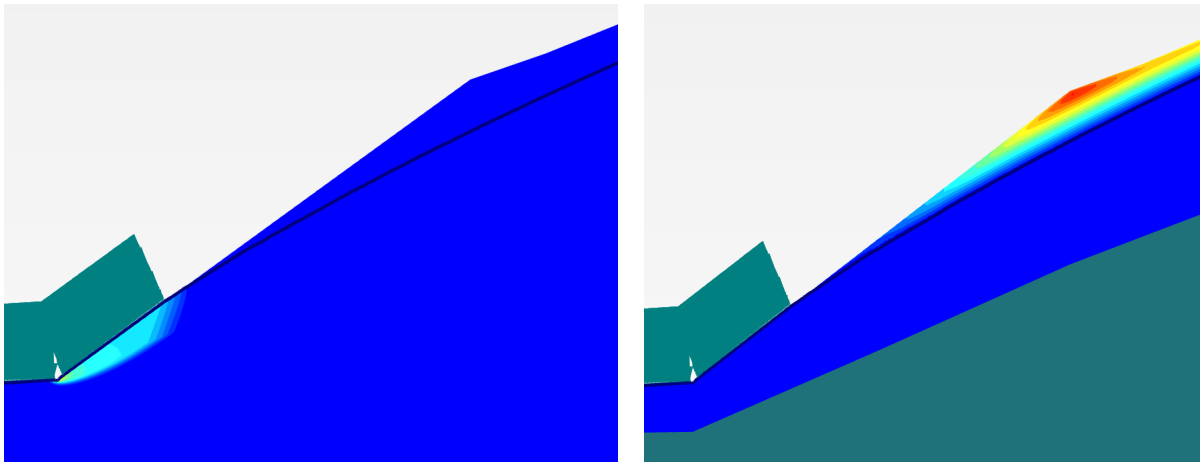

(d) at the end of 2nd series of rainfall

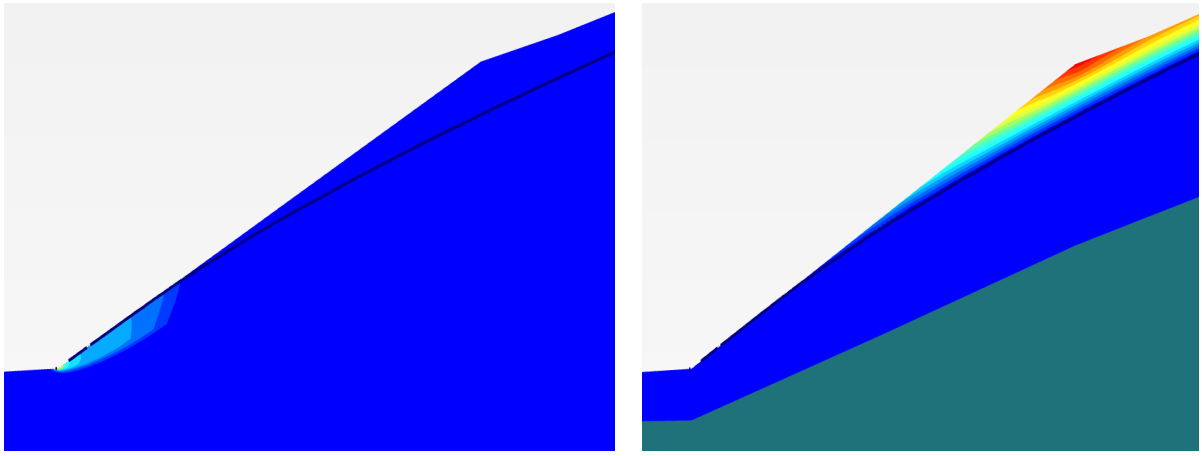

(e) before 3rd series of rainfall

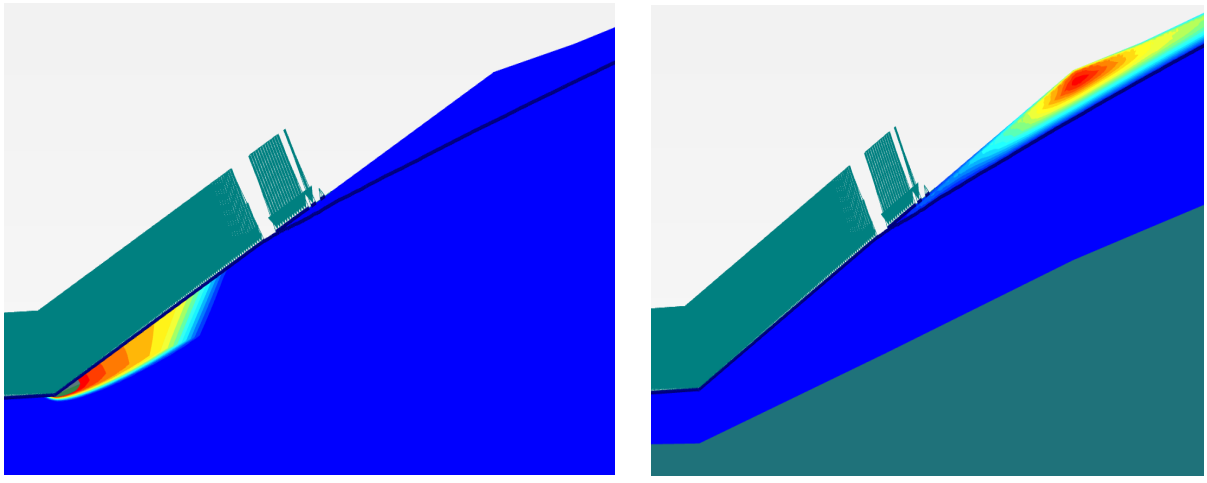

(f) at the end of 3rd series of rainfall

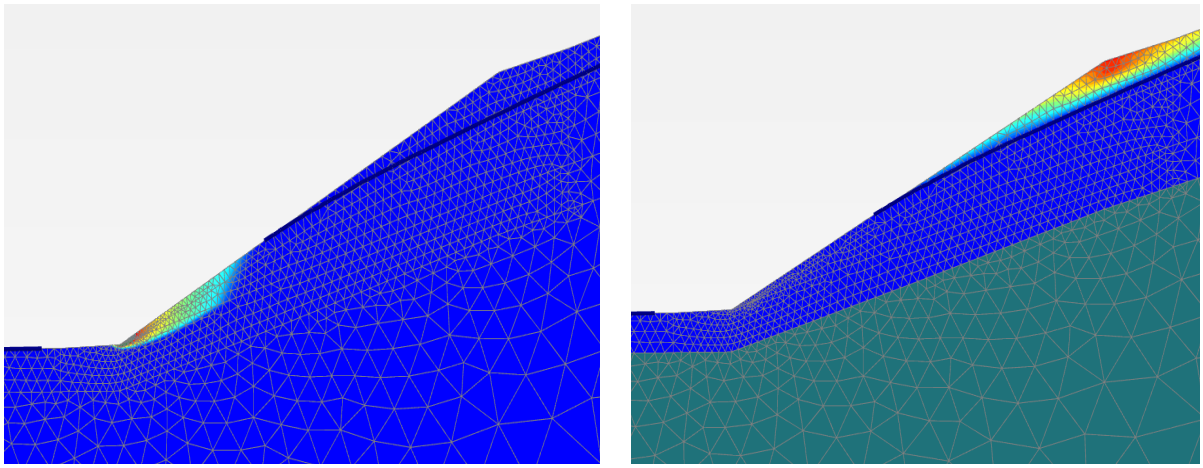

(g) at failure

Figure 5.30 The numerical modelling outputs for the condition of incremental displacements (left) and variation of negative pore-water pressures (right)

In Figure 5.30a, the results of incremental displacement and pore-water pressure for initial condition is shown. A constant value of -5kPa was set for the unsaturated region (above groundwater level), which essentially produced a uniformly contoured incremental displacement that covers the overall section of the slope. Then, after the 1st series rainfall (Figure 5.29b), higher negative pore-water pressure was built up at the crest, while elevation of groundwater table occurs at the toe of the slope. The displacement concentration is fully concentrated at the toe although there is an additional strength gained at the upper part of the slope; contributed by the defined cohesion and high magnitude of negative pore-water pressures. This greater displacement concentration caused by the elevated groundwater table has resulted in the decrease of FOS value.

After a long period of drying condition (Figure 5.30c), the position of groundwater table still remains at the same level but the magnitude of negative pore-water pressure is higher. This produces a higher concentration of incremental displacement that contributed to the lesser FOS. The development of these two components is observed to be similar for the conditions after the 2nd and 3rd series of wetting and drying cycles (Figure 5.30d, 5.30e and 5.30f). Eventually, due to the exceptional rainfall event that occurred immediately prior to the failure incident, the

elevation of groundwater table has reached a significant level within the slope, thus, giving the lowest value of FOS (Figure 5.30g).

From the descriptions made above, it is clear that the differences between both analyses are due to the different soil strengths. The additional cohesion defined for peak strength essentially produced a higher magnitude of shear strength that is not affected by the variation of pore-water pressure. In conclusion, the analysis using peak strength suggests that the slope was reasonably stable but gradually weakened as the amount of rainfall increased (indicated by the chain-dotted arrow). Furthermore, it also implies that an average value of strength property between peak state and critical state should be used in order to achieve a more representative FOS profile, similar to the suggestion made by Potts and Zdravkovic (2001).

5.5 Final Remarks

The occurrence of rainfall-induced slope failures is very common in Malaysia, with higher frequency particularly during the monsoon seasons. Based on the forensic geotechnical studies, the indication of the cause of these major slope failure events is highly related to the long periods of continuous or intense rainfall pattern that is believed to be linked to climate change. Therefore, the need for more research work and practical design approaches for slope design are highly essential in order to mitigate the risk of failure as minimal as possible.

This chapter presents the application of numerical modelling methods for tropical residual soil slope stability assessment, using rainfall as a surface boundary condition. The effect on slope stability is through the process of rainwater infiltration, which creates increases in pore-water pressure (or reduction in matric suctions) within the slope. The importance of considering the actual behaviour of the soil in stability analysis has also been highlighted through the presentation of numerical modelling work (using Plaxis 2D) that combined the equations for the flow (hydrological) and deformation (mechanical) assessments.

A reanalysis of a previous numerical study by incorporating models for both saturated and unsaturated conditions, using van Genuchten (1980) for the modelling

the soil water retention behaviour and the concept by Bishop (1959) for “effective” stress in unsaturated soils (implemented here using $\chi=S_r$), has been made. The analysis was carried out based on a research slope, reported by Tsaparas and Toll (2002), and described to be an instrumented tropical residual soil slope (called NTU-ANX), located on the campus of Nanyang Technological University (NTU), Singapore. An uncoupled analysis by SEEP/W and SLOPE/W software (GeoSlope International, 2007) was used in the earlier numerical investigation of the slope and was validated against field monitoring data that consisted of runoff data and pore-water pressure changes that were measured at several depths and locations on the slope. The objective of this analysis was to present a comparative study between the stability assessments using coupled and uncoupled analyses.

A comparison between coupled and uncoupled analyses was made against the field data at 0.5m depth. Reasonable agreement was seen between the two models. The models do explain the trends in fluctuation of pore-water pressures during rainfall through the patterns of inclinations and declinations at the right time periods during and after rainfall events.

Furthermore, the results from coupled analysis show the τ_m value decreased during both rainfall events. This is due to the increase in pore-water pressure which consequently produced a reduction in suction, weakening the soil. A sharp increase in pore water pressure caused a rapid drop in mobilised shear strength. However, during the drying period following a rain storm, it was seen that the pore water pressures dropped much more slowly and resulted in a gradual increase in strength. With the continuation of this scenario, a ‘ratcheting’ effect on soil strength would be caused when a series of regular rain storms with short periods of drying in between cause rapid loss of strength that is not recovered during the intermediate drying periods. The results are mirrored by degree of saturation, with rapid changes during wetting but taking longer to recover during drying.

The comparisons between the stability assessments were also made for the Factor of safety (FOS). For the uncoupled analysis is slightly higher compared to the results for the coupled analysis. Despite this difference in magnitude of FOS, which will be due to the difference in approach of SSR and Limit equilibrium methods, the trends of the curves show a very similar shape as both FOS decline and rise up

during and after rainfall infiltration. This implies that the adoption of unsaturated concepts for slope stability assessment is highly significant in order to mitigate the risk of failure, especially for slopes in tropical region.

For the incident of slope failure occurred in 2007 in Precinct 9, Putrajaya, a back analysis has been carried out by adopting the hydro-mechanical coupled model using Plaxis 2D. The objectives of this numerical analysis was to investigate the possible cause of the slope failure, as well as to further understand the effect of the infiltration mechanism on the strength behaviour of the slope prior to failure. The details of the tropical residual soils slope from Chapter 2, Chapter 3 and Chapter 4, were used which consist of groundwater table, slope geometry, hydrological and mechanical properties. These parameters were used together with time dependent boundary conditions (Rainfall data) in order to emulate the behaviour of the slope before failure. It was anticipated that the slope should produce a FOS higher than 1 prior to the failure incident and decreasing towards less than unity (FOS $\leq$ 1) due to the triggering factor of rainfall.

The results of pore-water pressures changes against time for the mid slope was used and compared for the points at 0.1m, 0.25m, 0.5m, 1.0m and 1.5m deep from the ground surface. It can be seen that the trends for the fluctuations of pore-water pressures are similar to the previous assessment for the NTU-ANX case, where the curves show inclinations and declinations at the right time periods during and after rainfall events. The distinction is less obvious at greater depths into the slope model due to the restriction of the amount of water flowing into the soil caused by the lower permeability with respect to water (permeability function). A wetting front has been formed close to the ground surface, where a large change in pore-water pressures is calculated. The effect also causes a rise of ground water table within the slope.

The mobilised shear strength (τ_m) is observed to decrease during the rainfall events caused by the increase in pore-water pressure. This reduction in strength is greater for soil near to the ground surface due to the build-up of the wetting front. Similar ‘ratcheting effect’ on soil strength can also be seen and is more apparent for the depth near to the ground surface. Similar observations for the degree of

saturation are made, with rapid changes during wetting but longer periods being necessary to recover during drying.

The results for Factor of safety (FOS) of the slope generally show a decline during and rise up after rainfall infiltrations. However, although the difference in magnitude between the maximum FOS and FOS at failure (FOS<1) is quite minimal (approximately 0.03), the overall trend of the curve does show reasonable agreement by the presentation of gradual declination before it was triggered to failure by the intense rainfall events. A factor of safety of less than 1.0 was calculated for the failure event. It can be concluded that the cause for the failure was due to the rise of groundwater table resulted from the adjustment process of pore water pressure to form hydrostatic equilibrium with the groundwater table

The failure event can be related to exceptionally high rainfall events in March 2007. These were the largest daily rainfalls observed for the whole 2007. This suggests that the slope was fairly stable before the incident took place but the failure was prompted by a very extreme amount of rainwater infiltration. The position of the slip failure with estimated incremental displacements contour, show a similar size of slope failure as indicated by the field observations of the failure in Chapter 2.

A further analysis using peak strength parameters showed that the FOS using peak strength does not explain the failure as the FOS remains above 1.0. However, it is clear that the value decreases towards FOS equal to 1 as the analysis continues towards the time of failure. Nevertheless, it seems that the critical state parameters are more suitable to match the observed failure.

Chapter 6
Conclusion and Recommendation for Future Works

6.1 Conclusion

This thesis describes the effects of climate variation on a tropical residual soil slope in Malaysia. The effects are generally associated with the changes in hydrological conditions within the slope and therefore it is important to further understand the natural characteristics of tropical residual soils. The findings can be used to generate a clear view of the hydro-mechanical behaviour of the slope through exposure to different climate events. Also, it can be used as further guidance for the mitigation and prevention to any unfavourable future implication such as landslides.

The study was presented in two parts. The first part concerned the presentation of the natural characteristics of the tropical residual soils, from soil samples obtained by soil sampling works that took place on a failed tropical residual soil slope in Precinct 9, Putrajaya, Malaysia. These soil properties were derived through the implementation of a series of laboratory works that consisted of the soil index classification tests, mechanical triaxial tests and hydrological tests (Chapters 2 to 4). Subsequently, these soil properties were used as input parameters for the advanced numerical modelling works using actual rainfall data as a surface boundary condition. Full details of these modelling works were described Chapter 5. This chapter presents a summary of the various conclusions that have been drawn out relative to the works carried out for both parts.

6.1.1 The natural characteristics of tropical residual soil

The inherent variations of engineering geology of residual soils are frequently unforeseen and also difficult to identify during the design stage. Many researchers have indicated that extra care should be taken when describing the actual behaviour of these tropical residual soils; especially in correspondence to climate changes. Soil-sampling works in May 2013 were successfully carried out at the top of the

slope to allow an investigation of the cause of failure to take place. This was done by using Durham University's state-of-the-art unsaturated soil testing facilities. Details of the slope and the soil sampling works were presented in Chapter 2.

Soil drilling procedures using foam as the flushing fluid were executed to ensure that the retrieved undisturbed soil samples were not subjected to irreversible damage either during sampling process (e.g. volumetric strains). A total number of 5 PVC sample tubes (75mm dia. x 1000m long) were successfully retrieved that represented the depth from 1m to 5m deep. Based on physical observation, the variation in weathering grade was seen clearly by the colour of the samples. For samples from 1m to 3m deep, the colour was reddish brown to brownish grey, while, a variation in colour from brown to yellowish could be seen in MZ3 tube, representing the depth at 3m to 4m. For samples in MZ4 (4m to 5m), the colour of the soil samples was dark grey with white stripes that represented the underlying bedrock due to its structural rigidity.

A series of index and classification tests were executed in order to classify the materials. In general, these tests proved that the index properties of the soil were highly connected to the variation in degree of weathering. The water content tests showed that for samples near to the ground surface (Layer 1), the soil had high natural water content. This could be explained by the leaching of minerals in the soil (weathering process) providing a more porous structure that was replaced by water, contributed by climatic events. This non uniform disintegration process also produced clay-based material that caused water to be retained instead of flowing down to the lower profile. Reasonably constant bulk density values were observed for this layer consistent with these high natural water content and clay materials.

However, for samples at lower depth (Layer 2), the weathering process of the parent bedrock was less advanced due to less exposure of surface climate variation. At this depth, the fabric of the soil seemed to maintain the original structure of the rock mass due to a higher degree of cementation between particles reflected by the lower weathering grade. This cementation was also associated with the lower content of clay material and less voids for water phase. The plot for Atterberg limits parameters clarified this suggestion.

The variation in degree of weathering was also reflected in the mechanical behaviour of the tropical residual soil (Chapter 3). This can be seen through the saturated test results obtained from all 6 triaxial samples from MZ1, MZ3 and MZ4 to represent layer 1 and layer 2 profiles. The results for the normalised stress paths obtained from the multistage saturated tests for layer 1 showed critical state stress ratio (M_s) equal to approximately 1.43. However, for the case of layer 2, stress ratio values ranged from 1.6 to 1.89. These differences were justified due to the visible dissimilarity in characteristics and thought to be related to the variation in degree of cementation of the sample (weathering grade).

The variation of the mechanical behaviour by climate variation can also be analysed from the comparison between both saturated and unsaturated tests. The multistage unsaturated constant water content triaxial tests (only done for layer 1), were conducted on 5 residual soil samples with 5 different initial suctions (4 of the samples were dried back before testing). Test were performed at constant water content to prevent the possibility of the natural packet fabric (soil aggregation) in the soil to be destroyed due to a suction controlled process (if wetted or saturated) and to preserve the 'in situ' condition of the soil.

The constant water content test results showed that the obtained stress ratio values (M_{p^*}), calculated based on the 'Bishop stress' concept, for unsaturated samples with lower suctions were higher than the stress ratio under saturated condition (M_s = 1.43). This showed that a single critical state parameter with degree of saturation (S_r) as the additional parameter, as suggested in the 'Bishop stress' approach, was insufficient.

To explain these additional strengths, the unsaturated strength was explained in terms of two stress components (M_a and M_b). The critical state stress ratio M_a is stress component relative to net stress (σ-u_a) and M_b is the stress ratio relative to the matric suction (u_a-u_w). This procedure was adopted to investigate the differences in strength with changes in suctions. The results showed that the values for M_a appeared to be progressive by increasing suction as M_b reduces towards zero. These scenarios were attributed to the occurrences of microscopic aggregations or packet fabric within the soil element, as reported by Toll (1990, 2000). As suction increased, higher degree of aggregation would be produced and caused the samples

to behave more like a coarser material explaining the increase in M_a. The decreased of degree of saturation (volumetric water content) within the soil, however, have forced withdrawal of the pore-water into packets and resulted into the reductions of M_b.

In addition, the determination of the critical state parameters based on the Extended Mohr Coulomb model (in q-p space) were implemented to interpret the results based on the assumption of using M_a equal to M_s. From the results, it was shown that an average of 49kPa additional strength value was needed by each sample in order to explain the actual strength value. This showed that under unsaturated conditions, the soil would gain additional strength, which explains the sustainability of tropical residual soil slope during dry season. With the imposition of an extreme infiltration event, failure can be induced due to rapid soil strength degradation.

To further understand the concept of unsaturated soil conditions, the implementation of hydrological tests is imperative (Chapter 4). The results from the tests can be used to describe the hydrological behaviour of the tropical residual soils that are generally associated with the movement of water seepage within the slope and the relationships with soil water content. To justify this, a total number of 13 samples of residual soil were tested for the derivation of both permeability and SWRC properties of layer 1 and layer 2. The SWRC is an unsaturated hydrological property that can be decribed as the ability of soil to attract and retain water and normally clarified based upon graphical approach and defined as Soil Water Retention Curve. The curve represents the relationships between water content and suction,

For the permeability tests, the results for layer 1 ranged between 3.96×10^{-7} m/s to 1.31×10^{-6} m/s, while values varied between 2.40×10^{-7} m/s to 1.26×10^{-6} m/s for layer 2. These variations were attributable to the inherent variation of degree of weathering. An average value of 8×10^{-7} m/s was used to represent the saturated coefficient of permeability for both layer 1 and 2.

The analysis for SWRC were carried out by adopting the axis translation technique using pressure plate apparatus and also by direct suction measurement technique using high capacity tensiometer for both continuous and stage methods of

water content change. These tests were implemented through the drying process from its natural conditions in order to minimise the possibilities of disturbance to these specimens. The results were presented in terms of gravimetric water content, volumetric water content and degree of saturation against suction.

In general, the SWRC pattern also reflected the degree of weathering. A steeper curve was observed for sample with higher fraction of coarse materials and gentler curve for samples with finer material. Moreover, it was also observed that the continuous method using high capacity tensiometer presented the most reliable data as compared to the rest of the tests. This signified the importance of continuous volume reading for the determination of SWRC in order to prevent experimental error during the handling for weight and volume measurements.

6.1.2 The advance numerical modelling of tropical residual soil slope

From previous works, it was recognised that the climate events would reduce soil strength, particularly with long periods of continuous or intense rainwater infiltration. For the case of slope stability, this reduction could induce failure. With extreme climate variation, the risk of failure could be accelerated and hence the application of numerical modelling methods for tropical residual soil slope stability assessment, using rainfall as a surface boundary condition was needed.

As reported in Chapter 5, the slope numerical analyses were carried out using Plaxis 2D software, by combining the equations for the hydrological and mechanical assessments (coupled model), based on the concept suggested by Bishop (1959). The first analysis was carried out for a research slope, reported by Tsaparas and Toll (2002) that was an instrumented tropical residual soil slope (called NTU-ANX), located on the campus of Nanyang Technological University (NTU), Singapore. The results were compared with uncoupled analysis, previously done by Tsaparas and Toll (2002), and validated against field monitoring data that consisted of runoff data and pore-water pressure changes that were measured at several depths and locations on the slope.

Reasonable agreement was seen between the two models. These models did explain the trends in fluctuation of pore-water pressures during rainfall through the patterns of inclinations and declinations at the right time periods during and after

rainfall events. Additionally, the coupled model managed to show the decrease of the mobilised shear strength, τ_m, during infiltration due to the increased pore-water pressure. However, the soil regained its strength during drying but the development was observed to be much slower as compared to wetting. It was discovered that a 'ratcheting' effect on soil strength would be caused when a series of regular rain storms with short periods of drying in between cause rapid loss of strength that is not recovered during the intermediate drying periods. In consequence, the variation in soil strength reflected the Factor of safety (FOS) of the slope. This implies that the adoption of unsaturated concepts for slope stability assessment is highly significant in order to mitigate the risk of failure, especially for slopes in tropical regions.

Similar modelling procedures were adopted to back analyse the incident of slope failure occurred in 2007 in Precinct 9, Putrajaya, The details of the tropical residual soils slope from Chapter 2, Chapter 3 and Chapter 4, as well as the rainfall data prior to the date of the failure incident, were used in order to implement this analysis. The slope stability assessment was expected to produce a FOS higher than 1 prior to the failure incident and decreasing towards less than unity (FOS $\leq$ 1) due to the triggering factor of rainfall.

In general, similar characteristics as the results for NTU-ANX were obtained from this analysis. A wetting front was formed close to the ground surface, where a large change in pore-water pressures was calculated that resulted in a rise of ground water table within the slope. The effect of the wetting front was also believed to have accelerated the 'ratcheting effect' on soil strength for this top layer. The overall trend of the FOS result did show a gradual declination before it was triggered to failure with FOS less than 1.0. Although the difference in magnitude between the maximum FOS and FOS at failure was small, the cause of failure can still be linked to the imposition of a very extreme amount of rainwater infiltration, caused by the rise of groundwater table. Furthermore, it was also discovered that the critical state soil parameters are more suitable to match the observed failure.

The fully coupled hydro-mechanical modelling also have proved that the cause to the incident of slope failure occurred in 2007 in Precinct 9, Putrajaya, Malaysia, was related to exceptionally high rainfall events in March 2007. With total amount of 140mm on the 20th and 60mm on 21st March 2007, the plot of daily rainfall

showed that these were the largest daily rainfalls observed for the whole 2007. This explained how the slope was fairly stable before the incident took place but eventually prompted to failure due to a very extreme climate variation.

Overall, it can be concluded that the natural characteristics of tropical residual soil slope are highly connected to the variation in degree of weathering and the historical background of its seepage condition. For slopes with a highly weathered top soil layer, the degree of cementation between particles for this layer will be less and will be weaker. The non-uniform disintegration process will cause the slope to be very heterogeneous which is also one of the factors that contribute to the variation of its properties. On the other hand, the effects of climate events can cause the slope to lose its strength due to the changes in hydrological condition. During a drying period, additional strength will be gained but with rainfall infiltration, this strength will rapidly deteriorate. This signifies the importance to implement advanced laboratory works as well as a hydro-mechanical numerical modelling for slope stability assessment, especially when dealing with tropical residual soil.

6.2 Recommendation for Future works

Taking into account the conclusions of this work, it is clear that climate plays an important role in the development of tropical residual soil. The effects are not only observed to influence its long-term characteristics (degree of weathering) but also on the short-term behaviours that prevail during drying and wetting seasons (transition from unsaturated into saturated condition). These characteristics can be highly heterogeneous as it also involves chemical weathering (leaching of soil minerals) that may alter the structure of the soil at both micro and macro levels. Thus, it is recommended to implement the study of the soil microstructure and mineralogy tests, such as X-ray diffraction (XRD) and Scanning electron microscopy (SEM), in order to further understand the role of these components towards the soil's natural characteristics.

From the study of mechanical behaviour of tropical residual soil, it was recognised that the soil would gain additional strength under unsaturated conditions.

Although, this additional strength was associated with the production of microscopic aggregations or packet fabric within the soil element, it can also be linked to the natural bonding between the particles that is based on the differences in the degree of cementation. The investigation of these particle cementation effects can be done, by implementing an additional series of mechanical tests, on the remoulded (destructed) tropical residual sample. The results can be compared with the obtained natural strength properties and hence the influence towards its strength behaviour can be investigated.

It has been highlighted that the application of the continuous method using high capacity tensiometer presented the most reliable data as compared to the rest of the tests. The advantage of using the technique was described due to its capability for continuous volume change readings without removing the soil sample for weight and volume measurements. However, the effect of cable stiffness on the mass measurement is still one of the concerns that need to be investigated as it may influence the actual characteristics of the SWRC. In the latest version of the equipment, wireless data logging has been adopted to eliminate the problem of cable stiffness. It would be useful to carry out additional SRWC test with the improved equipment to provide the most accurate SWRC of the tropical residual soil based on its actual characteristics.

A comparison study of permeability function using 2 different statistical model equations has been presented in Chapter 4. The results showed obvious differences in pattern between the shapes of the curves calculated from both methods. This indicates the danger in using such expressions without an experimental confirmation of their validity. Therefore, it is suggested to implement further experimental works on the permeability function of the soil. The findings will provide further indication on how this property would vary with suction.

Further research on the interrelation of hydraulic and mechanical behaviour in unsaturated soils has become a subject of great interest in geotechnical engineering practice. It is due to the fact that wetting and drying cycles, caused by the variation of climatic events, increases the stiffness and causes irreversible volumetric strain. As only ultimate limit states are concerned for stability analysis, this deformation effect was not employed in the presented analyses. This signifies the need for further

advance numerical modeling works for slope assessment, by incorporating constitutive models that include the deformation assessment as part of the analysis. The assessment should also include the application of finite element software that can provide the adoption of M_a, M_b or $(\emptyset_a, \emptyset_b)$ approach rather than relying on 'Bishop stress' method.

Lastly, it can be seen that the numerical modelling work implemented for Precinct 9 slope was not validated against any field data that include the measurement of pore water pressures changes. This is because the subsurface investigations and instrumentation programmes implemented by IKRAM did not involve the application of tensiometer that can provide data on the variation in pore water pressures within the slope. Therefore, it is necessary to adopt the technique for monitoring pore water pressures changes in engineered earth structures, such as slope. This data is not only useful to provide further understanding on the actual behaviour of seepage condition within a slope, but can also be used to validate the output of numerical modelling works in order to obtain the best simulation of the actual behaviour of the slope.

REFERENCES

AHMED, J., GHAZALI, M. A., MUKHLISIN, M., ALIAS, M. N. & TAHA, M. R. 2011. Effectiveness of horizontal drains in improving slope stability: A case study of landslide event in Putrajaya, Precinct 9, Malaysia. *Unsaturated Soils: Theory and Practice* 753-758.

ALI RAHMAN, Z. 2008. *The engineering behaviour of a weakly bonded soil including the unsaturated state.* Phd Dissertation, Durham University.

ANDERSON, M. G., COLLISON, A. J. C., HARTSHORNE, J., LLOYD, D. M. & PARK, A. 1996. Developments in Slope Hydrology-Stability Modelling for Tropical Slopes,. *Advances in Hillslope Processes,* 2**,** 799-821.

ATKINSON, J. H. 1993. *An introduction to the mechanics of soils and foundations.,* London, McGraw-Hill.

ATKINSON, J. H. & BRANSBY, P. L. 1978. *The mechanics of soils,* London, McGraw-Hill.

BERGMAN, E. F. & MCKNIGHT, T. L. 1993. *Introduction to geography*, Englewood Cliffs, New Jersey: Prentice Hall.

BIOT, M. A. 1941. General theory of three-dimensional consolidation. *Journal of Applied Physics,* 12**,** 155–164.

BISHOP, A.W. 1959. The Principle of Effective Stress. *Tecknisk Ukeblad* 39**,** 859-863.

BISHOP, A. W. & DONALD, I. B. 1961. The experimental study of partly saturated soils in the triaxial apparatus. *Proc. 5th Int. Conf. Soil Mechanics Foundation Engineering,* 1**,** 13–21.

BITTELLI, M. & FLURY, M. 2009. Errors in water retention curves determined with pressure plates and their effect on soil hydraulic properties. *soil Science Society Academy Journal,* 73**,** 1453–1460.

BLACK, D. K. & LEE, K. L. 1973. Saturating laboratory samples by back pressure. *ASCE Journal Soil Mechanics Foundation Engineering Division,* 99**,** 75-95.

BLIGHT, G. E. 1985. Residual soils in South Africa. *Sampling and testing of residual soils.*, 159-168.

BLIGHT, G. E. 1997. Mechanics of residual soils. *ISSMGE (TC25)*.

BOSO, M., ROMERO, E. & TARANTINO, A. 2003. The use of different suction measurement techniques to determine water retention curves. *Unsaturated soils: Experimental studies, (ed. Schanz T), Berlin: Springer-Verlag*, 171-181.

BRAND, E. W. 1981. Some Thoughts on Rainfall-Induced Slope Failures. *Proceedings of the 10th International Conference on Soil Mechanics and Foundation Engineering, Stockholm,* 3, 373-376.

BRAND, E. W. 1984. Landslides in Southeast Asia: A State of the Art Report. *Proceedings of the 4th International Symposium on Landslides, Toronto, Canada,* 1, 17-59.

BRAND, E. W. & PHILLIPSON, H. B. 1985. Sampling and testing of residual. *A review of International Practice. Southeast Asian Geotechnical Society.*: Hong Kong: Scorpio Press.

BRINKGREVE, R. B. J., SWOLFS, W. M. & ENGIN, E. 2010. PLAXIS 2D version 2010-11, Reference and Material models manuals.

BROOKS, R. H. & COREY, A. T. 1964. Hydraulics properties of porous media. *Colorado State University Hydrology Paper, Fort Collins,* 27.

BS1337 1990. Methods of test for soils of civil engineering purposes *Part 4: Compaction-related tests.* Milton Keynes: British Standard Institute.

BS5930 1999. The code of practice for site investigations. *British Standards Institution*.

BULUT, R. & LEONG, E. C. 2008. Indirect measurement of suction. *Geotechnical Geology Engineering*.

BURLAND, J. B. 1965. Some aspects of the mechanical behaviour of partly saturated soils. *Proc. Conf. On Moisture Equlibria and Moisture Changes in Soil Beneath Covered Areas* 270-278.

BURLAND, J. B. 1965a. The yielding and dilation of clay. *Geotechnique,* 15, 211-214.

CAMPBELL, G. S. 1974. A simple method for determining unsaturated conductivity from moisture retention data. *Soil Science,* 117**,** 311-314.

CAMPBELL, G. S. 1988. Soil water potential measurement: an overview. *Irrigation Science,* 9**,** 265–273.

CHATTERJEA, K. 1989. *Observations on the Fluvial and Slope Processes in Singapore and their Impact on the Urban Environment.* PhD thesis: School of Civil and Structural Engineering, Nanyang Technological University.

CHIU, C. F., CUI, Y. F., DELAGE, P., DE LAURE, E. & HAZA, E. Lessons learnt from suction monitoring during centrifuge modelling. *In:* CUI, Y. F., ed. Advanced experimental unsaturated soil mechanics, Tarantino, 2005. 3-8.

COLEMAN, J. D. 1962. Stress strain relations for partly saturated soil. *Géotechnique,* 12**,** 348-350.

COOLING, L. F. 1949. Soil mechanics and site exploration. Jounal of Institute of Civil Engineer, 18, 37-61.

CRESSWELL, H. P., GREEN, T. W. & MCKENZIE, N. J. 2008. The adequacy of pressure plate apparatus for determining soil water retention. *Soil Science Society Academy Journal,* 72**,** 41–49.

CRONEY, D. 1952. The movement and distribution of water in soils. *Geotechnique,* 3**,** 1-16.

CUNNINGHAM, M. R. 2000. The mechanical behaviour of a re-constituted unsaturated soil. *PhD Dissertation, Imperial College of Science, Technology and Medicine, London*.

DANE, J. H. & KLUTE, A. 1977. Salts effects on the hydraulic properties of a swelling soil. *Soil Science Soc. Of America,* 41**,** 1043-1049.

DAY, R. W. & AXTEN, G. W. 1989. Surficial Stability of Compacted Clay Slopes. *Journal of Geotechnical Engineering, ASCE,* 115**,** 577-580.

DELAGE P., SURAJ DE SILVA G.P.R. & DE LAURE E. 1987. A new triaxial apparatus for unsaturated soils. *9th Conf. Eur. Soil Mechanics and Foundation Engineering, Dublin, Balkema, Rotterdam,* 1, 26-28

DEUTCHER, M. S., GASMO, J. M., RAHARDJO, H., LEONG, E. C. & TANG, S. K. 2000. Field Measurements of Pore-Water Pressure Profiles in Residual Soil

Slopes of the Bukit Timah Granite Formation, Singapore. *Proceedings of the Asian Conference on Unsaturated Soils, UNSAT-ASIA 2000, Singapore*, 777-782.

DINEEN, K. & BURLAND, J. B. A new approach to osmotically controlled oedometer testing. *In:* DELAGE, A. A., ed. Unsaturated Soils, 1995. 459-465.

DYKES, A. P. & THORNES, J. B. 2000. Hillslope Hydrology in Tropical Rainforest Steeplands in Brunei. *Hydrological Processes,* 14, 215-235.

ESCARIO, V. & SÁEZ, J. 1986. The shear strength of partly saturated soils. *Géotechnique,* 36, 453-456.

ESHEL, G., LEVY, G. J., MEINGERLGRIN, U. & SINGER, M. J. 2003. Critical evaluation of the use of laser light scattering for particle size distribution analysis. *Soil Science Soc. Of America. Book Series*.

FOOKES, P. G. 1997. *Tropical Residual Soils: A Geological Society Engineering Group Working Party Revised Report,* Bath, Geological Society.

FOURIE, A. B. 1996. Predicting Rainfall-Induced Slope Instability. *Proceedings of Institution of Civil Engineers, Geotechnical Engineering,* 119, 211-218.

FOURIE, A. B. & PAPAGEORGIOU, G. 2001. Defining and appropriate steady state line for Merriespruit gold tailings. *Canadian Geotechnical Journal,* 38, 695-706.

FREDLUND, D. G. & BARBOUR, S. L. 1992. Integrated Seepage Modelling and Slope Stability Analyses: A Generalized Approach for Saturated/Unsaturated soils. *Geomechanics and Water Engineering in Environmental Management*, 3-35.

FREDLUND, D. G. & MORGENSTERN, N. R. 1977. Stress state variables for unsaturated soils. *J. Geotech. Eng. Div., ASCE,* 103, 447-466.

FREDLUND, D. G. & MORGENSTERN, N. R. 1978. STRESS STATE VARIABLES FOR UNSATURATED SOILS. *Journal of the Geotechnical Engineering Division-Asce,* 104, 1415-1416.

FREDLUND, D. G., MORGENSTERN, N. R. & WIDGER, R. A. 1978. Shear-Strength of Unsaturated Soils. *Canadian Geotechnical Journal,* 15, 313-321.

FREDLUND, D. G. & RAHARDJO, H. 1987. Soil mechanics principles for highway engineering in arid regions. *Transportation research record,* 1137**,** 1-11.

FREDLUND, D. G. & RAHARDJO, H. 1993. *Soila mechanics for Unsaturated Soils*, New York: Wiley.

FREDLUND, D. G. & XING, A. 1994. Equations for the soil-water characteristic curve. *Canadian Geotechnical Journal,* 31**,** 521–532.

FREDLUND, D. G., XING, A. & HUANG, S. 1994. Predicting the permeability function for unsaturated soils using the soil water characteristic curve. *Canadian Geotechnical Journal,* 31**,** 533-546.

GALAVI, V. 2010. *Groundwater flow, fully coupled flow deformation and undrained analysis in PLAXIS 2D and 3D* [Online]. Plaxis Report. Available: http://kb.plaxis.nl/.

GAN, J. K. M. & FREDLUND, D. G. 1988. Multistage direct shear testing of unsaturated soils. *ASTM Geotechnical Testing Journal,* 11**,** 132-138.

GASMO, J. M., HRITZUK, K. J., RAHARDJO, H. & LEONG, E. C. 1999. Instrumentation of an Unsaturated Residual Soil Slope. *Geotechnical Testing Journal,* 22**,** 128-137.

GASMO, J. M., RAHARDJO, H. & LEONG, E. C. 2000. Infiltration Effects on Stability of a Residual Soil Slope. *Computers and Geotechnics,* 26**,** 145-165.

GEE, G. W. & OR, D. 2002. Particle size analysis. *Soil Science Society of America,* 5**,** 255-293.

GEE, G. W., WARD, A. L., ZHANG, Z. F., CAMPBELL, G. S. & MATHISON, J. 2002. The influence of hydraulic nonequilibrium on pressure plate data. *Vadose Zone Journal,* 1**,** 172–178.

GENS, A. 2010. Soil environment interactions in geotechnical engineering. *Géotechnique,* 60**,** 3-74.

GEOGUIDE 3 1996. Tropical weathered in situ materials - Laboratory testing. *Public Works Department Malaysia*.

GREEN, R. E. & COREY, J. C. 1971. Calculation of Hydraulic Conductivity: A further evaluation of some predictive method. *Soil Science Society of America Proceedings,* 35**,** 3-8.

GUAN, Y. & FREDLUND, D. G. 1997. Use of the tensile strength of water for the direct measurement of high soil suction. *Canadian Geotechnical Journal,* 34**,** 604-614.

GUE, S. S. & TAN, Y. C. 2004. Guidelines for development in hill-sites. *In:* HUAT, B. B. K., GUE, S. S. & FAISAL, H. A. (eds.) *Tropical Residual Soils Engineering.* Taylor & Francis Group, London.

HAMDHAN, I. N. & SCHWEIGER, F. H. 2011. Slope Stability Analysis of Unsaturated Soil with Fully Coupled Flo- Deformation Analysis. *IAMG 2011, Salzburg, Austria*.

HEAD, K. H. 1992. *Manual of soil laboratory testing. Volume 1: Soil classification and compaction tests*, London Pentech Press.

HEAD, K. H. 1998. Manual of Soil Laboratory Testing Volume 3: Effective Stress Tests. *Chichester, John Wiley & Sons Ltd*.

HEINZ, W. F. 1989. Diamond drilling handbook. *2nd edn., W.F. Heinz, Halfway House, South Africa, S2Spp*.

HILF, J. W. 1956. An investigation of pore-water pressure in compacted cohesive soils. *Technical Memorandum*

HILLEL, D. 1982. Introduction to soil physics. *Academic Press, San Diego, CA.*

HO, D. Y. F. & FREDLUND, D. G. 1982. Increase in strength due to suction for two Hong Kong soils. *Proc. ASCE Specialty Conf. Engineering and COnstruction in Tropical and Residual Soils.***,** 263-295.

HO, K. M. Y., TSE, J. M. K. & NG, C. W. W. 2007. Influence of drying and wetting history and particle size on state-dependent soil-water characteristic curves (SDSWCCS). *3rd Asian Conference in Unsaturated Soils,***,** 213-218.

HODGE, R. A. L. & FREEZE, A. R. 1977. Groundwater Flow Systems and Slope Stability. *Canadian Geotechnical Journal,* 14**,** 466-476.

HOSSEINI, S. M., HAERI, M. S. & TOLL, D. G. 2005. Behaviour of gravely sand using critical state concepts. *Scientia Iranica,* 12**,** 167-177.

HUAT, B. B. K., ALIAS, A. & JAMALUDIN, S. 2004. Sampling and testing of tropical residual soils. *In:* HUAT, B. B. K., GUE, S. S. & FAISAL, H. A. (eds.) *Tropical Residual Soils Engineering.*: Taylor & Francis Group, London.

HUAT, B. B. K., DAVID, H. B. & AHMED, J. 2007. Slope Instability and Climate Change for Malaysia. *Proceedings of Expert Symposium Climate Change, Modelling, Impacts & Adaptations & Workshop on Climate Change and Slope Stability, National University of Singapore*, 127-134.

IKRAM 2007. Landslide at Precinct 9, Putrajaya, investigation and design of remedial works report. Kumpulan IKRAM Sdn. Bhd.

INTERGOVERNMENTAL PANEL ON CLIMATE CHANGE (IPCC). 2013. *Climate Change 2013 The Physical Science Basis Working Group I Contribution to the Fifth Assessment Report of theIntergovernmental Panel on Climate Change* [Online]. Available: https://www.ipcc.ch/pdf/assessment-report/ar5/wg1/WG1AR5_Frontmatter_FINAL.pdf

JAPANESE GEOTECHNICAL SOCIETY. 1998. *Method for Obtaining Undisturbed Soil Samples Using Rotary Triple-tube Sampler.* [Online]. Japan: Japanese Geotechnical Society. Available: https://www.jiban.or.jp/pdf_count/JGS1223-1995E.pdf.

JOMMI, C. 2000. Remarks on the constitutive modelling of unsaturated soils. *In* A. Tarantino & C. Mancuso (Eds), *Experimental Evidence and Theoretical Approaches in Unsaturated Soils, Rotterdam: Balkema,* 139-153.

JOTISANKASA, A. 2005. Collapse behaviour of a compacted silty clay. *PhD Dissertation, Imperial College of Science, Technology and Medicine, London*.

KARTHIKEYAN, M., TOLL, D. G. & PHOON, K. K. 2008. Prediction of changes in pore-water pressures response due to rainfall events. *In* Toll, D. G., Augarde, C. E., Gallipoli, D. & Wheeler, S.J. (Eds), *Unsaturated Soils: Advances in Geo-Engineering, Proc. 1st European Conf. Unsaturated Soisls, Durham, Leiden: CRC Press/Balkema,* 829-834

KARUBE, D. & KAWAI, K. 2001. The role of pore water in the mechanical behavior of unsaturated soils. *Geotechnical & Geological Engineering,* 19, 211-241.

KHALILI, N., HABTE, M. A. & S., Z. 2008. A fully coupled flow deformation model for cyclic analysis of unsaturated soils including hydraulic and mechanical hystereses. *Computers and Geotechnics,* 35, 872-889.

KHALILI, N. & KHABBAZ, M. H. 1998. A unique relationship for chi for the determination of the shear strength of unsaturated soils. *Geotechnique,* 48**,** 681-687.

KOMOO, I. 1985. Engineering properties of weatheredrock profiles in Peninsular Malaysia. *Proc. 8th SEA geotechnical conference***,** 3-81.

KONRAD, J. M. 1990. Minimum undrained strength versus steady state strength of sands. *Journal of the Geotechnical Engineering Division-Asce,* 34**,** 948-963.

KRAHN, J., FREDLUND, D. G. & KLASSEN, M. J. 1989. Effect of Soil Suction on Slope Stability at Notch Hill. *Canadian Geotechnical Journal,* 26**,** 269-278.

LADD, C. C. & LAMBE, T. W. 1963. The strength of undisturbed clay determined from undrained tests. Symposium on Laboratory Shear Testing of Soils, ASTM, 342–371.

LEACH, B. & HERBERT, R. 1982. The Genesis of a Numerical Model for the Study of the Hydrogeology of a Steep Hillside in Hong Kong. *Quarterly Journal of Engineering Geology,* 15**,** 243-259.

LEONG, E. C. & RAHARDJO, H. 1997. Permeability functions for unsaturated soils. *Journal of Geotechnical and Geoenvironmental Engineering Geology,* 123**,** 1118-1126.

LI, Q. & STANDING, J. 2014. Experimental Set up for Determining Soil Water Retention Curves for Granular Soils During Drying. *Acta Geologica Sinica (English Edition),* 88**,** 1875-1883.

LI, X. 1995. *Slope Stability in Unsaturated Residual Soils due to Rainfall.* PhD Dissertation, School of Civil and Structural Engineering, Nanyang Technological University.

LIEW, S. S. 2004. *Slope failures in tropical residual soils*. *In:* HUAT, B. B. K., GUE, S. S. & ALI, F. H., eds. Tropical Residual Soils Engineering, CRC Press, 73-100.

LITTLE, A. L. The engineering classification of residual tropical soils. Proc. specialty session on the engineering properties of Lateritic Soil. 7th International conference soil mechanics & foundation engineering, 1969 Mexico City. 1-10.

LIU, G., TOLL, D. G., KONG, L. & ASQUITH, J. D. 2016. Matric suction and volume characteristics of compacted clay soil un-der drying and wetting cycles. *submitted to ASTM Geotechnical Testing Journal*.

LOURENÇO, S. D. N. 2008. *Suction Measurements and Water Re-tention in Unsaturated Soils* [Online]. PhD Thesis, Durham University. Available: http://etheses.dur.ac.uk/1331/.

LOURENÇO, S. D. N., GALLIPOLI, D., TOLL, D. G., AUGARDE, C. E. & EVANS, F. 2011. A new procedure for the determination of the Soil Water Retention Curves by continuous drying using high suction tensiometers. *Canadian Geotechnical Journal*, 48, 2, pp. 327-335.

LOURENÇO, S. D. N., GALLIPOLI, D., TOLL, D. G. & EVANS, F. D. 2006. Development of a Commercial Tensiometer for Triaxial Testing of Unsaturated Soils. *Proc. 4th International Conference on Unsaturated Soils, Phoenix, USA, Geotech-nical Special Publication No. 147, Reston: ASCE,* 2**,** 1875-1886.

LOURENÇO, S. D. N., GALLIPOLI, D., TOLL, D. G., EVANS, F. D. & MEDERO, G. M. 2007. Determination of the Soil Water Retention Curve with Tensiometers. *Experimental Unsatu-rated Soil Mechanics, (ed. T. Schanz), Springer***,** 95-102.

LOW, T. H., FAISAL, H. A. & IBRAHIM A. S. 2012. An investigation on one of the rainfall-induced landslides in Malaysia. *Electronic Journal of Geotechnical Engineering,* 17, 435-449

LOW, T. H., FAISAL, H. A. & SARAVANAN, M. 2000. Suction and Infiltration Measurements on Cut Slope in Highly Heterogeneous Residual Soil. *Proceedings of the Asian Conference on Unsaturated Soils, UNSAT-ASIA 2000, Singapore***,** 807-811.

LUMB, P. 1975. Slope Failures in Hong Kong. *Quarterly Journal of Engineering Geology,* 8**,** 31-65.

MACARI, E. J., LAYMON, C. A. & COSTES, N. C. 1992. Hydrologic Field Instrumentation for a Small-Scale Experiment with Implication for Rain-Induced Slope Stability Analysis. *US Brazil NSF Geotechnical Workshop on Applicability of Classical Soil Mechanics Properties to Structured Soils***,** 79-88.

MADSEN, H. B., JENSEN, C. R. & BOYSEN, T. 1986. A comparison of the thermocouple psychrometers and the pressure plate methods for determination of soil water characteristic curves. *Journal Soil Science,* 37**,** 357-362.

MALAYSIA METEOROLOGY DEPARTMENT. 2009. *Scientific Report: Climate Scenarios for Malaysia 2001-2099* [Online]. Available: http://www.met.gov.my/images/pdf/nwp/climate-scenarios.pdf.

MATSUI, T. & SAN, K. C. 1988. Finite element stability analysis method for reinforced slope cutting. *Proceedings of the International Geotechnical Symposium on Theory and Practice of Earth Reinforcement, Fukuoka, Japan***,** 317–322.

MCDONELL, J. J. 1990. The Influence of Macropores on Debris Flow Initiation. *Quarterly Journal of Engineering Geology,* 13**,** 325-331.

MD. RAHIM, M. S. & TOLL, D. G. 2014. Fully Coupled Flow-Deformation Analyses of Infiltration and Matric Suctions within a Tropical Soil Slope. *Unsaturated Soils: Research & Applications, (Eds. N. Khalili, A. Russell & A. Khoshghalb), London: Taylor & Francis (CRC Press)***,** 1453-1458.

MEILANI, I., RAHARDJO, H., LEONG, E. C. & FREDLUND, D. G. 2002. Mini suction probe for matric suction measurements. *Canadian Geotechnical Journal,* 39**,** 1427-1432.

MENDES, J. 2011. *Assessment of the impact of climate change on an instrumented embankment: an unsaturated soil mechanics approach.* Phd Dissertation, Durham University.

MENDES, J., TOLL D.G. & EVANS, F. 2012. A double cell triaxial system for unsaturated soils testing. *2nd European Conference on Unsaturated Soils***,** 5-10.

MOONEY, M. A., FINNO, R. J. & VIGGIANI, M. G. 1998. A unique critical state for sands. *Journal of the Geotechnical Engineering Division-Asce,* 124**,** 1100-1108.

MUALEM, Y. 1986. hydraulic conductivity of unsaturated soils: prediction and Formulas. *Methods of soil analysis. Part 1. Physical and mineralogical*

methods. Second edition. Agronomy. Edited by A. Klute. American Society of Agronomy, Inc. and Soil Science Society of America, Inc. Madison, WI, USA, 799-823.

MUN, K. P. 1985. *Sampling and testing of residual soils in Malaysia,* Hong Kong, Scorpio Press.

MUTTAYA, P. & HUAT, B. B. K. 1994. Effect of treatment on engineering properties of local residual soils. *Journal of Institute of Engineers Malaysia,* 55, 29-41.

NEWILL, D. & DOWLING, J. W. F. 1969. Laterites in West Malaysia and Northern Nigeria. *Proc. of the specialty session engineering properties of lateritic soils VII ICSMFE. AIT. Bangkok.,* 2, 133-150.

NICHOLLS, R. A. 1990. Sampling techniques in soft ground and residual soils. *Proc. of seminar on geotechnical aspects of the north-south expressway.*, 1-7.

NITHIARAJ, R., TING W.H. & BALASUBRAMANIAM, A. S. 1996. Strength parameters of residual soils and application to stability analysis of anchored slopes. *Geotechnical Engineering,* 27, 55-81.

NIXON, I. K. & SKIPP, B. O. 1957. Airfield construction on overseas soil: Part 5. laterite. *Proc, Inst. Engrs. 36 (6258),* 36, 253-275.

NOGUCHI, T., MENDES J. & TOLL, D. G. 2012. Comparison of soil water retention curves obtained by filter paper, high capaci-ty suction probe and pressure plate. *Proc. 5th Asia-Pacific Conference on Unsaturated Soils, Pataya, Thailand*, 368-373.

OBERG, A. L. & SALLFORS, G. 1997. Determination of shear strength parameters of unsaturated silts and sands based on the water retention curve. *Geotechnical Testing Journal,* 20, 40-48.

OLDECOP, L. A. & ALONSO E.E. 2000. A model for rockfill compressibility. *Geotechnique,* 51, 127-139.

OOI, T. A. 1982. Malaysian soils and associated problems. *Geotechnical Engineering course.* University of Malaya, Kuala Lumpur.

OOI, T. A. 2004. Earthwork Practice in Malaysia. *Proc. Conference MGC 2004, Kuala Lumpur*, 45-58.

PERBADANAN PUTRAJAYA. 2015. *World first intelligent garden city.* [Online]. Available: http://www.putrajaya.gov.my [Accessed 05/08/2015.

PITTS, J. 1984. A review of geology and engineering Geology in Singapore. *Quarterly Journal of Engineering Geology* 17**,** 93-101.

PITTS, J. 1985. An Investigation of Slope Stability on the NTU Campus, Singapore. *Applied Research Project RPI/83, Nanyang Technological Institute, Singapore*.

POTTS, D. M. & ZDRAVKOVIC, L. 2001. *Finite Element Analysis in Geotechnical Engineering: Application*, Thomas Telford Limited.

PREMCHITT, J., BRAND, E. W. & CHEN, P. Y. M. 1994. Rain-Induced Landslides in Hong Kong. *Journal of Hong Kong Institution of Engineers***,** 43-51.

PUBLIC WORKS INSTITUTE OF MALAYSIA 1996. Tropical weathered in-situ materials.: Public Works Institute of Malaysia (IKRAM).

PUSHPARAJAH, E. & AMIN, L. L. 1977. Soils under Hevea in Peninsular Malaysia and their management. *Rubber Research Institute of Malaysia*

RAHARDJO, H., AUNG, K. K., LEONG, E. C. & REZAUR, R. B. 2004. Characteristics of residual soils in Singapore as formed by weathering. *Engineering Geology,* 73**,** 157-169.

RAHARDJO, H. & LEONG, E. C. 2006. Suction measurements. *Geotechnical Special Publication (ASCE),* 147**,** 81-104.

RAHARDJO, H., LEONG, E. C., DEUTCHER, M. S., GASMO, J. M. & TANG, S. K. 2000. Rainfall-Induced Slope Failures. *Geotechnical Engineering Monogrpah 3, NTU-PWD Geotechnical Researc Centre. Nanyang Technological University Singapore***,** 86.

RAHARDJO, H., LEONG, E. C., GASMO, J. M. & TANG, S. K. 1998. Assessment of Rainfall Effects on Stability of Residual Soil Slopes. *Proceedings of 2nd International Conference on Unsaturated Soils. Beijing, P.R. China* 1**,** 280-285.

RAHARDJO, H., LEONG, E. C. & REZAUR, R. B. 2003. Shear Strength Characteristics of Residual Soils in Singapore. *KEYNOTE LECTURE.*

Proceedings of the International Conference on Problematic Soils, Nottingham, United Kingdom, July 28-30.

RAHARDJO, H., LI, X. W., TOLL, D. G. & LEONG, E. C. 2001. The Effect of Antecedent Rainfall on Slope Stability. *Geotechnical and Geological Engineering,* 19**,** 369-399.

RAHARDJO, H., LIM, T. T., CHANG, M. F. & FREDLUND, D. G. 1994. Shear-strength characteristics of a residual soil. *Canadian Geotechnical Journal,* 32**,** 60-77.

RAHARDJO, H., ONG, B. H., REZAUR, R. B. & LEONG, E. C. 2007. Factors controlling instability of homogenous soil slopes under rainfall. *Journal of Geotechnical and Geoenvironmental Engineering Geology,* 133, 1532-1543.

RAJ, J. K. 1988. Drained shear strength of a weathered Graphitic-Quartz-Mica Schists. *Journal of Geotechnical Engineering,* 19**,** 253-267.

RAVIKOVITCH, P. I. & NEIMARK, A. V. 2002. Experimental confirmation of different mechanisms of evaporation from ink-bottle type pores: equilibrium, pore blocking, and cavitation. *Langmuir,* 18**,** 9830-9837.

RIDLEY, A. M. & BURLAND, J. B. 1993. A new instrument for the measurement of soil moisture suction. *Geotechnique,* 74**,** 321-324.

SCHNAID, F. & HUAT, B. 2012. Sampling and testing of tropical residual soils. *Handbook of Tropical Residual Soils Engineering*, 65-115.

SHUKRI, M., HUAT, B. B. K. & SUHAIMI, J. 2004. Index, engineering properties and classification of tropical residual soils. *In:* BUJANG, B. K. H., GUE, S. S. & FAISAL, H. A. (eds.) *Tropical Residual Soils Engineering.* Taylor & Francis Group, London.

SINGH, H. & HUAT, B. B. K. 2004. Origin, formation and occurence of tropical residual soils. *In:* HUAT, B. B. K., GUE, S. S. & FAISAL, H. A. (eds.) *Tropical Residual Soils Engineering.*: Taylor & Francis Group, London.

SOONG, N. K. & YAP, W. C. 1973. A study of the moisture characteristics of soils under rubber in Peninsular Malaysia. *Proc. of Malaysian society soil science conference on fert. and chem. of residual soils.* Kuala Lumpur, Malaysia.

SOWERS, G. F. 1985. Residual soils in United State. *Sampling and testing of residual soils: A review of International Practice.*

TAHA, M. R, MOFIZ, S. A. & HOSSAIN, M. K. 1999. Behaviour of georeinforced residual soil in triaxial test. *Proc. World Engineering Congress 99-Towards Engineering Vision: Global Challenges and Issues, 19th –22nd July, 1999, Kuala Lumpur,* 175–180.

TAN, H.S.A.,, TOLL, D. G. & PHOON, K. K. 2007. *Rainfall Induced Landslides – Why they occur and some mitigation measures.* [Online]. Available: http://www.cces.ethz.ch/latsis2007/program/CCESLatsisextended_abstract_Siew_Ann_Tan.pdf. .

TAN, B. K. 2004. Country case study: engineering geology of tropical residual soils in Malaysia. *In:* BUJANG, B. K. H., GUE, S. S. & FAISAL, H. A. (eds.) *Tropical Residual Soils Engineering.*: Taylor & Francis group, London.

TAN, S. B., TAN, S. L. & CHIN, Y. K. 1988. Soil Nailing for Slope Stabilisation in Singapore Residual Soils. *Proceedings of the 2nd International Conference on Geomechanics in Tropical Soils, Singapore, Balkema, Rotterdam***,** 285–292.

TARANTINO, A., GALLIPOLI, D., AUGARDE, C. E., DE GENNARO, V., G., R., , LALOUI, L., MANCUSO, C., MCCLOSKEY, G., MUNOZ, J., PEREIRA, J.-M., PERON, H., PISONI, G., ROMERO, E., RAVEENDIRARAJ, A., ROJAS, J. C., TOLL, D. G., TOMBOLATO, S. & WHEELER, S. 2011. Benchmark of experimental techniques for measuring and controlling suction. *Symposium in Print on Partial Saturation in Compacted Soils, Géotechnique,* 61**,** 303–312.

TERZAGHI, K. 1958. Design and performance of the Sasumua dam. *Proceedings of the Institution of Civil Engineers,* 9**,** 369–394.

TING, W. H., MUN, K. P. & TOH, C. T. 1982. Characteristics of a composite residual granite soil. *Proc. 7th SEA geotechnical conference.* Hong Kong.

TOKER, N., GERMAINE, J., SJOBLOM, K. & CULLIGAN, P. 2004. A new technique for rapid measurement of continuous soil moisture characteristic curves. *Géotechnique,* 54**,** 179-186.

TOLL, D. G. 1990. A Framework for Unsaturated Soil Behavior. *Geotechnique,* 40**,** pp. 31-44.

TOLL, D. G. 1999. A data acquisition and control system for ge-otechnical testing. *Computing Developments in Civil and Structural Engineering (eds. B. Kumar and B.H.V. Top-ping), Edinburgh: Civil-Comp Press***,** 237-242.

TOLL, D. G. 2000. The Influence of Fabric on the Shear Behaviour of Unsaturated Compacted Soils. *Advances in Unsaturated Geotechnics.*

TOLL, D. G. 2001. Rainfall-Induced Landslides in Singapore. *Proc. Institution of Civil Engineers. Geotechnical Engineering* 4**,** 211-216.

TOLL, D. G. 2012a. The behaviour of unsaturated soil. *In:* HUAT, B. B. K., TOLL, D. G. & PRASAD, A. (eds.) *Handbook of Tropical Residual Soils Engineering.* Leiden: CRC Press.

TOLL, D. G. 2012b. Tropical soils. *ICE Manual of Geotechnical Engineering Institution of Civil Engineers*.

TOLL, D. G., ASQUITH, J. D., FRASER, A., HASSAN, A. A., LIU, G., LOURENÇO, S. D. N., MENDES, J., NOGUCHI, T. & OSINSKI, P. 2015. Tensiometer techniques for determining soil water retention curves. *Keynote lecture Asia-Pacific Conference on Unsaturated Soil, Guilin, China*

TOLL, D. G., GALLIPOLI, D. & ALI RAHMAN, Z. 2008. Critical State conditions for an unsaturated artificially bonded soil. *Unsaturated Soils. Advances in Geo-Engineering.* Taylor & Francis.

TOLL, D. G., LOURENÇO, S. D. N. & MENDES, J. 2013. Advances in suction measurements using high suction tensiometers. *Engineering Geology,* 165**,** 29–37.

TOLL, D. G., MD RAHIM, M. S., KARTHIKEYAN, M. & TSAPARAS, I. Soil atmosphere interactions for analysing slopes in tropical soils. *In:* OKA, M., UZUOKA & KIMOTO, ed. Computer Methods and Recent Advances in Geomechanics, 2014. Taylor & Francis group, London, 1333-1338.

TOLL, D. G., MENDES, J., HUGHES, P. N., GLENDINNING, S. & GALLIPOLI, D. 2012. Climate change and the role of unsaturated soil mechanics. *Geotechnical Engineering Journal of the SEAGS & AGSSEA,* 42.

TOLL, D. G. & ONG, B. H. 2003. Critical-state parameters for an unsaturated residual sandy clay. *Geotechnique,* 53**,** 93–103.

TOLL, D. G., ONG, B. H. & RAHARDJO., H. 2000. Triaxial testing of unsaturated samples of undisturbed residual soil from Singapore. *Proceedings of the 1st Asian Conference on Unsaturated Soils (UNSATASIA 2000) Singapore, (eds. H. Rahardjo, D.G. Toll & E.C. Leong), Balkema, Rotterdam***,** 581-586.

TOMPSETT, G. A., KROGH, L., GRIFFIN, D. W. & CONNER, W. C. 2005. Hysteresis and scanning behavior of mesoporous molecular sieves. *Langmuir,* 21**,** 8214-8225.

TSAPARAS, I. 2002. *Field measurement and numerical modelling of infiltration and matric suctions within slopes* [Online]. PhD thesis: Durham University. Available: Durham E-Theses Online: http://etheses.dur.ac.uk/1715/.

TSAPARAS, I., RAHARDJO, H., TOLL, D. G. & LEONG, E. C. 2003. Infiltration Characteristics of Two Instrumented Residual Soil Slopes. *Canadian Geotechnical Journal,* 40**,** 1012-1032.

TSAPARAS, I. & TOLL, D. G. 2002. Numerical Analysis of Infiltration into Unsaturated Residual Soil Slopes. *Proc. 3rd International Conference on Unsaturated Soils, Recife, Brazil, Lisse: Swets & Zeitlinger. ,* 2**,** 755-762.

TUNCER, E. R. & LOHNES, R. A. 1977. An engineering classification for basalt-derived lateritic soils. *Engineering Geology,* 4**,** 319-339.

VAN GENUCHTEN, M. T. 1980. A closed-form equation for predicting the hydraulic conductivity of unsaturated soil. *Soil Science Soc. Of America,* 44**,** 892-898.

VAN GENUCHTEN, M. T., LEIJ, F. J. & YATES, S. R. 1991. The RETC Code for Quantifying the Hydraulic Functions of Unsaturated Soils. *Robert S. Kerr Environmental Research Laboratory, US Environmental Protection Agency, USA.*

VANAPALLI, S. K., FREDLUND, D. G. & PUFAHL, D. E. 1999. The influence of soil structure and stress history on the soil-water characteristics of a compacted till. *Géotechnique,* 49**,** 143-159.

VANAPALLI, S. K., FREDLUND, D. G., PUFAHL, D. E. & CLIFTON, A. W. 1996. Model for the prediction of shear strength with respect to soil suction. *Canadian Geotechnical Journal,* 33**,** 379-392.

VAQUERO, J. L. 2007. Soil suction measurement using the pressure plate technique within the MUSE network. *Project report, Durham University.*

VARGAS, J. E. A., VELLOSO, R. C., DE CAMPOS, T. M. P. & FILHO, L. M. C. 1990. Saturated-Unsaturated Analysis of Water Flow in Slopes of Rio De Janeiro, Brazil,. *Computers and Geotechnics,* 10**,** 247-261.

VAUGHAN, P. R. 1985. Pore Pressures due to Infiltration into Partly Saturated Slopes. *Proceedings of the 1 st International Conference on Tropical, Lateritic and Saprolitic Soils, Brasilia,* 2**,** 61-71.

WANG, X. & BENSON, C. H. 2004. Leak-free pressure plate extractor for measuring the soil water characteristic curve. *Geotech. Test. J.,* 27**,** 163-172.

WANG, Z., WU, L. & WU, Q. J. 2000. Water-entry value as an alternative indicator of soil water-repellency and wettability. *J. Hydrology,* 231–232**,** 76–83.

WEI, J., HENG, Y. S., CHOW, W. C. & CHONG, M. K. 1991. Landslide at Bukit Batok Sports Complex. *Proceedings of the 9th Asian Regional Geotechnical Conference, Singapore*

WEST, G. & DUMBLETON, M. J. 1970. The mineralogy of tropical weathering illustrated by some West Malaysian soils. *Q. J. Engineering Geology,* 3**,** 25-40.

WHEELER, S. J. 1988. The undrained shear srength of soils containing large gass bubbles. *Geotechnique,* 38**,** 397-413.

WHEELER, S. J. & KARUBE, D. 1996. Constitutive modelling in unsaturated soils. *1st International Conference on Unsaturated Soils.*

WHEELER, S. J. & SIVAKUMAR, V. 1995. An elastoplastic critical state framework for unsaturated soil. *Geotechnique,* 45**,** 35-53.

WILSON, G. W., BARBOUR, S. L. & D.G., F. 1995. The Prediction of Evaporative Fluxes from Unsaturated Surface. *Proceedings of the 1 st International Conference on Unsaturated Soils. UNSAT 95, Paris***,** 423-429.

WIND, P. G. 1955. Field Experiment Concerning Capillary Rise of Moisture in Heavy Clay Soil. *Soil Science,* 85**,** 228-232.

WOLLE, C. M. & HACHICHI, W. 1989. Rain-Induced Landslides in South-eastern Brazil. *Proceedings of the 12th International. Conf. on Soil Mechanics and Foundation Engineering, Rio de Janeiro***,** 1639-1642.

YAMAMURO, J. A. & LADE, P. V. 1998. Steady state concepts and static liquefaction of silty sands. *Geotechnical & Geoenvironmental Engineering,* 124**,** 868-877.

YANG, K. S. & TANG, S. K. 1997. Stabilising the Slope of Bukit Gombak. *Proceedings of the 3rd Young Geotechnical Engineers Conference, Singapore***,** 589–605.